Karoo Aquifers

Deformations, Hydraulic and Mechanical Properties

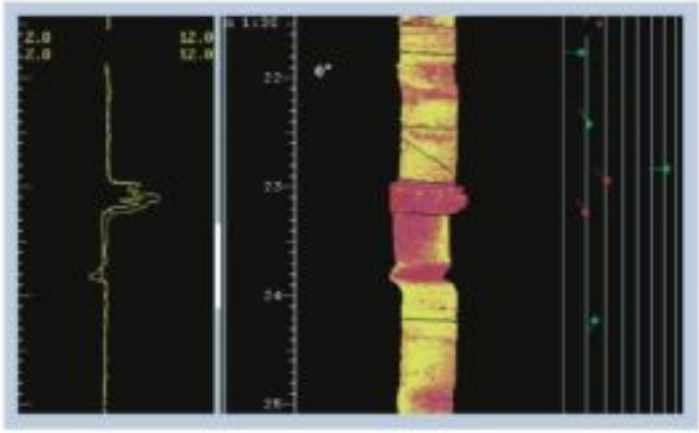

by

J.F. Botha and A.H. Cloot

Draft Report to the Water Research Commission on the Project:
'Flow and Transport Characteristics of Groundwater in Karoo Formations'
Project Leader: J. F. Botha

May 2004

Die Instituut vir Grondwaterstudies
Universiteit van die Vrystaat
Posbus 339 Bloemfontein 9300

The Institute for Groundwater Studies
University of the Free State
P.O. Box 339 Bloemfontein 9300

ACKNOWLEDGEMENTS

The research in this report emanated from a project funded by the Water Research Commission entitled:

'Flow and Transport Characteristics of Groundwater in Karoo Formations'

The Steering Committee responsible for the project consisted of the following persons:

Dr K.C. Pietersen	Water Research Commission (Chairman)	
Mr H.M. du Plessis	Water Research Commission	
Prof J.M. van Bever Donker	Univ of the Western Cape	
Prof Y. Xu	Univ of the Western Cape	
Dr E.H. Stettler	Council for Geoscience	
Dr P. Dzanga	Nuclear Energy Corporation of South Africa	
Mr E. van Wyk	Department of Water Affairs and Forestry	
Dr E.C. Murray	Environmentek, CSIR	
Prof G.J. van Tonder	University of the Free State	
Prof J.F. Botha	University of the Free State	Research Team
Prof A.H. Cloot	University of the Free State	Research Team

The financing of the project by the Water Research Commission and the contributions of members of the Steering Committee are hereby gratefully acknowledged.

The authors would also like to take this opportunity to express their sincere thanks to the following institutions and people, without whose help the investigation could not have been carried out:

The University of the Orange Free State for the facilities provided in conducting this research.

The Institute for Groundwater Studies, in particular the Director, Prof F.D.I. Hodgson, and Prof G.J. van Tonder for their assistance and encouragement during the investigation.

EXECUTIVE SUMMARY

1 GENERAL

Aquifers in the Karoo formations of South Africa are usually considered as unreliable sources of water, as illustrated by the difficulties experienced by towns such as Dealesville, Dewetsdorp and Philippolis with water supply schemes based on boreholes. However, as pointed out by (Botha *et al.*, 1998) in a previous study for the Water Research Commission these aquifers must contain considerable volumes of water, otherwise it will be difficult to explain the large quantities of water pumped daily from mines and buildings located in and on the formations respectively. One reason advanced by Botha and his co-workers for this seeming discrepancy is that the behaviour of a stressed Karoo aquifer is determined by its very complex geometry, consisting of multi-porous rocks interspersed by a few bedding-parallel fractures. To neglect this geometry in the management and operation of these aquifers, which incidentally is not discussed in textbooks on groundwater resources, can only cause severe damage to the aquifer or even ruin it completely. Indeed, there is sufficient reason to believe that the inability of previous investigators to take the internal geometry of Karoo aquifers into account must be regarded as the main reason for the difficulties experienced with these aquifers, and why people distrust them. The real problem with these aquifers might thus be more a management problem than a shortage of water.

2 BACKGROUND TO THE STUDY

A common view of the Karoo formations in the past was that the rocks are very tight and that the formations can only store water in vertical and sub-vertical fractures. However, the investigations of Botha and his co-workers have shown that this is not the case. Vertical and sub-vertical fractures do occur quite frequently in these formations, but they only serve as preferential flow paths during the recharge of the aquifers and not as storage units. The major storage units of water in Karoo aquifers are the formations themselves, while the bedding-parallel fractures serve as the conduits of water in these aquifers. A borehole in a Karoo aquifer therefore only has a significant yield if it intersects one (or more, but usually only one) bedding-parallel fracture. Although these fractures often extend over large areas, they can only store a limited volume of water, because of the sizes of their apertures, which are of the order of 10 mm. The apertures, nevertheless, are large enough to allow them to transmit water rapidly to any point in the aquifer where the fracture is present and there is a demand for water.

The American hydrologist O.E. Meinzer already argued in 1928 that aquifers (be it only confined aquifers) are compressible from observations of the following phenomena (Meinzer, 1928).

a) Manifestations of land subsidence within oil fields.

b) Larger discharge volumes obtained from pumping than calculated from recharge.

c) Lag in head decline and nature of the hydraulic gradient surrounding a pumped borehole.

d) Water level responses associated with the changing earth tides.

Nevertheless, the compressibility of an aquifer is habitually neglected in groundwater investigations, because the magnitudes of these phenomena are small and difficult to observe in practice. However, this does not imply that compressibility can be neglected in the case of water-yielding fractures with apertures of similar dimensions. Such fractures could still deform even though the deformation might not be recognized during normal field investigations of an aquifer. Indeed, there are strong indications that the bedding-parallel fractures in the Karoo formations are particularly susceptible to such deformations. For example, the complaint: *'my*

borehole has dried up', often heard from people who depend on Karoo aquifers for their water supply, may be the result of a bedding-parallel fracture that collapsed locally. The hydraulic tests, discussed in Botha *et al.* (1998), also indicated that deformations might affect the yield of a borehole in the Karoo formations adversely.

Since deformations seemed to play such an important role in Karoo aquifers and very little information was available in the existing literature on groundwater resources at the time that the project of Botha and his co-workers ended, the Water Research Commission was again approach for funds to investigate this phenomenon in more detail.

3 OBJECTIVES OF THE STUDY

The aims of the present study as set out in the original proposal to the Water Research Commission were as follows:

a) Confirm and expand the existing knowledge on the physical nature of Karoo aquifers, with special reference to the role that the flow field and deformation play in their behaviour.

b) Determine how the physical nature of Karoo aquifers influences the dispersion of contaminants.

c) Incorporate the new knowledge into the existing three-dimensional numerical flowmodel.

d) Expand the three-dimensional flow-model to account for mass transport in Karoo aquifers.

e) Combine the information gained in the previous investigations and develop efficient management and protection strategies for these aquifers that will improve their reliability as sources of potable water and protect them against pollution.

The first step taken in this investigation was to expand the three-dimensional model developed for Karoo formations during the project *'The analysis and interpretation of aquifer tests in secondary aquifers'* for the Water Research Commission to account for deformations. The computer program developed for this purpose was originally based on a three-dimensional Cartesian description of the aquifer, as it was anticipated that suitable computer resources might become available nationally during the duration of the project. Unfortunately, the latter expectation did not materialize and the program had to be scaled down to radial-symmetric, cylindrical coordinates.

The devaluation of the South African Rand between the time the proposal was submitted to the Water Research Commission and when the project actually began meant that that there were not sufficient funds to purchase a suitable flow meter. The project team therefore concentrated their efforts on the development of the deformation model. This model showed that deformations might play a much larger role in the behaviour of aquifers in general, and not only Karoo aquifers, than originally thought. This means that one should use a model that also takes the mechanical properties of the aquifer into account and not a model that only depends on the classical hydraulic parameters (specific storativity and hydraulic conductivity), when modelling the flow of groundwater in practice. One approach to determine these parameters (Young's modulus and Poisson's ratio) is through electrokinetic surveys. The Water Research Commission was therefore approach with the request, supported by the Steering Committee, to include an investigation of electrokinetic surveys in the project, which the Commission accepted.

Although significant results were obtained with the electrokinetic surveys (Fourie *et al.*, 2000), it later became clear that a full investigation of the method would take a much longer time than originally anticipated and that it could not be completed even during the extension of this project. The surveys could fortunately be continued through grants from the National Research Foundation to the Project Leader. However, this meant that the original objectives of the investigation had to be modified. The results of the electrokinetic surveys will therefore not be included in this report, but a separate report will be submitted to the Water Research Commission after the conclusion of the project.

The deformation model was supplemented with the two-dimensional mass transport model of Verwey and Botha (1992) to study mass transport in an aquifer subject to deformations. However, this showed that there is no significant difference between mass transport in a deformable and a rigid aquifer, provided that the discharge rate of a borehole is not so high as to cause oscillations in the water levels of the aquifer and the mass transport model becomes unstable. This report will therefore concentrate on a discussion of the deformation model.

4 METHODOLOGY USED IN THE INVESTIGATIONS

4.1 The Nature of Deformations

All material bodies on earth, including the earth itself, change their shape, or *deform*, to some degree when acted on by an external force. Some bodies regain their original shape once the external force is removed, but others retain all or a degree of the deformation induced by the force. Typical examples of the first type of body include the elastic band and the well-known coiled spring. These bodies are consequently known as *elastic bodies*. The other *inelastic bodies* all retain some degree of deformation—commonly referred to as *residual deformations*. A number of inelastic bodies, which retain the full deformation, such as clay, are known as *plastic bodies*. The deformation of a body is essential caused by the interaction between the molecules in the body, *which act even when no external forces are applied to the body*. These interactions, which ensure the existence of a solid state and its *strength*—the ability of the solid medium to withstand applied forces—are conventionally studied in the *theory of elasticity*. However, the theory of elasticity is not so much concerned with the internal forces themselves, but rather with the effects of the forces.

4.2 Aquifer Deformations

Since real bodies differ considerably in their composition, the internal interactions differ widely from one body to the next. Two approaches are therefore commonly used to study the behaviour of a body in the theory of elasticity—experimental and theoretical. Previous experience has shown that a combination of the two approaches provides the best way to study the behaviour of deformable bodies. Although an attempt was made to develop equipment and observational techniques for this purpose, the progress was slower than expected. The present study therefore had to be limited to a more theoretical approach.

Previous studies on the deformations of aquifers have in the past always been based on the generalized linear law of Hooke, which is one of the keystones of the theory of elasticity (Biot, 1956; Hsieh, 1996; Burbey, 1999). This law, unfortunately, does not allow one to study residual information, which could be important in Karoo aquifers. Since the linear law of Hooke cannot account for residual deformations, a new non-linear form of the law was introduced to study residual deformations in aquifers.

There are no analytical solutions available for the coupled flow and momentum equations that arise from the application of both the linear and non-linear forms of Hooke's law to the flow of groundwater through deformable aquifers, at least not to the knowledge of the authors. The finite element method (Botha and Pinder, 1983; Huyakorn and Pinder, 1983) was therefore used to approximate the equations and a computer program was developed for the numerical computations of solutions.

The computer program was first used to study a model for a hypothetical aquifer system similar to the one used by Hsieh (1996), mainly with the view to test and verify the present model. After this has been achieved the model was used to study the behaviour of the aquifer on the Campus Test Site.

5 DISCUSSION

5.1 The Aquifer of Hsieh

Two very interesting results emerged from a study of the deformations in the aquifer of Hsieh, The first is that the vertical displacements, which developed in the aquifer during the pumping of a borehole, are restricted to the interfaces of the aquifer and confining layers where the elastic parameters are discontinuous. The second is that the deformation causes the aquifer to contract towards the screened segment of the borehole, both horizontally and vertically, while the confining layers contract horizontally and extend vertically.

5.2 The Aquifer on the Campus Test Site

No significant differences were detected in the spatial distribution of the drawdowns or the vertical deformation of Hsieh's aquifer, between the linear and non-linear laws of Hooke, at least for the time scales used in the simulations. However, the situation changed drastically when the model was applied to the aquifer on the

Campus Test Site with its bedding-parallel fracture. Although the simulated drawdowns and displacements remained smooth for all simulations with the linear law of Hooke, the fracture experienced significant deformations if the discharge rate of the borehole exceeded a certain limit. The same also applies in the case of the non-linear law of Hooke, except for the introduction of residual deformations with magnitudes that depend quadratically on the discharge rate of the borehole. These residual deformations ultimately led to a chaotic behaviour of both the simulated drawdowns and displacements at high discharge rates. The model thus clearly support the view expressed in Botha *et al.* (1998) that too high discharge rates could damage a borehole and a Karoo aquifer permanently.

An interesting prediction by the model is that no deformations will form in the aquifer, even under the non-linear law of Hooke, if the discharge rate of the borehole is kept below a certain value. However, this behaviour is typical of all deformable bodies and there is no reason to expect that aquifers should behave otherwise. Knowledge of this limiting discharge rate of boreholes obviously would enhance the management of aquifers considerably. Unfortunately, the limiting discharge rate depends intrinsically on the hydraulic and mechanical parameters of an aquifer that vary considerably from aquifer to aquifer. The parameter can therefore only be determined through detailed field investigations.

The non-linear law of Hooke caused constrictions to develop in the fracture immediately after the pump is switched on, if the discharge rate of the borehole exceeds the limiting rate. The magnitudes of the constrictions increase very quickly at first, but then approach a pseudo steady state within a few hours of pumping (two in the case of the model). A series of simulations was performed to try to find to what extent the pumping of the borehole will affect the fracture in the model of the Campus Site. Two basic assumptions were made in these simulations.

a) The borehole is pumped intermittently for a continuous period of 8 h a day each day of the year, which is similar to the practice followed by many municipalities that depend on groundwater for their supply of water.

b) The borehole will dry up once the horizontal aquifer slice with an aperture of 50 mm (the fracture) has been closed due to the formation of residual constrictions.

The last assumption, which is based on the observation of Botha *et al.* (1998) that a borehole in a Karoo aquifer will only yield water if it intersects a horizontal fracture, allows one to derive an *expected mechanical life* for the borehole, defined as *the time it will take residual constrictions to reduce the aperture of the fracture to zero*.

According to the results of the simulations, summarized in Table 1, a borehole on the Campus Site will fail in less than six years, if pumped at a rate of 8,3 $m^3 h^{-1}$ for 8 h a day, every day of the year. However, the results also indicate that the fracture will suffer no significant mechanical damages, if the discharge rate is kept at or below 1,4 $m^3 h^{-1}$. The mechanical properties of a fractured aquifer are therefore as important as the hydraulic properties of the aquifer in designing a discharge rate for a production borehole in such an aquifer. More attention should therefore be paid to the mechanical properties of the aquifer in the management and control of well fields.

The fact that constrictions develop very quickly in the fracture at early times of pumping and then approach a pseudo steady state suggests that it would be more advantageous to pump a borehole for extended periods, rather than intermittently. For example, pump the borehole once for 24 hours in a cycle of 72 hours rather than three times for eight hours each, as is usually done in water supply schemes. This procedure will increase the expected mechanical life of the borehole by a factor of 3 for a given discharge rate. Longer periods of pumping will increase this time proportionally. A very important conclusion that can be drawn from this behaviour of boreholes is that an aquifer can be completely destroyed if a new borehole replaces every

Table 1 Expected mechanical life (T_g) of the borehole in the model of the Campus Test Site pumped intermittently for a continuous period of 8 h a day, every day of the year, as a function of the discharge rate (Q).

Q ($m^3 h^{-1}$)	1,4	2,8	4,1	5,5	8,3
T_g (y)	Unlimited	34,85	21,68	11,54	5,10

borehole that failed in the aquifer. It is therefore of the utmost importance that boreholes in water-supply schemes must be pumped at rates that will prevent mechanical damage to the borehole, to protect the aquifer for future generations.

There are in general three mechanisms that contribute to the volume of water pumped from an aquifer through a borehole: the expansion of the water caused by a reduction in pressure due to pumping, water that flows into the aquifer across the boundaries and matrix compression. The last two mechanisms are commonly referred to as water released from storage. The deformation model showed that magnitudes of the dilatational strains, created in the aquifer during the pumping of a borehole, increase with the discharge rate, but decreases with distance from the pumped borehole. The significance of this result immediately becomes clear if it is remembered that the dilatational strain represents the volume of water released from matrix compression during the pumping of a borehole. The three-dimensional hydraulic parameter specific storativity or its two-dimensional equivalent (storativity), which represent the volume of water released from storage in the conventional theory of groundwater flow, are therefore not independent parameters, but functions of both the discharge rate and distance from a pumped borehole. This behaviour, illustrated in Figure 1, has been observed previously by Bredenkamp *et al.*, (1995) and Botha *et al.*, (1998) in analyses of conventional hydraulic tests, but could not be explained by the authors.

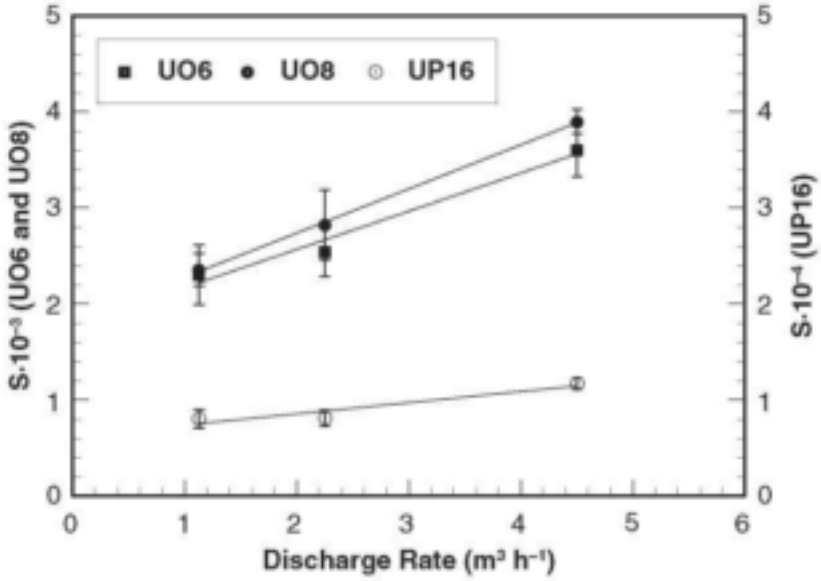

Figure 1 Storativity values for three boreholes on the Campus Test Site derived from a series of hydraulic tests in which Borehole UO5 was pumped at different discharge rates (Botha *et al.*, 1998). The variation between the maximum and minimum storativity values, expressed as a percentage of the minimum values are: UO6 56%, UO8 65% and UP16 46%.

The equivalence of the dilatational strain and water released from storage during the pumping of a borehole allows one to determine the areas in the aquifer from where the borehole obtains it water. The graphs of the normalized radial dilatational yield (the ratio of the water released per unit thickness of the aquifer divided by the total volume of water released) in Figure 2, indicates, for example, that a borehole on the Campus Test Site withdraws all its water from areas adjacent to the fracture. The fracture itself contributes almost nothing to the yield, but serve as the main conduit of water to the borehole.

An analysis of the sensitivity of the model to changes in the discharge rate, hydraulic conductivity, shear modulus and porosity revealed three very interesting properties of deformable aquifers.

a) The magnitudes of the deformations increase linearly with the discharge rate of a borehole and inversely with the shear modulus. The more rigid and aquifer is, the less likely will the withdrawal of water causes deformations in the aquifer.

b) The porosity of an aquifer has no effect on the drawdowns caused by the withdrawal of water from the aquifer, but it can affect the magnitudes of the deformations slightly.

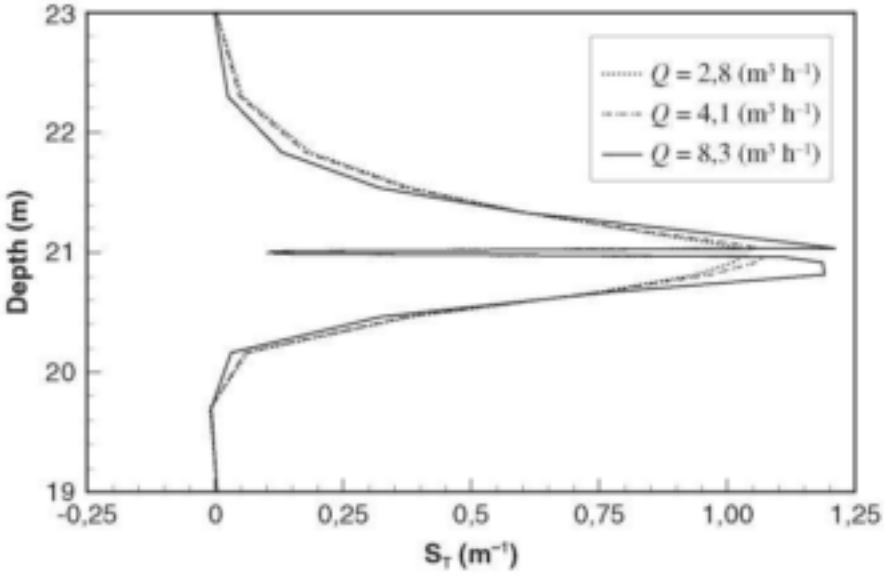

Figure 2 Graphs of normalized radial dilatational yield computed from the non-linear deformation model of the Campus Test Site after pumping the borehole at rates of 2,8 $m^3 h^{-1}$, 4,1 $m^3 h^{-1}$ and 8,3 $m^3 h^{-1}$ for a period of 8 h.

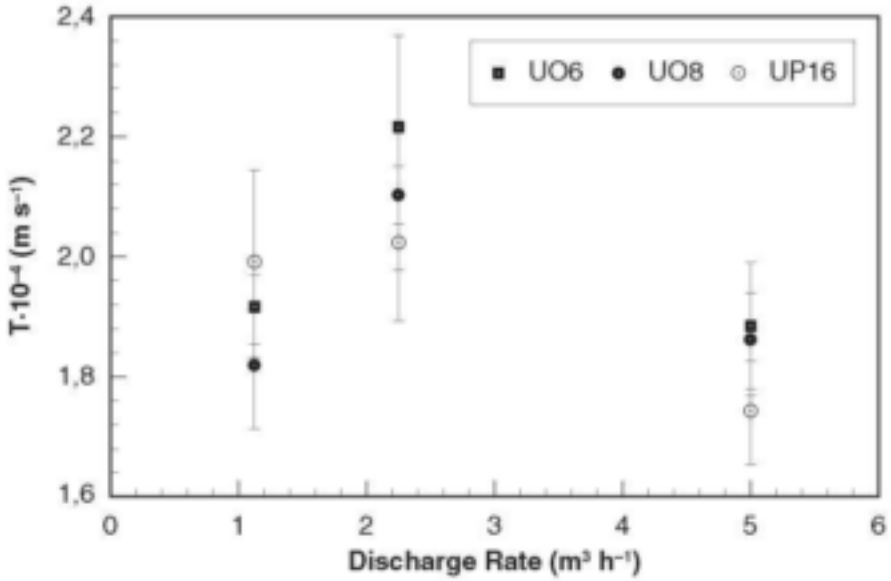

Figure 3 Dependence of the Theis-fitted *T*-values on the discharge rate of a borehole as determined from constant rate tests performed on Borehole UO5 at the Campus Test Site (Botha *et al.*, 1998).

c) The magnitudes of the deformations depend inversely on the hydraulic conductivity of an aquifer.

A detailed analysis of the model, however, revealed that the last property arises from the assumption in the present model that the hydraulic conductivity does not depend in the deformations. A physical more acceptable interpretation is that the hydraulic conductivity is also a function of the deformations and therefore should depend on the discharge rate of a borehole and the distance from the borehole, as illustrated in Figure 3.

6 CONCLUSIONS AND RECOMMENDATIONS

There are a number of results that followed from the present study that are of the utmost importance for the practical use, management and control of groundwater resources.

a) The pumping of a borehole causes deformations in an aquifer.

b) The magnitudes of the deformations depend linearly on the discharge rate and decrease with distance from the pumped borehole.

c) Groundwater levels observed in the field are implicit functions of the deformations.

d) The specific storativity of an aquifer is determined by the dilatational strains associated with the deformations and therefore depends on both the discharge rate of the borehole and the distance from the borehole.

e) The hydraulic conductivity of an aquifer is determined by properties of the rock matrix and the deformations and therefore depends on both the discharge rate of the borehole and the distance from the borehole.

There are two properties of aquifer deformations that will have a significant impact on the management and control of groundwater resources. The first is the magnitudes of the deformations and the second the nature of the deformations, i.e. whether the deformations are linear or non-linear.

Since the deformations are small, it is tempting to assume that the dilatational strain will also be small and can be neglected from the practical point of view. Unfortunately, this cannot be done, since such an assumption implies that one must also neglect the release of water by vertical matrix compression in the conventional theory of groundwater flow. The real difficulty is how to detect the deformations and how to apply them in the management of an aquifer. Since there are no methods available today that can be used to detect the deformations directly and unobtrusively, the only viable option is to observe the behaviour of the aquifer continuously. This strategy of course requires a complete revision of many practices currently applied in the management and control of groundwater resources.

The reason why it is important to know whether the deformations are linear or non-linear is briefly the following. Linear deformations will only act during the time a borehole is pumped and then disappear, without causing any damage to the borehole or aquifer. Non-linear deformations, on the other hand, will generate residual deformations that accumulate with time; thereby damaging the aquifer permanently and eventually may lead to the complete destruction of the aquifer. The present study and the work of (Botha *et al.*, 1998) suggest that the deformations in Karoo aquifers are non-linear and therefore build-up steadily over the years, but this should be confirmed by further field investigations.

The discovery that the specific storativity and hydraulic conductivity of an aquifer depend on the discharge rate of a borehole has far reaching consequences for the management of groundwater resources. To show this, consider the case where the management of an aquifer is based on a mathematical model derived from the conventional two-dimensional groundwater flow equation, as is often the practice today. A common approach used to develop such a model is to determine a few values for the storativity, S, and the transmissivity, T, of the aquifer from a few hydraulic tests performed on the aquifer. These parameters and water levels observed previously in a few boreholes are then used to derive a new set of storativities and transmissivities from the mathematical model that are supposed to be unique to the aquifer. This set of parameters is then combined with prescribed discharge rates for production boreholes to simulate the future behaviour of water levels in the aquifer with the mathematical model. However, this approach can be criticized for several reasons of which the following two are perhaps the most important.

a) The discharge rates used for the hydraulic tests will in most cases differ from the discharge rates of production boreholes for which the model is intended, which means that the S and T values derived from the hydraulic tests are not really valid for the model. There is thus no reason why the derived set of storativities and transmissivities or water levels simulated with the model should be representative of the aquifer.

b) The mathematical methods commonly used in the fitting of groundwater models are restricted to the degrees of freedom allowed for in the given model. The only way that these methods can handle the situation, where the given parameters depend on an additional parameter (not originally specified in the model), is to spread the dependence on the additional parameter over the given parameters. The parameters derived in this way will not only depend on one another, but may also loose their original physical interpretation.

A model for an observable derived by fitting a subset of the parameters, on which the observable actually depends, to a given set of realizations of the observable, will of course always describe the realizations of the observable with the accuracy specified in the fitting procedure. However, this does not mean that such a *phenomenological model* (as these models are sometimes called) will be able to describe all future realizations of the observable and that it can be used to obtain values of the observable in domains outside the one for which the model was derived originally. Extrapolation is an ill-conditioned mathematical exercise, i.e. small variations in one or more of the parameters can lead to large variations in the extrapolated values of the observable. There is thus no assurance that the extrapolated values will be true realizations of the observable, unless the whole fitting procedure is repeated, and it can be illustrated unambiguously that the model is not sensitive to extrapolations, which may be the case if the distance or time over which the model is extrapolated is small. It is therefore possible that a phenomenological groundwater model will predict the future behaviour of water levels in an aquifer within the accuracy normally associated with field observations in the immediate future, but not over extended periods. The question thus arises whether the inability of conventional, phenomenological, groundwater models to account for deformations, may not account for the heterogeneities often associated with hydraulic parameters derived from such models.

The preceding discussion is broadly based on procedures used in the development of numerical models for aquifers. However, the same arguments can also be applied to conventional hydraulic tests, although the results of this study question the value of such tests.

The most unexpected result of the present study is that the motion of groundwater in an aquifer stressed by the pumping of boreholes is essentially controlled by the discharge rates of the boreholes and not the specific storativity or hydraulic conductivity as in the conventional theory of groundwater flow. The reason for this is that both these parameters are functions of the deformations created by the pumping of the boreholes and that the magnitudes of the deformations depend linearly on the discharge rate of the boreholes. It is therefore natural to ask: *Why are deformations of aquifers commonly neglected in investigations of groundwater resources, notwithstanding the fact that* Biot, (1941) *published the first significant paper on aquifer deformation more than 60 years ago*?

One answer to this question is that the effects deformations have on the parameters and variables observed in the field develop slowly with time and thus difficult to detect with the insensitive equipment used today in investigations of groundwater resources. It may therefore take a long time to notice the effects of the deformations, unless brought to the front by disastrous phenomena, such as the 'dried-up' borehole in Karoo aquifers. The result is that the effects are often not noticed or simply discarded in field investigations. However, such an approach could have dire consequences, not only for communities that depend today on groundwater for their supply of water, but perhaps more importantly for future generations. It is therefore paramount that more attention should be given to develop methods to observe the effects of deformations in the field, especially for Karoo aquifers on which properties the model discussed in this report is mainly based.

Two approaches can be used to observe deformations, or their effects, in the field: a qualitative approach and a quantitative approach. Qualitative methods could include, for example, the repetition of conventional hydraulic tests with different discharge rates. Quantitative methods, on the other hand, would consist of detailed theoretical and laboratory studies of the relation between observed drawdowns, deformations and the permeability of an aquifer and the verification of the results through actual field observations. Since it is not clear now how to relate the permeability to the deformations, it is recommended that preference should be given to laboratory and theoretical studies of the dependence of the permeability on deformations. Many laboratory techniques could be used to investigate the dependence of the permeability on deformations. However, there is only one method the project team is aware of that may be suitable for field investigations—the electrokinetic technique.

The advantage of the electrokinetic technique is that it is based on the same equations that govern the poro-elastic model developed in this study, with the addition of Maxwell's equations that govern the behaviour of electromagnetic fields. The method could therefore be used in principle to observe the effects that deformations have on the aquifer directly and to delineate regions of different mechanical properties in the aquifer. Although some positive results have been obtained with the method during the present study, the progress has been slow because of the lack of suitable equipment and financial resources to develop appropriate equipment to compare the theoretical results with field observations.

The present report deals exclusively with results derived from a mathematical model for deformation in aquifers. Although some observational data from the aquifer on the test site of the Institute for Groundwater Studies at the Campus of the University of the Free State have been used in the development of the model and some of the predictions of the model could be verified qualitatively with field data, the model must be regarded as generic. It is the hope of the authors that it will someday be possible to confirm the conclusions derived from the model in this report, or another appropriate model, with actual field data.

7 REFERENCES

Biot, M. A. (1941) General theory of three-dimensional consolidation. *Journal of Applied Physics.* **12**, 155–164.

Biot, M. A. (1956) Theory of propagation of elastic waves in a fluid-saturated porous solid. I. Low frequency range. *Journal of the Acoustical Society of America.***28** (2), 168–178.

Botha, J. F. and Pinder, G. F. (1983) *Fundamental Concepts in the Numerical Solution of Differential Equations.* John Wiley & Sons, New York, N.Y.

Botha, J. F., Verwey, J. P., Van der Voort, I., Vivier, J. J. P., Buys, J., Colliston, W. P. and Loock, J. C. (1998) *Karoo Aquifers. Their Geology, Geometry and Physical Behaviour*. WRC Report No 487/1/98. Water Research Commission, P.O. Box 824, Pretoria 0001.

Bredenkamp, D. B., Botha, L. J., Van Tonder, G. J. and Janse van Rensburg, H. J. (1995) *Manual on Quantitative Estimation of Groundwater Recharge and Aquifer Storativity*. WRC Report No TT 73/95. Water Research Commission, P.O. Box 824, Pretoria 0001.

Burbey, T. J. (1999) Effects of horizontal strain in estimating specific storage and compaction in confined and leaky aquifer systems. *Hydrogeology Journal.* **7**, 512–532.

Fourie, F. D., Botha, J. F., Grobbelaar, R. and van Tonder, G. J. (2000) Application of the electrokinetic sounding technique for geohydrological investigations in a fractured rock aquifer system. In: Proceedings of the *XXXth IAH Congress on Groundwater: Past achievements and Future Challenges.* O. Sililo (eds.) Cape Town, South Africa. A.A. Balkema, Rotterdam.

Hsieh, P. A. (1996) Deformation-induced changes in hydraulic head during ground-water withdrawal. *Ground Water.* **34** (6), 1082–1089.

Huyakorn, P. S. and Pinder, G. F. (1983) *Computational Methods in Subsurface Flow.* Academic Press, Inc., New York, N.Y.

Meinzer, O. E. (1928) Compressibility and elasticity of artesian aquifers. *Geology.* **23**, 263–291.

Verwey, J. P. and Botha, J. F. (1992) *A Comparative Study of Two- and Three-dimensional Groundwater Models*. WRC Report No 271/1/92. Water Research Commission, P.O. Box 824, Pretoria 0001.

CONTENTS

Chapter 4

Approximation of the Governing Equations with the Finite Element Method

Chapter 5

The Hypothetical Aquifer of Hsieh

Chapter 6

The Campus Test Site

Chapter 7

Sensitivity Analysis

Chapter 8

Summary and Recommendations

LIST OF FIGURES

Chapter 1

Introduction

Chapter 2

Introduction to the Theory of Elasticity

Chapter 3

Groundwater Flow through Deformable Aquifers

Chapter 4

Approximation of the Governing Equations with the Finite Element Method

Chapter 5

The Hypothetical Aquifer of Hsieh

Chapter 6

The Campus Test Site

Chapter 7

Sensitivity Analysis

LIST OF TABLES

LIST OF SYMBOLS

1 PHYSICAL SYMBOLS

1.1 Latin Symbols

$\mathbf{B}$	=	Body forces per unit volume of the body	[M L^{-1} T^{-1}]
e	=	Dilatational strain or volumic dilatation	[1]
E	=	Longitudinal or Young's modulus of elasticity	[M T^{-1}]
e	=	Mean elongation in the body at a given point	[1]
$\mathbf{e}$	=	Strain tensor	[1]
$\mathbf{e}^0$	=	Residual strains induced by stresses	[1]
$\mathbf{e}^1$	=	Strains dependend on the stresses and pressure	[1]
$e_{\alpha\beta}$,e_{ij}	=	The $\alpha\beta$-th or ij-th elements of the strain tensor	[1]
e_{xx}, e_{yy}, e_{zz}	=	Extensional strains in the x-, y- and z directions	[1]
e_{XX}, e_{YY}, e_{ZZ}	=	Extensional strains in the principal X-, Y- and Z directions	[1]
F_κ	=	Strength of sources or sinks of the specie κ	[T^{-1}]
g	=	Acceleration of gravity	[L T^{-2}]
G	=	Shear transverse modulus of elasticity	[M T^{-1}]
$\mathbf{i}$, $\mathbf{j}$, $\mathbf{k}$	=	The unit Cartesian vectors	[1]
$\mathbf{K}$	=	Hydraulic conductivity tensor	[L T^{-1}]
$\mathbf{k}$	=	Permeability tensor of the rock matrix	[L^2]
L, M, N	=	Direction cosines in the coordinates $\{X, Y, Z\}$	[1]
l, m, n	=	Direction cosines of $\mathbf{n}$	[1]
m, n	=	Characteristic constants for a given soil	[1]
$\mathbf{P}$	=	Total stress acting on the surface area $\Delta\mathcal{A}$	[M L^{-1} T^{-2}]
$p(\mathbf{x}, t)$	=	Fluid pressure	[M L^{-1} T^{-2}]
$\mathbf{q}$	=	Darcy velocity	[L T^{-1}]
r	=	Average stress across area $\Delta\mathcal{A}$	[M L^{-1} T^{-2}]
$\mathbf{r}$	=	Radius or displacement vector	[L]
$\mathbf{S}$	=	Surface forces per unit area of a body	[M L^{-1} T^{-2}]
$\mathbf{u}$	=	Displacement vector	[L]
u,v, w	=	Cartesian components of the displacement vector	[L]
$\mathbf{v}$	=	Velocity of the centre of mass	[L T^{-1}]
$\mathbf{v}^\kappa$	=	Velocity of material specie κ	[L T^{-1}]
$\mathbf{x}$	=	Cartesian coordinates (x, y, z)	[L]
X, Y, Z	=	Principal Cartesian coordinates	[L]
x, y, z	=	Cartesian coordinates	[L]
$\mathbf{X}$, $\mathbf{Y}$, $\mathbf{Z}$	=	Cartesian stress component vectors	[M L^{-1} T^{-2}]
X_i, Y_i, Z_i	=	The i-th component of the Cartesian stresses	[M L^{-1} T^{-2}]

1.2 Greek Symbols

α	=	Characteristic constant of a given soil	[M^{-1} T]
α	=	Volumetric compressibility of the rock matrix	[M^{-1} T]
α, β, γ	=	Direction angles of the vector, $\mathbf{n}$	[1]
α_{xy}	=	Angle of rotation in the plane Oxy	[1]

β	=	Isothermal compressibility of the water	[M^{-1} T]
$\Delta\mathcal{A}$	=	Elementary area	[L^2]
$\Delta\mathcal{A}_0$	=	Proper sample area	[L^2]
ΔM_a	=	Elementary mass of air	[M]
ΔM_m	=	Elementary mass of rock matrix	[M]
ΔM_w	=	Elementary mass of water	[M]
$\Delta\mathbf{P}$	=	Resultant force vector	[M L^2 T^{-1}]
ΔS	=	Elementary area element	[L^2]
Δt	=	Time increment from time t_n to t_{n+1}	[T]
ΔV	=	Elementary volume element	[L^3]
ΔV_0	=	Proper sample volume	[L^3]
ΔV_a	=	Elementary volume of air	[L^3]
ΔV_m	=	Elementary volume of rock matrix	[L^3]
ΔV_w	=	Elementary volume of water	[L^3]
$\Delta x, \Delta y, \Delta z$	=	Increments in the Cartesian coordinates	[L]
ε	=	Porosity of a porous medium	[1]
ε_0	=	Residual porosity of the medium	[1]
$\varphi(\mathbf{x}, t)$	=	Piezometric head of groundwater	[M T^{-1}]
λ, μ	=	Lame's coefficients	[M T^{-1}]
ν	=	Poisson's ratio	[1]
θ	=	An arbitrary angle	[1]
θ, κ, λ	=	Invariants of the strain tensor	[1]
Θ, K, Λ	=	Invariants of the stress tensor	[1]
θ_κ	=	Volumetric fraction of the material specie κ	[1]
θ_w^r	=	Residual water contents of soil	[1]
θ_w^s	=	Saturated water contents of soil	[1]
ρ	=	Density of a body at a given point in space	[M L^{-3}]
ρ_κ	=	Density of material specie κ	[M L^{-3}]
ρ_w	=	Density of the water	[M L^{-3}]
$\boldsymbol{\sigma}$	=	Stress tensor	[M T^{-1}]
σ	=	Trace of the stress tensor $\boldsymbol{\sigma}$	[M T^{-1}]
$\boldsymbol{\sigma}_0$	=	Residual strains associated with $\mathbf{e}_o$	[M T^{-1}]
$\boldsymbol{\sigma}^1$	=	Non-linear strain tensor corresponding to $\mathbf{e}^1$	[M T^{-1}]
$\sigma_{\alpha\beta}, \sigma_{ij}$	=	The $\alpha\beta$-th or ij-th elements of the stress tensor	[M T^{-1}]
σ^C	=	Limiting compressive stress of rock grains	[M T^{-1}]
σ^T	=	Maximum tensile stress of rock matrix	[M T^{-1}]
$\omega_x, \omega_y, \omega_z$	=	Angles of rotation around axes (x, y, z)	[1]
ξ, η, ζ	=	Cartesian coordinates	[L]

2 MATHEMATICAL SYMBOLS

2.1 Latin Symbols

$\hat{\mathbf{p}}^n$	=	Finite element approximation vector of $p(\mathbf{x}, t)$
$\boldsymbol{\nabla}$	=	Gradient or nabla operator
$\mathbf{d}^r, \mathbf{s}^0, \mathbf{s}^\lambda, \mathbf{b}^m$	=	Finite element approximation vectors
D_z	=	Partial derivative with respect to the variable z
$\mathbf{f}, \mathbf{b}$	=	Finite element approximation vectors
$\mathbf{I}$	=	Unit Cartesian tensor
$\mathbf{L}$	=	Arbitrary differential operator
$l_k(t)$	=	Lagrange interpolation polynomials
$\mathbf{M}, \mathbf{H}, \mathbf{V}, \mathbf{W}$	=	Finite element approximation matrices
$\mathbf{n}$	=	Outwardly directed unit normal vector to a surface
$\mathbf{P}, \mathbf{Q}, \mathbf{R}$	=	Finite element approximation matrices
s	=	A line segment
$u(\mathbf{x})$	=	Arbitrary function in the variables $\mathbf{x}$

$\hat{\mathbf{u}}(\mathbf{x}, t)$	=	Finite element approximation of $u(\mathbf{x}, t)$
$\hat{\mathbf{u}}^{\kappa}$	=	Finite element approximation vector of $\mathbf{u}(\mathbf{x}, t)$
w, a, m	=	Subscripts denoting water, air and rock species (κ)
$\mathbf{x}$	=	Set of independent variables

2.2 Greek Symbols

$\delta\Omega$	=	Boundary of Ω
$\Phi(x, y, z)$	=	Potential function
$\phi_j(\mathbf{x})$	=	Set of known, piecewise continuous polynomials
$\boldsymbol{\gamma}$	=	Finite element approximation vector
λ	=	General eigenvalue parameter
Ω	=	Domain of a specie or medium

CHAPTER 1

INTRODUCTION

1.1 BACKGROUND TO THE STUDY

Aquifers in the Karoo formations of South Africa are usually considered as unreliable sources of water, as illustrated by the difficulties experienced by towns such as Dealesville, Dewetsdorp and Philippolis with water supply schemes based on boreholes. However, as pointed out by (Botha *et al.*, 1998) in a previous study for the Water Research Commission these aquifers must contain considerable volumes of water, otherwise it will be difficult to explain the large quantities of water pumped daily from mines and buildings located in and on the formations respectively. One reason advanced by Botha and his co-workers for this seeming discrepancy is that the behaviour of a stressed Karoo aquifer is determined by its very complex geometry, consisting of multi-porous rocks interspersed by a few bedding-parallel fractures. To neglect this geometry in the management and operation of these aquifers, which incidentally is not discussed in textbooks on groundwater resources, can only cause severe damage to the aquifer or even ruin it completely. Indeed, there is sufficient reason to believe that the inability of previous investigators to take the internal geometry of Karoo aquifers into account must be regarded as the main reason for the difficulties experienced with these aquifers, and why people distrust them. The real problem with these aquifers might thus be more a management problem than a shortage of water.

A common view of the Karoo formations in the past was that the rocks are very tight and that the formations can only store water in vertical and subvertical fractures. However, the investigations of Botha *et al.* (1998) have shown that this is not the case. Vertical and subvertical fractures do occur in these formations, but they only serve as preferential flow paths during the recharge of the aquifers and not as storage units. The major storage units of water in Karoo aquifers are the formations themselves, while the bedding-parallel fractures serve as the conduits of water. A borehole in a Karoo aquifer therefore only has a significant yield if it intersects one (or more, but usually only one) bedding-parallel fracture. Although these fractures can extend over large areas, they can only store a limited volume of water, because of the sizes of their apertures, which are of the order of 10 mm. The apertures, nevertheless, are large enough to allow them to transmit water rapidly to any point in the aquifer where the fracture is present and there is a demand for water. This behaviour of Karoo aquifers presents a considerable challenge to the efficient management and control of these aquifers.

The American hydrologist O.E. Meinzer already argued in 1928 that aquifers (be it only confined aquifers) are compressible from observations of the following phenomena (Meinzer, 1928).

a) Manifestations of land subsidence within oil fields.

b) Larger discharge volumes obtained from pumping than calculated from recharge.

c) Lag in head decline and nature of the hydraulic gradient surrounding a pumped borehole.

d) Water level responses associated with the changing earth tides.

Since the magnitudes of these phenomena are small and difficult to observe in normal groundwater investigations, the compressibility of an aquifer is habitually neglected in groundwater investigations. However, this does not imply that compressibility can be neglected in the case of water-yielding fractures. Such fractures could still deform even though the deformation might not be recognized during normal field investigations of an aquifer. Indeed, there are strong indications that the bedding-parallel fractures in the Karoo formations are particularly susceptible to such deformations. For example, the complaint: '*my borehole has dried up*', often heard from people who depend on Karoo aquifers for their water supply, may be the result of a bedding-parallel fracture that collapsed locally. This interpretation is supported by the fact that it is often possible to drill a new, successful borehole within a short distance from the one that 'dried up'. Another, less spectacular, but probably related, phenomenon is a borehole whose yield decreases with time. The phenomenon has never been discussed in the literature, to the knowledge of the authors, but discussions with farmers indicated that it is quite common in Karoo boreholes older than 10 years. The hydraulic tests, discussed in Botha *et al.* (1998), also indicated that deformations might affect the yield of a borehole in the Karoo formations adversely.

As mentioned in Botha *et al.* (1998) none of the common observational techniques used in their investigations gave any indication of the extent to which a water-yielding fracture may be deformed, either through the pumping of a borehole or other causes. This only became apparent when one of the high-yielding boreholes on the test site of the Institute for Groundwater Studies, commonly known as the Campus Test Site, was imaged with an acoustic televiewer in June 1996 by the consulting firm BPB Instruments Ltd. The borehole was also surveyed geophysically on two previous occasions; the first one carried out by the Department of Water Affairs and Forestry on 1992-06-04 and the second one by BPB Instruments Ltd on 1993-12-01. The bedding-parallel fracture, associated with all high-yielding boreholes on the site, is clearly visible at a depth of 23,0 m on the composite image of all three surveys in Figure 1–1. However, neither the subvertical fracture, between 22,5 and 23,0 m, nor the highly warped zone at 23,8 m in the image of the June 1996 survey, appear on the scans of the earlier surveys. These features must therefore have developed after December 1993, possibly through the reactivation of existing planes of weakness, caused by the extensive hydraulic tests performed on this borehole. There is therefore no doubt that pumping activities can deform bedding-parallel fractures and boreholes in Karoo aquifers.

Since deformations seemed to play such an important role in Karoo aquifers and very little information was available in the existing literature on groundwater resources at the time that the project of Botha and his co-workers ended, the Water Research Commission was again approach for funds to investigate this phenomenon in more detail.

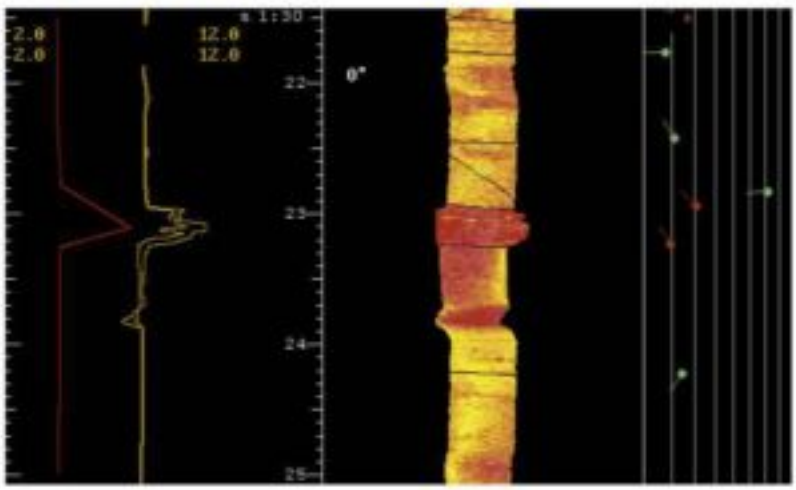

Figure 1–1 Calliper and acoustic scanner images of Borehole UO5 on the Campus Test Site. The position of the main water-yielding fracture is shown by the calliper curve on the left, and its orientation by the tadpoles on the right.

1.2 OBJECTIVES OF THE STUDY

The aims of the present study as set out in the original proposal to the Water Research Commission were as follows:

a) Confirm and expand the existing knowledge on the physical nature of Karoo aquifers, with special reference to the role that the flow field and deformation play in their behaviour.

b) Determine how the physical nature of Karoo aquifers influences the dispersion of contaminants.

c) Incorporate the new knowledge into the existing three-dimensional numerical flow-model.

d) Expand the three-dimensional flow-model to account for mass transport in Karoo aquifers.

e) Combine the information gained in the previous investigations and develop efficient management and protection strategies for these aquifers that will improve their reliability as sources of potable water and protect them against pollution.

The first step taken in this investigation was to expand the three-dimensional model developed for Karoo formations during the project *'The analysis and interpretation of aquifer tests in secondary aquifers'* for the

Water Research Commission to account for deformations. The computer program developed for this purpose was originally based on a three-dimensional Cartesian description of the aquifer, as it was anticipated that suitable computer resources might become available nationally during the duration of the project. Unfortunately, the latter expectation did not materialize and the program had to be scaled down to radial-symmetric, cylindrical coordinates.

The devaluation of the South African Rand between the time the proposal was submitted to the Water Research Commission and when the project actually began meant that that there were not sufficient funds to purchase a suitable flow meter. The project team therefore concentrated their efforts on the development of the deformation model. This model showed that deformations might play a much larger role in the behaviour of aquifers in general, and not only Karoo aquifers, than originally thought. This means that one should use a model that also takes the mechanical properties of the aquifer into account and not a model that only depends on the classical hydraulic parameters (specific storativity and hydraulic conductivity), when modelling the flow of groundwater in practice. One approach to determine these parameters (Young's modulus and Poisson's ratio) is through electrokinetic surveys. The Water Research Commission was therefore approach with the request, supported by the Steering Committee, to include an investigation of electrokinetic surveys in the project, which the Commission accepted.

Although significant results were obtained with the electrokinetic surveys (Fourie *et al.*, 2000), it later became clear that a full investigation of the method will take a much longer time than originally anticipated and that it could not be conpleted even during the extension of this project. The surveys could fortunately be continued through grants from the National Research Foundation to the Project Leader. However, this meant that the original objectives of the investigation had to be modified. The results of the electrokinetic surveys will therefore not be included in this report, but a separate report will be submitted to the Water Research Commission after the conclusion of the project.

The deformation model was supplemented with the two-dimensional mass transport model of Verwey and Botha (1992) to study mass transport in an aquifer subject to deformations. However, this showed that there is no significant difference between mass transport in a deformable and a rigid aquifer, provided that the discharge rate of a borehole is not so high as to cause oscillations in the water levels of the aquifer and the mass transport model becomes unstable. This report will therefore concentrate on a discussion of the deformation model.

1.3 METHODOLOGY USED IN THE INVESTIGATIONS

All material bodies on earth, including the earth itself, change their shape, or *deform*, to some degree when acted on by an external force. Some bodies regain their original shape once the external force is removed, but others retain all or a degree of the deformation induced by the force. Typical examples of the first type of body include the elastic band and the well-known coiled spring. These bodies are consequently known as *elastic bodies*. The other *inelastic bodies* all retain some degree of deformation—commonly referred to as *residual deformations*. A number of inelastic bodies, which retain the full deformation, such as clay, are known as *plastic bodies*.

Since real bodies differ considerably in their composition, the internal interactions differ widely from one body to the next. Two approaches are therefore commonly used to study the behaviour of a body in the theory of elasticity—experimental and theoretical. Previous experience has shown that a combination of the two approaches provides the best way to study the behaviour of deformable bodies. Although an attempt was made to develop equipment and observational techniques for this purpose, the progress was slower than expected. The present study therefore had to be limited to a more theoretical approach.

Studies of deformations in aquifers have in the past always been based on the linear law of Hooke (Biot, 1941; Hsieh, 1996; Burbey, 1999, 2001). This law, unfortunately, does not allow one to study residual deformations, which could be important in Karoo aquifers according to Figure 1–1. Since the linear law of Hooke cannot account for residual deformations, a new non-linear form of the law was introduced to study residual deformations in aquifers.

There are no analytical solutions available for the coupled flow and momentum equations that arise from the application of both the linear and non-linear forms of Hooke's law to the flow of groundwater through

deformable aquifers, at least not to the knowledge of the authors. The finite element method (Botha and Pinder, 1983; Huyakorn and Pinder, 1983) was therefore used to approximate the equations and to develop a computer program for the numerical computations.

1.4 STRUCTURE OF THE REPORT

The deformation of a body is essential caused by the interaction between the molecules in the body, *which act even when no external forces are applied to the body*. These interactions, which ensure the existence of a solid body and its *strength*—the ability of the body to withstand applied forces—are conventionally studied in the *theory of elasticity*. However, the theory of elasticity is not so much concerned with the internal forces themselves, but rather with the effects of the forces. This theory is a rather specialized field of Physics that has not attracted the attention of groundwater investigators very much. However, the situation is changing, judging from the number of papers that recently appeared in the groundwater literature on the subject, e.g. Hsieh (1996); Burbey, (1999, 2001) and Zijl *et al.* (2002). It was therefore thought worthwhile to include a brief overview of the theory in Chapter 2. This is followed by a discussion of the linear and non-linear forms of Hooke's law and their application to the flow of groundwater through deformable aquifers in Chapter 3.

The computer program was first used to develop a model for a hypothetical aquifer system similar to the one discussed by (Hsieh, 1996), mainly with the view to test and verify the present model, but also to have a reference for the investigations of the aquifer on the Campus Test Site. The model, discussed in Chapter 5, was able to reproduce all the results of Hsieh and indicated that the vertical displacements, which developed in the aquifer during the pumping of a borehole, are restricted to the interfaces of the aquifer and confining layers where the elastic parameters are discontinuous. An interesting observation about this model, which is not discussed by Hsieh, is that the deformation causes the aquifer to contract towards the screened segment of the borehole, both horizontally and vertically, while the confining layers contract horizontally and extend vertically, with magnitudes that decrease with distance from the borehole. This behaviour could be responsible for the observation that the storativity values, derived from conventional aquifer tests, tend to decrease with distance from the borehole that is pumped during such a test (Bredenkamp *et al.*, 1995; Botha *et al.*, 1998).

No significant differences were detected in the spatial distribution of the drawdowns or the vertical deformation of Hsieh's aquifer, between the linear and non-linear laws of Hooke, at least for the time scales used in the simulations. However, the situation changed drastically in the case of the model for the aquifer on the Campus Test Site, which is discussed in Chapter 6. Although the simulated drawdowns and displacements remained smooth for all simulations with the linear law of Hooke, the fracture experienced significant deformations if the discharge rate of the borehole exceeded a certain limit. The same also applies to the non-linear law of Hooke, except that both the simulated drawdowns and displacements now display a highly chaotic behaviour at high discharge rates. The non-linear law also introduces residual deformations with magnitudes that depend quadratically on the discharge rate of the borehole. The model thus clearly support the view of Botha *et al.* (1998) that too high discharge rates could damage not only a borehole, but also the Karoo aquifer itself permanently.

An interesting prediction by the model is that no deformations will form in the aquifer, even under the non-linear law of Hooke, if the discharge rate of the borehole is kept below a certain value. However, this behaviour is typical of all deformable bodies and there is no reason to expect that aquifers should behave otherwise. Knowledge of this limiting discharge rate of boreholes obviously would enhance the management of aquifers considerably. Unfortunately, the limiting discharge rate depends intrinsically on the hydraulic and mechanical parameters of an aquifer that vary considerably from aquifer to aquifer. The parameter can therefore only be determined through detailed field investigations.

The non-linear law of Hooke caused constrictions to develop in the fracture immediately after the pump is switched on, if the discharge rate of the borehole exceeds the limiting rate. The magnitudes of the constrictions increase very quickly at first, but then approach a pseudo steady state within a few hours of pumping (two in the case of the model). The residual deformation of a fracture therefore follows a similar pattern as the drawdowns caused by pumping boreholes in natural aquifers. This property of the constrictions suggests that it would be more advantageous to pump a borehole that intersect a bedding-parallel fracture for extended periods, rather than intermittedly. For example, pump the borehole once for 24 hours in a cycle of 72 hours

rather than three times for eight hours each, as is usually done in water supply schemes. The existence of residual deformations suggests that it might be advantageous to introduce another parameter into the concept of the sustainable yield for a borehole—the *expected mechanical life of a borehole*—defined as *the time it will take residual constrictions to reduce the aperture of the fracture to zero*.

The deformation model also showed that the volume of water released from storage is directly related to the dilatational strain created in the aquifer by pumping the borehole and that the magnitude of the dilatational strain increases with the discharge rate, but decreases continuously with distance from the pumped borehole. This behaviour of the dilatational strain implies that the three-dimensional hydraulic parameter specific storativity and its two-dimensional equivalent (storativity) are not independent parameters as assumed in the conventional theory of groundwater flow, but functions of both the discharge rate and distance from a pumped borehole

A rather unusual property of aquifers that emerged from the sensitivity analysis of the parameters in the model for the Campus Test Site, discussed in Chapter 7, is that the magnitudes of the vertical displacements are related to the inverse of the hydraulic conductivity. However, this behaviour can be ascribed to the assumption that the hydraulic conductivity is independent of the deformations in the present model, which forces the deformations to depend on the hydraulic conductivity of the aquifer. A physical more meaningful interpretation is that the deformations actually affect the permeability of the aquifer. The advantage of this interpretation is that it can explain the dependence of the transmissivity on the discharge rate of a borehole and the distance from the pumped borehole observed by Botha *et al.* (1998). The hydraulic conductivity, like the storativity, is therefore not an independent parameter, as assumed in the conventional theory of groundwater flow. It is important to remember though that the permeability is a tensor that also depends on various properties of the rock matrix, particularly the orientation of the grains, and therefore cannot be described in terms of the deformations alone, as is the case with the specific storativity.

The results discussed in this report are all based on conclusions derived from what may be called a generic model for the aquifer on the Campus Test Site of the Institute for Groundwater Studies at the University of the Free State. While such a model can provide valuable insight into the physical behaviour of an aquifer, it can never replace field observations. Unfortunately, very little attention was paid to deformations in previous field studies of aquifers. There is therefore no field data that could be used to verify the results of this investigation quantitatively. One approach that could be used to obtain the necessary field data and a few recommendations for future work are discussed in Chapter 8.

CHAPTER 2

INTRODUCTION TO THE THEORY OF ELASTICITY

2.1 INTRODUCTION

All material bodies on earth change their shape, or *deform*, to some degree when acted on by an external force. Some bodies regain their original shape once the external force is removed, but others retain all or some degree of the *deformation*. Typical examples of the first type of body include the elastic band and the well-known coiled spring. These bodies are consequently known as *elastic bodies*. The other *inelastic bodies* all retain some degree of deformation. A number of inelastic bodies, which retain the full deformation, such as clay, are known as *plastic bodies*. This behaviour of bodies caused considerable difficulties for the 18th and early 19th century physicists and mathematicians, who was used to the idea of a *rigid body*—a body that retains its shape *no matter what force is acting on it*. This concept arose from the view that the internal forces in a body should cancel pairwise mutually, because of Newton's third law of motion. The deformation of bodies, on the other hand, clearly indicates that this is not necessarily the case. The theory of elasticity therefore essentially entails the study of internal forces in a solid body. These forces, which arise form the interaction between the molecules in the body, ensure the existence of a solid body as such and hence its *strength*. They also act when no external forces are applied to the body.

The theory of elasticity is not so much concerned with the internal forces themselves, but rather with the effects of the forces. However, it is important to know what kind of forces will act on the body and how a body will react to these forces to determine the effects that the forces will have on the body. The discussion therefore begins with a brief overview of the internal forces, commonly known as *stresses*, in Section 2.2. This is followed a discussion of the geometrical theory of strain in Section 2.3 that describes the geometrical behaviour of a body when forced to deform. It should be obvious that stresses and strains alone cannot be instrumental in solving physical problems associated with the deformation of bodies under the action of forces. This can only be achieved, once a suitable physical law has been established that relates the stresses and strains in the body. This law generally known as the law of Hooke is discussed in Section 2.4.

2.2 THE THEORY OF STRESS

2.2.1 General

According to the atomic theory of matter, a body can only deform under the action of external forces if the mutual positions, hence the distances, between the atoms or molecules in the body change. The action of external forces that produce deformations in a body must therefore introduce additional internal forces in the body, according to Newton's second law of motion. One must therefore first convert the internal forces in question into external forces to study the deformation of a body. To achieve this, consider the situation of a body in equilibrium cut into two parts by a plane, $\mathscr{P}$, as in Figure 2–1. This plane intersects the lines of forces of interaction between molecules situated on its two sides. If one now removes part $\mathscr{B}$ from the body, the interaction forces between the molecules on the plane will be unbalanced in part $\mathscr{A}$, but the rest of the forces will remain in equilibrium.

Consider now the elementary area $\Delta\mathscr{A}$ within of the plane $\mathscr{P}$ that is very smaller than the dimensions of the plane, but considerably larger than the square of the largest distance between the individual molecules on the plane. This area will be intersected by a large number of lines of forces left unbalanced by the removal of $\mathscr{B}$. Let $\mathbf{\Delta P}$ denote the resultant force vector of these now external forces. The ratio

$$r = \frac{\mathbf{\Delta P}}{\Delta\mathscr{A}}$$

is known as the *average stress* of the internal forces in the body across the area $\Delta\mathscr{A}$. If one now contracts the contour, $\mathscr{C}$, around the area $\Delta\mathscr{A}$, the resultant force vector will decrease indefinitely. However, it is possible that the ratio, r, approaches a limit as $\Delta\mathscr{A}$ approaches a value $\Delta\mathscr{A}_0$, henceforth referred to as a *proper sample*

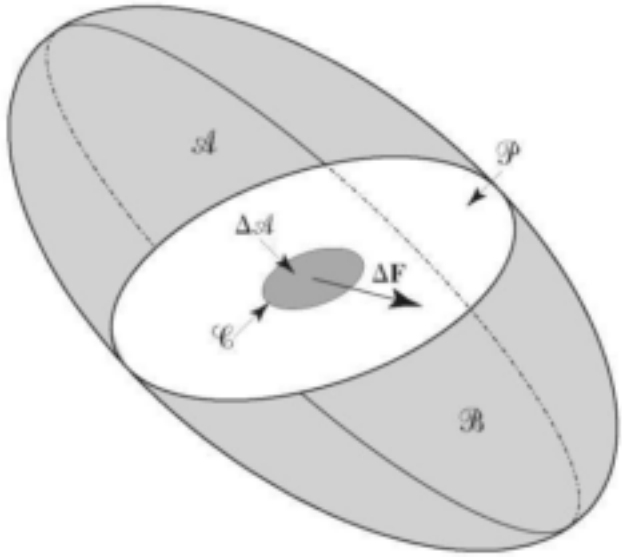

Figure 2–1 Schematic diagram of the internal forces acting on a body.

area. This limiting ratio

$$\lim_{\Delta\mathscr{A}\to\Delta\mathscr{A}_c} \frac{\Delta\mathbf{P}}{\Delta\mathscr{A}}$$

is called the *stress of internal forces,* or simply the *stress,* exerted at the centre point of $\Delta\mathscr{A}$ lying in the plane of the section through the body. The notion of stress is therefore a fundamental measure of the intensity of internal forces at an internal point of a body in the theory of elasticity. Notice that stress, as defined here, has the dimensions of force per length^2 and depends on the orientation of the plane $\mathscr{P}$.

2.2.2 The State of Stress in a Body

Stress or more appropriately, *total stress*—the stress per unit area—has the same dimensions as pressure, but differs from pressure in that stress depends on the direction in which it is measured and is therefore not a scalar. It is therefore very important that one uses a good notational system to describe stress. One approach to achieve this is to characterize the stress plane by its outwardly directed unit normal vector, **n**, as illustrated in Figure 2–2. This allows one to introduce a Cartesian coordinate system, (X, Y, Z) in Figure 2–2, with its Z–axis pointing in the direction of **n** and the X and Y axes perpendicular to it and each other in the plane of $\Delta\mathscr{A}$

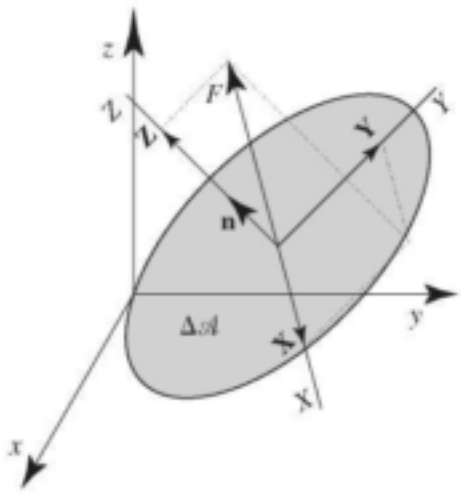

Figure 2–2 Schematic diagram of the total stress, **P**, acting on the surface area $\Delta\mathscr{A}$ in Figure 2–1, with (x, y, z) and (X, Y, Z) two Cartesian coordinate systems.

Although this coordinate system can be used to decompose the stress into its three mutually orthogonal Cartesian component vectors (**X**, **Y**, **Z**) in Figure 2–2, the decomposition is not unique, as one can still rotate the X and Y axes in the plane of Δs. Stresses are consequently more commonly related to a coordinate system fixed in space, such as the one denoted by (x, y, z) in Figure 2–2. However, as shown in Figure 2–3 for the **Z** component vector of Δ **P**, each of the component vectors can again be decomposed into three components in the (x, y, z) coordinate system. This means that stress is characterized by nine quantities

$$(X_x, X_y, X_z), (Y_x, Y_y, Y_z), (Z_x, Z_y, Z_z)$$

in the fixed coordinate system. Stress is therefore a more general quantity than just a vector, called a *tensor* — a quantity that that does not depend only on magnitude and direction, but also the direction in which it is measured, as can be seen from the fact that Δs in Figure 2–2 can be arbitrarily orientated in space.

As shown in Figure 2–3, the stress Z_z acts perpendicular to the xy-plane in the direction of the z-axis, while Z_x and Z_y act in the plane. The same obviously also apply to the stresses X_x and Y_y and their associated components. The stresses X_x, Y_y and Z_z are therefore known as the *normal stresses*, while the other six stresses are known as *shearing stresses*.

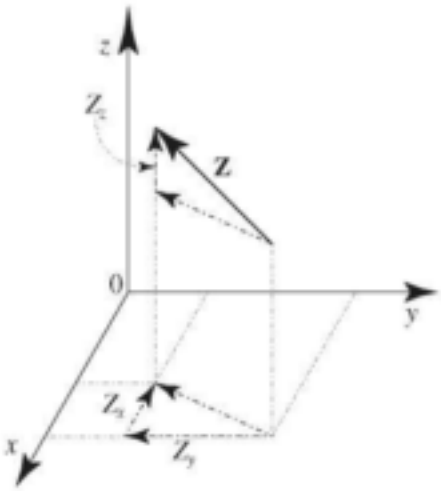

Figure 2–3 Schematic decomposition of the Z-component vector of **P** in the (x, y, z) coordinate system of Figure 2–2.

The notation used above, which is the same as that used in the classical treatises on elasticity, e.g. Filonenko-Borodich (1965) and Love (1927), has the advantage that it clearly distinguishes between the different elements of the stress tensor. However, the current practise is to denote the tensor itself by the symbol $\boldsymbol{\sigma}$ and its elements by $\sigma_{\alpha\beta}$ (or σ_{ij}), where α and β (i and j in the latter case) denote the coordinates x, y and z. Since this notation has some notational advantages, it will also be used from now on.

The stresses in a body may of course vary from point to point and with time. They are therefore, generally speaking, functions of the spatial coordinates and the time, that is

$$\sigma_{\alpha\beta} = \sigma_{\alpha\beta}(x, y, z, t) \qquad (\alpha, \beta = x, y \text{ or } z)$$

One can consequently always use Taylor's series to express a variation in $\sigma_{\alpha\beta}$ over a small distance, say Δx, as

$$\sigma_{\alpha\beta}(x + \Delta x, y, z, t) = \sigma_{\alpha\beta}(x, y, x, t) + \Delta x \partial_x \sigma_{\alpha\beta}(x, y, x, t)$$

2.2.3 Equations of Motion

Assume that an infinitesimal element in the form of a parallelepiped with three pairs of faces parallel to the planes of the Cartesian coordinate system xyz in Figure 2–2 has been cut from a solid. The actions of the

removed parts of the body upon the isolated element can then be represented by the $6\times3 = 18$ components of the stresses acting on each of the faces, as shown in Figure 2–4. Also, assume that there exist a number of so-called *body forces*, the force of gravity, for example, that acts on the body from which the parallelepiped was cut. Let X, Y, and Z represent the Cartesian components of the body forces per unit mass of the body and

$$\mathbf{u} = \mathbf{i}u + \mathbf{j}v + \mathbf{k}w \tag{2.1}$$

the displacement of the body caused by the forces, with $\mathbf{i}$, $\mathbf{j}$, $\mathbf{k}$ the unit Cartesian vectors and (u, v, w) the Cartesian components of $\mathbf{u}$. Also let Δx, Δy and Δz be the lengths of the parallelepiped's edges, $\Delta V = \Delta x \Delta y \Delta z$ its volume, ρ the density of the body at a given point in space and

$$\boldsymbol{\sigma} = \begin{pmatrix} \sigma_{xx} & \sigma_{xy} & \sigma_{xz} \\ \sigma_{yx} & \sigma_{yy} & \sigma_{yz} \\ \sigma_{zx} & \sigma_{zy} & \sigma_{zz} \end{pmatrix}$$

the stress tensor at points on of the faces of the parallelepiped that pass through the origin of the Cartesian coordinate system in Figure 2–4. Taylor's theorem can then be used to express the stresses on the opposite faces of the parallelepiped in the form given in Figure 2–4.

According to Newton's second law of motion the resultant of the stresses and the body forces in every one of the directions must be equal to the product of the mass of parallelepiped and the acceleration it experiences in that direction. Consider for example the x-direction. It follows from Figure 2–4 that the resultant of the stresses in this direction is given by

$$[\sigma_{xx} + (\mathrm{D}_x\sigma_{xx})\Delta x - \sigma_{xx}]\Delta y\Delta z + [\sigma_{yx} + (\mathrm{D}_y\sigma_{yx})\Delta y - \sigma_{yx}]\Delta x\Delta z + [\sigma_{zx} + (\mathrm{D}_z\sigma_{zx})\Delta z - \sigma_{zx}]\Delta x\Delta y$$

while the body forces and accelerations are given respectively by

$$X\rho\Delta x\Delta y\Delta z \quad \text{and} \quad \rho\Delta x\Delta y\Delta z\mathrm{D}_t^2 u$$

The equation of motion in the x-direction is therefore of the form

$$\mathrm{D}_x\sigma_{xx} + \mathrm{D}_y\sigma_{yx} + \mathrm{D}_z\sigma_{zx} + X\rho = \rho\mathrm{D}_t^2 u$$

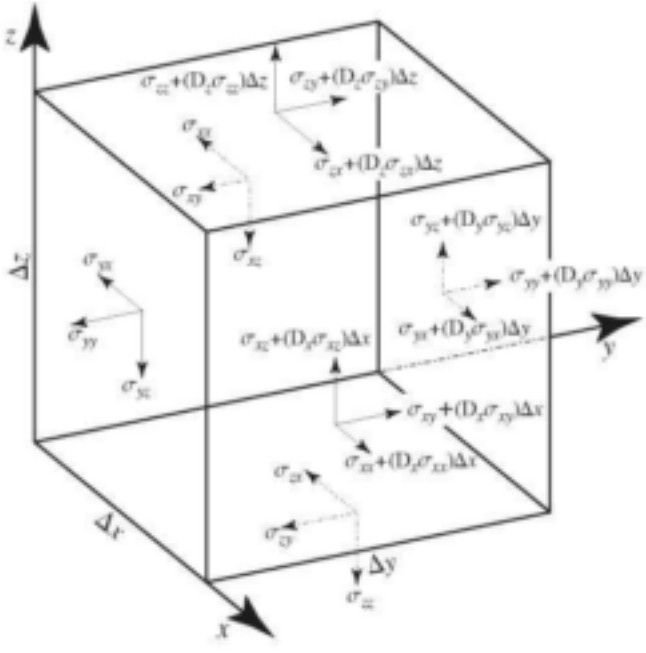

Figure 2–4 Distributions of stresses across the six faces of a parallelepiped.

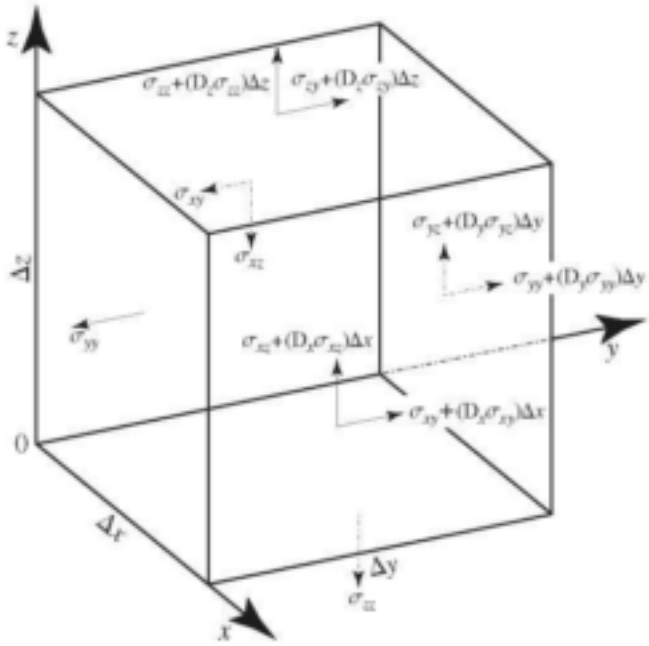

Figure 2–5 Stress components that can rotate the elementary volume element around the Ox -axis.

where the identical terms in the first expression have been cancelled and use was made of the fact that the volume of the parallelepiped is (by assumption) not equal to zero. Similar expressions can also be derived for the other directions. The behaviour of a deformable solid is therefore governed by the three equations of motion

$$\begin{aligned} &D_x\sigma_{xx} + D_y\sigma_{yx} + D_z\sigma_{zx} + X\rho = \rho D_t^2 u \\ &D_x\sigma_{xy} + D_y\sigma_{yy} + D_z\sigma_{zy} + Y\rho = \rho D_t^2 v \\ &D_x\sigma_{xz} + D_y\sigma_{yz} + D_z\sigma_{zz} + Z\rho = \rho D_t^2 w \end{aligned} \tag{2.2}$$

Stresses are internal forces and should therefore balance one another under normal conditions, according to Newton's third law of motion. This means that they cannot set a body in motion by themselves through translation or rotation. The translational constraints are automatically satisfied by Equation (2.2), as can be seen by equating the components of the acceleration $D_t^2\mathbf{u}$ on its right hand side with zero.

To derive equivalent expressions for the rotations, consider the rotation of the elementary volume element about a suitable axis, e.g. the Ox-axis. As shown in Figure2–5, only 10 of the 18 stress components can contribute to such a rotation (components that act perpendicular to the axis and do not pass through the axis). To ensure that the volume element does not rotate about this axis, the sum of the moments of the stresses and the body forces must be zero. If it assumed that moments in the clockwise direction is positive, the moments caused by the stress components can be expressed as

$$\begin{aligned} &[\sigma_{zy} + (D_x\sigma_{zy})\Delta x - \sigma_{zy}]\Delta y\Delta z\frac{\Delta z}{2} + [\sigma_{xz} - \sigma_{xz} - (D_x\sigma_{xz})\Delta x]\Delta y\Delta z\frac{\Delta y}{2} \\ &+ [\sigma_{yy} + (D_y\sigma_{yy})\Delta y - \sigma_{yy}]\Delta x\Delta z\frac{\Delta z}{2} - [\sigma_{yz} + (D_y\sigma_{yz})\Delta y]\Delta x\Delta z\Delta y + \\ &+ [\sigma_{zz} - \sigma_{zz} - (D_z\sigma_{zz})\Delta z]\Delta x\Delta y\frac{\Delta y}{2} + [\sigma_{zy} + (D_z\sigma_{zy})\Delta z]\Delta x\Delta y\Delta z \end{aligned}$$

or if simplified and divided by the volume of the volume element

$$[D_x\sigma_{xy} + D_y\sigma_{yy}]\frac{\Delta z}{2} - [D_x\sigma_{xz} + D_z\sigma_{zz}]\frac{\Delta y}{2} + [D_z\sigma_{zy}\Delta z - D_y\sigma_{yz}\Delta y] + (\sigma_{zy} - \sigma_{yz})$$

while that caused by the body forces can be expressed as

$$+Y\rho\frac{\Delta z}{2} - Z\rho\frac{\Delta y}{2}$$

Since the volume element is by assumption very small, terms containing the length of one of the element's sides can be neglected. The volume element will therefore not rotate about the Ox-axis provided that

$$\sigma_{zy} = \sigma_{yz}$$

The same line of reasoning can also be used to show that

$$\sigma_{xy} = \sigma_{yx} \quad \text{and} \quad \sigma_{yz} = \sigma_{zy}$$

This is the law of reciprocity for shearing stresses. The stress tensor is consequently a symmetric tensor.

$$\boldsymbol{\sigma} = \begin{pmatrix} \sigma_{xx} & \sigma_{xy} & \sigma_{xz} \\ \sigma_{xy} & \sigma_{yy} & \sigma_{yz} \\ \sigma_{xz} & \sigma_{yz} & \sigma_{zz} \end{pmatrix} \tag{2.3}$$

It is important to note that the stress tensor in Equation (2.3) contains six quantities that are functions of the coordinates of the point in question, but that there are only three equations in Equation (2.2) which relates them. The equations of motion in the theory of elasticity are thus indeterminate. The reason for this is that the discussion has thus far not been concerned with the conditions of deformation and the physical properties of a given elastic body, properties on which the state of stress in a body depends undoubtedly. For example, the equations of motion in Equation (2.2) only relate stresses over areas parallel to the coordinate planes, but say nothing about stresses on arbitrary orientated planes in the body. This applies in particular to the surface of the body, the main area where external forces will act on a body, which cannot be divided into parallelepipeds. It is therefore necessary to give attention to stresses over an area inclined arbitrarily to the coordinate planes.

2.2.4 Surface Conditions

To obtain relations for an arbitrary orientated plane, consider the infinitesimal tetrahedron bounded by three planes parallel to the coordinate planes and a fourth plane intersecting all three coordinate axes, as in Figure 2–6. Let α, β and γ denote the direction angles that the outwardly directed unit vector, **n**, normal to the plane abc with area ΔS, makes with the coordinate axes (x, y, z). The areas of the other three faces can then be expressed as the projections of ΔS onto the coordinate planes.

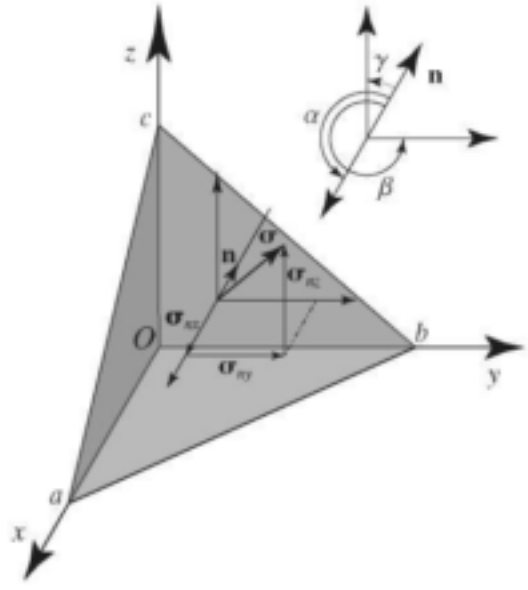

Figure 2–6 Schematic view of an infinitesimal tetrahedral element cut from a deformable body.

$$\text{area } Oac = \Delta S \cos\alpha$$
$$\text{area } Obc = \Delta S \cos\beta$$
$$\text{area } Oab = \Delta S \cos\gamma$$

In addition, let σ_{nx}, σ_{ny}, σ_{nz} be the component vectors of the total stress $\boldsymbol{\sigma}$, acting on the area abc. Since the plane abc is fixed in the tetrahedron, the component vectors of $\boldsymbol{\sigma}$ must be balanced by the stresses across the other three faces. This will be the case if their magnitudes in a given direction cancel. For example,

$$\sigma_{nx}\Delta S = \sigma_{xx}\Delta S\cos\alpha + \sigma_{xy}\Delta S\cos\beta + \sigma_{xz}\Delta S\cos\gamma \tag{2.4}$$

or if divided by ΔS,

$$\sigma_{nx} = \sigma_{xx}\cos\alpha + \sigma_{xy}\cos\beta + \sigma_{xz}\cos\gamma$$

and similarly for the other two component vectors. It is custom to express these boundary equations in the form

$$\begin{aligned}\sigma_{nx} &= \sigma_{xx}l + \sigma_{xy}m + \sigma_{xz}n\\ \sigma_{ny} &= \sigma_{xy}l + \sigma_{yy}m + \sigma_{yz}n\\ \sigma_{nz} &= \sigma_{xz}l + \sigma_{yz}m + \sigma_{zz}n\end{aligned} \tag{2.5}$$

where

$$l = \cos\alpha, \quad m = \cos\beta, \quad n = \cos\gamma$$

are the components of $\mathbf{n}$ also known as the direction cosines of $\mathbf{n}$.

It is important to note that the body forces are not involved in these equations since they are small quantities of the third order, for instance the body force in the x-direction is given by

$$\rho X \frac{dx\,dy\,dz}{6}$$

while all terms in Equation (2.4) are of the second order.

If ΔS approaches zero as a limit; Equation (2.5) can be viewed as the relation between the stresses at a point on an oblique area with the normal unit vector $\mathbf{n}$ and those on the three areas parallel to the coordinate planes. If this face was cut from the surface of the body, one can view $\boldsymbol{\sigma}_{nx}$, $\boldsymbol{\sigma}_{ny}$ and $\boldsymbol{\sigma}_{nz}$ as the component vectors of the stress caused by external forces or *loads* applied on the surface on the given body. In this case, Equation (2.5) gives a relation between the external load and internal forces, i.e., the *boundary conditions* that the stress in a body must satisfy when subjected to external forces. If applied in conjunction with Equation (2.2), these equations will ensure that the equations of motion in the theory of elasticity are determinate.

2.2.5 Principal Areas and Principal Stresses

In the previous discussion, the total stress, $\boldsymbol{\sigma}$, at a point on the plane abc was decomposed into three components of a Cartesian coordinate system $\{x, y, z\}$. However, any other coordinate system could have been used for this purpose. A particular interesting choice is the coordinate system with one axis parallel to the normal vector, $\mathbf{n}$, of the plane and the other two in the plane, such as the coordinate system $\{\xi, \eta, \zeta\}$ in Figure 2–7. Let $\{l_k, m_k, n_k\}$ $(k = \xi, \eta, \zeta)$ denote the direction cosines of the new axes, which implies that $\{l_\zeta, m_\zeta, n_\zeta\}$ will be identical to the direction cosines $\{l, m, n\}$ used above. The normal stress on the area abc will then be nothing else than the sum of the projections of stresses $\boldsymbol{\sigma}_{nx}$, $\boldsymbol{\sigma}_{ny}$, $\boldsymbol{\sigma}_{nz}$ onto the normal $\mathbf{n}$ that is

$$\begin{aligned}\sigma_{\zeta\zeta} &= \sigma_{nx}l_\zeta + \sigma_{ny}m_\zeta + \sigma_{nz}n_\zeta\\ &= \sigma_{xx}l_\zeta^2 + \sigma_{yy}m_\zeta^2 + \sigma_{zz}n_\zeta^2 + 2\sigma_{xy}l_\zeta m_\zeta + 2\sigma_{xz}l_\zeta n_\zeta + 2\sigma_{yz}m_\zeta n_\zeta\end{aligned} \tag{2.6}$$

where use has been made of the law of reciprocity for shearing stresses. Expressions for the shearing stresses, $\sigma_{\xi\zeta}$ and $\sigma_{\eta\zeta}$, can be obtained similarly.

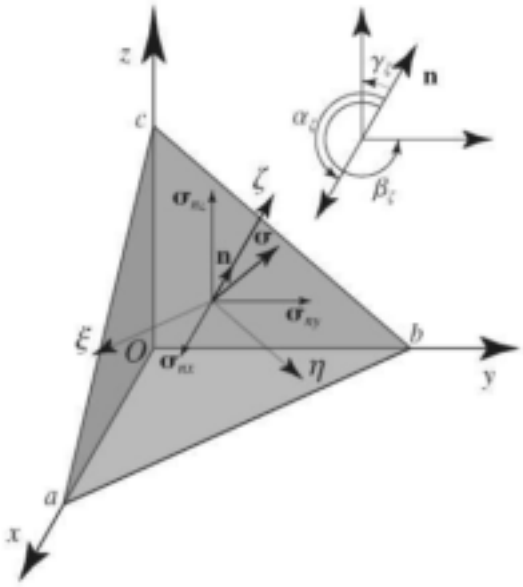

Figure 2–7 Relations between the total stress, $\boldsymbol{\sigma}$, at a point on a plane in a body and a coordinate system with one axis in the direction of the normal vector of the plane and the other two situated in the plane.

$$\begin{aligned}\sigma_{\xi\xi} &= \sigma_{nx} l_\xi + \sigma_{ny} m_\xi + \sigma_{nz} n_\xi \\ &= \sigma_{xx} l_\xi l_\xi + \sigma_{yy} m_\xi m_\xi + \sigma_{zz} n_\xi n_\xi + \\ &\quad \sigma_{xy}(l_\xi m_\xi + l_\xi m_\xi) + \sigma_{xz}(l_\xi n_\xi + l_\xi n_\xi) + \sigma_{yz}(m_\xi n_\xi + m_\xi n_\xi)\end{aligned}$$

$$\begin{aligned}\sigma_{\eta\zeta} &= \sigma_{nx} l_\eta + \sigma_{ny} m_\eta + \sigma_{nz} n_\eta \\ &= \sigma_{xx} l_\eta l_\zeta + \sigma_{yy} m_\eta m_\zeta + \sigma_{zz} n_\eta n_\zeta + \\ &\quad \sigma_{xy}(l_\eta m_\zeta + l_\zeta m_\eta) + \sigma_{xz}(l_\eta n_\zeta + l_\zeta n_\eta) + \sigma_{yz}(m_\eta n_\zeta + m_\zeta n_\eta)\end{aligned} \tag{2.7}$$

Equations (2.6) and (2.7) state the important proposition that if the stresses over three mutually perpendicular elementary areas at a point O are known, one can calculate all three components of stress, $[\sigma_\xi, \sigma_\eta, \sigma_\zeta]$, over a fourth area determined by its outward normal **n**. Indeed, one can actually proceed further and construct two more areas with outward normals in the directions of ξ and η. The stresses over these areas will be expressed by formulas of the same form as Equations (2.6) and (2.7), for instance

$$\begin{aligned}\sigma_{\xi\xi} &= \sigma_{nx} l_\xi + \sigma_{ny} m_\xi + \sigma_{nz} n_\xi \\ &= \sigma_{xx} l_\xi^2 + \sigma_{yy} m_\xi^2 + \sigma_{zz} n_\xi^2 + 2\sigma_{xy} l_\xi m_\xi + 2\sigma_{xz} l_\xi n_\xi + 2\sigma_{yz} m_\xi n_\xi\end{aligned}$$

This decomposition will yield nine formulas [three of the type in Equation (2.6) and six of the type in Equation (2.7)] expressing the stress components in terms of the new coordinate system

$$\boldsymbol{\sigma} = \begin{pmatrix} \sigma_{\xi\xi} & \sigma_{\xi\eta} & \sigma_{\xi\zeta} \\ \sigma_{\xi\eta} & \sigma_{\eta\eta} & \sigma_{\eta\zeta} \\ \sigma_{\xi\zeta} & \sigma_{\eta\zeta} & \sigma_{\zeta\zeta} \end{pmatrix} \tag{2.8}$$

This expression for the stress tensor is exactly of the same form as the expression in Equation (2.3), except that the components now refer to a different coordinate system. The formulas in Equations (2.6) and (2.7) (remember there are nine of them) therefore describe the transformation of the stress tensor from one coordinate system to another.

The previous result raises the question if there does not exist a coordinate system; say $\{X, Y, Z\}$ with direction cosines $\{L, M, N\}$, in which $\boldsymbol{\sigma}$ can be expressed as

$$\boldsymbol{\sigma} = \begin{pmatrix} \sigma_{XX} & 0 & 0 \\ 0 & \sigma_{YY} & 0 \\ 0 & 0 & \sigma_{ZZ} \end{pmatrix} \tag{2.9}$$

This implies that one should be able to express Equation (2.5), which is nothing more than a set of linear equations in the direction cosines, $\{l, m, n\}$, in the form

$$\begin{pmatrix} \sigma_{xx} & \sigma_{xy} & \sigma_{xz} \\ \sigma_{xy} & \sigma_{yy} & \sigma_{yz} \\ \sigma_{xz} & \sigma_{yz} & \sigma_{zz} \end{pmatrix} \begin{pmatrix} L \\ M \\ N \end{pmatrix} = \lambda \begin{pmatrix} 1 & 0 & 0 \\ 0 & 1 & 0 \\ 0 & 0 & 1 \end{pmatrix} \begin{pmatrix} L \\ M \\ N \end{pmatrix} = \begin{pmatrix} \sigma_{nX} \\ \sigma_{nY} \\ \sigma_{nZ} \end{pmatrix} \tag{2.10}$$

It is not difficult to see that this will be the case if one can choose λ in such a way that

$$\begin{pmatrix} \sigma_{xx} - \lambda & \sigma_{xy} & \sigma_{xz} \\ \sigma_{xy} & \sigma_{yy} - \lambda & \sigma_{yz} \\ \sigma_{xz} & \sigma_{yz} & \sigma_{zz} - \lambda \end{pmatrix} \begin{pmatrix} L \\ M \\ N \end{pmatrix} = 0 \tag{2.11}$$

As shown in courses on linear algebra, see e.g. Strang (1976), this will be the case iff (read if and only if) the determinant of the coefficient matrix vanish, i.e.

$$\det \begin{pmatrix} \sigma_{xx} - \lambda & \sigma_{xy} & \sigma_{xz} \\ \sigma_{yx} & \sigma_{yy-\lambda} & \sigma_{yz} \\ \sigma_{zx} & \sigma_{zy} & \sigma_{zz} - \lambda \end{pmatrix} = 0$$

This is a cubic polynomial of the form

$$\lambda^3 - \Theta\lambda^2 + \mathrm{K}\lambda - \Lambda = 0 \tag{2.12}$$

in which the coefficients have the following values

$$\begin{aligned} \Theta &= \sigma_{xx} + \sigma_{yy} + \sigma_{zz} \\ \mathrm{K} &= \det \begin{pmatrix} \sigma_{xx} & \sigma_{xy} \\ \sigma_{yx} & \sigma_{yy} \end{pmatrix} + \det \begin{pmatrix} \sigma_{xx} & \sigma_{xz} \\ \sigma_{zx} & \sigma_{zz} \end{pmatrix} + \det \begin{pmatrix} \sigma_{yy} & \sigma_{yz} \\ \sigma_{zy} & \sigma_{zz} \end{pmatrix} \\ \Lambda &= \det \begin{pmatrix} \sigma_{xx} & \sigma_{xy} & \sigma_{xz} \\ \sigma_{yx} & \sigma_{yy} & \sigma_{yz} \\ \sigma_{zx} & \sigma_{zy} & \sigma_{zz} \end{pmatrix} \end{aligned} \tag{2.13}$$

It is known that the three roots of Equation (2.12), called the *eigenvalues* of the coefficient matrix in Equation (2.10), are all real, since the matrix is symmetric (Strang, 1976). Moreover, the roots cannot depend on the coordinate system used to compute the components of $\boldsymbol{\sigma}$ in Equation (2.10), because this would imply that $\boldsymbol{\sigma}$ could assume different directions, contrary to its definition in Section 2.2.2. This implies that the coefficients, Θ, K and Λ, in Equation (2.13) must also be independent of the coordinate system. In mathematical language, such coefficients are said to be *invariant* under a transformation of coordinates.

Substitution of the eigenvalues of Equation (2.10) into Equation (2.11) will each yield a different solution for the vector $\{L, M, N\}$, or rather a vector of the form $\{cL, cM, cN\}$, since the solutions are not unique and any vector of the latter form will satisfy Equation (2.11). An interesting property of these solutions, known as the *eigenvectors* of the coefficient matrix in Equation (2.10), is that they are orthogonal to one another (Strang, 1976). They can therefore be used to define the axes of a new coordinate system, after the normalization

property of the direction cosines

$$l^2 + m^2 + n^2 = 1$$

has been used to determine the coefficient c. The axes of this coordinate system are conventionally known as the *principal axes* and the three eigenvalues as the *principal components of the stress tensor*, or simply *principal stresses*, denoted by σ_{XX}, σ_{YY} and σ_{ZZ} in Equation (2.9).

The principal axes allow one to interpret the stress tensor geometrically. Let *OXY*, *OYZ* and *OZX* denote the three *principal areas* defined by the normalized eigenvectors of Equation (2.10), in which case Equation (2.5) reduces to

$$\begin{aligned} \sigma_{nX} &= \sigma_{XX} L \\ \sigma_{nY} &= \sigma_{YY} M \\ \sigma_{nZ} &= \sigma_{ZZ} N \end{aligned} \tag{2.14}$$

This means that one can interpreted the total stress, $\boldsymbol{\sigma}$, in this coordinate system as a vector with components given by Equation (2.14). If the normal stresses are taken as distance scales along the three axes, i.e.

$$\sigma_{XX} L = X, \quad \sigma_{YY} M = Y, \quad \sigma_{ZZ} N = Z$$

X, Y, and Z must satisfy the equality

$$\frac{X^2}{\sigma_{XX}^2} + \frac{Y^2}{\sigma_{YY}^2} + \frac{Z^2}{\sigma_{ZZ}^2} = L^2 + M^2 + N^2 = 1 \tag{2.15}$$

This is the equation of an ellipsoid commonly known as the *stress ellipsoid* or the ellipsoid of Lame, illustrated in Figure 2–8. Depending on the values of σ_{XX}, σ_{YY} and σ_{ZZ}, one the three semi-axes is the longest, another the shortest and the third one in between. If two of the principal stresses are equal (for instance, $\sigma_{YY} = \sigma_{ZZ}$),

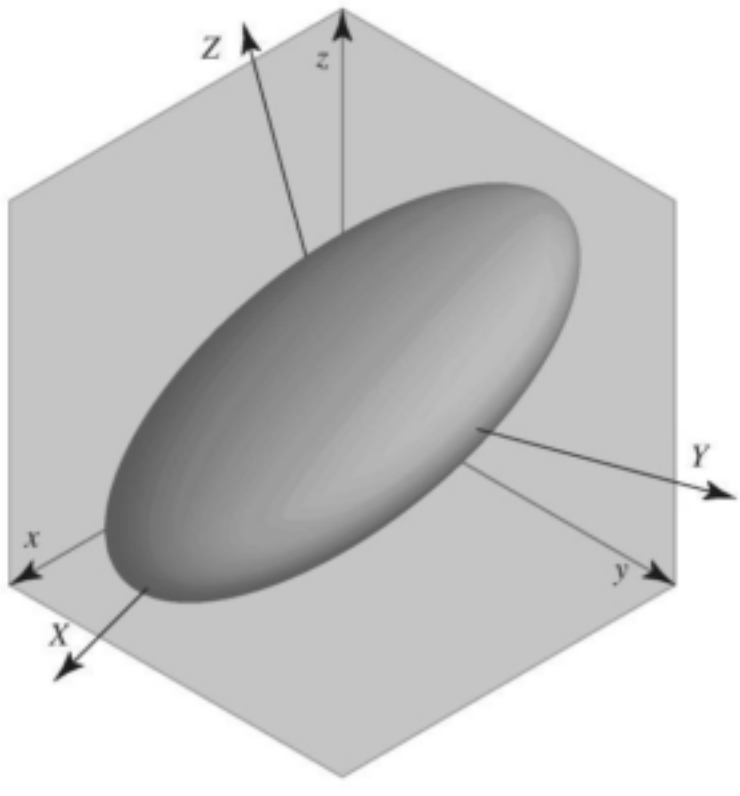

Figure 2–8 Schematic representation of the stress ellipsoid.

Lame's ellipsoid is an ellipsoid of revolution and the state of stress at a given point is symmetrical with respect to the third axis, OX.

2.3 GEOMETRICAL THEORY OF STRAIN

2.3.1 Strains and Displacements

Consider the case of an elastic body fixed in space. Such a body cannot be displaced as a rigid body, but any point in the body can be displaced if the body or a part of the body is deformed in one way or another. Let $M(x, y, z)$ be a point in this elastic body and $M(x', y', z')$ its position after the body has been deformed by some force, with (u, v, w) the components of the displacement, as illustrated in Figure 2–9. Since the displacements will vary from point to point, the components will be functions of (x, y, z), that is

$$u = u(x, y, z)$$
$$v = v(x, y, z)$$
$$w = w(x, y, z)$$

The major consequence of the deformation of the body is that it changes its shape. This means that the length of the edges and the initially right angles between the faces of an infinitesimal parallelepiped, such as the one in Figure 2–10, will change during the deformation. One approach to estimate these changes is to examine the elongations (linear deformations) of the edges dx, dy and dz of the parallelepiped and the distortions of the original right angles, α, β and γ in Figure 2–10. For this purpose, use will be made of the projections of the parallelepiped on the coordinate planes. Take, for instance, the projection of the elementary parallelpiped, ΔP, on the plane Oxy in Figure 2–10. Let, AB $(= dx)$ and AC $(= dy)$ denote the positions of the edges of ΔP before deformation and $A'B'$, $A'C'$ their positions after the deformation, as illustrated in Figure 2–11. If the displacement of point A along the axis Ox is u, the projection of the displacement of the point B along the same axis can be expressed through Taylor's theorem as

$$u + \delta u = u + (\mathrm{D}_x u)dx$$

The elongation of this edge per unit length, known as the *extensional strain* in the x-direction, is consequently given by

$$e_{xx} = (\mathrm{D}_x u)dx \Big/ dx = \mathrm{D}_x u$$

Similarly, if the displacement of the point A along the axis Oy is v, the projection of the displacement of the point C along the same axis can be expressed as

$$v + \delta v = v + (\mathrm{D}_y v)dy$$

and the extensional strain in the y-direction as

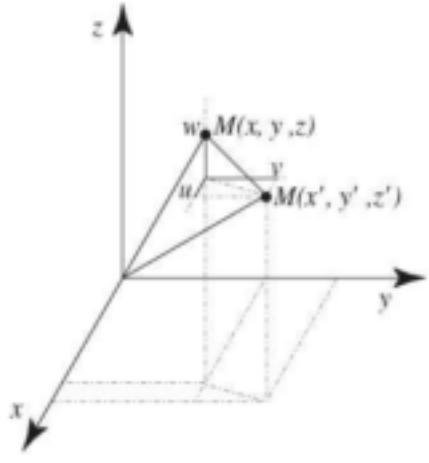

Figure 2–9 Displacement of a point $M(x, y, z)$ in an elastic body after a deformation of the body.

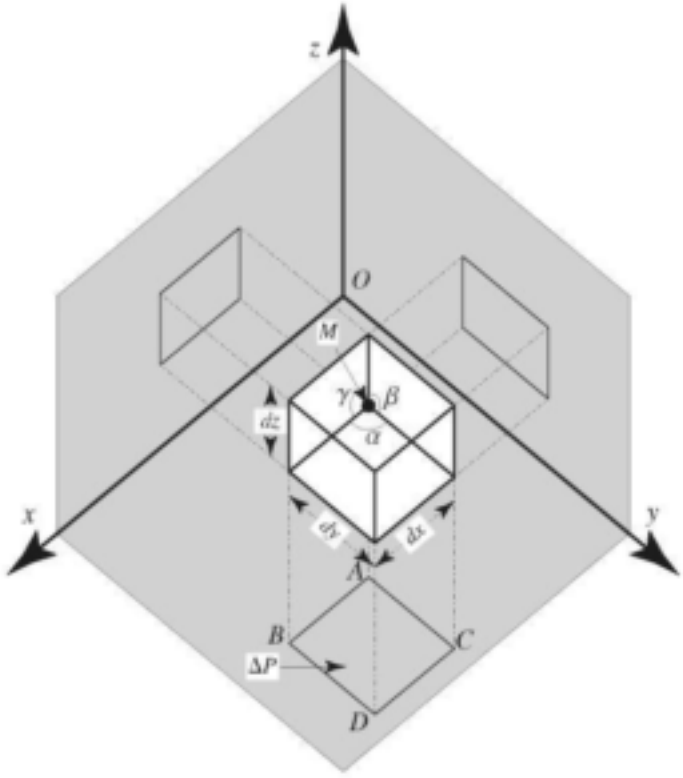

Figure 2–10 An infinitesimal parallelepiped taken from an elastic body, and its projections on the coordinate planes of a Cartesian coordinate system.

$$e_{yy} = (\mathrm{D}_y v)dy \Big/ dy = \mathrm{D}_y v$$

A similar line of reasoning can be used to show that the extensional strain of the edge dz through the point M in Figure 2–10 is given by

$$e_{zz} = (\mathrm{D}_z w)dz \Big/ dz = \mathrm{D}_z w$$

It is important to note that the extensional strains are not the only deformations suffered by the elementary area in Figure 2–11; the edges have also been rotated. For example the edge $AB = dx$ has been rotated through the angle α_{xy} in the plane Oxy. If it is assumed that the deformations are very small, the magnitude of this angle can be approximated as

$$\alpha_{xy} \simeq \tan \alpha_{xy} = \frac{B'B''}{A'B''} = \frac{(\mathrm{D}_x v)dx}{dx + (\mathrm{D}_x u)dx} = \frac{\mathrm{D}_x v}{1 + \mathrm{D}_x u} \simeq \mathrm{D}_x v \tag{2.16}$$

assuming that $\mathrm{D}_x u = e_{xx} \ll 1$. The angle of rotation of the edge $AC = dy$ in the plane Oxy can be similarly approximated as

$$\alpha_{yx} \simeq \tan \alpha_{yx} = \frac{C'C''}{A'C''} = \frac{(\mathrm{D}_y u)dy}{dy + (\mathrm{D}_y v)dy} = \frac{\mathrm{D}_y u}{1 + \mathrm{D}_y v} \simeq \mathrm{D}_y u$$

The total distortion of the right angle BAC

$$e_{xy} = \alpha_{xy} + \alpha_{yx} = \mathrm{D}_x v + \mathrm{D}_y u$$

is conventionally called the *shearing strain* in the plane Oxy. Similar expressions for the shearing strains in the other two coordinate planes can be obtained by considering the corresponding projections of the infinitesimal parallelepiped in Figure 2–10, or by a cyclic change of the subscripts for the shearing strain in

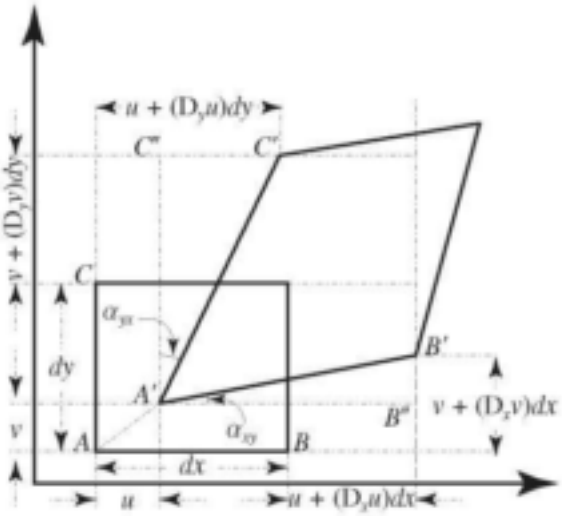

Figure 2–11 Plan view of the face P' in Figure 2–10.

the plane Oxy. The deformation of point M in Figure 2–10 can consequently be characterized by six basic relations: the three extensional strains

$$e_{xx} = \mathrm{D}_x u, \quad e_{yy} = \mathrm{D}_y v, \quad e_{zz} = \mathrm{D}_z w \tag{2.17}$$

and the three shearing strains

$$e_{xy} = \mathrm{D}_x v + \mathrm{D}_y u, \quad e_{yz} = \mathrm{D}_y w + \mathrm{D}_z v, \quad e_{zx} = \mathrm{D}_z u + \mathrm{D}_x w \tag{2.18}$$

It is sometimes more convenient to use the halves of the shear angles and define a new set of shearing strains, which are related to those introduced above through the relations

$$\begin{aligned} 2\bar{e}_{xy} &= e_{xy} = \mathrm{D}_x v + \mathrm{D}_y u \\ 2\bar{e}_{yz} &= e_{yz} = \mathrm{D}_y w + \mathrm{D}_z v \\ 2\bar{e}_{zx} &= e_{zx} = \mathrm{D}_z u + \mathrm{D}_x w \end{aligned} \tag{2.19}$$

One particular advantage of this notation is that it allows one to express the strains as

$$\begin{pmatrix} e_{xx} & \bar{e}_{xy} & \bar{e}_{xz} \\ \bar{e}_{xy} & e_{yy} & \bar{e}_{yz} \\ \bar{e}_{xz} & \bar{e}_{yz} & e_{zz} \end{pmatrix} = \frac{1}{2}[\,\boldsymbol{\nabla}\mathbf{u} + (\boldsymbol{\nabla}\mathbf{u})^T\,] \tag{2.20}$$

The previous discussion of the strains is based on the assumption that the deformation causes the infinitesimal parallelepiped to increase in the length (the displacement of point B to the right is greater than that of point A in Figure 2–11). *Positive extensional strains are therefore conventionally associated with elongations and negative extensional strains with contractions of the body*. Furthermore, if the function v grows with increasing x, $\mathrm{D}_x v$ and the angle α_{xy} will be positive according to Equation (2.16), that is the segment AB rotates from the positive x-axis to the positive y-axis. Since the same situation also occurs in the case of α_{xy}, where AC rotates from the positive y-axis to the positive x-axis, a positive shearing strain, $e_{xy} > 0$, is an indication that the deformation caused the right angle between the positive x and y to decrease. The same rule obviously also applies to the shearing strains in the other two planes. Positive shearing strains are for this reason conventionally associated with a decrease in the angle between two adjacent coordinate plains and negative shearing strains with an increase in the same angle.

Equations (2.18) and (2.19) are linear relations between the six elements of strain, e_{xx}, e_{yy}, e_{zz}, e_{xy}, e_{yz} and e_{zx}, and the nine partial derivatives of the displacement components u, v and w

$$\begin{pmatrix} D_x u & D_y u & D_z u \\ D_x v & D_y v & D_z v \\ D_x w & D_y w & D_z w \end{pmatrix} \tag{2.21}$$

The components of the principal diagonal of this matrix are elongations [see the three relations in Equation (2.17)]. The remaining components represent the angles of rotation of the edges of the elementary parallelepiped, shown in Figure 2–10, about the x, y and z-axes. One could therefore also express the matrix in Equation (2.21) as

$$\begin{pmatrix} e_{xx} & \alpha_{xy} & \alpha_{xz} \\ \alpha_{yx} & e_{yy} & \alpha_{yz} \\ \alpha_{zx} & \alpha_{zy} & e_{zz} \end{pmatrix} \tag{2.22}$$

where the first subscript of α denotes the elementary segment (dx, dy, dz) that is rotated and the second subscript the axis in the direction of which the rotation takes place.

It is important to note that it is impossible to invert Equations (2.17) and (2.18), that is express the nine derivatives of the displacements in terms of the six components of strain. This is a clear indication that the previous geometrical representation of deformations at a given point is incomplete. To complete the representation, consider once again the projection $ABCD$ of the parallelepided in Figure 2–10 on the Oxy plane in the case where $dx = dy = dz$ and the elongations $e_{xx} = e_{yy} = e_{zz} = 0$. As shown in Figure 2–12, there are two situations to consider. The first is the case of 'simple shear' parallel to the x-axis, in Figure 2–12 (a), where the diagonal AD of the parallelepiped is rotated through the angle ϑ to the new position AD'. If it is assumed that the distance between the point D' and the point D'' on the circle ADD'' with centre at B can be neglected, the cosine rule of trigonometry can be used to show, that

$$\vartheta' > \angle DAD'' = \varphi/2$$

This implies that

$$\vartheta' = -\tfrac{1}{2} D_y u$$

because in the case under consideration $D_y u > 0$, while AD must be rotated in the clockwise direction to reach AD', which is customarily regarded as a negative angle in kinematics.

A similar line of reasoning applied to simple shear along the y-axis, see Figure 2–12 (b), yields

$$\vartheta'' = -\tfrac{1}{2} D_x u$$

The general shear that the parallelepiped may experience because of a rotation around the z-axis is therefore of the form

$$\vartheta = \vartheta' + \vartheta'' = -\tfrac{1}{2}(D_y u - D_x v) = -\tfrac{1}{2}(\alpha_{yx} - \alpha_{xy})$$

The same approach can also be used to derive analogous formulas for the angles of the diagonals of the elementary cube's faces in the yz and zx faces, when rotated about the x- and y-axes respectively. It is custom to denote these so-called *angles of rotation*, (ω_x, ω_y, ω_z) as

$$\begin{aligned} 2\omega_x &= D_y w - D_z v \\ 2\omega_y &= D_z u - D_x w \\ 2\omega_z &= D_x v - D_y u \end{aligned} \tag{2.23}$$

These equations added to Equations (2.17) and (2.18), or (2.19), complete the picture of deformations at a given point.

A simple but very important case of the relation between the displacement and strain components, arises when the displacements u, v, w are linear functions of the coordinates

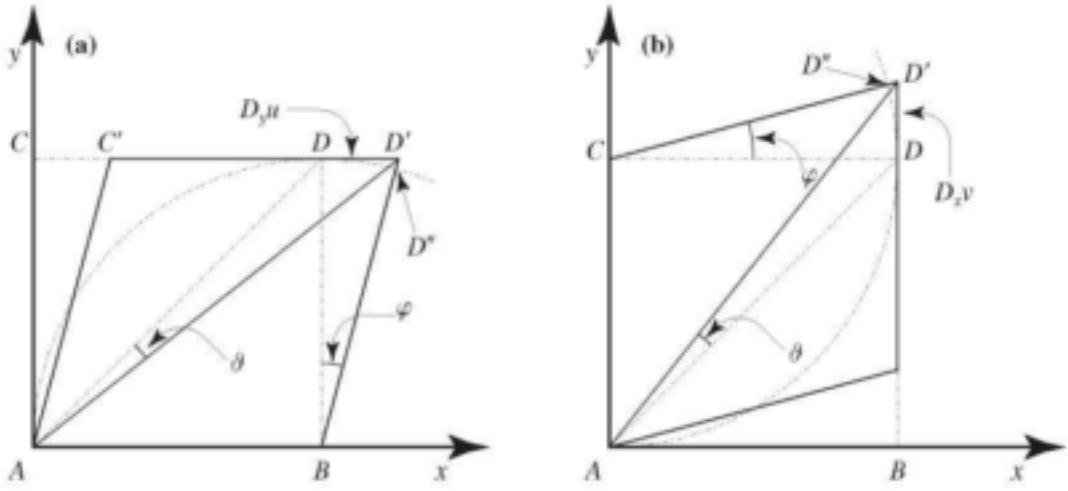

Figure 2–12 Deformations of the projection *ABCD* of the parallelepided in Figure 2–10 on the *O*xy-plane in the case where the elongations $e_{xx} = e_{yy} = e_{zz} = 0$.

$$\begin{aligned} u &= u_0 + c_{11}x + c_{12}y + c_{13}z \\ v &= v_0 + c_{21}x + c_{22}y + c_{23}z \\ w &= w_0 + c_{31}x + c_{32}y + c_{33}z \end{aligned} \tag{2.24}$$

The components of strain in Equations (2.17) and (2.18) as well as the components of rotation in Equation (2.23) will then all be constants. Such a deformation is said to be *homogeneous*.

The basic characteristic of deformation is to convert a given body into another body in which each point (x, y, z) in the body moves to another point

$$x' = x + u, \quad y' = y + v, \quad z' = z + w$$

It is evident that in the case of the homogeneous deformation given in Equation (2.24), each plane (or straight line) is transformed into a plane (or a straight line), while two parallel planes (or straight lines) are likewise transformed into two parallel planes (or straight lines). A rectangular parallelepiped, on the other hand will be transformed into an oblique parallelepiped, in general. It must be remembered though that small quantities of orders higher than 1 were disregarded in deriving Equation (2.23). The deformation defined by these equations will consequently be homogeneous only in a very small region isolated in the body. The elementary parallelepiped in Figure 2–10 will therefore be converted into an oblique parallelepiped, but its opposite faces will remain plane and mutually parallel.

Consider now the case where the strain components in Equations (2.17) and (2.18) are all zero, and the body does not deform. The coefficients in Equation (2.24) must then satisfy the set of equations

$$c_{11} = c_{22} = c_{33} = 0, \quad c_{21} = -c_{12} = r, \quad c_{31} = -c_{13} = -q, \quad c_{32} = -c_{23} = p$$

in which case Equation (2.24) reduces to the kinematical expressions for the infinitesimal displacements of an absolute rigid body

$$\begin{aligned} u &= u_0 - ry + qz \\ v &= v_0 + rx - pz \\ w &= w_0 - qx + py \end{aligned} \tag{2.25}$$

where u, v, w represent translatory displacements of the body with

$$p = \omega_x, \quad q = \omega_y, \quad r = \omega_z$$

the angles of rotation about the coordinate axes, as can be seen by substituting Equation (2.25) into Equation (2.23). It is therefore a custom in the theory of elasticity to say that Equation (2.25) represents a *'rigid body displacement'*.

Now consider the inverse case when the components of rotation in Equation (2.23) vanish, that is

$$D_y w = D_z v, \quad D_z u = D_x w, \quad D_x v = D_y u$$

This means that the curl of the displacement vector, **u**,

$$\mathbf{i}(D_y w - D_z v) + \mathbf{j}(D_z u - D_x w) + \mathbf{k}(D_x v - D_y u) \equiv 0$$

The displacements in a 'pure deformation' can therefore always be represented through a potential function $\Phi(x, y, z)$ given by

$$\begin{aligned} d\Phi(x, y, z) &= D_x \Phi(x, y, z)dx + D_y \Phi(x, y, z)dy + D_z \Phi(x, y, z)dz \\ &= u\,dx + v\,dy + w\,dz \end{aligned}$$

2.3.2 Compatibility Equations

It follows from the preceding discussion that the displacement of a given point in an elastic body is determined by the three functions

$$u(x, y, z), \; v(x, y, z), \; w(x, y, z)$$

while the deformation at the given point is determined by the six strain components

$$e_{xx}, \; e_{yy}, \; e_{zz}, \; e_{xy}, \; e_{xz}, \; e_{yz}$$

However, Equations (2.17) and (2.18) show that it will not be possible to prescribe the six components of strain arbitrarily if the three displacements are specified, since they depend on the first derivatives of the displacements. There must therefore exist certain relations among them. To show that this is indeed the case, consider the following derivatives of the first two extensional strains in Equation (2.17)

$$D_{yy} e_{xx} = D_{yy,x} u, \quad D_{xx} e_{yy} = D_{xx,y} v$$

or on adding up these equations by members

$$D_{yy} e_{xx} + D_{xx} e_{yy} = D_{yy,x} u + D_{xx,y} v = D_{xy}(D_y u + D_x v) = D_{xy} e_{xy}$$

Similar expressions can also be derived for the other two shearing strains, by a cyclic change of the subscripts. This yields the first group of relations

$$\begin{aligned} D_{yy} e_{xx} + D_{xx} e_{yy} &= D_{xy} e_{xy} \\ D_{zz} e_{yy} + D_{yy} e_{zz} &= D_{yz} e_{yz} \\ D_{xx} e_{zz} + D_{zz} e_{xx} &= D_{zx} e_{zx} \end{aligned} \tag{2.26}$$

The second group of relations can be obtained by differentiating Equation (2.18) as follows:

$$\begin{aligned} D_z e_{xy} &= D_{zx} v + D_{zy} u \\ D_x e_{yz} &= D_{xy} w + D_{xz} v \\ D_y e_{zx} &= D_{yz} u + D_{yx} w \end{aligned}$$

which can also be expressed as

$$D_x e_{yz} + D_y e_{zx} - D_z e_{xy} = 2D_{xy} w$$

Differentiating this equation once more with respect to z and observing that

$$D_{xyz} w = D_{xy} e_{zz}$$

one finds that

$$D_z[D_x e_{yz} + D_y e_{zx} - D_z e_{xy}] = 2D_{xy} e_{zz}$$

A cyclic change of the subscripts will yield two additional equations of the same form. This yields the additional system of equations

$$\begin{aligned} D_x[D_y e_{zx} + D_z e_{xy} - D_x e_{yz}] &= 2D_{yz} e_{xx} \\ D_y[D_z e_{xy} + D_x e_{yz} - D_y e_{zx}] &= 2D_{zx} e_{yy} \\ D_z[D_x e_{yz} + D_y e_{zx} - D_z e_{xy}] &= 2D_{xy} e_{zz} \end{aligned} \tag{2.27}$$

that must be satisfied by the extensional and shearing strains. These equations and those in Equation (2.26) are called the equations of continuity or compatibility for the strain components. Since the equations were first derived by Saint-Venant, they are often called Saint-Venant's equations.

2.3.3 Displacements and Strains

The main emphasis in the preceding discussion was to express the components of the strains and rotations as functions of the derivatives of the displacements. However, the inverse is of course also true

$$\begin{aligned} D_x u &= e_{xx} & D_y u &= \bar{e}_{xy} - \omega_z & D_z u &= \bar{e}_{xz} + \omega_y \\ D_x v &= \bar{e}_{xy} + \omega_z & D_y v &= e_{yy} & D_z v &= \bar{e}_{yz} - \omega_x \\ D_x w &= \bar{e}_{xz} - \omega_y & D_y w &= \bar{e}_{yz} + \omega_x & D_z w &= e_{zz} \end{aligned} \tag{2.28}$$

or expressed in matrix notation

$$\begin{pmatrix} D_x u & D_y u & D_z u \\ D_x v & D_y v & D_z v \\ D_x w & D_y w & D_z w \end{pmatrix} = \begin{pmatrix} e_{xx} & \bar{e}_{xy} & \bar{e}_{xz} \\ \bar{e}_{xy} & e_{yy} & \bar{e}_{yz} \\ \bar{e}_{xz} & \bar{e}_{yz} & e_{zz} \end{pmatrix} + \begin{pmatrix} 0 & -\omega_z & +\omega_y \\ +\omega_z & 0 & -\omega_x \\ -\omega_y & +\omega_x & 0 \end{pmatrix} \tag{2.29}$$

provided that Saint-Venant's equations are satisfied.

The first matrix on the right-hand hand side of this equation is symmetric and represents a pure deformation (without rotation), while the second matrix is antisymmetric and represents a rigid body rotation (without deformation). This suggests that one can interpret the partial derivatives of the displacements in Equation (2.21) as a tensor that can be resolved into a symmetric tensor of pure deformation and an antisymmetric tensor of rigid body rotation. This full tensor is sometimes called the tensor of relative displacements.

The equalities in Equation (2.28) may be regarded as differential equations that describe the spatial variations of the displacements u, v and w. This means that if the components of strain and rotation are given at all points of a body, the displacements themselves can be found by integrating the equalities in Equation (2.28). Take for example, the equations in the first line of Equation (2.28). If the previous interpretation is true, the right-hand members of these equations must be partial derivatives of the same function, $u(x, y, z)$, which can be eliminated to obtain the following set of equations

$$\begin{aligned} D_y e_{xx} = D_x(\bar{e}_{xy} - \omega_z), \quad D_z e_{xx} &= D_x(\bar{e}_{xz} + \omega_y) \\ D_y(\bar{e}_{xz} + \omega_y) &= D_z(\bar{e}_{xy} - \omega_z) \end{aligned} \tag{2.30}$$

or after rearranging the terms

$$\begin{aligned} D_x \omega_z &= +D_x \bar{e}_{xy} - D_y e_{xx} \\ D_x \omega_y &= -D_x \bar{e}_{xz} + D_z e_{xx} \\ D_x \omega_x &= +D_y \bar{e}_{xz} - D_z \bar{e}_{xy} \end{aligned} \tag{2.31}$$

where use has been made of the identity

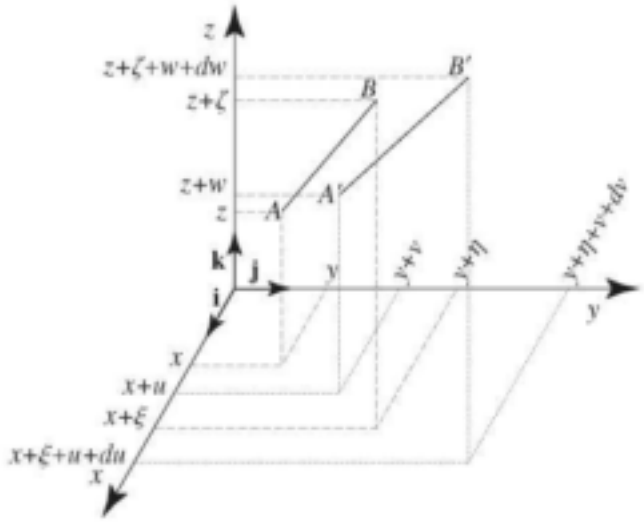

Figure 2–13 Changes in the length and position of an infinitesimal line segment within a deformable body caused by an infinitesimal deformation the body.

$$D_x\omega_x + D_y\omega_y + D_z\omega_z = 0 \tag{2.32}$$

that follows if one differentiates the three equations in Equation (2.22) with x, y, and z respectively and then add the three derivatives.

The same procedure can also be used to eliminate v and w from the second and third equations in Equation (2.28). This will yield six more equations, in addition to Equation (2.31), that relates the nine partial derivatives of the components of rotation to the partial derivatives of the components of strain (analogous to Equation (2.28) for u, v, w), from which ω_x, ω_y and ω_z can be eliminated. This will again yield nine equalities that depend only the second derivatives of the strain components, but only the six that coincide with those in Equations (2.26) and (2.27) will be independent. Saint-Venant's compatibility conditions are therefore the necessary conditions if one wants to use Equations (2.17) and (2.18) to determine the displacements from the given strain components, at least in the case of a simply connected body with no through cavities.

2.3.4 Tensor Character of the Strain at a given Point in a Body

The deformation at a given point in a body will be completely determined if one can compute the unit elongation of any infinitesimal line segment drawn from that point. Let AB in Figure 2–13 be such an infinitesimal line segment that assumes the position and shape of $A'B'$ after the deformation. Also let

$$\mathbf{r} = \mathbf{i}dx + \mathbf{j}dy + \mathbf{k}dz = \mathbf{i}\xi + \mathbf{j}\eta + \mathbf{k}\zeta$$

be the radius vector of AB, where $(\mathbf{i}, \mathbf{j}, \mathbf{k})$ are the Cartesian unit vectors and

$$\begin{aligned}\mathbf{r}' &= \mathbf{i}[x+\xi+u+du-(x+u)] + \mathbf{j}[y+\eta+v+dv-(y+v)] + \mathbf{k}[z+\zeta+w+dw-(z+w)] \\ &= \mathbf{i}(\xi+du) + \mathbf{j}(\eta+dv) + \mathbf{k}(\zeta+dw)\end{aligned}$$

the radius vector of $A'B'$. Since AB is an infinitesimal line segment, Taylor's theorem can be used to express the difference between $\mathbf{r}$ and $\mathbf{r}'$ as

$$d\mathbf{r} = \mathbf{r}' - \mathbf{r} = \mathbf{i}d\xi + \mathbf{j}d\eta + \mathbf{k}d\zeta = \mathbf{i}du + \mathbf{j}dv + \mathbf{k}dw$$

where terms with order higher than one in du, dv and dw has been neglected. If it is further kept in mind that u, v and w are functions of x, y and z, the differentials that appear in this equation can be expressed as

$$\begin{aligned} d\xi &= D_x u\,dx + D_y u\,dy + D_z u\,dz &&= \xi D_x u + \eta D_y u + \zeta D_z u \\ d\eta &= D_x v\,dx + D_y v\,dy + D_z v\,dz &&= \xi D_x v + \eta D_y v + \zeta D_z v \\ d\zeta &= D_x w\,dx + D_y w\,dy + D_z w\,dz &&= \xi D_x w + \eta D_y w + \zeta D_z w \end{aligned} \tag{2.33}$$

Another application of Taylor's theorem, in which terms with orders higher than one are again neglected, to this equation yields

$$sds = \xi d\xi + \eta d\eta + \zeta d\zeta$$

or if divided by s^2

$$\frac{ds}{s} = \frac{\xi}{s}\frac{d\xi}{s} + \frac{\eta}{s}\frac{d\eta}{s} + \frac{\zeta}{s}\frac{d\zeta}{s} \tag{2.34}$$

The left-hand term in this equation represents the elongation of the segment s per unit length caused by changes in ξ, η and ζ, which can be expressed through Equations (2.33), (2.17) and (2.19) as

$$\begin{aligned} e_s &= \mathrm{D}_x u l^2 + \mathrm{D}_y v m^2 + \mathrm{D}_z w n^2 + (\mathrm{D}_x v + \mathrm{D}_y u) lm + (\mathrm{D}_y w + \mathrm{D}_z v) mn + (\mathrm{D}_z u + \mathrm{D}_x w) nl \\ &= e_{xx} l^2 + e_{yy} m^2 + e_{zz} n^2 + 2\bar{e}_{xy} lm + 2\bar{e}_{yz} mn + 2\bar{e}_{zx} nl \end{aligned} \tag{2.35}$$

where

$$l = \frac{\xi}{s}, \quad m = \frac{\eta}{s}, \quad n = \frac{\zeta}{s}$$

are the direction cosines of the segment s. This equation is exactly of the same form as Equation (2.6), which shows that the quantities

$$\begin{pmatrix} \mathrm{D}_x u & \mathrm{D}_y u & \mathrm{D}_z u \\ \mathrm{D}_x v & \mathrm{D}_y v & \mathrm{D}_z v \\ \mathrm{D}_x w & \mathrm{D}_y w & \mathrm{D}_z w \end{pmatrix} \text{ and } \begin{pmatrix} e_{xx} & \bar{e}_{xy} & \bar{e}_{xz} \\ \bar{e}_{yx} & e_{yy} & \bar{e}_{yz} \\ \bar{e}_{zx} & \bar{e}_{zy} & e_{zz} \end{pmatrix} \tag{2.36}$$

are also tensors. The first of the matrices in Equation (2.36) is consequently known as the *tensor of relative displacements* and the second as the *strain tensor* at a given point in a body.

A knowledge of the tensors in Equation (2.36) completely determines the deformation of a body at a given point in the same way as a knowledge of the nine components of the stress tensor in Equation (2.8) determines the state of stress at a given point in a body. The same line of reasoning used in the analysis of the stress tensor in Section 2.2.5 can consequently also be applied to the strain tensor. This implies that the strain tensor also will have three principle axes along which the shearing deformations vanish and three principle elongations, e_{XX}, e_{YY} and e_{ZZ} given by the three real roots of the equation

$$e^3 - \theta e^2 + \kappa e - \lambda = 0$$

where

$$\begin{aligned} \theta &= e_{xx} + e_{yy} + e_{zz} \\ \kappa &= \det\begin{pmatrix} e_{xx} & \bar{e}_{xy} \\ \bar{e}_{yx} & e_{yy} \end{pmatrix} + \det\begin{pmatrix} e_{xx} & \bar{e}_{xz} \\ \bar{e}_{zx} & \sigma_{zz} \end{pmatrix} + \det\begin{pmatrix} e_{yy} & \bar{e}_{yz} \\ \bar{e}_{zy} & \sigma_{zz} \end{pmatrix} \\ \lambda &= \det\begin{pmatrix} e_{xx} & \bar{e}_{xy} & \bar{e}_{xz} \\ \bar{e}_{yx} & e_{yy} & \bar{e}_{yz} \\ \bar{e}_{zx} & \bar{e}_{zy} & e_{zz} \end{pmatrix} \end{aligned} \tag{2.37}$$

This implies that one can always express Equation (2.35) in terms of the principle axes (X, Y, Z) as

$$e_{XX} X^2 + e_{YY} Y^2 + e_{ZZ} Z^2 = \pm\beta^2 \qquad (\beta^2 = s^2 e_s)$$

which represent a surface in three-dimensional space. The form of this surface will clearly depend on the signs of the principal elongations (e_{XX}, e_{YY}, e_{ZZ}). If all three the principle elongations have the same sign, the surface is an ellipsoid representing either an extension (if the principal elongations are positive) or compression (if the principal elongations are negative) at the point (X, Y, Z) in the body. Otherwise, the surface will consist

of a combination of hyperboloids of one and two sheets, separated by an asymptotic cone.

2.3.5 Dilatational Strain and Strain Invariants

Consider an infinitesimal element of a body with volume dV (= $dxdydz$) subject to extensional strains alone. The new volume of the element after deformation can then be expressed through Equation (2.35) as

$$\begin{aligned} dV + \delta(dV) &= dx(1+e_{xx})dy(1+e_{yy})dz(1+e_{zz}) \\ &= dxdydz(1+e_{xx}+e_{yy}+e_{zz}+e_{xx}e_{yy}+e_{xx}e_{zz}+e_{yy}e_{zz}+e_{xx}e_{yy}e_{zz}) \end{aligned}$$

By neglecting, the last four terms in parentheses, which are small quantities of the second and third order, the *dilatational strain* (also known as the volumic dilatation or simply dilatation)

$$\frac{\delta(dV)}{dV} = e_{xx} + e_{yy} + e_{zz} \tag{2.38}$$

is seen to be nothing else than the invariant θ of the strain tensor in Equation (2.37).

An interesting and very important application of the dilatational strain arises in the case where the strain tensor in Equation (2.36) is decomposed in two tensors

$$\mathbf{e} = \begin{pmatrix} e_{xx}-\epsilon & \overline{e}_{xy} & \overline{e}_{xz} \\ \overline{e}_{yx} & e_{yy}-\epsilon & \overline{e}_{yz} \\ \overline{e}_{zx} & \overline{e}_{zy} & e_{zz}-\epsilon \end{pmatrix} + \begin{pmatrix} \epsilon & 0 & 0 \\ 0 & \epsilon & 0 \\ 0 & 0 & \epsilon \end{pmatrix}$$

If

$$\epsilon = \tfrac{1}{3}(e_{xx} + e_{yy} + e_{zz})$$

represents the mean elongation in the body at a given point, the second tensor above represents the situation where an element isolated at a given point in a body receives equal elongations in all directions, while its strain surface is a sphere. Such an element will always remain similar to itself, although its volume may change. Since

$$(e_{xx}-\epsilon) + (e_{yy}-\epsilon) + (e_{zz}-\epsilon) = e_{xx} + e_{yy} + e_{zz} - 3\epsilon = 0$$

the first tensor in the previous equation is often referred to as the *strain deviator* and used to characterize the change in the shape of the element not caused by a change in its volume. This interpretation is not merely a formal operation; it reflects the physical properties of the phenomenon of deformation, since real materials behave differently to changes in their volumes and shapes.

2.4 THE LAW OF HOOKE

2.4.1 General

The preceding discussion has concentrated exclusively on two aspects of the deformation that a natural body may experience: the theory of stresses that describes the forces acting on the body and the theory of strains that describes the geometrical behaviour of the body. It should be obvious that these two theories alone cannot be instrumental in solving physical problems associated with the deformation of bodies under the action of external forces. This can only be achieved, once a suitable physical law has been established that relates the stresses and strains in the body. As indicated by the previous discussion, such a law could be quite complex with the general form

$$\begin{aligned} \sigma_{xx} &= \sigma_{xx}(e_{xx}, e_{yy}, e_{zz}, e_{xy}, e_{yz}, e_{zx}) \\ \sigma_{yy} &= \sigma_{yy}(e_{xx}, e_{yy}, e_{zz}, e_{xy}, e_{yz}, e_{zx}) \\ \sigma_{zz} &= \sigma_{zz}(e_{xx}, e_{yy}, e_{zz}, e_{xy}, e_{yz}, e_{zx}) \\ \sigma_{xy} &= \sigma_{xy}(e_{xx}, e_{yy}, e_{zz}, e_{xy}, e_{yz}, e_{zx}) \\ \cdots &= \cdots \cdots \cdots \\ \sigma_{zx} &= \sigma_{zx}(e_{xx}, e_{yy}, e_{zz}, e_{xy}, e_{yz}, e_{zx}) \end{aligned} \tag{2.39}$$

However, as shown by numerous laws of physics, the exact form of the law may very well depend on the nature of the body investigated and therefore could vary from body to body. Indeed, experiments over the years have indicated that all natural bodies can be conveniently divided into one of two classes: *homogeneous* and *inhomogeneous* bodies. A homogeneous body is a body whose structure and composition are the same at all its points, while the structure and composition of an inhomogeneous body vary from point to point.

The existing theory of elasticity deals almost exclusively with homogeneous bodies. However, even among homogeneous bodies one has to distinguish between isotropic bodies—bodies whose properties are the same in all directions—and anisotropic bodies whose properties depends on the direction in which they are measured. For example, many crystals display a homogeneous structure, but their elastic and optical properties vary with direction.

The simplest form that the relations in Equation (2.39) can assume, is a set of linear equations with the general form

$$\sigma_{\alpha\beta} = a_{xx}^{\alpha\beta} e_{xx} + a_{yy}^{\alpha\beta} e_{yy} + a_{zz}^{\alpha\beta} e_{zz} + a_{xy}^{\alpha\beta} e_{xy} + a_{yz}^{\alpha\beta} e_{yz} + a_{zx}^{\alpha\beta} e_{zx} \tag{2.40}$$

that often arises in the study of homogeneous isotropic bodies, such as steel rods and springs. Since the British physicist Robert Hooke was the first person to study the deformation of this type of body scientifically, it is common practice to refer to the relations in Equation (2.40) as *Hooke's law* and those in Equation (2.39) as the *Generalized Law of Hooke*.

No one has yet succeeded in deriving a theoretical expression for Hooke's law that applies to all homogeneous bodies. Investigations of deformable bodies are consequently conventionally based on the so-called *tensile test diagram* (or simply tensile diagram) of the given body. Examples of this diagram, which represents the relation between the tensile (normal) stress σ_{xx} and unit elongation (e_{xx}) in a bar, are illustrated in Figure 2–14. The shape of a tensile diagram varies not only considerably from one material to the next, but also depends on the chemical composition and structure of the materials.

The simplest form of a tensile diagram is a straight-line, such as the initial segment OA of the diagram in Figure 2–14(a). This behaviour, which is characteristic of metals possessing ductile properties, such as mild steels with low carbon content, is conventionally expressed mathematically as

$$\sigma_{xx} = E e_{xx} \tag{2.41}$$

where E is known as the longitudinal modulus of elasticity or *Young's modulus*, while the stress at the terminal point, A, is called the *proportional limit*.

Investigations of tensile diagrams have shown that the longitudinal elongation of a bar in simple tension, e_{xx}, is usually accompanied by equal lateral deformations $e_{yy} = e_{zz}$ of opposite sign (i.e., contractions), and that these deformations are proportional to the primary elongation e_{xx}, that is

$$e_{yy} = e_{zz} = -\nu e_{xx} \tag{2.42}$$

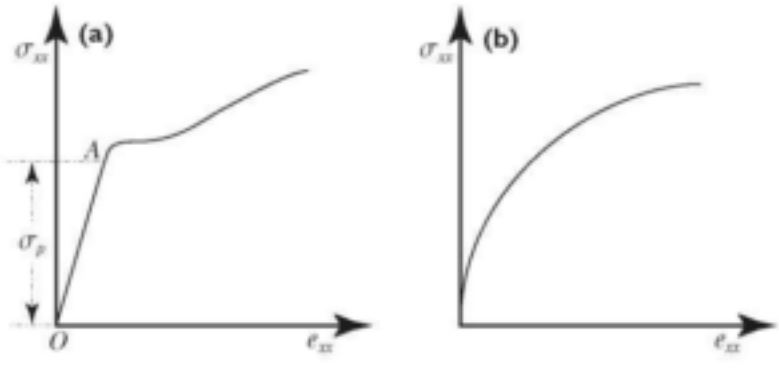

Figure 2–14 Schematic illustration of tensile test diagrams for (a) ductile materials and (b) brittle materials.

The proportionality parameter, ν, is again a constant for a given material, but varies from material to material. This dimensionless number, known as *Poisson's ratio*, is sometimes replaced by its reciprocal, usually denoted by m, and called *Poisson's number*.

The numerical value of Young's modulus, E, varies over a very wide range. For example, it is approximately equal to 2,1 10^{11} Pa for steel and 9,8 10^{9} Pa for wood. Poisson's ratio, ν, on the other hand, is always a proper fraction smaller than 0,5 as will be shown later.

As shown in Figure 2–14 (b) the tensile diagram for brittle materials, such as hard alloy steels, cast iron and stone, has no initial straight-line portion. However, it is sometimes possible to approximate a segment of the curve with a straight line and apply Hooke's law in studies of brittle materials, albeit conditionally.

Experiments have also shown that the shearing stresses on the faces of an elementary parallelepiped is directly proportional to the shearing strains, that is

$$\sigma_{xy} = Ge_{xy}, \quad \sigma_{yz} = Ge_{yz}, \quad \sigma_{zx} = Ge_{zx}$$

as long as the tensile diagram of the material display a linear segment. The proportionality factor, G, in this relation is called the modulus of elasticity in shear or the *transverse modulus of elasticity*, while the relations are known as Hooke's law in shear. Notice that G and E both have the same dimensions as stress.

The transverse modulus of elasticity is also a characteristic but not independent parameter of a material, since it is related to the other two parameters through the equation

$$G = \frac{E}{2(1+\nu)} \tag{2.43}$$

as will be shown in Section 2.4.2. It is therefore only necessary to determine two of these parameters in practical applications of Hooke's law—usually E and G.

2.4.2 Strains as Functions of Stresses

The preceding discussion has focussed mainly on the relations between a few elements of the stress and strain tensors that can be determined experimentally. In this and the following sections, this information will be used to establish explicit expressions for Hooke's law, Equation (2.40), in the case of a homogeneous, isotropic material. Assume for this purpose that normal stresses do not cause shear deformations and that shearing stresses do not cause elongations in the direction of their action in a homogeneous isotropic material, such as the parallelepiped with unit edges in Figure 2–15. If the stress σ_{xx} were acting alone, the unit elongation in the x-direction would be

$$e'_{xx} = \sigma_{xx}/E$$

according to Equation (2.41). However, as pointed out above, the stresses σ_{yy} and σ_{zz} will reduce this by the amounts

$$e''_{xx} = -\nu\frac{\sigma_{yy}}{E} \quad \text{and} \quad e'''_{xx} = -\nu\frac{\sigma_{zz}}{E}$$

according to Equation (2.42). The actual elongation along the x-axis will consequently be given by

$$e_{xx} = \frac{1}{E}[\sigma_{xx} - \nu(\sigma_{yy} + \sigma_{zz})]$$

and similarly for the y- and z-directions. These relations are also often expressed as

$$\begin{aligned} e_{xx} &= \frac{1}{E}[(1+\nu)\sigma_{xx} - \nu\Theta] \\ e_{yy} &= \frac{1}{E}[(1+\nu)\sigma_{yy} - \nu\Theta] \\ e_{zz} &= \frac{1}{E}[(1+\nu)\sigma_{zz} - \nu\Theta] \end{aligned} \tag{2.44}$$

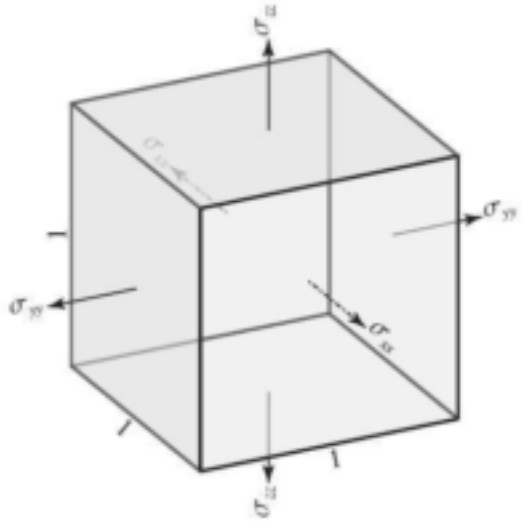

Figure 2–15 A parallelepiped with edges equal to unity, subjected to the action of normal forces.

where Θ is the first invariant defined in Equation (2.13) , a form that is more convenient for some computations. The relations between shearing strains and stresses are simply taken in the form given above

$$e_{xy} = \frac{\sigma_{xy}}{G} = \frac{2(1+\nu)}{E}\sigma_{xy}, \quad e_{yz} = \frac{\sigma_{yz}}{G} = \frac{2(1+\nu)}{E}\sigma_{yz}, \quad e_{zx} = \frac{e_{zx}}{G} = \frac{2(1+\nu)}{E}\sigma_{zx} \tag{2.45}$$

Equations (2.44) and (2.45) represents Hooke's law for a homogeneous material in which the strains are expressed as functions of the stresses.

It is interesting to note that the two invariants Θ and θ in Equations (2.13) and (2.37) allows one to express the sum of the members of Equation (2.44)

$$e_{xx} + e_{yy} + e_{zz} = \frac{1}{E}[(1+\nu)(\sigma_{xx} + \sigma_{yy} + \sigma_{zz}) - 3\nu\Theta]$$

as

$$\theta = \frac{1-2\nu}{E}\Theta \tag{2.46}$$

i.e., the unit volume expansion, θ, is proportional to the sum of three normal stresses Θ. This equation, known as the volumetric form of Hooke's law, is the reason why $\nu \leq ½$. To see this, one merely has to note that the volume of the element under consideration cannot decrease if it undergoes an extension along all three the axes, that is if

$$\sigma_{xx} > 0, \quad \sigma_{yy} > 0, \quad \sigma_{zz} > 0$$

This means that both θ and Θ must be larger than zero. However, as shown by Equation (2.46) this will be true iff

$$\nu \leq ½$$

2.4.3 Stresses as Functions of Strains

As derived in the previous section, Hooke's law expresses the strains as functions of the stresses. However, it is often necessary to have the law in the inverse form. One approach to achieve this is to use Equation (2.46) and replace Θ in Equation (2.44) with θ . This yields, for example.

$$e_{xx} = \frac{1}{E}\left[(1+\nu)\sigma_{xx} - \frac{E\nu}{1-2\nu}\theta\right]$$

and hence

$$\sigma_{xx} = \frac{E\nu}{(1+\nu)(1-2\nu)}\theta + \frac{E}{1+\nu}e_{xx}$$

or in more compact form

$$\sigma_{xx} = \lambda\theta + 2\mu e_{xx}$$

By using the two parameters introduced here

$$\lambda = \frac{E}{(1+\nu)(1-2\nu)} \quad \text{and} \quad \mu = \frac{E}{2(1+\nu)} = G \tag{2.47}$$

known as Lame's coefficients, the inverse form of Hooke's law in Equations (2.44) and (2.45) can be expressed as

$$\begin{gathered}\sigma_{xx} = \lambda\theta + 2\mu e_{xx},\ \sigma_{yy} = \lambda\theta + 2\mu e_{yy},\ \sigma_{zz} = \lambda\theta + 2\mu e_{zz} \\ \sigma_{xy} = \mu e_{xy},\ \sigma_{yz} = \mu e_{yz},\ \sigma_{zx} = \mu e_{zx}\end{gathered} \tag{2.48}$$

One advantage of Lame's coefficients is that they present one with two combinations of the three deformation parameters, E, ν and G and hence represents a reduction in parameters. The inverse relations of course also exist. The first one, $G \equiv \mu$, follows directly from Equation (2.47), while the other two

$$E = \mu\frac{3\lambda + 2\mu}{\lambda + \mu}, \quad \nu = \frac{\lambda}{2(\lambda + \mu)}$$

can be obtained by solving Equation (2.47) simultaneously for E and ν.

It is important to note that Lame's coefficients are always positive, or in mathematical notation $\lambda > 0$ and $\mu > 0$. This property follows directly from Equation (2.47), if it is kept in mind that $E > 0$, by definition, while $\nu \leq ½$.

CHAPTER 3

GROUNDWATER FLOW THROUGH DEFORMABLE AQUIFERS

3.1 INTRODUCTION

From the physical point of view, a porous material is nothing more than a skeleton of solid particles interspersed with a large number of interstices. In the case of aquifers the grains of the geological formation in which the aquifer occurs form the skeleton, while the interstices vary from huge solution caverns (in dolomites and limestones) to subcapillary openings in clays (Bear, 1979). These interstices are conventionally divided into two classes:

Original interstices—created by the geological processes; operative at the time the formation was formed.

Secondary interstices—that developed after the formation was formed.

If one keeps the mechanisms that led to the formation of the Karoo aquifers in mind Botha *et al.* (1998), it is not strange to find that both classes of interstices are import for groundwater flow in Karoo aquifers. This applies in particular to the following two types of interstices, illustrated in Figure 3–1.

Pores—these are interstices with dimensions so small that their boundaries restrict the flow of water in all three spatial directions.

Fractures—caused by stresses, to which the earth's mantle was subjected in the past. The sizes of these fractures can vary from huge fissures, extending over hundreds of kilometres, to microscopic fractures. The flow in fractures therefore often resembles flow in pores, but they can also form channels, although the latter type of flow has not been detected in Karoo aquifers.

The interstices not only define the flow paths for a fluid in the geological formations of the earth, but their sizes also play a significant role in the ability of the formations to transmit water. If the interstices are large, the interactions between their boundaries and water will be negligible, with the result that water can flow freely through them. Conversely, the large boundary interactions present in small interstices will restrict the flow of water considerably. These variations in the sizes and interconnections of the interstices make it very difficult to describe the flow of groundwater with a set of mathematical relations. Nevertheless, there is an approach that proofed to be very useful in the study of groundwater flow—*the mechanics of continuous media* also known as the continuum approach.

The continuum approach, which is briefly discussed in Section 3.2, is conventionally applied only to the flow of water and the transport of dissolved solids in the earth's subsurface. However, Biot (1941) has already extended the approach to include the study of aquifer deformations with the linear law of Hooke. However, there are strong indications that the aquifers in Karoo formations may deform non-linearly (Botha *et al.*, 1998). It was consequently decided to extend Biot's work to the non-linear deformation of aquifers. The model developed for this purpose is discussed in Section 3.3.

3.2 THE MECHANICS OF CONTINUOUS MEDIA

3.2.1 The Proper Sample Volume

A basic assumption in the continuum approach is that the subsurface of the earth can be viewed as a mathematical continuum consisting of three components—water, air and the rock matrix—and that the interactions between the three components can be described with the help of an elementary volume element

$$\Delta V = \Delta x_1 \Delta x_2 \Delta x_3 = \Delta V_w + \Delta V_a + \Delta V_m \tag{3.1}$$

and an elementary mass element

$$\Delta M = \Delta M_w + \Delta M_a + \Delta M_m \tag{3.2}$$

Figure 3–1 Examples of (a) fractured and (b) porous interstices that are important for the flow of groundwater in Karoo aquifers.

where the subscripts w, a and m refer to the water, air and rock matrix respectively, as illustrated in Figure 3–2.

A common assumption in the continuum approach is that the volume element is much larger than the sizes of the interstices, but still small enough to consider it as an infinitesimal for mathematical purposes. This assumption may pose some difficulties for the partially fractured Karoo formations. However, as shown by Botha *et al.* (1998), this is not the case, since the apertures of the fractures of interest in Karoo aquifers are only a few millimetres wide and usually filled with mud and clay particles.

The assumptions in the continuum approach are, strictly speaking, incompatible and caution must be exercised in applying the approach. This contradiction can be easily illustrated by considering the behaviour of the ratio

$$e = \frac{\Delta V_w + \Delta V_a}{\Delta V}$$

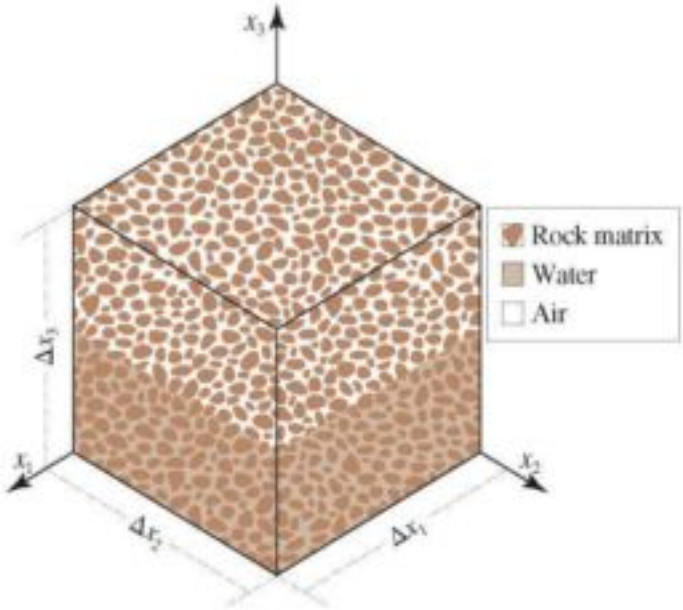

Figure 3–2 Illustration of an elementary volume element in a Cartesian coordinate system with axes x_i ($i = 1, 2, 3$) fixed in space, commonly used to describe the earth's subsurface as a porous continuum.

at a point P within ΔV. Experience has shown; see Figure 3–3, that this ratio is in general a function of the volume of the element, due to the heterogeneity of the global medium, but approaches a fixed value as ΔV approaches a certain value, ΔV_{max} say, from above. At this point, the material becomes locally homogeneous and e remains constant until ΔV reaches another limit (ΔV_{min} say), after which it begins to oscillate between 1, if P is situated in an interstice, and 0, if P is situated in the rock matrix. The idea to describe the subsurface of the earth as a mathematical continuum therefore only make sense if there exists a suitable elementary volume, ΔV_0 say, such that one can assign a unique ratio

$$e = \lim_{\Delta V \to \Delta V_0} \frac{\Delta V_w + \Delta V_a}{\Delta V} \quad (\Delta V_{min} \le \Delta V_0 \le \Delta V_{max}) \\ = \frac{dV_w + dV_a}{dV} \tag{3.3}$$

to every point P in the domain of interest. A medium whose voids satisfy Equation (3.3) is commonly

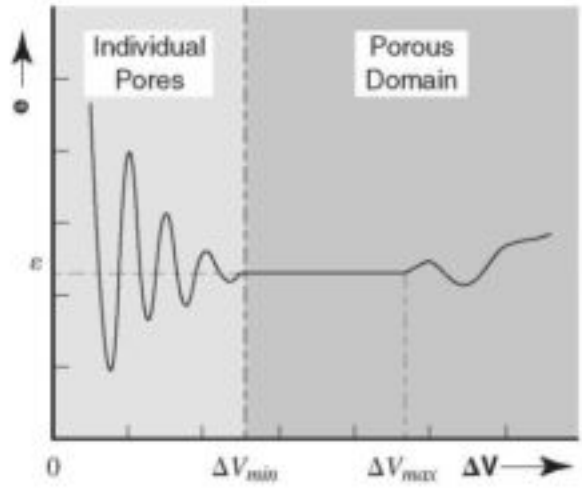

Figure 3–3 Effect of the size of the elementary volume element on the ratio e.

referred to as a porous medium and the ratio, , as the *porosity* of the medium, while the volume element ΔV_0 is known as the *proper sample volume* for the medium. See Botha (1996) for a detailed discussion of this volume element.

It should be noticed that the previous definition does not imply that the porosity must remain constant throughout the domain of interest—it can vary from point to point within the medium and with time. The only requirement is that there must exist a proper sample volume for every point P in the domain of interest, henceforth denoted by the symbol Ω.

3.2.2 A Deformable Model for Groundwater Flow

A proper sample volume from the subsurface of the earth will contain the same three species, water air and rock matrix, as the elementary volume element in Figure 3–2. The chain rule for differentiation and the definitions in Equations (3.1) and (3.2) can therefore be used to express the density of the total mass, dM, within a proper sample volume as

$$\rho = \frac{dM}{dV} = \frac{dM_w}{d\Omega_w}\frac{d\Omega_w}{d\Omega} + \frac{dM_a}{d\Omega_a}\frac{d\Omega_a}{d\Omega} + \frac{dM_m}{d\Omega_m}\frac{d\Omega_m}{d\Omega} = \rho_w\theta_w + \rho_a\theta_a + \rho_m\theta_m \tag{3.4}$$

The quantities ρ_κ and θ_κ introduced here are known as the density and the volumetric fraction of the material specie κ ($= w, a, m$). By using these quantities and assuming that each of the material species satisfy the law of mass conservation, which states that any variation in the mass of a specific specie, κ, within a given volume, Ω, of the medium must be related to one or both of the following two processes.

a) A specie can only be added to or removed from the volume Ω by sources or sinks respectively.

b) A specie in the volume element $d\Omega$, located within Ω, can only interact with the same (or another) specie in the environment of $d\Omega$ across the boundary of $d\Omega$.

The law of mass conservation for a specie κ in the fixed volume, Ω, with boundary $d\Omega$, can therefore be expressed in mathematical form as (Batchelor, 1967)

$$\frac{d}{dt}\int_\Omega \rho_\kappa\theta_\kappa d\Omega = -\int_{d\Omega} \rho_\kappa\theta_\kappa \mathbf{v}^\kappa\cdot\mathbf{n}\,dA + \int_\Omega \rho_\kappa F_\kappa d\Omega \quad (\kappa = w, a, m) \tag{3.5}$$

where $\mathbf{n}$ is the outside-directed unit vector normal to the boundary $d\Omega$, F_κ the strength of any sources or sinks of the specie κ within Ω, and $\mathbf{v}^k$ the velocity of the specie κ relative to the coordinate system (x_1, x_2, x_3).

Equation (3.5) expresses the law of mass conservation in integral form, which is not always easy to manage, even mathematically. Fortunately, it is not difficult to transform Equation (3.5) into a more manageable differential relation. This can be achieved by using Gauss' theorem to replace the surface integral in Equation (3.5) with a volume integral, which yields the so-called continuum equation for the material specie κ

$$\mathrm{D}_t(\rho_\kappa\theta_\kappa) = -\nabla\cdot(\rho_\kappa\theta_\kappa\mathbf{v}^\kappa) + \rho_\kappa F_\kappa \tag{3.6}$$

where

$$\nabla = \mathbf{e}_1\mathrm{D}_{x_1} + \mathbf{e}_2\mathrm{D}_{x_2} + \mathbf{e}_3\mathrm{D}_{x_3}$$

is the well-known nabla or gradient operator, $(\mathbf{e}_1, \mathbf{e}_2, \mathbf{e}_3)$ the unit Cartesian vectors in the direction of the three axes (x_1, x_2, x_3) and

$$\mathrm{D}_\xi f = \frac{d}{d\xi} f$$

is the *total derivative* of the function f with respect to the independent variable ξ. The law of mass conservation for all three species can consequently be expressed through Equation (3.4) as

$$\mathrm{D}_t\rho = -\nabla\cdot\sum_\kappa \rho_\kappa\theta_\kappa\mathbf{v}^\kappa + \sum_\kappa \rho_\kappa F_\kappa = -\nabla\cdot(\rho\mathbf{v}) + \sum_\kappa \rho_\kappa F_\kappa \quad (\kappa = w, a, m) \tag{3.7}$$

where **v** is the velocity of the centre of mass of the proper sample volume in the coordinate system (x_1, x_2, x_3) defined by the equation

$$\rho\mathbf{v} = \sum_{\kappa} \rho_{\kappa}\beta_{\kappa}\mathbf{v}_{\kappa}, \quad (\kappa = w, a, m)$$

It is important to note that Equation (3.7) describes only the behaviour of the three species within and across the boundary of Ω and not the motion of the species. To account for the latter, one must also derive an expression for the displacements of the species. This can be achieved by invoking Newton's second law of motion, which states that the time variation of the momentum of a body is equal to the sum of the external forces acting on the body.

As pointed out in Section 2.1, a solid body, with volume $d\Omega$ and surface area dA, will normally experience two kinds of forces: *surface forces,* which act on the surface of the body and *body forces*, which act on the total body. Let **S** denotes the surface forces per unit area of the surface of such a body, **B** the body forces per unit volume of the body, ρ the density and **v** the velocity of the body. According to Newton's second law of motion, an elementary volume element of such a body, $d\Omega$, with surface area dA, must satisfy the so-called equation of motion,

$$\frac{d}{dt}(\rho\mathbf{v})d\Omega = \mathbf{S}dA + \mathbf{B}d\Omega$$

The motion of the total body can therefore be described by the equation

$$\int_{\Omega} \frac{d}{dt}(\rho\mathbf{v})d\Omega = \int_{\partial\Omega} \mathbf{S}dA + \int_{\Omega} \mathbf{B}d\Omega \tag{3.8}$$

As discussed in Section 2.2.4, the surface forces in Equation (3.8) can be expressed through Equation (2.5) as

$$\mathbf{S} = \mathbf{n}\cdot\boldsymbol{\sigma}$$

with $\boldsymbol{\sigma}$ the symmetric stress tensor introduced in Equation (2.3), which assumes in the case of the coordinate system (x_1, x_2, x_3) the form

$$\boldsymbol{\sigma} = \begin{pmatrix} \sigma_{11} & \sigma_{12} & \sigma_{13} \\ \sigma_{12} & \sigma_{22} & \sigma_{23} \\ \sigma_{13} & \sigma_{23} & \sigma_{33} \end{pmatrix}$$

This means that one can use Gauss' theorem to rewrite Equation (3.8) in the form

$$\int_{\Omega} \frac{d}{dt}(\rho\mathbf{v})d\Omega = \int_{\Omega} \nabla\cdot\boldsymbol{\sigma}d\Omega + \int_{\Omega} \mathbf{B}d\Omega \tag{3.9}$$

Since the volume element, $d\Omega$, is arbitrary and by definition not equal to zero, Equation (3.9) can only be satisfied if the integrand vanishes identically, that is iff

$$\frac{d}{dt}(\rho\mathbf{v}) = \nabla\cdot\boldsymbol{\sigma} + \mathbf{B}$$

The main difference between the solid body, discussed above, and the subsurface of the earth under consideration, is that the latter consists of three different material species. This means that the motion of the subsurface of the earth must satisfy not one but three equations of motion

$$\frac{d}{dt}(\rho_{\kappa}\mathbf{v}_{\kappa}) = \nabla\cdot\boldsymbol{\sigma}^{\kappa} + \mathbf{B}^{\kappa} \quad (\kappa = w, a, m) \tag{3.10}$$

The set of partial differential equations, defined by Equations (3.6) and (3.10), represents the mathematical

description of the motion of a proper sample volume in the subsurface of the earth. However, these equations are not complete, in the sense that they do not provide explicit expressions for the stresses and the densities. They cannot therefore be solved unless supplemented with a set of constitutive relations. If it is assumed that the earth's subsurface, where groundwater occurs, is isothermal and that the concentration of dissolved solids in the water is negligible, these relations will only depend on the displacement, **u**, of the volume element and the pressure, p, of the fluid, that is

$$\boldsymbol{\sigma}^e = \boldsymbol{\sigma}^e(\mathbf{u}), \quad \rho_w = \rho_w(p), \quad \rho_s = \rho_s(p) \tag{3.11}$$

Equations (3.6), (3.10) and (3.11) form a set of highly, non-linear equations that is very difficult to solve, even numerically. The next section will consequently be devoted to a discussion of a more manageable model, but one still able to describe most of the properties of groundwater flow in the subsurface of the earth.

3.3 SIMPLIFIED DEFORMABLE MODEL FOR GROUNDWATER FLOW

3.3.1 The Water Specie

Although the air content plays an important role in the dynamics of unsaturated flow, experience has shown that its influence on the evolution of the rock matrix is minimal, especially in saturated flow. The air specie will therefore be dropped from Equations (3.6), (3.10) and (3.11) in the following discussion. It will also be assumed that the velocity of the water with respect to the rock matrix ($\mathbf{v}_r^w$) is laminar. This implies that one can use Darcy's law to relate the velocity of the water to the so-called Darcy velocity, **q**. This law is conventionally expressed in the form (Bear, 1979)

$$\mathbf{q} = \theta_w \mathbf{v}_r^w = -\mathbf{K}\nabla\varphi \tag{3.12}$$

where **K** is the hydraulic conductivity tensor and φ the *piezometric head* of the water, defined as

$$\varphi = x_3 + \int_0^p \frac{dp}{\rho_w g} \tag{3.13}$$

with g the acceleration of gravity. This allows one to express the velocity of water in the coordinate system (x_1, x_2, x_3) as

$$\mathbf{v}^w = \mathbf{v}_r^w + \mathbf{v}^m$$

where $\mathbf{v}^m$ is the velocity of the rock matrix in the coordinate system (x_1, x_2, x_3) and the flux of water as

$$\theta_w \mathbf{v}^w = \theta_w(\mathbf{v}_r^w + \mathbf{v}^m) = -\mathbf{K}\cdot\nabla\varphi + \theta_w \mathbf{v}^m$$

This equation substituted into Equation (3.6) yields the following expression for the mass conservation of the water

$$\mathrm{D}_t(\rho_w\theta_w) = \nabla\cdot[\rho_w(\mathbf{K}\cdot\nabla\varphi - \theta_w\mathbf{v}^m)] + \rho_w F_w \tag{3.14}$$

It follows from its definition in Equation (3.6) that the volumetric fraction of the water, θ_w, or *water content* as it is more commonly known, is the ratio of two volumes—the volume of water in a proper sample element and the volume of the element. Since water is a compressible fluid, one would expect that θ_w should depend on the water pressure, p, and the stresses exerted on the proper sample volume, that is

$$\theta_w = \theta_w(\boldsymbol{\sigma}, p)$$

The relation between θ_w and p in an unsaturated and undeformed soil is usually expressed through the so-called *water retention curve* of the soil (Botha, 1996). Since this curve can only be determined experimentally, a number of attempts have been made to approximate it analytically (El-Kadi, 1985), the best known of which is probably the one suggested by Van Genuchten (1980)

$$\theta_w(p) = \Theta(p) = \begin{cases} \theta_w^r + (\theta_w^s - \theta_w^r)[1 + (\alpha p)^n]^{-m} & (p < 0) \\ \theta_w^s & (p \geq 0) \end{cases} \tag{3.15}$$

where θ_w^r and θ_w^s are known as the residual and saturated water contents respectively, while α, m and n are characteristic constants for a given soil. The saturated water content is of course nothing else than the porosity, ε, of the soil as defined in Equation (3.3).

As shown in Section 2.3.4 the change in a body caused by stresses can be described by the dilatational strain defined in Equation (2.37), denoted here and in the rest of this discussion by the symbol e, which can also be expressed through Equation (2.35) in terms of the displacement of the volume element, $\mathbf{u}$, as

$$e = \nabla \cdot \mathbf{u} \tag{3.16}$$

Notice that e is negative when the element is compressed by the stresses and positive when stretched. In the case of a porous medium the main effect of the stresses will be to deform the porous matrix and hence to change its porosity. The water contents of the deformable and saturated subsurface of the earth could therefore be described with an equation of the form

$$\theta_w(\boldsymbol{\sigma}, p) = \varepsilon = \varepsilon_0 + e(\boldsymbol{\sigma}, p) = \varepsilon_0 + e(x, y, z, t) \tag{3.17}$$

where ε_0 is the residual porosity of the medium caused by previous stresses.

The density of the water, ρ_w, will certainly also be affected by the stresses experienced by the proper sample volume and the pressure exerted by the fluid. However, these two forces do not act independently on the density, since both of them exist only internally in the volume element. A change in one will therefore cause a change in the other one. It is consequently convenient to describe the effect of both these forces through the well-known constitutive relation for the density of a fluid

$$\mathrm{D}_p \rho_w = \beta \rho_w$$

where β is the isothermal compressibility of the water, in other words

$$\rho_w(\mathbf{x}, t) = \rho_w^0 \exp[\beta p(\mathbf{x}, t)]$$

If it is assumed that the velocity of the matrix, $\mathbf{v}^m$, is small, this assumption and Equation (3.17) allows one to rewrite Equation (3.14) in the form

$$\rho_w \mathrm{D}_t e + \beta \rho_w \varepsilon \mathrm{D}_t p = \nabla \cdot [\rho_w (\mathbf{K} \nabla \varphi)] + \rho_w F_w \tag{3.18}$$

A fluid is, by definition, a body that cannot sustain surface tensions. It hence follows, from Figure 2–6 and Equation (2.5) that for a fluid in equilibrium one must have

$$\sigma_{nn} = \sigma_{xx} l = \sigma_{nn}, \quad \sigma_{ny} = \sigma_{yy} m = \sigma_{nn}, \quad \sigma_{nz} = \sigma_{zz} n = \sigma_{nn} \tag{3.19}$$

The normal stress in all directions at a point in a fluid, which is nothing else than the fluid pressure, is therefore the same throughout the fluid and a scalar. Moreover, since ordinary fluids cannot be stretched, the fluid pressure must always be compressive. The stress tensor, $\boldsymbol{\sigma}^f$, for a fluid is therefore of the form

$$\boldsymbol{\sigma}^f = -p \begin{pmatrix} 1 & 0 & 0 \\ 0 & 1 & 0 \\ 0 & 0 & 1 \end{pmatrix} = -p\mathbf{I}$$

where $\mathbf{I}$ is the unit Cartesian tensor. Equation (3.19) is therefore nothing else than the mathematical representation of the well-known law of Pascal.

The pressure of the water will of course only act on that part of the proper sample volume from the subsurface

of the earth occupied by the water. The stress tensor for the water in a fully saturated rock matrix is therefore of the form

$$\boldsymbol{\sigma}^w = -\varepsilon p\mathbf{I} \tag{3.20}$$

where ε is the porosity of the medium, as defined in Equation (3.3).

It is interesting to observe that the left hand side of Equation (3.18) can in the case of a saturated medium also be expressed through Equations (3.17) and (3.13) and the assumption that ε_0 is a constant as

$$\rho_w^2 g(\mathrm{D}_p e + \beta\varepsilon)\mathrm{D}_t\varphi = \rho_w^2 g(\mathrm{D}_p\varepsilon + \beta\varepsilon)\mathrm{D}_t\varphi \tag{3.21}$$

The assumptions that the grains of the rock matrix are incompressible and that the external stresses remains constant, allows one to express the volumetric compressibility of the rock matrix defined as

$$\alpha = -\frac{1}{V_b}\mathrm{D}_\sigma V_b = \frac{1}{1-\varepsilon}\mathrm{D}_p\varepsilon$$

Substitution of this result into Equation (3.21) yields

$$\rho_w^2 g(\mathrm{D}_p e + \beta\varepsilon)\mathrm{D}_t\varphi = \rho_w^2 g[(1-\varepsilon)\alpha + \beta\varepsilon]\mathrm{D}_t\varphi = \rho_w S_0 \mathrm{D}_t\varphi$$

The only difference between this equation and the equation conventionally used to describe the flow of groundwater in saturated rocks is the replacement of the volumetric compressibility of the rocks in the specific storativity, S_0, with the dilatational strain. In other words the dilatational strain is the real physical mechanism controlling the specific storativity, S_0, of an aquifer. This relation is very important for the management and control of boreholes, because the dilatational strain is a function of the displacement vector, **u**, which may not only depend on the compressibility of the rock matrix, but also other parameters such as the discharge rate of a borehole.

3.3.2 The Rock Matrix Specie

If it is assumed that there are no sources or sinks of the rock matrix specie and that the solids in the matrix are incompressible (ρ_m is a constant), the continuum equation for the rock matrix in Equation (3.6) reduces to

$$\mathrm{D}_t(1-\boldsymbol{\varepsilon}) = -\nabla\cdot[(1-\boldsymbol{\varepsilon})\mathbf{v}^m] \tag{3.22}$$

and its equation of motion, Equation (3.10), to

$$\rho_s(1-\varepsilon)\frac{d}{dt}\mathbf{v}^m = \nabla\cdot\boldsymbol{\sigma}^m + \mathbf{B}^m$$

where use was made of the relations $\theta_m = (1-\varepsilon)$ and $\rho_m = \rho_m(1-\varepsilon)$. It will again be assumed that $\mathbf{v}^m$, which is nothing else than the time derivative of the displacement experienced by the rock matrix, henceforth denoted by **u**, is small. The convective terms in the equation of motion for the rock matrix may therefore be neglected and the total time derivative replaced by its equivalent partial derivative, to obtain

$$\rho_s(1-\varepsilon)D_t^2\mathbf{u} = \nabla\cdot\boldsymbol{\sigma}^m + \mathbf{B}^m \tag{3.23}$$

This equation will obviously not be complete, unless explicit expressions are provided for the stress tensor and the body forces. To achieve this, notice that $\boldsymbol{\sigma}^m$ will, according to Newton's third law of motion, consists of two components—the stresses experienced by the rock matrix, $\boldsymbol{\sigma}$, and its interaction with the fluid pressure. It thus follows from Equation (3.20) that the stress tensor for a water saturated rock matrix in the subsurface of the earth, is of the form

$$\boldsymbol{\sigma}^m = \boldsymbol{\sigma} + \varepsilon p\mathbf{I} \tag{3.24}$$

If it is assumed that the deformations experienced by the rock matrix are small, the law of Hooke, Equation (2.37), can be used to relate the stress tensor, $\boldsymbol{\sigma}$, to the strain tensor, **e**, and hence the displacements **u**. Biot (1941), see also Equations (2.46) and (2.47), express these relations in the form

$$
\begin{aligned}
\sigma_{11} + \varepsilon p &= 2G(e_{11} + \frac{\nu}{1-2\nu} e) \\
\sigma_{22} + \varepsilon p &= 2G(e_{22} + \frac{\nu}{1-2\nu} e) \\
\sigma_{33} + \varepsilon p &= 2G(e_{33} + \frac{\nu}{1-2\nu} e) \\
\sigma_{12} = 2G\bar{e}_{12}, \quad \sigma_{13} &= 2G\bar{e}_{13}, \quad \sigma_{23} = 2G\bar{e}_{23}
\end{aligned}
\tag{3.25}
$$

and the strains as

$$
\begin{aligned}
e_{11} &= \frac{1}{E}[\sigma_{11}(1+\nu) - \nu\sigma + (1-2\nu)p] \\
e_{22} &= \frac{1}{E}[\sigma_{22}(1+\nu) - \nu\sigma + (1-2\nu)p] \\
e_{33} &= \frac{1}{E}[\sigma_{33}(1+\nu) - \nu\sigma + (1-2\nu)p] \\
e_{12} = \frac{\sigma_{12}}{2G}, \quad e_{13} &= \frac{\sigma_{13}}{2G}, \quad e_{23} = \frac{\sigma_{23}}{2G}
\end{aligned}
\tag{3.26}
$$

with

$$\sigma = \sigma_{11} + \sigma_{22} + \sigma_{33}$$

the trace of the stress tensor $\boldsymbol{\sigma}$.

An implicit consequence of Hooke's law is that the body will return to its original form once the influence of the stresses is removed, which is not the case with many rock types such as clays. Moreover, experiments with various kinds of materials have shown that the relations in Equations (3.25) and (3.26) are usually only valid for very small strains and that the relations become non-linear as the magnitudes of the deformations increase, even in the case of moderate strains, see e.g. Jaeger (1969) for examples. Since the inter-granular stresses in rocks are very large, (Bear, 1972), the possibility exists that rocks may not obey the linear relations in Equations (3.25) and (3.26), especially near boreholes, which are pumped at high discharge rates. In such cases the rock may not regain its original form once the stress is removed, but retain a *residual strain*. This suggests that it would be more appropriate to use a form of Hook's law, such as the one illustrated in Figure 3–4, and express the strains as

$$\mathbf{e} = \mathbf{e}^0 + \mathbf{e}^1(\boldsymbol{\sigma}, p) \tag{3.27}$$

where $\mathbf{e}^0$ denotes the residual strains induced by stresses and $\mathbf{e}^1$ the dependence of the strains on the stresses and pressure.

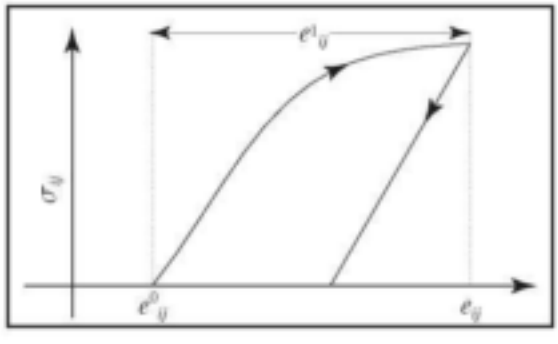

Figure 3–4 Schematic illustration of a non-linear tensile diagram.

As mentioned above, the rock matrix may be regarded as a system of grains interspersed by a series of voids. It is therefore natural to assume that such a system will ultimately break up if subjected to large stresses in tension, and contracts when compressed by the stresses. If it is assumed that the grains in the matrix are incompressible this behaviour can be characterized by two sets of stresses: σ^T the maximum tensile stress before the matrix breaks up, and σ^C a limiting compressive stress, which can be interpreted theoretically as the stress at which the grains begin to deform.

Although there are a large number of functions that could be used to represent the non-linear behaviour of the stresses and strains in Figure 3–4, the present discussion will be based on the following non-linear relation

$$e^1_{ij} = \frac{\sigma^T_{ij}\sigma^C_{ij}}{E(\sigma^T_{ij}+\sigma^C_{ij})} \ln \frac{\sigma^T_{ij}(\sigma^1_{ij}+|\sigma^C_{ij}|)}{|\sigma^C_{ij}|(\sigma^T_{ij}-\sigma^1_{ij})} \quad (i,j=1,2,3) \tag{3.28}$$

where $\boldsymbol{\sigma}^1$ is the tensor with elements given by the numerators of the expressions for e_{ij} in Equation (3.26)

$$\begin{aligned} \sigma^1_{ii} &= [\sigma_{ii}(1+\nu) - \sigma\nu + (1-2\nu)p] \\ \sigma^1_{ij} &= (1+\nu)\sigma_{ij} \qquad (i,j=1,2,3) \end{aligned} \tag{3.29}$$

The approximation of $\mathbf{e}^1$ in Equation (3.28) has two advantages. The first is that it reduces to the linear expressions for the strains in Equation (3.26), if

$$|\sigma^C_{ij}| = \alpha\sigma^T_{ij} \quad \text{and} \quad \sigma^1_{ij}/\sigma^T_{ij} \to 0$$

as shown by the Taylor series of the components of $\mathbf{e}^1$

$$e^1_{ij} = \frac{\sigma^1_{ij}}{E}\left[1-(1-\alpha)\frac{\sigma^1_{ij}}{2\alpha\sigma^T_{ij}} + (1-\alpha+\alpha^2)\frac{(\sigma^1_{ij})^2}{3(\alpha\sigma^T_{ij})^2} + \cdots + O\left(\frac{\sigma^1_{ij}}{\alpha\sigma^T_{ij}}\right)^n\right]$$

This approximation is very useful because it can be used to linearize Equation (3.28), and to represent the linear leg of the relation in Figure 3–4. The second advantage is that it represents many of the properties of the stress-strain relations for rocks, as presented in Jaeger (1969). These include a plastic behaviour whenever the stresses become very large and the strengthening of the material under compression. This behaviour is best seen by comparing the various curves for rocks in Jaeger with the graph of the inverse of Equation (3.28)

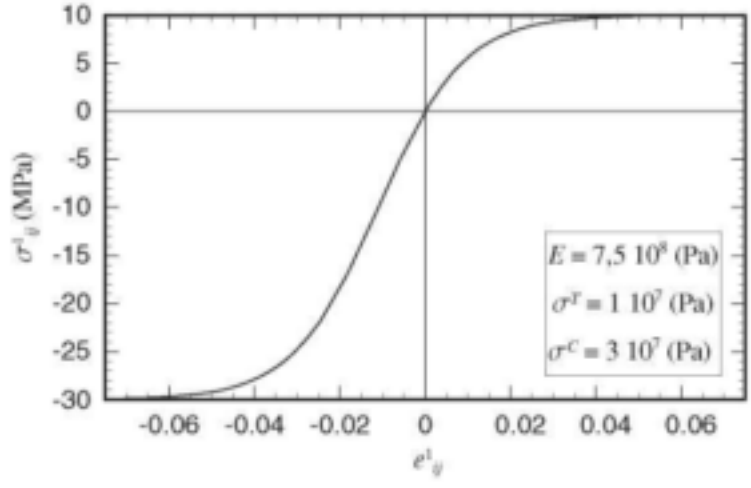

Figure 3–5 Graph of the inverse of the relation in Equation (3.28). ($E = 7{,}5\times10^8$ Pa, $\sigma_{ij}{}^T = 10^7$ Pa, $|\sigma_{ij}{}^C| = 3\times10^7$ Pa)

$$\sigma_{ij}^{1} = (\sigma_{ij}^{T} \mid \sigma_{ij}^{C} \mid)\frac{\exp[w(e_{ij}^{1})]-1]}{\mid \sigma_{ij}^{C} \mid \exp[w(e_{ij}^{1})]+\sigma_{ij}^{T}}, \qquad w(e_{ij}^{1}) = \frac{e_{ij}^{1}E(\mid \sigma_{ij}^{C} \mid +\sigma_{ij}^{T})}{\mid \sigma_{ij}^{C} \mid \sigma_{ij}^{T}} \tag{3.30}$$

in Figure 3–5.

Equations (3.28) and (3.30) applies only in the case where the magnitudes of the stresses and strains increase non-linearly in Figure 3–4. The linear leg, which represents the situation where the magnitudes decrease, will be described by the linear law of Hooke in Equations (3.25) and (3.26) until the rock matrix reached a state of zero stress. The residual constant, $\mathbf{e}_o$ or s_{ij}, is then updated, after which the stresses or strains are once again allowed to evolve according to Equations (3.28) and (3.30). These equations will in future be referred to as the non-linear law of Hooke.

3.3.3 Summary of the Simplified Model

The previous discussion suggests that it would still be possible to satisfy the main objective of the present investigation—the effect that the pumping of a borehole will have on the deformation of an aquifer— by describing the behaviour of the aquifer with the following simplified set of equations.

$$\rho_w \mathrm{D}_t e + \beta\rho_w \varepsilon \mathrm{D}_t p = \nabla\cdot[\rho_w(\mathbf{K}\nabla\varphi)] + F_w \tag{3.18}$$

$$\rho_s(1-\varepsilon)D_t^2\mathbf{u} = \nabla\cdot\boldsymbol{\sigma}' + \mathbf{B}' \tag{3.23}$$

$$\theta_w(\boldsymbol{\sigma}, p) = \varepsilon = \varepsilon_0 + e(\boldsymbol{\sigma}, p) \tag{3.17}$$

$$\mathbf{e} = \mathbf{e}^0 + \mathbf{e}^1(\boldsymbol{\sigma}, p) \tag{3.26}$$

$$e_{ij}^{1} = \frac{\sigma_{ij}^{T}\sigma_{ij}^{C}}{E(\sigma_{ij}^{T}+\sigma_{ij}^{C})}\ln\frac{\sigma_{ij}^{T}(\sigma_{ij}^{1}+\mid \sigma_{ij}^{C} \mid)}{\mid \sigma_{ij}^{C} \mid (\sigma_{ij}^{T}-\sigma_{ij}^{1})} \quad (i,j=1,2,3) \tag{3.27}$$

$$\begin{aligned} \sigma_{ij}^{1} &= [\sigma_{ii}(1+\sigma) - \sigma s + (1-2\sigma)p] \\ \sigma_{ij}^{1} &= (1+\sigma)\sigma_{ij} \qquad (i,j=1,2,3) \end{aligned} \tag{3.28}$$

$$e = \nabla\cdot\mathbf{u} = e_{11} + e_{22} + e_{33} \tag{3.16}$$

Although these equations are mathematically considerably simpler than the more exact equations in Section 3.2.2, it would still be very difficult to solve them analytically, if possible. A computer program, based on the Petrov-Galerkin finite element approximation of the equations, was therefore developed to solve the equations numerically. This program and the approximations used in it are described in the next chapter.

CHAPTER 4

APPROXIMATION OF THE GOVERNING EQUATIONS WITH THE FINITE ELEMENT METHOD

4.1 THE FINITE ELEMENT METHOD

The finite element approximation for the solution of a differential equation is so well-known and described in the literature, see e.g. Pinder and Gray (1977), Botha and Pinder (1983) and Verwey and Botha (1992), that only the principles of the method needed in the solution of the differential equations of Section 3.4 will be described here.

The basic principle behind the approximation, which is a member of the larger class of methods known as the method of weighted residuals (Finlayson, 1972), is to approximate the dependent variable $u(\mathbf{x})$ in a differential equation such as

$$\mathbf{L}u(\mathbf{x}) = F \tag{4.1}$$

as the sum of a set of known, piecewise continuous polynomials, $\phi_j(\mathbf{x})$ say, in the independent variables, $\mathbf{x}$,

$$u(\mathbf{x}) = \sum_{j=1}^{n} u_j \phi_j(\mathbf{x}) \tag{4.2}$$

The unknown coefficients, u_j, is now determined by substituting this sum into Equation (4.1), multiplying the residual with a suitable weighting function, $w_i(\mathbf{x})$, and forcing the set of so-called weighted ed residuals

$$w_i(\mathbf{x})[\sum_{j=1}^{n} u_j \phi_j(\mathbf{x}) - F] \quad (i = 1, \quad ,n)$$

to zero in some average sense. In the case of the Galerkin finite element method this is achieved by integrating the residuals over the domain of the differential equation, Ω, and equate each residual to zero. This operation generates, in general, a set of algebraic equations of the form

$$\int_{\Omega} \phi_i(\mathbf{x})[\mathbf{L}\sum_{j=1}^{n} u_j \phi_j(\mathbf{x}) - F]d\Omega = 0 \quad (i = 1, \quad ,n) \tag{4.3}$$

that can be solved for the unknown u_j, which on substitution into Equation (4.2) will yield an approximate solution of Equation (4.1).

It is possible to apply the method of weighted residuals to any set of independent variables, $\mathbf{x}$. However, experience with differential equations of practical interest, where $\mathbf{x}$ usually consists of the three spatial coordinates, (x, y, z) and the time t, has shown that a more accurate solution of the differential equation can be obtained by using the semi-discrete approximation

$$\hat{u}(\mathbf{x},t) = \sum_{j=1}^{N} u_j(t)\phi_j(\mathbf{x}) \quad (\mathbf{x} = x, y, z) \tag{4.4}$$

for the spatial coordinates and a low-order finite difference approximation for the time derivative (Botha and Pinder, 1983). For example, if Δt represents an increase in time from t_n to t_{n+1}, the function $u_j(t)$ and its first derivative in time can be approximated through the linear Lagrange interpolation polynomials,

$$l_k(t) = \frac{t - t_{k+1}}{t_k - t_{k+1}}, \quad l_{k+1}(t) = \frac{t - t_k}{t_k - t_k}$$

as

$$u_j(t) \simeq l_k(t)u_j(t_k) + l_{k+1}(t)u_j(t_{k+1})$$
$$\mathrm{D}_t u_j(t) \simeq \frac{u_j(t_{k+1}) - u_j(t_k)}{\Delta t} \tag{4.5}$$

A similar expression can also be derived for the second time derivative by approximating $u_j(t)$ with the second order Lagrange interpolation polynomials

$$l_{k-1}(t) = \frac{(t-t_k)(t-t_{k+1})}{(t_{k-1}-t_k)(t_{k-1}-t_{k+1})}, \quad l_k(t) = \frac{(t-t_{k-1})(t-t_{k+1})}{(t_k-t_{k-1})(t_k-t_{k+1})},$$
$$l_{k+1}(t) = \frac{(t-t_{k-1})(t-t_{k-1})}{(t_k-t_{k-1})(t_k-t_{k+1})}$$

This yields the expressions

$$u_j(t) \simeq l_{k-1}(t)u_j(t_{k-1}) + l_k(t)u_j(t_k) + l_{k+1}(t)u_j(t_{k+1})$$
$$\mathrm{D}_t^2 u_j(t) \simeq \frac{u_j(t_{k-1}) - u_j(t_k) + u_j(t_{k-1})}{2\Delta t^2} \tag{4.6}$$

4.2 DISCRETIZATION OF THE GOVERNING EQUATIONS

4.2.1 The Conservation of Fluid Mass

The governing equation for the conservation of fluid mass in Equation (3.18) is strictly only valid for incompressible fluid flow. To apply it to compressible fluid flow one must express the Darcy flux in terms of the permeability of the medium instead of the hydraulic conductivity (De Marsily, 1986) that is set

$$\mathbf{K}\nabla\varphi(\mathbf{x},t) = \frac{\mathbf{k}}{\mu}\nabla(p + \rho_w g z)$$

Although it is possible to relate the permeability tensor, $\mathbf{k}$, to the porosity of a porous medium (Botha, 1996)—hence the deformation of the medium—the models used for this purpose are very simplistic and not of much use in practice. This dependence will consequently be neglected in the following discussion. Since there is not very much information available on the tensorial properties of the permeability for Karoo aquifers, it will also be assumed that the permeability is a scalar that the medium is isothermal and that the viscosity of the fluid is a constant. By using these assumptions and Equation (3.16) to replace the dilatation with its equivalent expression in terms of the displacement vector, $\mathbf{u} = \mathbf{i}u_x + \mathbf{j}u_y + \mathbf{k}u_z$, the equation governing the conservation of fluid mass in a deformable porous medium and a compressible fluid is found to be of the form

$$\rho_w \mathrm{D}_t \nabla\cdot\mathbf{u} + \beta\rho_w \varepsilon \mathrm{D}_t p = \nabla\cdot[\rho_w(\frac{k}{\mu}\nabla(p + \rho_w g z)] + F_w \tag{4.7}$$

If the vectors

$$\hat{\mathbf{u}}(t) = \{\mathbf{u}_0(t), \mathbf{u}_1(t), \cdots \mathbf{u}_N(t)\}$$
$$\hat{\mathbf{p}}(t) = \{p_0(t), p_1(t), \cdots p_N(t)\} \tag{4.8}$$

are used to denote the time-dependent coefficients of the semi-discrete approximations for the displacement and pressure respectively, the system of equations arising from the finite element discretization of Equation (4.7) can be expressed symbolically as

$$\mathbf{P}\cdot\mathrm{D}_t\hat{\mathbf{u}}(t) + \mathbf{Q}\mathrm{D}_t\hat{\mathbf{p}}(t) + \frac{k}{\mu}[\mathbf{R}\,\hat{\mathbf{p}}(t) + \mathbf{b}] = \boldsymbol{\gamma} + \mathbf{f} \tag{4.9}$$

or if Equation (4.5) is used to approximate the time derivatives, $D_t\hat{\mathbf{u}}(t)$ and $\hat{\mathbf{p}}(t)$

$$\mathbf{P}\cdot\hat{\mathbf{u}}^{n+1} + \hat{\mathbf{p}}^{n+1}(\mathbf{Q} + \frac{k}{\mu}\mathbf{R}\Delta t) = \mathbf{P}\cdot\hat{\mathbf{u}}^{n} + \mathbf{Q}\,\hat{\mathbf{p}}^{n} + (\boldsymbol{\gamma} + \mathbf{f} - \frac{k}{\mu}\mathbf{b})\Delta t \tag{4.10}$$

The symbols **P**, **Q** and **R** in these equations are matrices with elements

$$p_{ij} = \int_\Omega \rho_w(\mathbf{x},t)\phi_i(\mathbf{x})\nabla\phi_j(\mathbf{x})d\Omega$$
$$q_{ij} = \int_\Omega \beta e(\mathbf{x},t)\rho_w(\mathbf{x},t)\phi_i(\mathbf{x})\phi_j(\mathbf{x})d\Omega$$
$$r_{ij} = \int_\Omega \rho_w(\mathbf{x},t)(1+\beta g z)\nabla\phi_i(\mathbf{x})\cdot\nabla\phi_j(\mathbf{x})d\Omega$$

while **f**, $\boldsymbol{\gamma}$ and **b** are vectors with elements

$$f_i = \int_\Omega \rho_w(\mathbf{x},t)\phi_i(\mathbf{x},t)F(\mathbf{x},t)d\Omega$$
$$\gamma_i = \int_S \rho_w(\mathbf{x},t)\gamma(\mathbf{x},t)\phi_i(\mathbf{x},t)dS$$
$$b_i = \int_\Omega g\rho_w^2(\mathbf{x},t)\mathrm{D}_z\phi_i(\mathbf{x},t)d\Omega$$

where

$$\gamma(\mathbf{x},t) = \mathbf{n}\cdot(k/\mu)\phi_i(\mathbf{x})\nabla\varphi(\mathbf{x},t)$$

represents a Neumann boundary condition and therefore only exists if the prescribed boundary conditions entail either a non-homogeneous Neumann or a Cauchy boundary condition.

4.2.2 The Equation of Motion

The discretization procedure used above for the equation of mass conservation can also be applied to the equation of motion, if provision is made for the non-linearities in the stresses associated with the matrix skeleton.

To begin, notice that the equation of motion in Equation (3.23) can be expressed through Equation (3.24) as

$$\rho_s(1-\varepsilon)D_t^2\mathbf{u} = \nabla\cdot(\boldsymbol{\sigma} + \mathbf{I}\varepsilon p) + \mathbf{B}^m$$

where p, is the fluid pressure, ε the porosity of the medium, $\boldsymbol{\sigma}$ the stresses created by forces other than the water pressure and **I** the unit matrix. Multiplication of this equation by the basis function, $\phi_i(\mathbf{x})$, and the application of Green's theorem to the right hand side of the equation yield

$$\int_\Omega \rho_s(1-\varepsilon)\phi_i(\mathbf{x})D_t^2\mathbf{u}d\Omega = -\int_\Omega \nabla\phi_i(\mathbf{x})\boldsymbol{\sigma}d\Omega + \int_\Omega \phi_i(\mathbf{x})\nabla\cdot\mathbf{I}\varepsilon p d\Omega + \int_\Omega \phi_i(\mathbf{x})\mathbf{B}^m d\Omega + \int_{\delta\Omega}\phi_i(\mathbf{x})\boldsymbol{\sigma}\cdot\mathbf{n}dS \tag{4.11}$$

where **n** is the unit normal vector on the outside of the boundary, $\delta\Omega$, of Ω. The first term on the right hand side of Equation (4.11) can be simplified by replacing $\boldsymbol{\sigma}$ with the linearized form of $\boldsymbol{\sigma}'$ in Equation (3.30), expressed in terms of the dilatational strain, e, and strains, **e**, as defined in Equation (2.20),

$$\mathbf{e} = \frac{1}{2}[\nabla\mathbf{u} + (\nabla\mathbf{u})^T]$$

as

$$\boldsymbol{\sigma} \simeq \boldsymbol{\sigma}_0 + 2G[\mathbf{e} + \{\nu/(1-2\nu)\}\mathbf{I}e]$$

to obtain

$$\int_\Omega \nabla\phi_i(\mathbf{x})\boldsymbol{\sigma}d\Omega = \int_\Omega G\,\nabla\phi_i(\mathbf{x})[\nabla\mathbf{u} + (\nabla\mathbf{u})^T + \{\nu/(1-2\nu)\}\mathbf{I}e]d\Omega + \int_\Omega \nabla\phi_i(\mathbf{x})\boldsymbol{\sigma}_0 d\Omega$$

The spatial finite element approximation of Equation (4.11) is therefore given by

$$\mathbf{M}D_t^2\hat{\mathbf{u}}(t) + \mathbf{H}\hat{\mathbf{u}}(t) + \mathbf{V}\hat{\mathbf{u}}^T(t) - \mathbf{W}\hat{\mathbf{p}}(t) = \left(\frac{\nu}{1-2\nu}\right)\mathbf{d}^e + \mathbf{s}^0 + \mathbf{b}^m + \mathbf{s}^b$$

or if Equation (4.6) is used to approximate the time derivative, $D_t^2\hat{\mathbf{u}}(t)$

$$\mathbf{M}\hat{\mathbf{u}}^{n+1} + (\Delta t)^2\left[\mathbf{H}\hat{\mathbf{u}}^{n+1} + \mathbf{V}\hat{\mathbf{u}}^{n+1} - \mathbf{W}\mathbf{p}^{n+1}\right] = \mathbf{M}\left[2\mathbf{u}^n - \mathbf{u}^{n-1}\right] + (\Delta t)^2\left[\left(\frac{\nu}{1-2\nu}\right)\mathbf{d}^e + \mathbf{s}^0 + \mathbf{b}^m + \mathbf{s}^b\right] \tag{4.12}$$

The symbols $\hat{\mathbf{u}}(t)$ and $\hat{\mathbf{p}}(t)$ are as defined in Equation (4.8), while **M**, **H**, **V** and **W** are matrices with elements

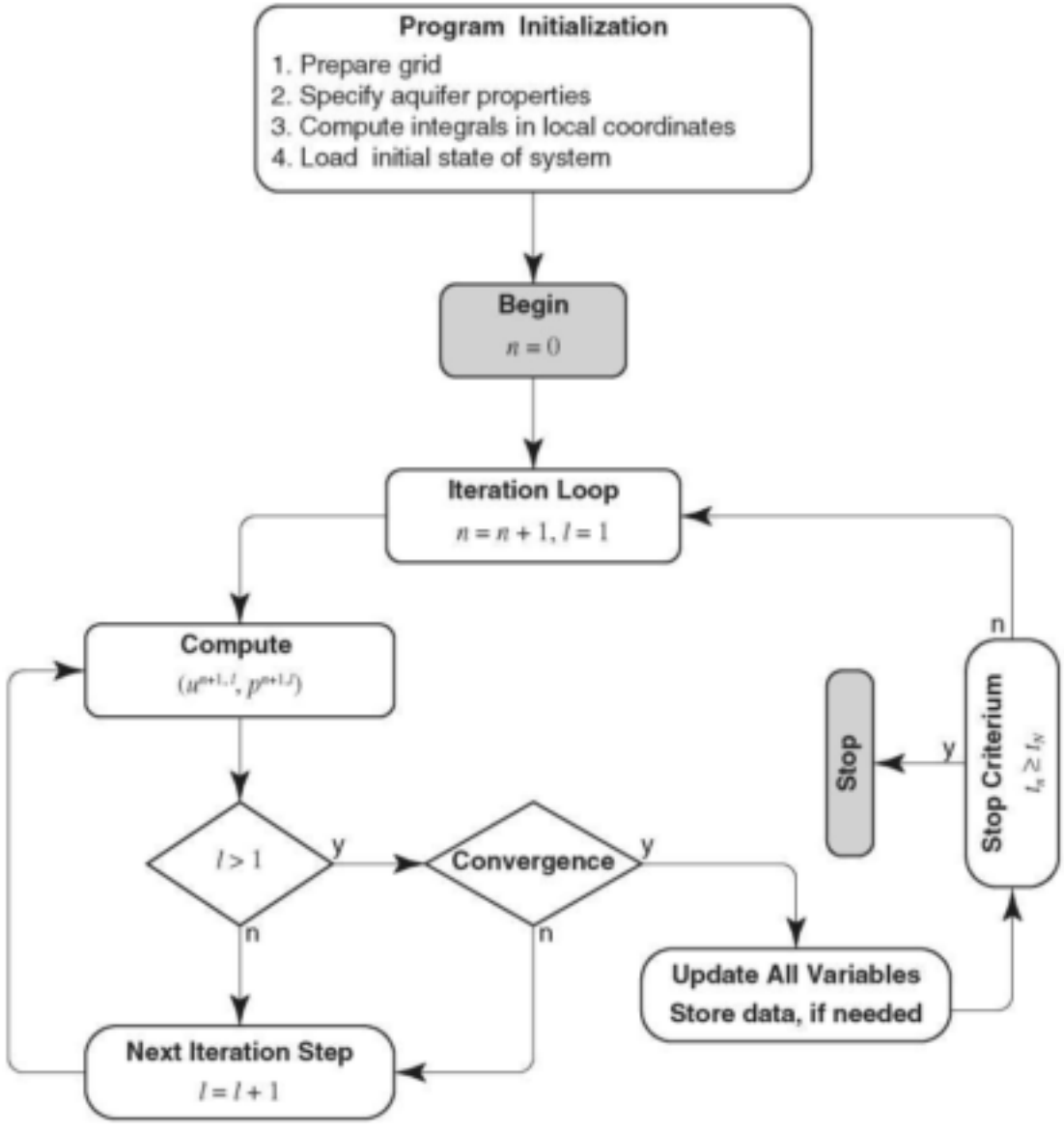

Figure 4–1 Flow chart of the general algorithm used to solve the system of equations given by Equation (4.11) and (4.12).

$$m_{ij} = \int_{\Omega} \phi_i(\mathbf{x}) \rho_s (1-\varepsilon) \phi_j(\mathbf{x}) d\Omega$$
$$h_{ij} = \int_{\Omega} G \nabla \phi_i(\mathbf{x}) \cdot \nabla \phi_j(\mathbf{x}) d\Omega$$
$$v_{ij} = \int_{\Omega} G \nabla \phi_i(\mathbf{x}) \cdot [\nabla \phi_j(\mathbf{x})]^T d\Omega$$
$$w_{ij} = \int_{\Omega} \phi_i(\mathbf{x}) \varepsilon \nabla \phi_j(\mathbf{x}) d\Omega$$

and $\mathbf{d}^e$, $\mathbf{s}^0$, $\mathbf{s}^b$ and $\mathbf{b}^m$ vectors with elements

$$d_i^e = \int_{\Omega} G \nabla \phi_i(\mathbf{x}) \mathbf{I} e \, d\Omega$$
$$s_i^0 = \int_{\Omega} \nabla \phi_i(\mathbf{x}) \cdot \boldsymbol{\sigma}_0 d\Omega$$
$$b_i^m = \int_{\Omega} \phi_i(\mathbf{x}) \mathbf{B}^m d\Omega$$
$$s_i^b = \int_{\partial\Omega} \phi_i(\mathbf{x}) \boldsymbol{\sigma} \cdot \mathbf{n} dS$$

Equations (4.10) and (4.12) represents a set of four equations, which can be used to solve for the four unknowns $\hat{\mathbf{u}}^{n+1}$ and $\hat{\mathbf{p}}^{n+1}$. It is important though to note this system of equations has to be solved iteratively if $\boldsymbol{\sigma}$ is non-linear, as illustrated by the flow chart of the general algorithm in Figure 4–1.

CHAPTER 5

THE HYPOTHETICAL AQUIFER OF HSIEH

5.1 INTRODUCTION

The first step taken in evaluating the numerical algorithms derived in Chapter 4 was to develop a computer program in Fortran and apply it to a hypothetical aquifer similar to the one considered by Hsieh (1996). The aquifer is 100 m thick and confined by two less permeable layers. The upper layer is also 100 m thick, but the lower one extends to a depth of 5 000 m. The water table in the aquifer coincides with the land surface, which is the top of the first layer, as illustrated schematically in Figure 5–1. A borehole that penetrates all three units fully is cased throughout both confining layers but screened over the thickness of the aquifer. Groundwater is pumped at a constant rate of 5 10^{-2} $m^3 s^{-1}$ from the borehole. The basic properties of the aquifer, the boundary conditions and the finite element mesh used to model the aquifer are described in Section 5.2. This is followed by a discussion of the results obtained with the model in Section 5.3.

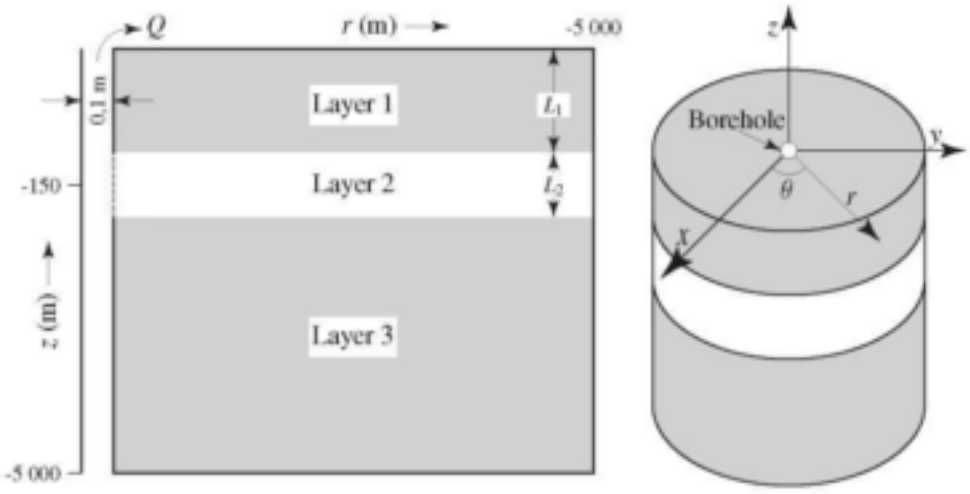

Figure 5–1 Schematic representation of the hypothetical porous aquifer used to test the present model.

5.2 AQUIFER PROPERTIES

5.2.1 Aquifer Parameters

The aquifer and fluid parameters used in modelling the hypothetical aquifer are listed in Table 5-1. If applied in a conventional groundwater model these parameters would yield a vertical matrix compressibility of

$$\alpha = \frac{1-2\nu}{2G(1-\nu)} = 1{,}1\,10^{-7}\ \mathrm{Pa}^{-1} \tag{5.1}$$

and a specific storativity for the aquifer of

$$S_0 = \rho_w g(\alpha + \epsilon\beta) = 1{,}2\,10^{-5}\ \mathrm{m}^{-1} \tag{5.2}$$

The vertical matrix compressibility and specific storativity of the two confining layers are 1,1 10^{-8} Pa^{-1} and 1,1 10^{-6} m^{-1} respectively.

5.2.2 Boundary and Initial Conditions

Since the aquifer system is radially symmetric, the numerical model was restricted to a vertical cross-section

Table 5-1 Values of the physical properties used in the numerical simulations of the hypothetical aquitard.

Parameter	Aquifer	Layers 1 and 3	Unit
Fluid Compressibility (β)	4,4 10^{-10}	4,4 10^{-10}	[Pa^{-1}]
Soil Density (ρ_s)	2,5 10^{+3}	2,5 10^{+3}	[kg m^{-3}]
Hydraulic Conductivity (K)	1,0 10^{-4}	1,0 10^{-7}	[m s^{-1}]
Young's Modulus (E)	7,5 10^{+8}	7,5 10^{+7}	[Pa]
Poisson's Ratio (ν)	0,25	0,25	[1]
Porosity (ε)	0,25	0,40	[1]

of the aquifer that extended from the borehole, with a radius of 0,1 m to an outer boundary at a distance of 5 km and a depth of 5 km. The outer boundary was considered as impervious and subject to constant stresses. The bottom boundary was also considered as impervious and rigid, i.e. the boundary was not subject to displacements. The reason for this choice of the two boundaries was to ensure that they were sufficiently distant from the borehole, so as not to influence the behaviour of the aquifer near the borehole. The boundary at the land surface was considered free of applied forces and deformable, and subject to a constant piezometric head. No radial displacements were allowed at the borehole casing, while the vertical component of the boundary traction was assumed to remain constant. This allowed the aquifer matrix to move vertically along the screen. It was further assumed that the pumping caused a uniform flux of water across the entire thickness of the aquifer, but that no water entered the borehole across the casing in the two confining layers.

5.2.3 Finite Element Implementation

The finite element mesh used for the 5 km by 5 km domain consisted of 30 columns and 80 rows of rectangular finite elements with variable sizes to prevent numerical oscillations, which required elements as thin as 0,01 m along the interfaces between the aquifer and the confining layers, as illustrated in Figure 5–2.

Two sets of numerical simulations where performed with this finite element mesh: (a) with a linear stress-strain relation and (b) with the generalized non-linear law of Hooke, as described in Section 3.2.2.

5.3 RESULTS

5.3.1 The Linear Stress-Strain Case

The general behaviour of the aquifer system observed with the linear stress-strain relation can be summarized as follows. The pressure dropped rapidly close to the borehole when pumping began; see Figure 5–3. As shown in Figures 5–4 and 5–5, this caused the rock matrix to deform in both the horizontal and vertical directions. The deformations in the radial direction (u_r) at first increased continuously near the borehole, until they reached a maximum value, not far from the borehole, after which they began to decrease continuously. Notice also, how the position of the maximum deformation in the radial direction moved away from the borehole with time. The vertical displacements, u_z, on the other hand, were essentially restricted to the interfaces of the aquifer and confining layers, where the elastic parameters are discontinuous.

The simulated drawdown in the aquifer behaves similarly to drawdowns computed with models that do not take the deformation of the aquifer into account, in that it decreases continuously with time throughout the aquifer. The largest drawdowns also occur within the aquifer and not the confining layers, as shown in Figure 5–6 (a). The displacements of the rock matrix follows a similar pattern, see Figure 5–6 (b) and (c). However, there are some slight differences. For example, the position of the maximum horizontal displacement tends to move away from the borehole with time, while the absolute maxima of the vertical displacement remains on the interfaces of the aquifer and confining layers, although the domain of influence widens on both sides of the interfaces.

Another interesting feature of the contour maps in Figure 5–6, is that the drawdown and displacements all display a local symmetry about the centre plane of the aquifer at a depth of 150 m, at least for the time scales considered in the simulation.

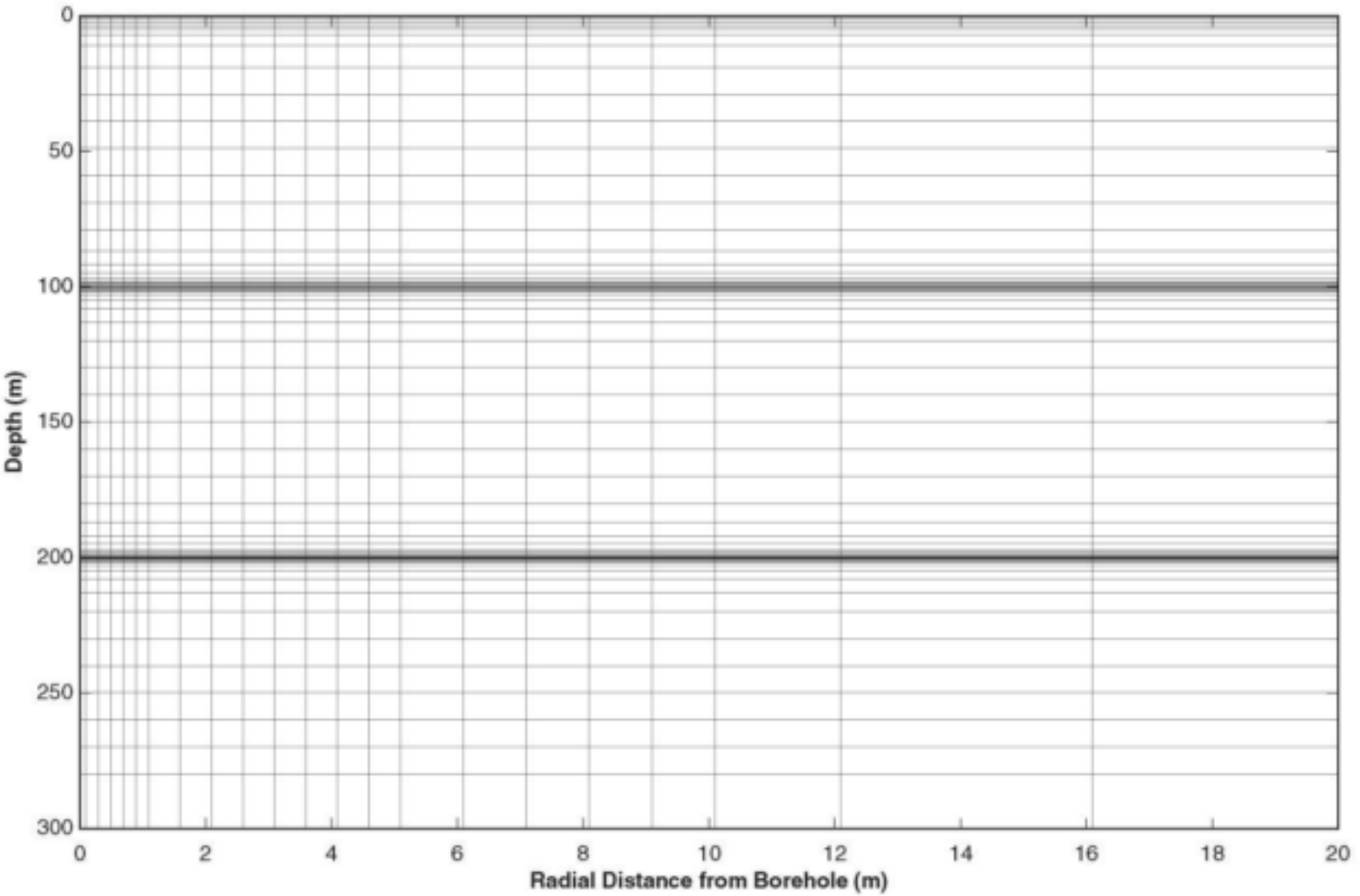

Figure 5–2 A cross-section of the finite element mesh used in the simulation of the hypothetical aquifer.

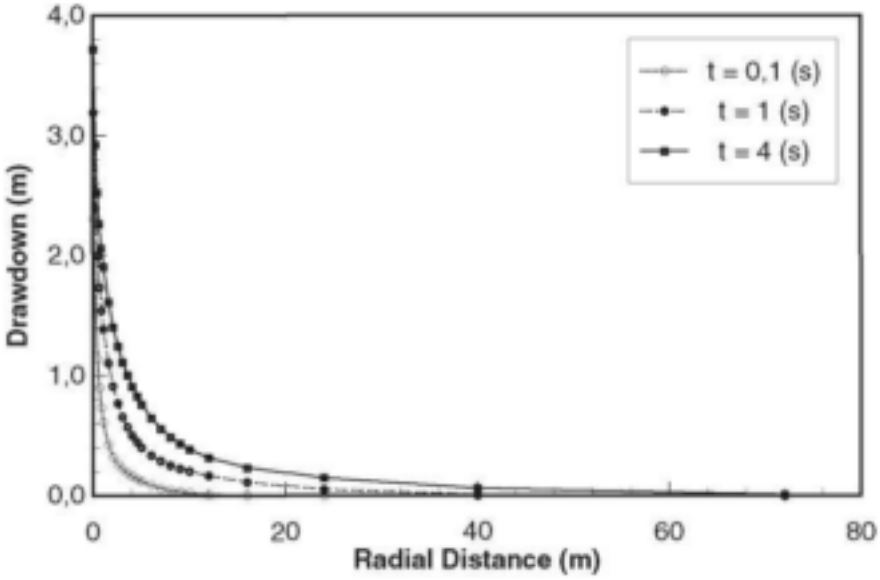

Figure 5–3 Evolution of the piezometric pressure across the centre plane of the aquifer at a few times after pumping the borehole began.

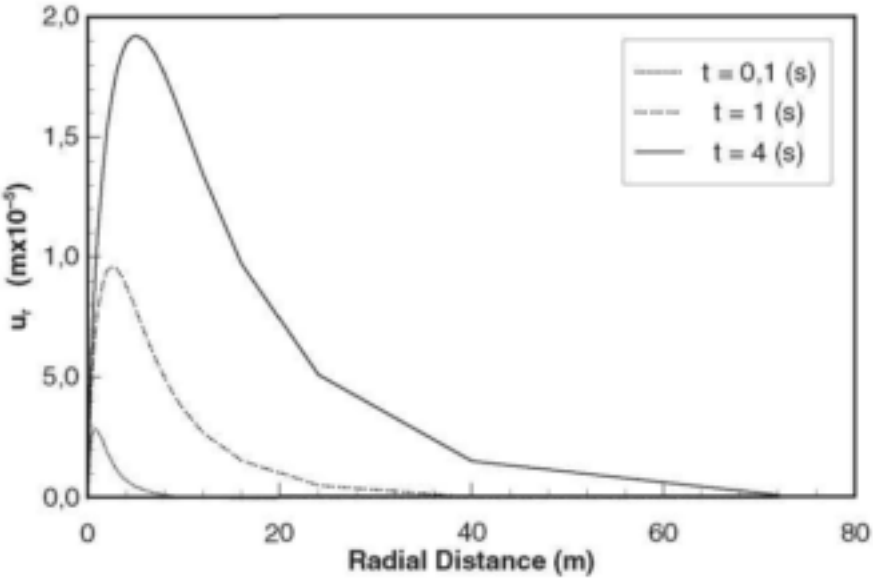

Figure 5–4 Evolution of the radial displacement (u_r) across the centre plane of the aquifer at a few times after pumping the borehole began.

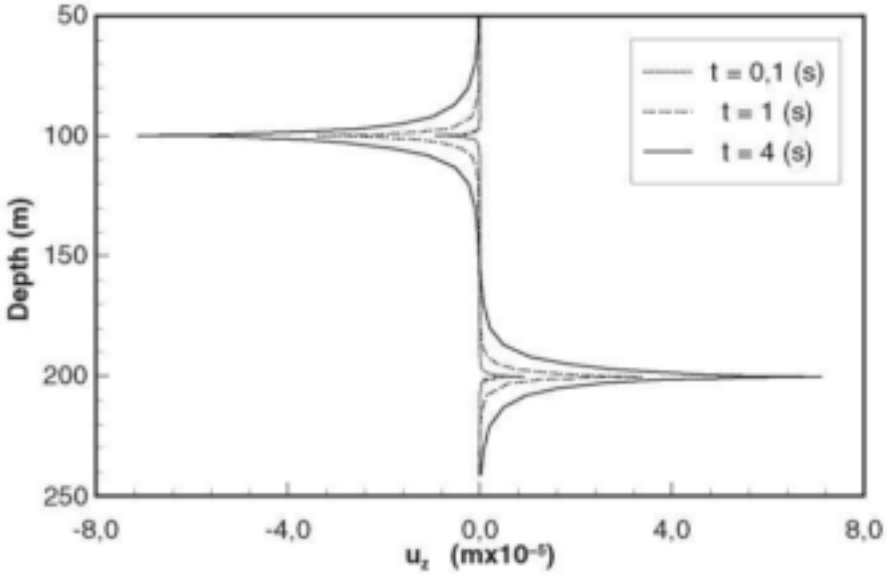

Figure 5–5 Evolution of the vertical displacement (u_z) across the interfaces of the aquifer and two confining layers at a few times after pumping the borehole began.

Very little, if any, attention is usually paid to the deformation of the rock matrix in models of groundwater flow. However, as shown by the contour maps of the displacements (magnified 40 000 times) in a 40 m by 150 m vertical cross-section of the aquifer system in Figure 5–7, the shape of the rock matrix is influenced by the pumping. As can be seen from the figure, the rock matrix tends to contract towards the screened segment of the borehole, both horizontally (the deflection of the vertical lines toward the screen) and vertically (the decrease in the thickness of the aquifer. This deformation is also shared by the confining layers, which tend to contract horizontally and extend vertically. The contraction of the aquifer rocks and the vertical extension of the rocks in the confining layers must obviously affect not only the porosity of the aquifer system, but also the pressure distribution and thus the ability of the aquifer to yield water to the borehole. It is also interesting to note that the extent at which the rock matrix is deformed in Figure 5–7 decreases with distance. This phenomenon may therefore be responsible for a very perplexing observation—that the storativity values, derived from conventional aquifer tests, tend to decrease with distance from the borehole that is pumped during such a test (Botha *et al.*, 1998; Bredenkamp *et al.*, 1995).

The previous conjecture was investigated further by comparing the behaviour of the piezometric heads in the deformable aquifer with the piezometric heads in an aquifer where the deformation is ignored. As shown by the contour maps in Figure 5–8, the two sets of drawdowns differ completely. For, not only are the drawdowns considerably lower in the in the deformed model, especially near the borehole, but the borehole now also obtain water from the confining layers. There is thus more water available near the borehole in the deformed model, than in the conventional model. However, this excess of water disappears with distance from the borehole. The only way in which a conventional model can account for this excess of water is to display a higher storativity in the vicinity of the borehole that is pumped, than at an observation borehole farther away.

5.3.2 The Non-linear Stress-Strain Relation

As shown in Figure 5–7, the largest vertical displacements occur on the interfaces between the aquifer and confining layers. The interfaces are consequently also subject to the largest strains and the section of the aquifer most likely to be deformed permanently by excessive strains. It is thus quite possible that the linear law of Hooke will not be applicable in the neighbourhood of the interfaces. A second set of computations was therefore performed with the deformable model, but using the non-linear law of Hooke described in Section 3.3.2, with the values of Young's modulus given in Table 5-1 and $|\sigma^c| = \sigma^T = 1{,}64\ 10^5$ Pa for the aquifer and $1{,}64\ 10^4$ Pa for the confining layers, taken from Bredthauer (1957) and Handin and Hager (1957). This non-linear curve was discretized into 14 linear strips, for computational purposes with a limit of $e = 4{,}5\ 10^{-3}$, as illustrated in Figure 5–9.

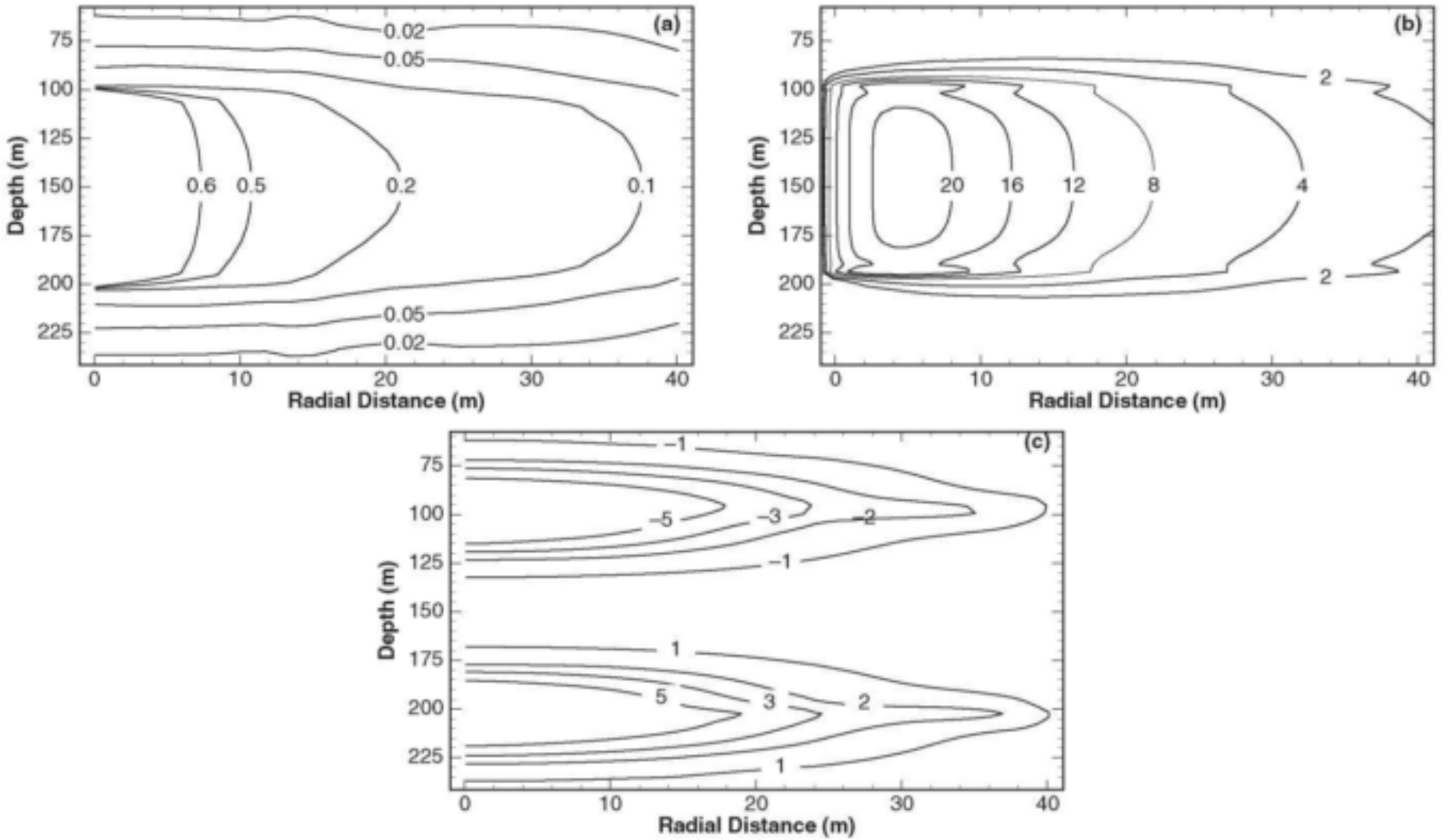

Figure 5–6 Contour maps of the simulated drawdown in the hypothetical aquifer and the deformation of the rock matrix after 5 s of pumping the borehole. [(a) drawdown (m), (b) horizontal and (c) vertical displacement of the rock matrix (mm)].

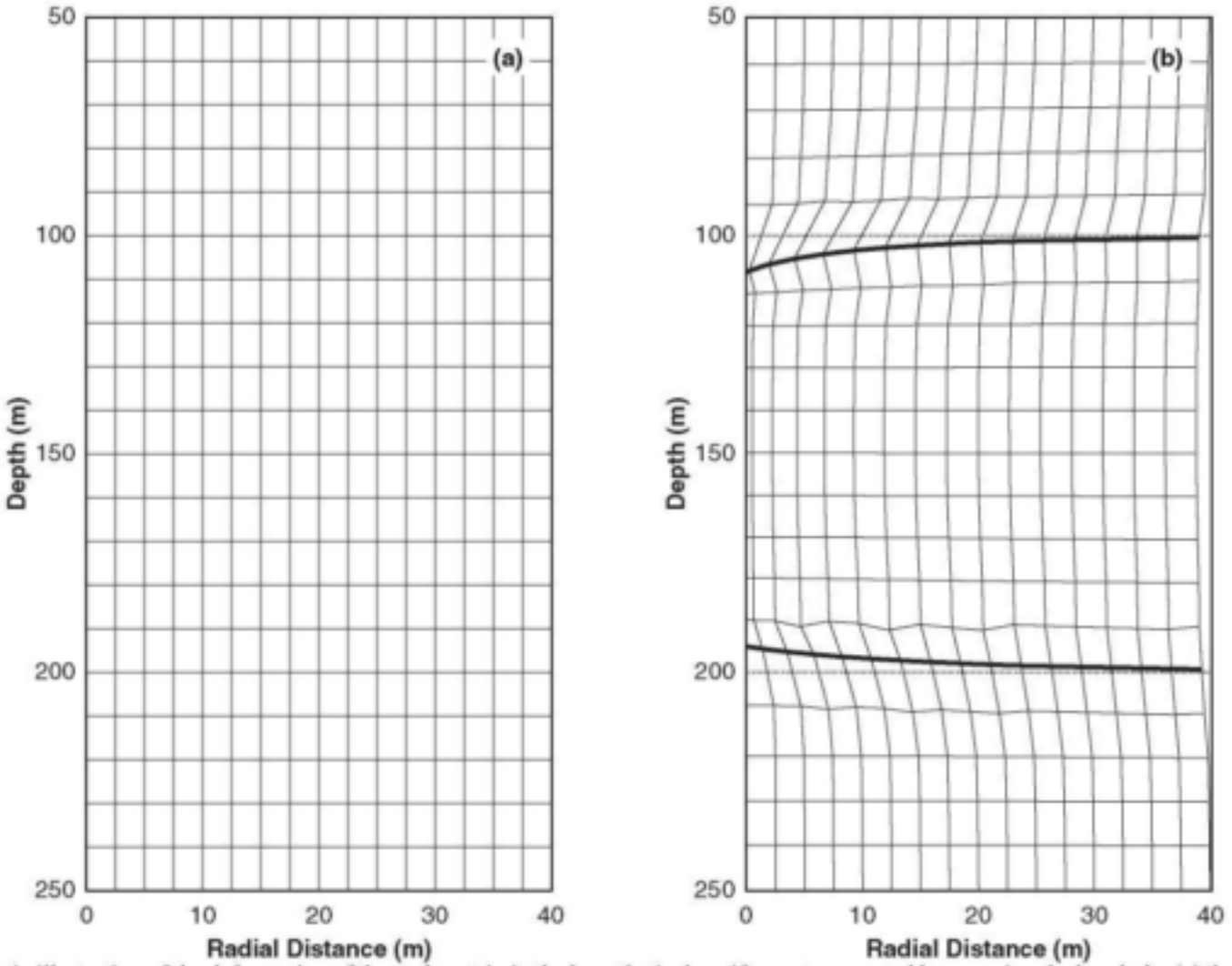

Figure 5–7 Schematic illustration of the deformation of the rock matrix in the hypothetical aquifer system created by pumping the borehole: (a) the initial non-deformed state and (b) the deformed state after 20 s of pumping with a 40 000 magnification of the displacements. (The bold lines indicate the interfaces of the aquifer and confining layers.)

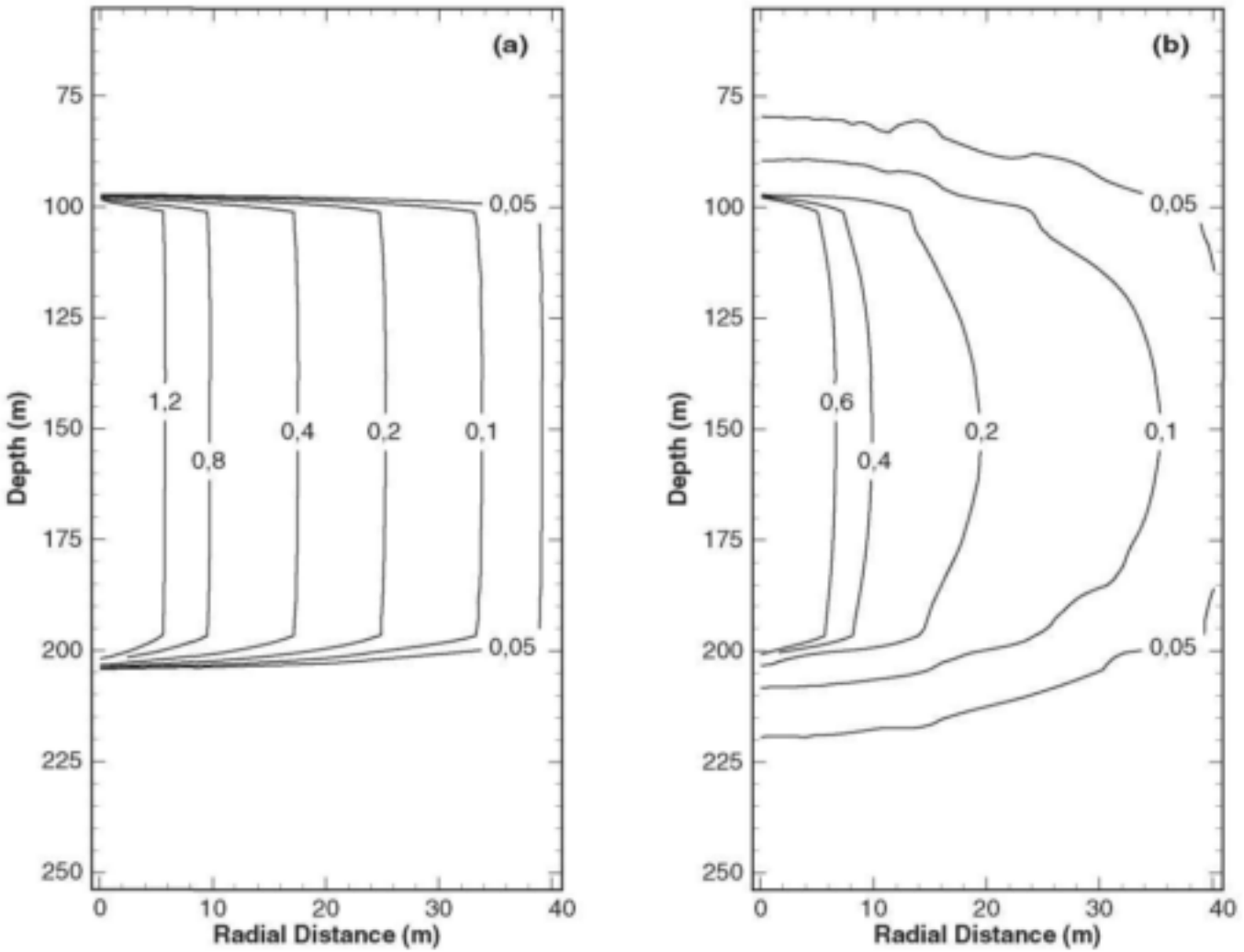

Figure 5–8 Contour maps of the drawdowns computed for the hypothetical aquifer with (a) the conventional groundwater flow model and (b) the deformable model, after pumping the borehole for 4 s.

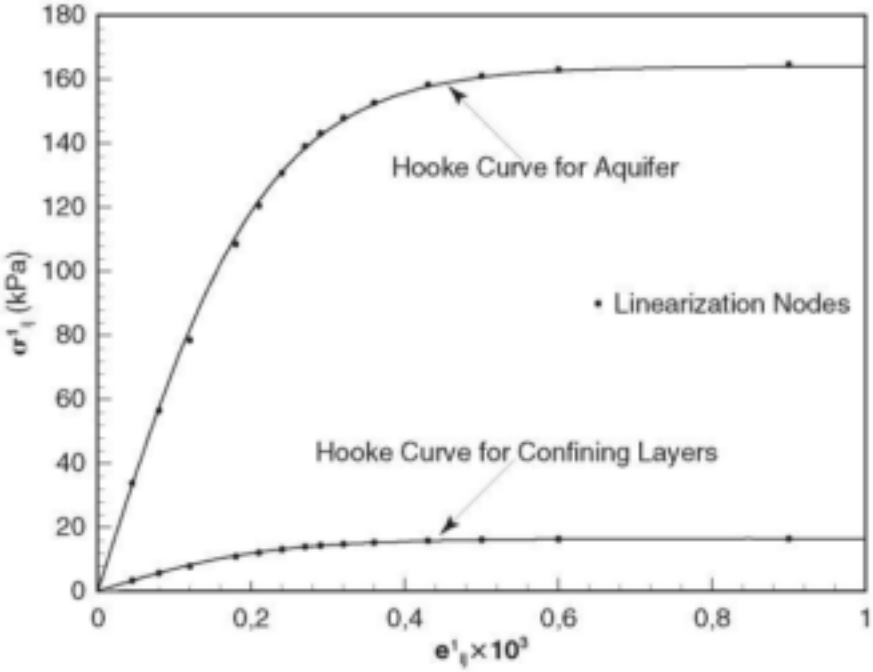

Figure 5–9 The discretized non-linear stress-strain functions.

The displacements in the non-linear model followed very much the same pattern as those obtained for the linear case at early times, as could have been expected, because the strains are then still small and behave linearly. However, a time is soon reached where the stresses and strains move off the section of the non-linear law of Hooke, which may be regarded as linear. The cross-sections of the aquifer system where the non-linear behaviour is observed after 5 s, 10 s and 15 s of pumping, are illustrated in Figures 5–10 and 5–11 for the radial and vertical deformations respectively.

According to these figures, the non-linear behaviour tends to propagate along the nodes in the neighbourhood of the interfaces between the aquifer and confining layers and around the borehole in the aquifer. This behaviour of the non-linear deformations could not only enhance the vertical deformations, with respect to the linear case, but also break the symmetry of the deformation profile, present in the drawdowns and deformations computed with the linear law of Hooke, and deform the aquifer permanently. However, the non-linear law of Hooke does not have a significant effect on the spatial distribution of the drawdown or the vertical deformation of the aquifer, at least for the time scale used to compute the values displayed in Figures 5–12 and 5–13. Nevertheless, one would expect that a significant non-linear effect could develop later, or if the borehole is pumped at a higher rate. Indeed, a review of the computed displacements revealed that the rock matrix already experienced a slight permanent deformation in some areas, illustrated in Figure 5–14, even after pumping the borehole for only 15 s, but at a discharge rate of 2,5 10^{-1} $m^3 s^{-1}$.

5.4 CONLUSION

It is of course not possible to compare the results of the simulations discussed here quantitatively with the results of Hsieh (1996). However, as shown by a comparison of Figures 5–6, 5–8 and 5–12 with his Figure 3 and Figure 5–7 with his Figure 2, it would seem that the present model agree very much with his model, be it only qualitatively. It is unlikely that the two models will agree to such an extent if the present model contains significant errors, especially if the complexity of the two models is taken into account.

Two very interesting results followed from both models. The first, which is not discussed by Hsieh (1996), is that the vertical displacements are essentially restricted to the interfaces of the aquifer and confining layers where the elastic parameters are discontinuous. The second is that the deformation causes the aquifer to contract towards the screened segment of the borehole, both horizontally and vertically, while the confining layers contract horizontally and extend vertically. This contraction of the aquifer rocks and the vertical extension of the rocks in the confining layers must obviously affect not only the porosity of the aquifer

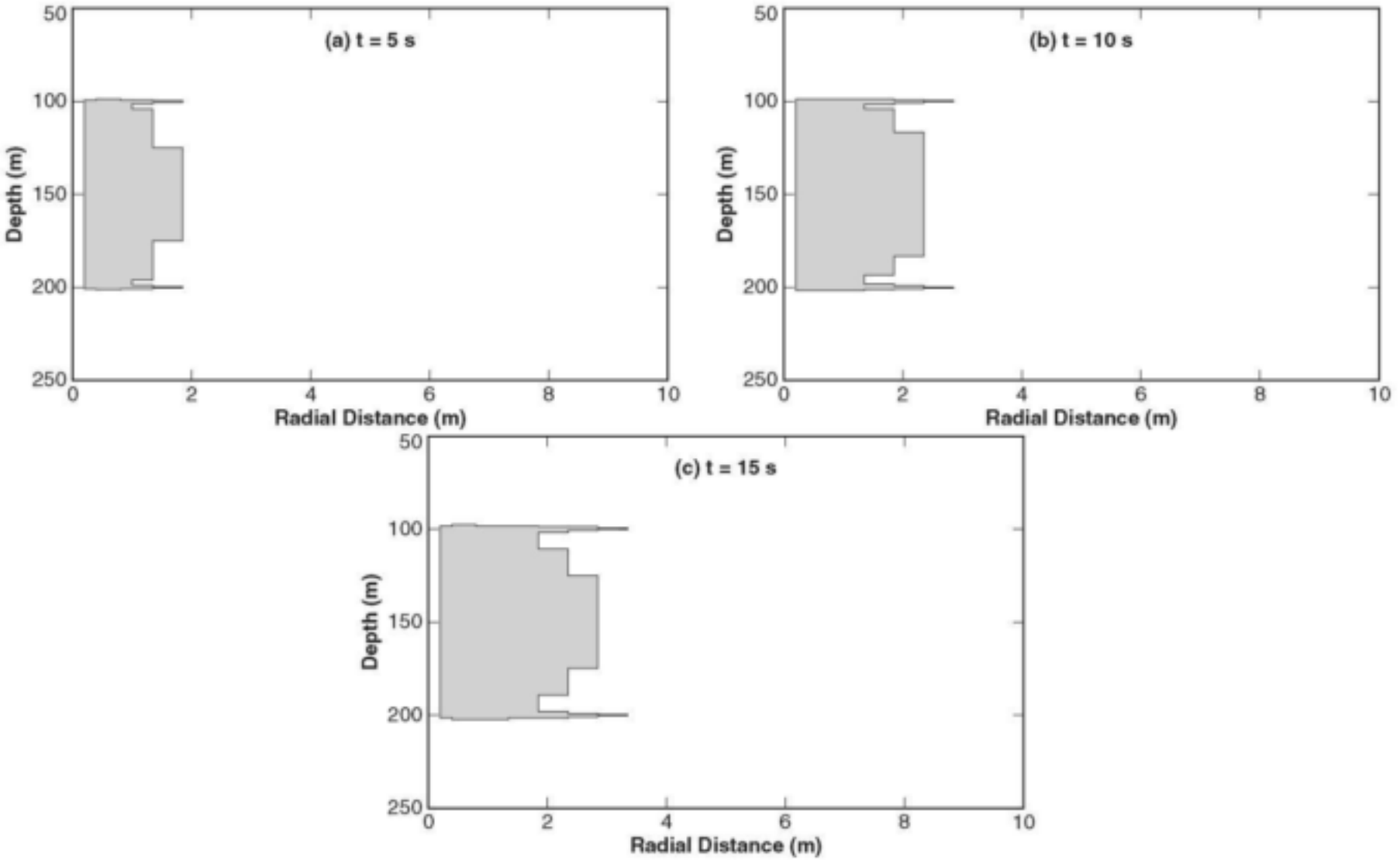

Figure 5–10 Vertical cross-sections (not to scale) of the areas in the aquifer system subjected to non-linear radial strain, after simulation times of 5 s, 10 s and 15 s.

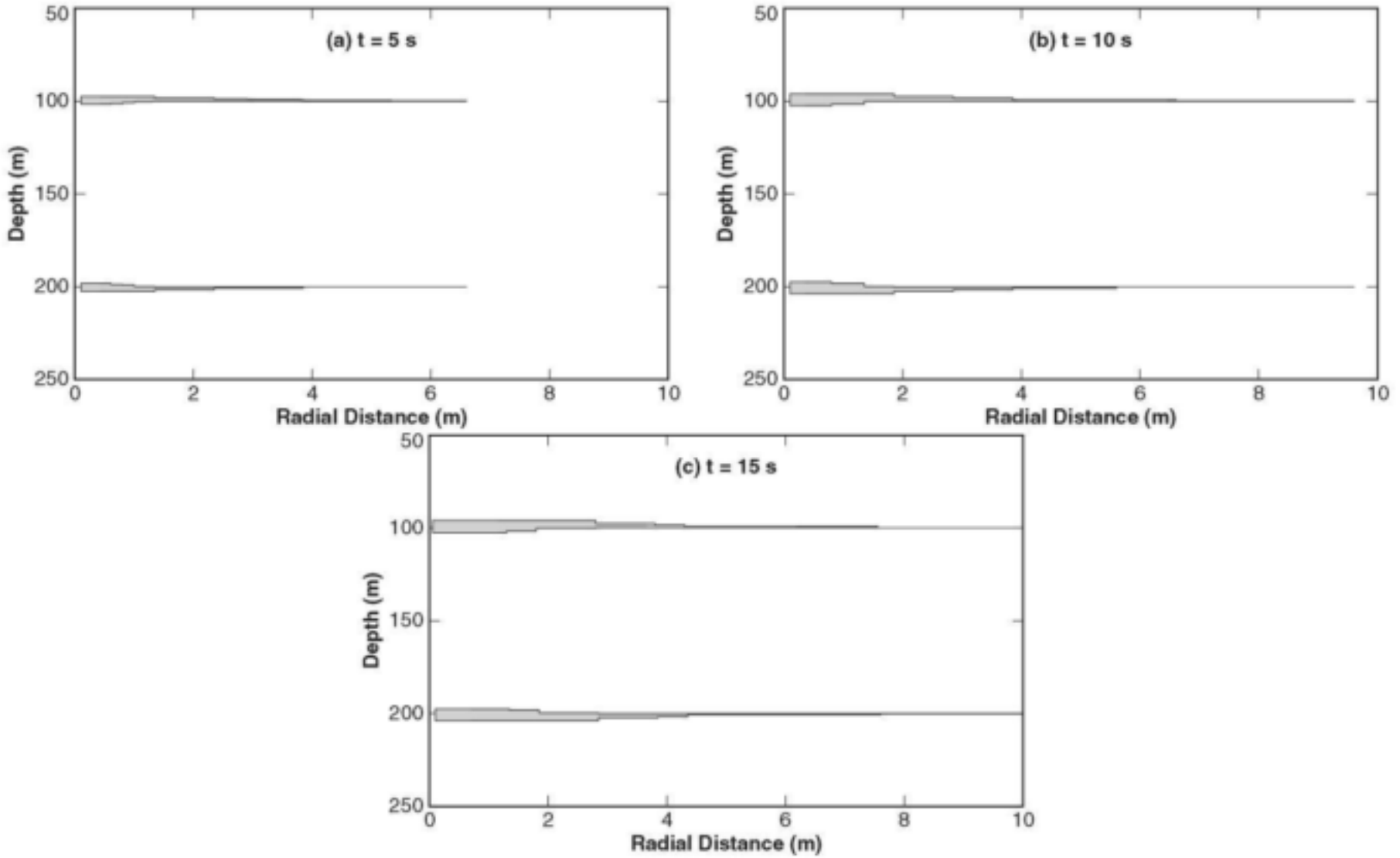

Figure 5–11 Vertical cross-sections (not to scale) of the areas in the aquifer system subjected to non- linear vertical strain, after simulation times of 5 s, 10 s and 15 s.

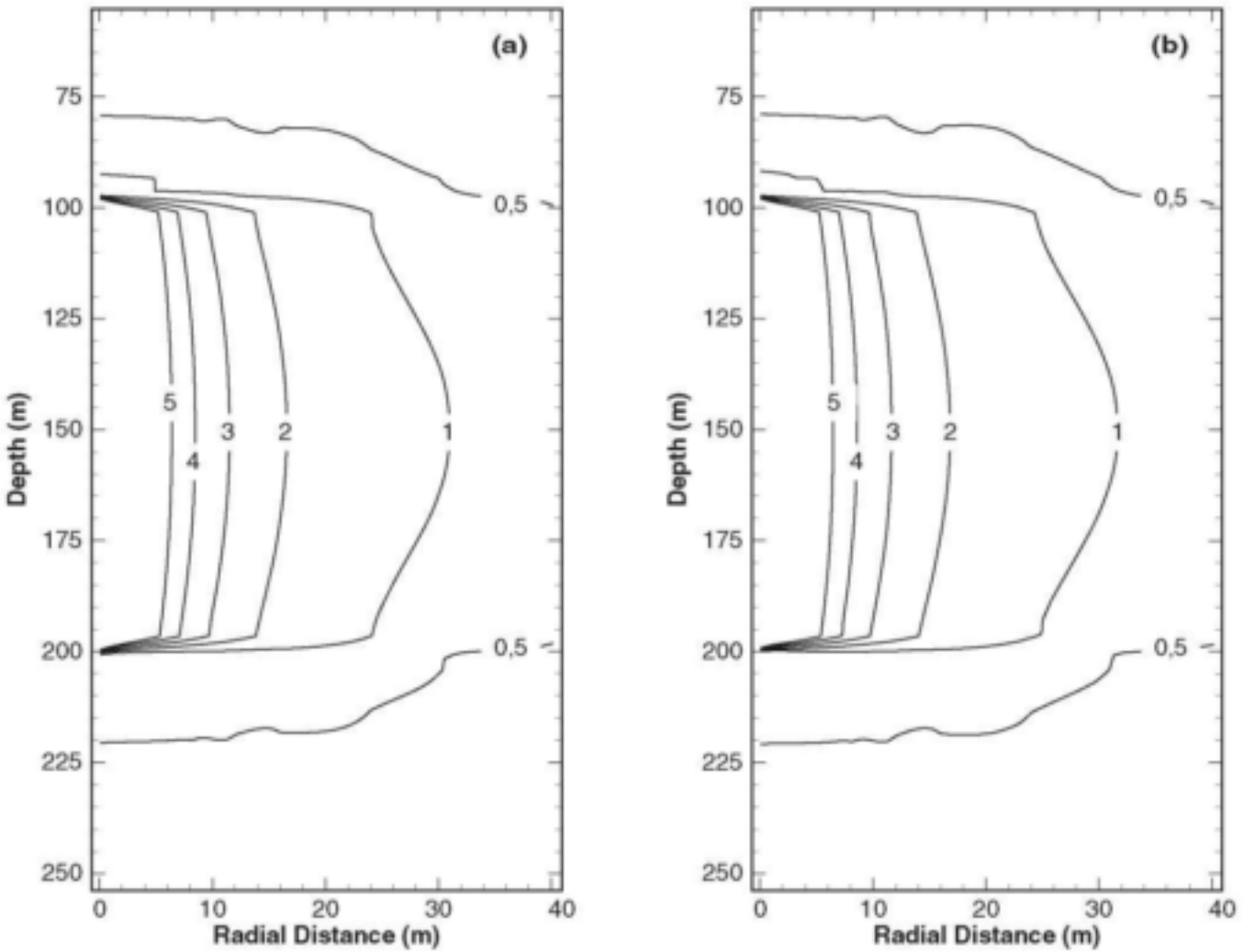

Figure 5–12 Contours (not to scale) of the drawdown (m) in the hypothetical aquifer computed with (a) the linear and (b) the non-linear law of Hooke, 15 s after pumping began.

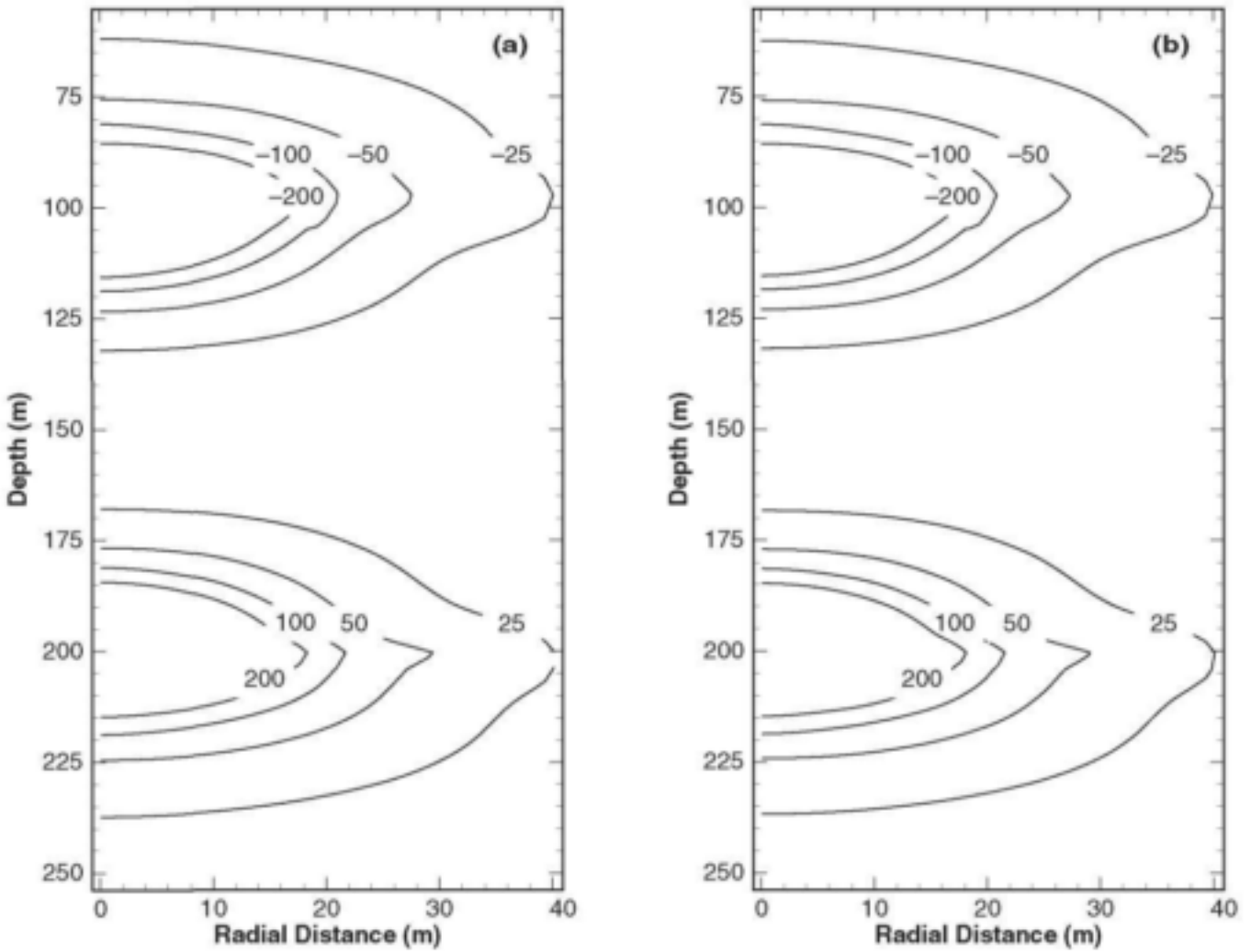

Figure 5–13 Contours (not to scale) of the vertical displacements in the hypothetical aquifer with (a) the linear and (b) the non-linear law of Hooke, 15 s after pumping began.

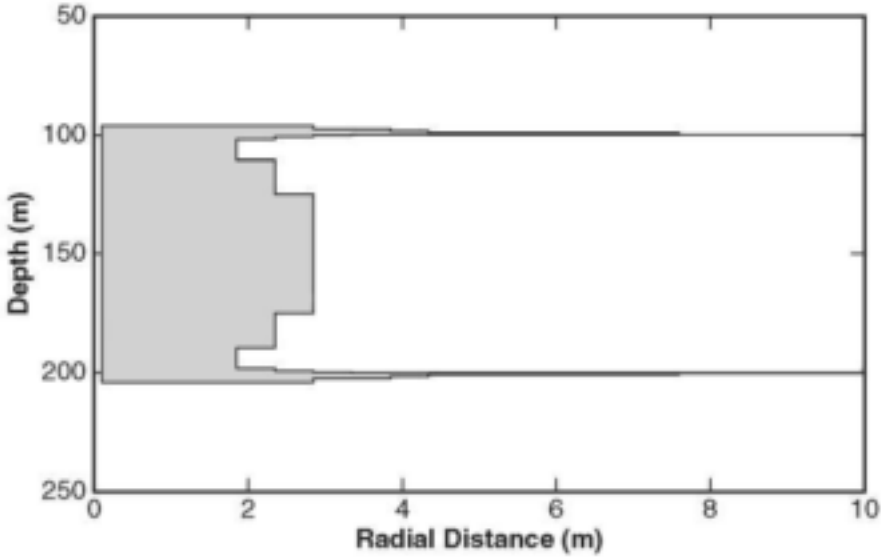

Figure 5–14 The shaded area indicates the area where permanent residual deformations had been observed in the aquifer system after pumping the borehole for 15 s at a rate of $2{,}510^{-1}\,m^3\,s^{-1}$.

system, but also the pressure distribution and thus the ability of the aquifer to yield water to the borehole. The fact that the extent of the deformation decreases with distance, suggests that the deformation of an aquifer during pumping, may be responsible for the very puzzling observation that the storativity values, derived from conventional aquifer tests, tend to decrease with distance from the borehole that is pumped during such a test. This conclusion is supported by the fact that the simulated drawdowns in the deformed model are considerably lower than in a conventional model, especially near the borehole. There is thus more water available near the borehole in the deformed model, than in the conventional model. However, this excess of water disappears with distance from the borehole.

CHAPTER 6

THE CAMPUS TEST SITE

6.1 INTRODUCTION

The aquifer system used to evaluate the elastic model developed in Chapters 2 and 3 is not typical of aquifers in South Africa, although it imitates the aquifers in the Karoo formations superficially. These formations, which still display the geometry of a porous medium, but with large variations in porosity, are sometimes intersected by bedding-parallel fractures. Botha *et al.* (1998) consequently, refer to them as *multi-porous, fractured aquifers*. The bedding-parallel fractures often have significant apertures (~1–10 mm) and underlie horizontal areas of several square kilometres. The groundwater flow-field in these aquifers and the drawdown in boreholes, therefore, differ considerable from that predicted by the conventional theory of flow through a porous medium. An example of this difference is illustrated in Figure 6–1. This figure compares the drawdown observed in a typical Karoo borehole near the town of Philippolis south-west of Bloemfontein, with the drawdowns computed from the type curve of Gringarten and Ramey (1974) for a horizontal fracture and the Theis curve Theis (1935) for a conventional porous aquifer. A more detailed discussion of the drawdowns and the various fits can be found in Van Tonder *et al.* (2001).

The bedding-parallel fractures in the Karoo formations are usually surrounded by highly permeable, limonite-stained, alteration zones with thicknesses that vary from 1 mm to 1 m for the fracture in the aquifer on the Campus Test Site at the University of the Free State. The cementation of the grains in the alteration zones has been reduced considerably by the diffusion of oxygen-rich water from the embedded fractures. The alteration zones and the embedded bedding-parallel fractures could therefore be highly susceptible to elastic deformations in the aquifer. It therefore seemed logical to apply the present model to the aquifer on the Test Site of the Institute for Groundwater Studies on the campus of the University of the Free State in Bloemfontein (South Africa).

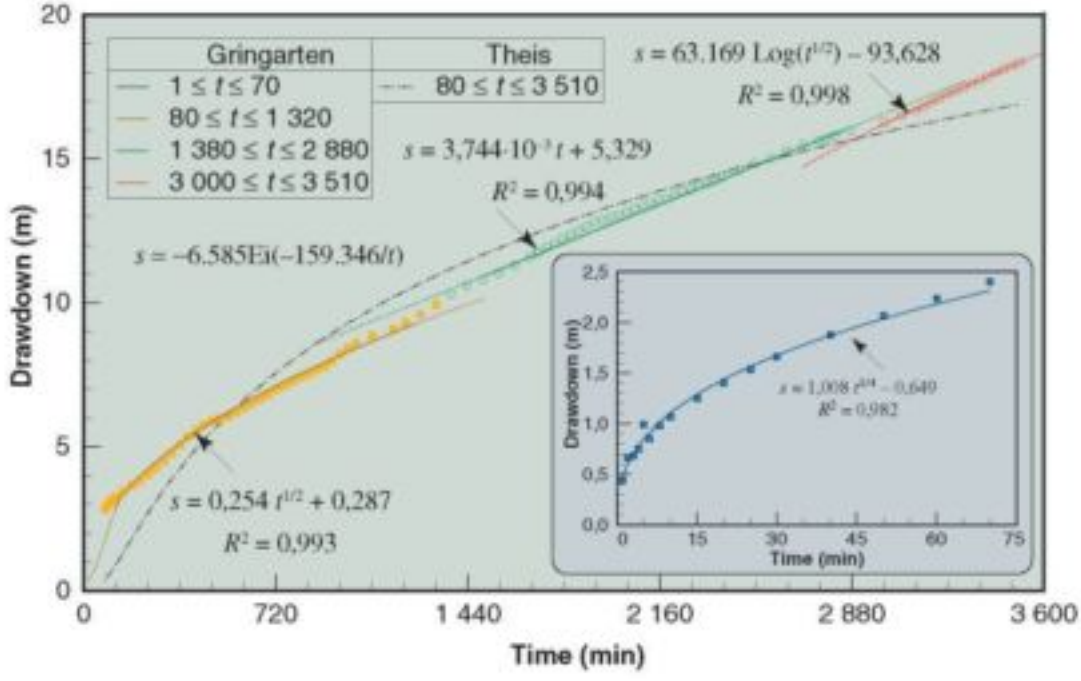

Figure 6–1 The drawdown observed in borehole A05 at Philippolis by Botha *et al.* (1996) fitted to the type curve of Gringarten and Ramey (1974) for an aquifer intersected by a horizontal fracture and the Theis curve for a horizontal porous aquifer.

The site, commonly known as the Campus Test Site, covers an area of approximately 180×192 m², where 24 percussions and 7 core-boreholes have been drilled to date, with positions given in Figure 6–2. As shown in Figure 6–3, three aquifers are present in the mudstones and sandstones from the Adelaide Subgroup of the Karoo Supergroup of formations that underlie the site. The top aquifer is a phreatic aquifer situated in the upper mudstone layers on the site. This aquifer is separated from the middle and main aquifer by a layer of carbonaceous shale 0,5 m to 4 m thick. The main aquifer occurs in an 8 m to 10 m thick sandstone layer. The third aquifer occurs in the mudstone layers that underlie the sandstone unit and is more than 100 m thick (Botha *et al.*, 1998).

A major characteristic of the main aquifer is the presence of a horizontal fracture; see Figure 6–3, that coincide approximately with the centre plane of the main aquifer. The fracture has an aperture of approximately 10 mm, see Figure 6–4, but the adjacent 200 mm of the sandstone on both sides of the fracture is also highly permeable.

A major feature of the aquifer on the Campus Test Site is that the 12 boreholes with significant yields

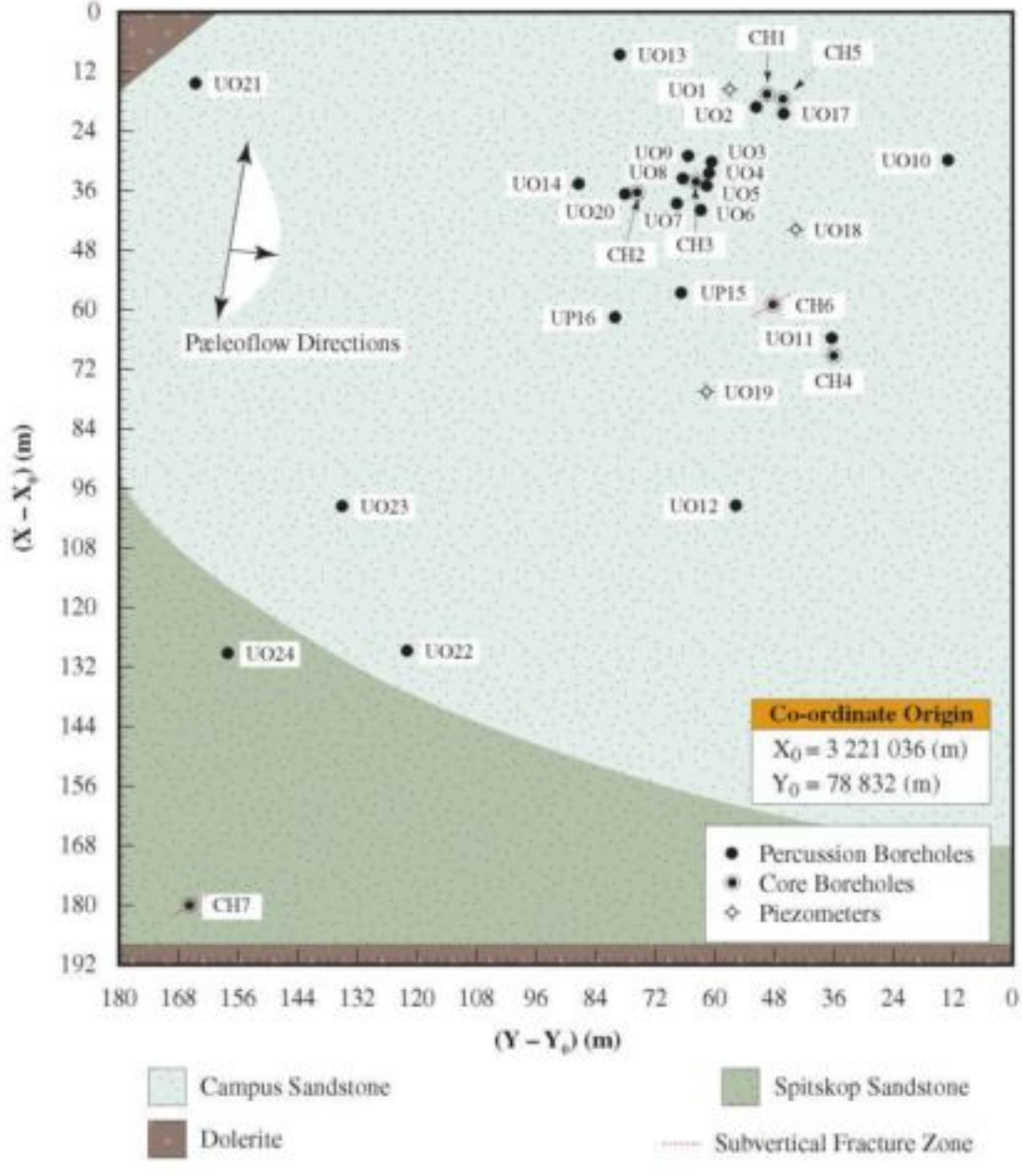

Figure 6–2 Map of the boreholes on the Campus Test Site.

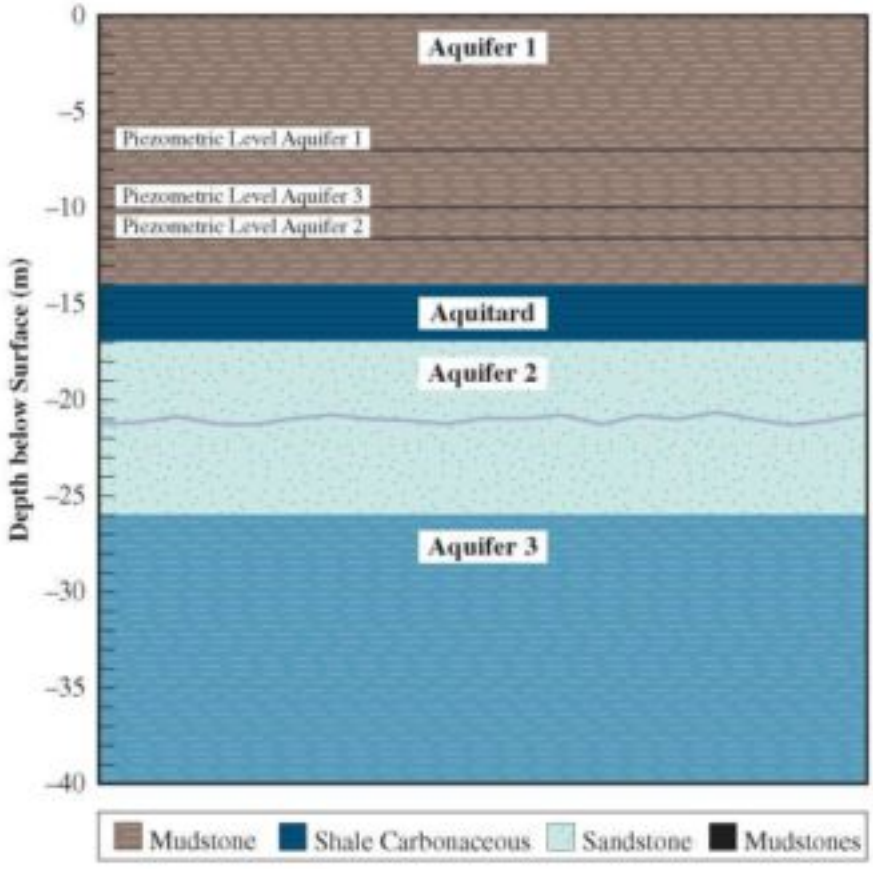

Figure 6–3 Schematic diagram of the different geological formations and aquifers present on the Campus test Site.

Figure 6–4 Photograph of a core sample that intersected the horizontal fracture on the Campus Test Site, displaying the fracture.

(> 4 $m^3 h^{-1}$) all intersect the fracture. The remaining boreholes do not intersect the fracture and have yields less than 0,1 $m^3 h^{-1}$. This and other observations on boreholes drilled in the Karoo formations led Botha *et al.* (1998) to conclude that bedding parallel fractures are the main conduits of water towards boreholes in the Karoo formations, but that the formations themselves serve as the main reservoirs of water. It this stand to reason, that any damage to a fracture that serves as the conduit of water for a borehole could affect the yield of a borehole adversely. Indeed, there are ample data to support the view that the so-called 'dried-up borehole', which is so characteristic of aquifers in the Karoo formations, is caused by a collapse of its conduit fracture and not a shortage of water.

There are a number of reasons why bedding-parallel fractures may collapse. However, field observations and discussions with farmers indicated that the deformation of the fracture, caused by excessive and prolonged pumping, probably contributes the most to the collapse of such fractures. Since there did not (and still does not) exist suitable equipment to study the behaviour of the fractures in the field, the Water Research Commission was approached for funds to develop a deformable groundwater flow model that could be used to study the behaviour of the fractures theoretically. It was there logical to apply the model developed in Chapters 2 and 3 to Karoo aquifers.

Although any Karoo aquifer could be used for this purpose, as indeed proposed in the original proposal to the Water Research Commission, it became clear during the development of the model that such an investigation will be a waste of time and money, unless backed by field observations. The present study will therefore be confined to the aquifer on the Campus Test Site, which is one of the best-known aquifers in the world.

The basic concepts of the numerical model develop for this aquifer (henceforth referred to as the *Campus Test Site Model*), are discussed in Section 6.2. This is followed by a discussion of the numerical simulations performed with this model in Section 6.3 with a summary and discussion of the results in Section 6.4.

6.2 DEFORMATION MODEL FOR THE CAMPUS TEST SITE

6.2.1 General

The Institute for Groundwater Studies have previously undertaken a detailed study of the Campus Test Site, including the development of a full three-dimensional model in Cartesian coordinates to simulate and understand the results of hydraulic tests performed on the site (Botha *et al.*, 1998). The deformation model developed in this project for the site was consequently based on this model. Indeed, the deformation model must reduce to the model developed by Botha and his co-workers if deformations are neglected. The real difference between the models is the number of differential equations that one needs to solve—one in a conventional three-dimensional Cartesian flow model and four in the corresponding deformation model.

It was known at the time of developing the deformation model that three-dimensional groundwater models require extensive computer resources and that the model developed by Botha *et al.* (1998) already needed all the resources available at of the Computing Centre of the University of the Free State to execute. Nevertheless, it was decided to develop the deformation model as a full, three-dimensional model in Cartesian coordinates, because the computer resources at the University increased considerably since the investigation of Botha and his co-workers and it was anticipated that more sophisticated equipment would become available during the project. Unfortunately, the latter expectation did not materialize. The investigation therefore had to be restricted to the radial-symmetric, cylindrical model used for the hypothetical aquifer of Hsieh in Chapter 5.

6.2.2 Hydraulic Parameters

Of particular importance in the development of any model for an aquifer is the availability of sufficient information on what Botha (1994) called relational parameters. In the case of a conventional three-dimensional groundwater flow model these parameters are: the hydraulic conductivity tensor and the specific storativity, to which must be added Young's modulus (E) and Poisson's ratio (ν) in the case of the deformation model.

The principal components for the Cartesian hydraulic conductivity tensor, (K_{XX}, K_{YY}, K_{ZZ}) and the specific storativity of the aquifer are known from the calibration of the three-dimensional model of Botha *et al.* (1998). These values, given in Table 6-1, were consequently also used in the development of the Cartesian

Table 6-1 Principal components of the hydraulic conductivity tensor and storativities used in modelling the Campus Aquifer.

Depth Below	Hydraulic Conductivity (m s^{-1})			Storativity	E
Soil Surface (m)	K_X	K_Y	K_Z	(m^{-1})	(Pa)
0,00	1,035.10^{-06}	1,035.10^{-06}	1,000.10^{-08}	1,0.10^{-04}	7,25.10^{+07}
5,00	1,035.10^{-06}	1,035.10^{-06}	1,000.10^{-08}	1,0.10^{-04}	7,25.10^{+07}
10,00	4,990.10^{-06}	1,035.10^{-06}	1,000.10^{-08}	1,0.10^{-04}	7,25.10^{+07}
15,00	7,191.10^{-08}	5,234.10^{-08}	1,948.10^{-11}	1,0.10^{-04}	7,25.10^{+07}
17,00	3,610.10^{-07}	1,988.10^{-07}	1,117.10^{-11}	1,0.10^{-04}	7,25.10^{+07}
20,00	3,280.10^{-06}	1,208.10^{-06}	1,117.10^{-11}	1,0.10^{-04}	7,25.10^{+07}
20,75	3,428.10^{-05}	1,234.10^{-05}	4,638.10^{-09}	1,0.10^{-04}	7,25.10^{+07}
20,95	3,428.10^{-05}	1,234.10^{-05}	4,638.10^{-09}	1,0.10^{-04}	7,25.10^{+07}
21,00	3,428.10^{-05}	1,234.10^{-05}	4,638.10^{-09}	1,0.10^{-04}	7,25.10^{+07}
21,05	3,428.10^{-05}	1,234.10^{-05}	4,638.10^{-09}	1,0.10^{-04}	7,25.10^{+07}
21,25	3,428.10^{-05}	1,234.10^{-05}	4,638.10^{-09}	1,0.10^{-04}	7,25.10^{+07}
22,00	3,747.10^{-07}	1,988.10^{-07}	9,638.10^{-10}	1,0.10^{-04}	7,25.10^{+07}
25,00	5,638.10^{-07}	2,678.10^{-07}	9,638.10^{-10}	1,0.10^{-04}	7,25.10^{+07}
32,50	6,521.10^{-08}	3,567.10^{-08}	9,830.10^{-10}	1,0.10^{-04}	7,25.10^{+07}
40,00	7,172.10^{-08}	5,223.10^{-08}	9,830.10^{-10}	1,0.10^{-04}	7,25.10^{+07}
Fracture	9,000.10^{-03}	9,000.10^{-03}	9,000.10^{-03}	1,0.10^{-05}	7,25.10^{+07}

deformation model for the Campus Test Site. However, the forced reduction of the three-dimensional Cartesian model to the radial-symmetric, cylindrical model meant that the horizontal components of the hydraulic tensor had to be transformed to the radial component in cylindrical coordinates, by using the relation (Tyldesley, 1975)

$$K_{rr} = K_{xx}\cos^2\theta + K_{yy}\sin^2\theta$$

between the radial hydraulic conductivity, K_{rr}, and the components, K_{xx} and K_{yy} in the Cartesian xy-plane, where θ is the angle between the x-axis in Cartesian coordinates and the radial axis (r) in cylindrical coordinates, as illustrated in Figure 6–5. In the discussion below, this angle was fixed at $\pi/4$ and K_{rr} computed as

$$K_{rr} = (K_{xx} + K_{yy})/2$$

Since there is no information available on the elastic properties of the Karoo formations, the specific storativities in Table 6-1 were used to derive the approximate values for Young's modulus given in Table 6-1, while Poisson's ratio was fixed at 0,25.

6.2.3 Finite Element Implementation

The finite element implementation of the model followed essentially the same procedure used in the case of Hsieh's hypothetical aquifer in Chapter 5. The main difference is that the domain of the aquifer was reduced to 520 m in the radial direction and 50 m in depth. This of course necessitated the introduction of a new finite element mesh. Of particular importance in the design of this mesh was the position of the fracture that exists at a depth of 21 m in the aquifer and the effect that may have on the convergence and accuracy of the numerical solution. A number of numerical experiments were therefore performed to determine a suitable spacing for the finite element mesh. These experiments showed that convergence and accuracy of the model can be assured, if the domain of 520×50 m^2 is divided into 28 columns and 46 rows with six of the rows spaced at vertical distances of 0,01 m, 0,2 m and 0,3 m above and below the centre plane of the aquifer. Figure 6–6 displays a section of this mesh adjacent to the borehole.

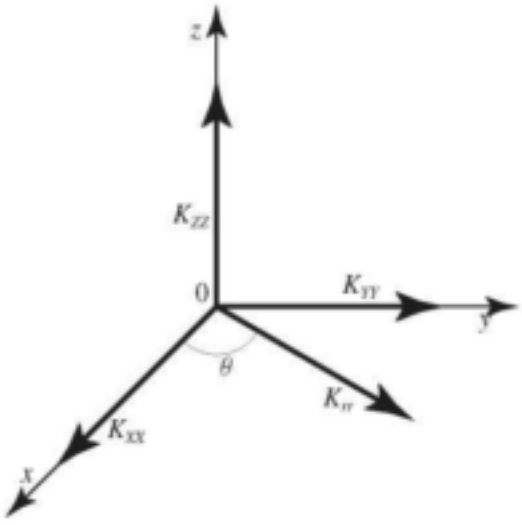

Figure 6–5 Relation between the radial component, K_{rr}, of the hydraulic conductivity tensor in cylindrical coordinates and its principle Cartesian components.

6.2.4 Boundary Conditions

The boundary conditions used with the Campus Test Site model were similar to that used with the hypothetical aquifer of Hsieh in Chapter 5. The outer boundary was again considered as impervious and subject to constant stresses and the bottom boundary as impervious and rigid. The boundary at the land surface was also considered free of applied forces, but deformable and subject to a constant piezometric head. Although it would have been nice to allow the borehole wall to deform, as observed by Botha *et al.* (1998), this additional freedom increased the computational time considerably. No radial displacements were therefore allowed along the borehole wall, but the prescribed constant vertical traction along the wall allowed the borehole to deform vertically. It was also assumed that the borehole received its water only from the fracture, taken as a slice centred at a depth of 21 m and 100 mm thick, as in the model of Botha *et al.* (1998).

6.3 NUMERICAL SIMULATIONS

6.3.1 Behaviour of the Aquifer with the Linear Law of Hooke

The first set of simulations with the model of the Campus test Site was restricted to the linear law of Hooke. The first simulation considered the situation where a hypothetical constant rate test was performed for 2 h on one of the high-yielding boreholes on the site with a discharge rate of 1,8 $m^3\ h^{-1}$.

The first and most noticeable difference between this aquifer and the aquifer of Hsieh in Chapter 5 is the way in which the drawdowns in the two aquifers behave. While the simulated drawdowns in Hsieh's aquifer steadily increase in time, see Figure 5–3, the drawdowns in the Campus Test Site model, display a dependence on the position in the aquifer. In the fracture, its immediate neighbourhood and the region below it, the drawdowns increase steadily with time, as expected. However, there is a region, centred at approximately 800 mm above the fracture, where the simulated drawdowns decrease with time, after the pump was switched on. This situation persisted for several minutes; see Figure 6–7 (a), before the drawdown began to increase with time. It is worth noticing that this situation was not restricted to the direct neighbourhood of the pumped borehole, but was also observed at distances of up to 50 m from the borehole, as shown in Figure 6–7 (b). This behaviour may serve as a numerical illustration of the somewhat paradoxal phenomenon that the water level in an observation borehole begins to rise the moment the pump is switched on in the production borehole, often observed during hydraulic tests of Karoo boreholes (Botha *et al.*, 1998). Since it is impossible to explain this phenomenon in the conventional theory of groundwater flow, its existence must be attributed to the deformation of the rock matrix in the deformation model. That this is indeed the case is confirmed by the drawdowns for the same model aquifer predicted by the conventional theory of groundwater flow in Figure 6–8, where the drawdowns are increasing continuously at all times and throughout the aquifer.

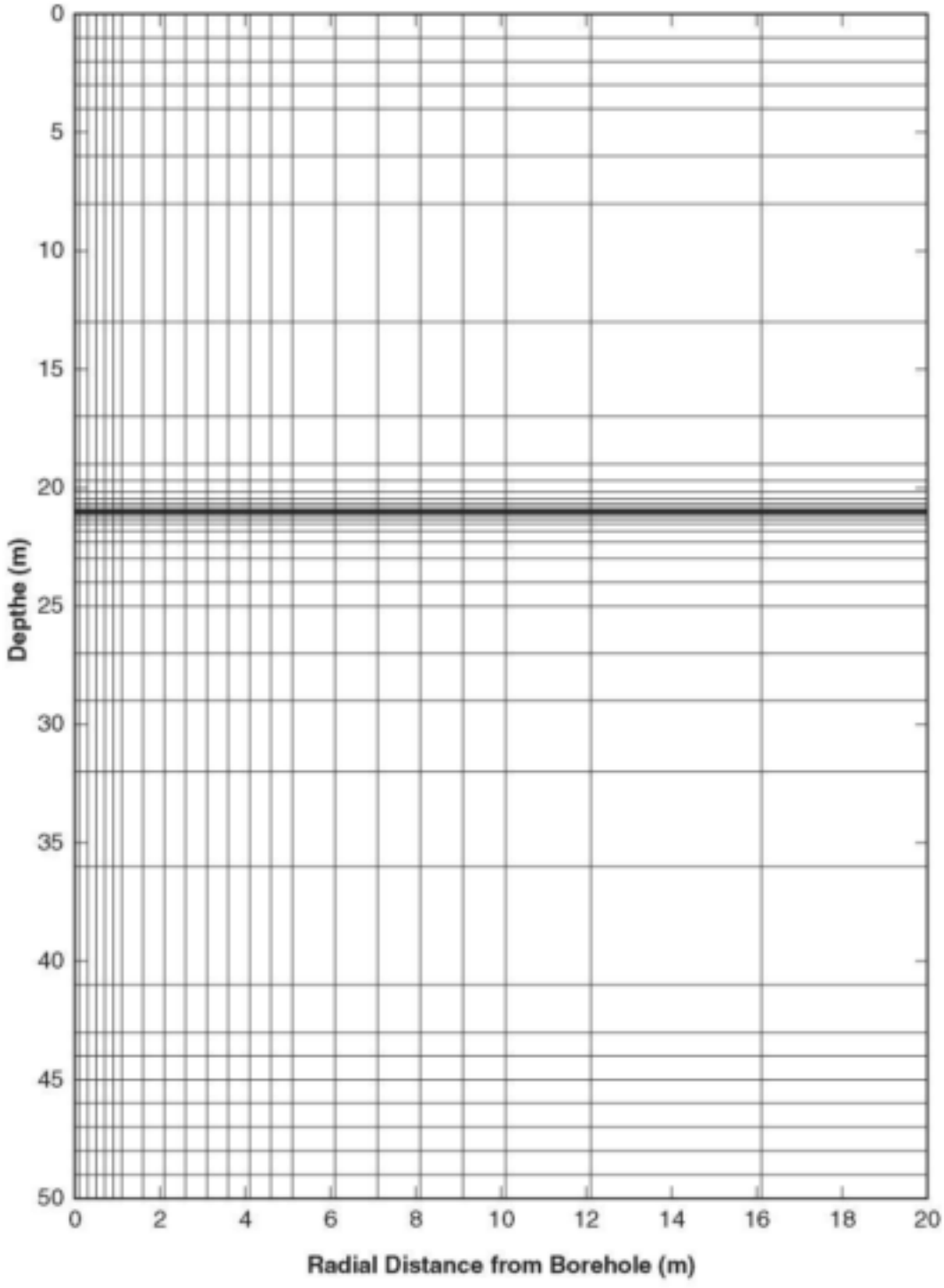

Figure 6–6 A cross-section of the finite element mesh used in simulations with the Campus Test Site model.

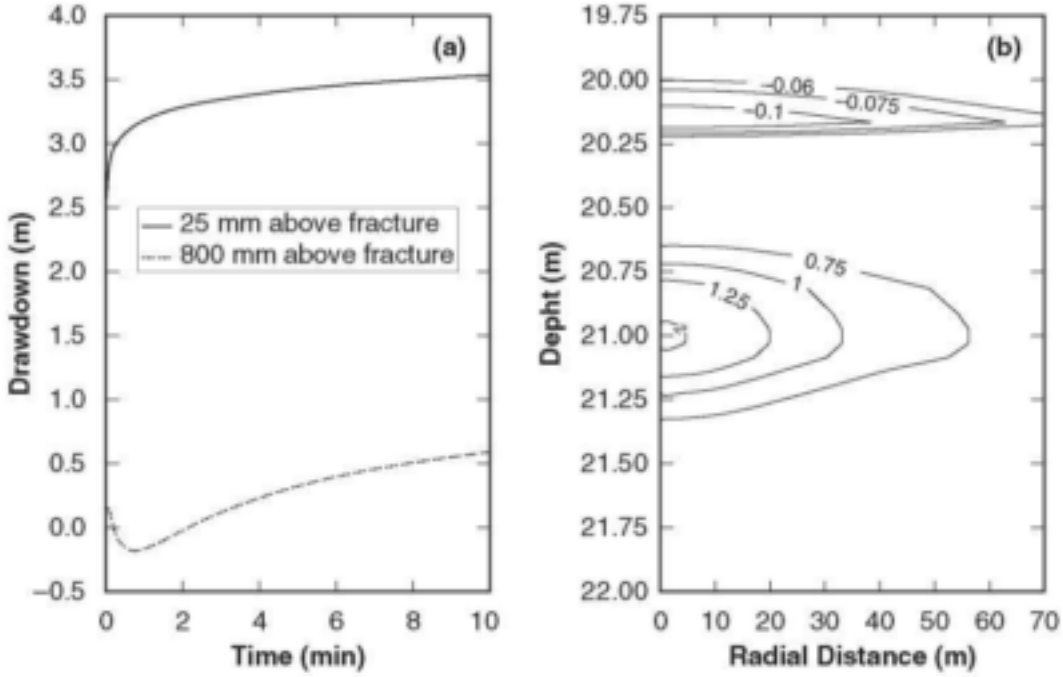

Figure 6–7 Simulated drawdowns (m) for the hypothetical aquifer test on the Campus Test Site with deformation of the aquifer. (a) Drawdowns observed in the rock matrix above the fracture, and (b) a vertical contour map of drawdowns after 45 s of pumping.

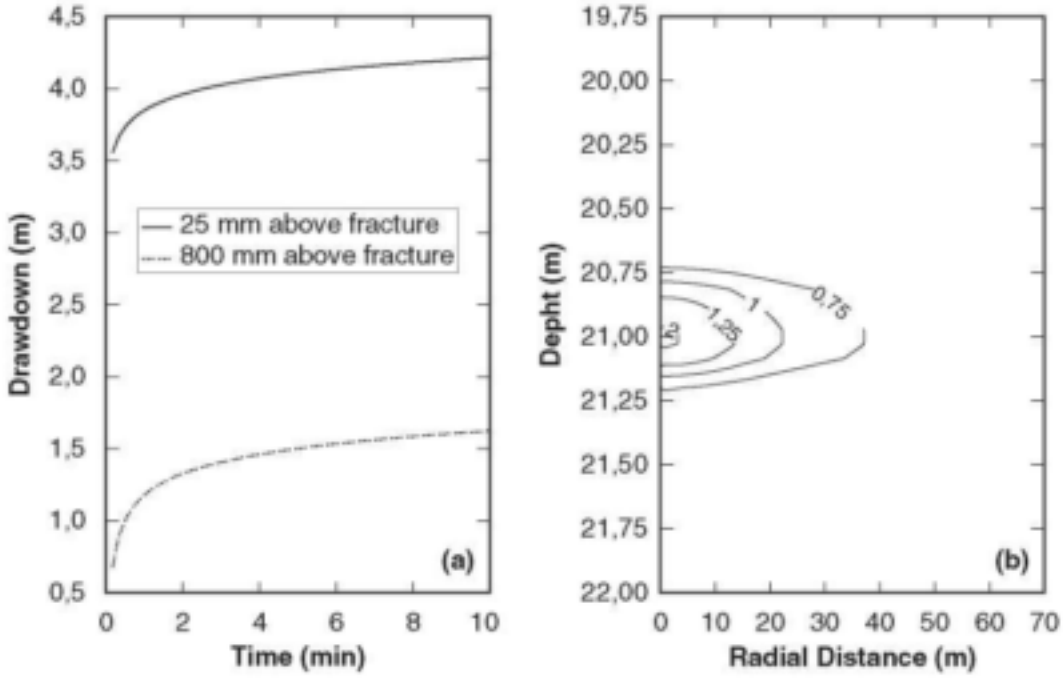

Figure 6–8 Simulated drawdowns (m) for the hypothetical aquifer test on the Campus Test Site without deformation of the aquifer. (a) Drawdowns observed in the rock matrix above the fracture, and (b) a vertical contour map of drawdowns after 45 s of pumping.

It might come as a surprise to find that the drawdowns in Figures 6–7 (a) and 6–8 (a) differ by as much as 0,7 m. However, as will be shown below, the models used to compute them have completely different physical interpretations.

The behaviour of the Campus Test Site model differs in another respect from that of Hsieh in that no sharp vertical deformations were generated along the discontinuous interfaces of the fracture, but at a vertical distance of approximately 0,25 m above and below the fracture. This feature is illustrated in Figure 6–9, which display a contour map of the simulated vertical displacements, u_z, observed after the borehole has been pumped for 15 minutes. The contours, moreover, show that the fracture tends to bend vertically and that the magnitude of the bending is a non-linear function of the radial distance. This behaviour can be seen more clearly in the detailed contours of u_z in Figure 6–10, which indicate that the displacements very much resembles a non-linear wave. It is also interesting to observe that the displacements above the fracture are all negative, while those below the fracture are all positive. Since the magnitudes of the negative displacements are larger than that of the positive displacements below the fracture plane, the pumping of the borehole tend to push the

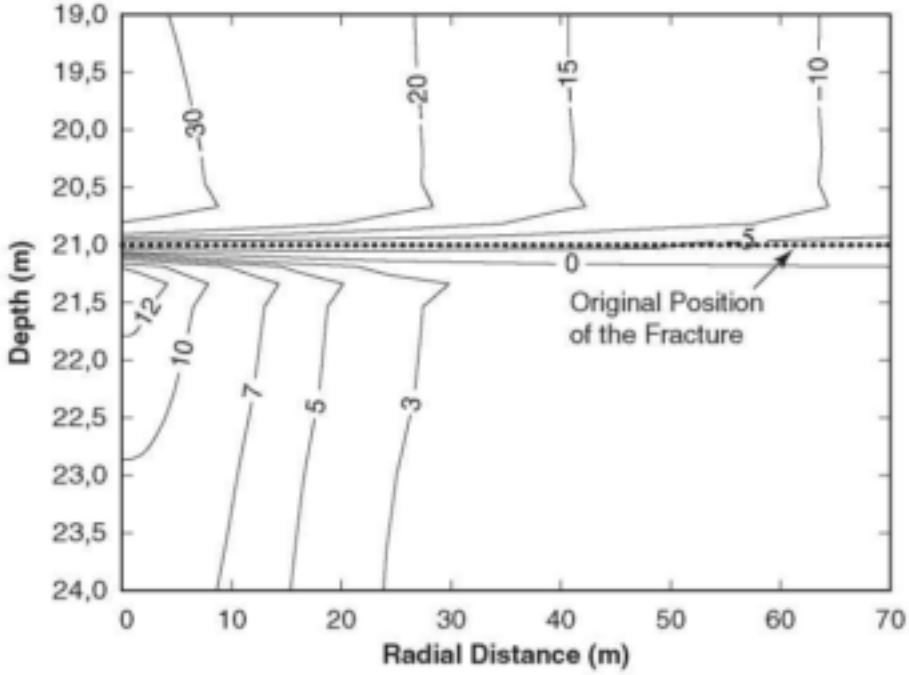

Figure 6–9 A contour map of the vertical displacements (in μm) across a vertical section of the fractured aquifer after 15 minutes of pumping.

fracture plane downwards. Notice also that the contours do not intersect the fracture plane perpendicularly. The bending of the upper plane of the fracture is therefore different from that of the lower plane, for a given radial distance, which implies that the pumping of the borehole tends to compress the fracture to a degree that decreases with distance from the borehole.

The restitution phase of the aquifer was also simulated. This was achieved by switching the pump off after two hours, but continue the computation for another two hours. As shown by the contours in Figure 6–11, the drawdowns in and near the fracture plane declined very quickly with time, but stayed stable or even increased for a period of several minutes at distances farther away from the fracture plane. This behaviour, illustrated more clearly in Figure 6–12, is particularly noticeable in two regions of the aquifer. The first region stretches from the soil surface to a plane situated at approximately 200 mm above the fracture plane, and the second region from a plane at a depth of 200 mm below the fracture plane downwards.

A very interesting and unusual feature of the drawdowns in Figure 6–12 is the increase in the drawdown for the point 200 mm above the fracture after the pump was switched off. It might be argued that this behaviour is an artefact in the present model. However, a similar and more pronounced effect was actually observed

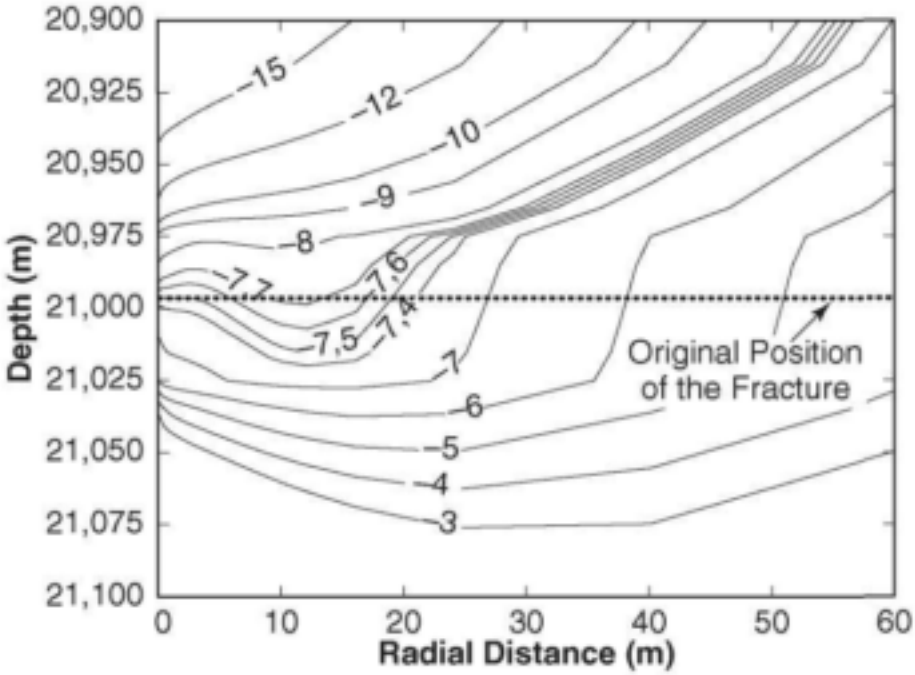

Figure 6–10 Enlarged view of the vertical displacement contours in Figure 6–9 in the domain adjacent to the fracture.

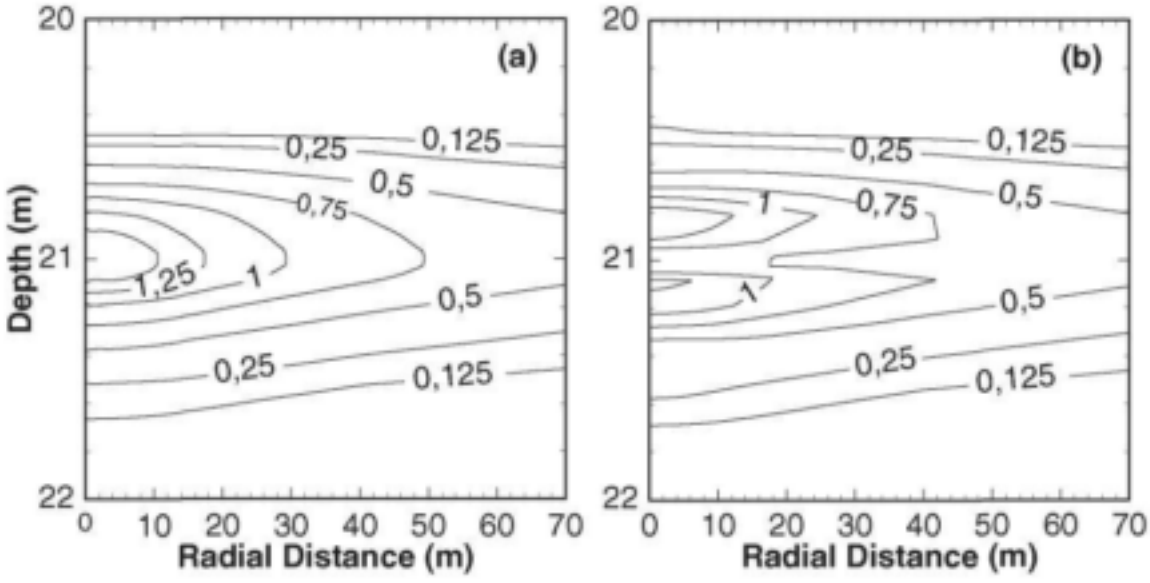

Figure 6–11 Contours of the simulated drawdowns (m) in a vertical section of the Campus Test Site around the fracture during the hypothetical aquifer test with Campus Test Site model: (a) after 2 hours of pumping and (b) 45 s after the pump was switched off.

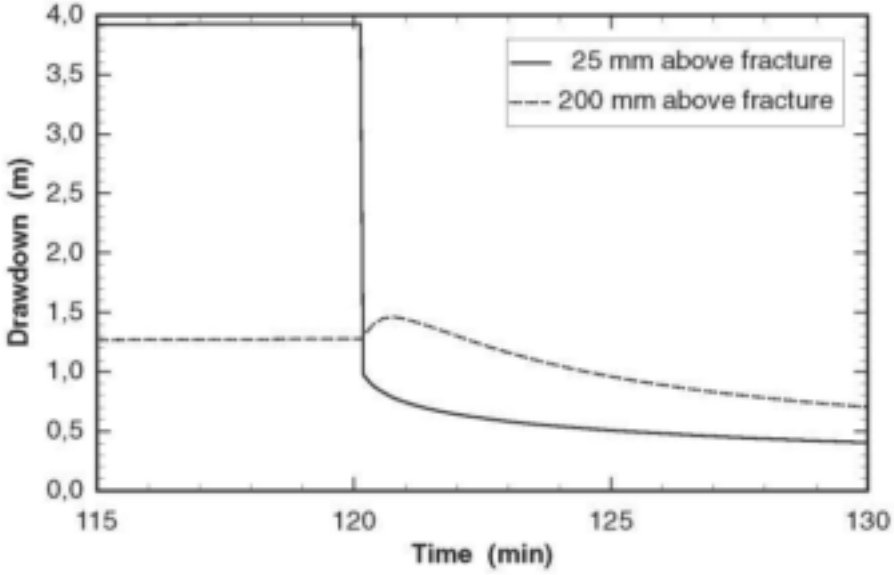

Figure 6–12 Transient evolution of the simulated drawdowns on the wall of the borehole 25 mm and 200 mm above the fracture plane during the hypothetical hydraulic test performed with Campus Test Site model.

during a constant rate test performed on 1995-06-01 at the Campus Test site. In this test, Borehole UP15, that intersect the fracture was pumped, while the water levels in three other boreholes, UO5, UO20 and UO11 were monitored continuously with pressure transducers. Boreholes UO5 and UO20, which are the highest yielding boreholes on the site, both intersect the fracture and are situated approximately 20 m from UP 15, while UO11, which does not intersect the fracture, is situated approximately 30 m from UP15. (See Figure 6–2 for the exact positions of the boreholes.) The test began with a discharge rate of 9,72 $m^3 h^{-1}$, which was reduced to 3,6 $m^3 h^{-1}$ after 140 min, when the water level in UP15 dropped to the level of the pump intake and continued for another 40 min after which the pump was switched off. As shown by the graphs of the drawdowns in Figure 6–13, the drawdowns in UO5 and UO20 behaved very similar to that of the pumped borehole, UO15, in that their water levels began to restore as soon as the pump was switched off. The water level in Borehole UO11, however, continued to decline for approximately 30 minutes after the pump was switched off, before

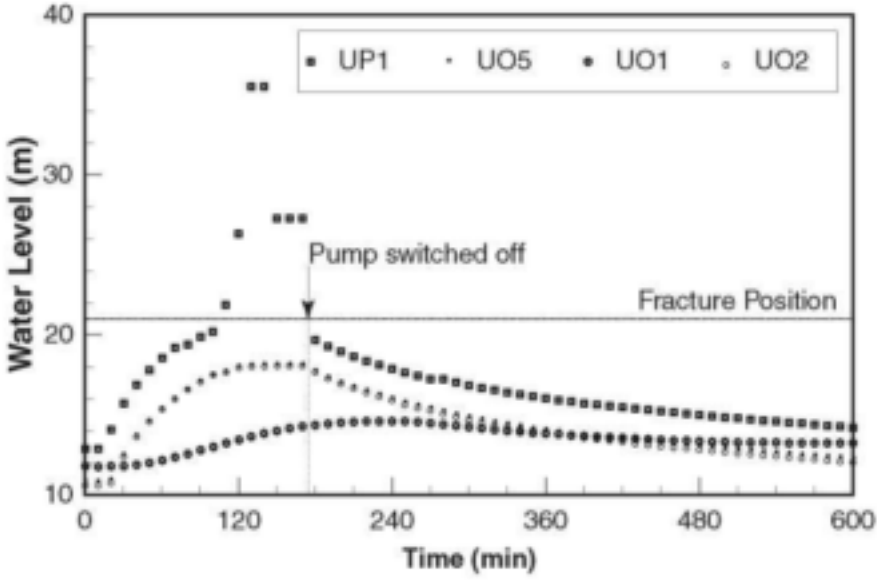

Figure 6–13 Graphs of the water levels in boreholes UO5, UO11, UP15 and UO20 observed during the constant rate test performed on 1995-06-01 at the Campus Test Site (Botha *et al.*, 1998).

it began to restore slowly. It was therefore thought worthwhile to see to what extent the deformation model could account for the behaviour of the drawdowns observed during this hydraulic test. The numerical simulation for the hypothetical aquifer was therefore repeated, but with the pumping rate replaced by the rates used in the actual test.

It is obviously impossible to represent the positions of the boreholes fully in a symmetric cylindrical model, especially one based on the finite element approximation. The following procedure was consequently used to assign positions for the boreholes in the present model. Since UO5 and UO20 both intersect the fracture, the positions of the two boreholes were represented by a point situated 25 mm above the fracture and 24 m away from the borehole (UP15) in Figure 6–6, while the position of UO11 was represented by a point 200 mm above the fracture and 30 m away from UO15. It was also necessary to reduce the discharge rate after 120 min instead of the 140 min used in the actual test and to restrict the simulation period to approximately 300 min to keep the computational time within acceptable limits.

Although one cannot really expect that the simulated pressure heads at a single node must represent the water levels in an open borehole, the results of the simulation in Figure 6–14, nevertheless, show a strong similarity between the computed and observed values. Not only do the drawdowns at the point representing boreholes UO5 and UO20 follow the same pattern as in the original test, but the drawdown at the point representing Borehole UO11 again tends to increase after the pump was switched off, albeit only for approximately 5 minutes. However, one cannot expect to simulate such behaviour in detail without sufficient knowledge of the mechanical properties of the aquifer. Nevertheless, it is interesting to note that the model was able to simulate a perplexing observation during the performance of the actual test—a rise of approximately 75 mm in the water level of borehole UO11 during the first two minutes of pumping. The rise, unfortunately, is too small to see in Figure 6–13 and is only just visible in Figure 6–14. This behaviour has been observed previously in Karoo boreholes, but it is usually not monitored in hydraulic tests, or simply neglected in the analysis of such tests (Hsieh, 1996). Moreover, it is virtually impossible to notice this behaviour if the readings during the test are taken manually, since the magnitude of the feature is not very large. Nevertheless, there is no doubt that the feature is real. Since no conventional groundwater flow model can account for this behaviour, there is this little doubt that deformations play a significant role in the physical behaviour not only of Karoo aquifers, but also of aquifers in general.

6.3.2 Behaviour of the Aquifer with the Non-linear Law of Hooke

The approximation of the non-linear law of Hooke in Equation (3.29) with the piecewise linear polynomial in Figure 5–9, can be viewed as the replacement of Young's modulus, E, which is independent of the strains, with a new parameter that varies with the magnitude of the strains. The possibility therefore exists that non-linear stresses with large magnitudes can cause larger deformations in a body than linear stresses with the same magnitude. This behaviour is illustrated by the contours in Figure 6–15 of the simulated vertical displacements in the Campus Test Site model that developed after pumping the borehole for 2 h at the constant discharge rate of 1,4 m^3h^{-1}, using the linear law of Hooke and the non-linear stress-strain relation in Equation (3.29).

It is interesting to note that the enhancement of the displacements by the non-linear stress-strain relation in Figure 6–15 occur mainly on both sides of the horizontal fracture and not the fracture itself. The magnitudes of the displacements in and around the fracture are almost unaffected, but the magnitudes of the vertical strains in the neighbourhood of the fracture increase. This behaviour is especially noticeable near the borehole and below the fracture, where the vertical density of the contour lines in Figure 6–15 (b) is denser than that of the contour lines in Figure 6–15 (a). However, the non-linear stress-strain relation does not change the distribution of displacements markedly in the radial direction.

The most important consequence of the non-linear stress-strain relation is that it allows the aquifer to deform non-linearly. Two points, P_0 and P_1 say, in the same neighbourhood of a body and subject to the same value of Young's modulus will experience very much the same displacements in the linear case. For example, a linear displacement of P_0 must necessarily be accompanied by a similar linear displacement of P_1. However, this is no longer true in the non-linear case, where P_0 may still experience a linear displacement, while P_1 experience a non-linear displacement. The behaviour of a body subjected to a non-linear stress-strain relation could therefore differ completely from its behaviour when subjected to a linear stress-strain relation.

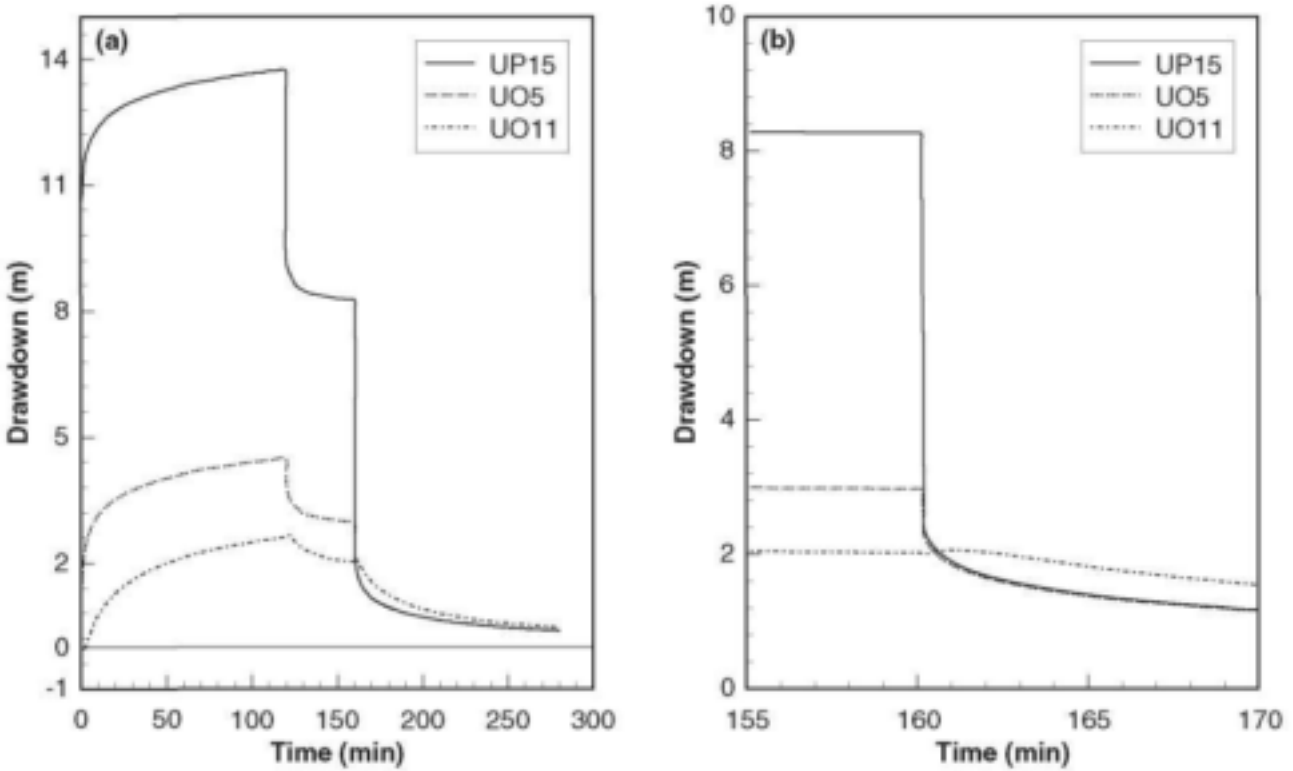

Figure 6–14 Graphs of the drawdowns in boreholes UO5, UO11 and UP15 simulated with the deformation model and the linear law of Hooke for the constant rate test performed on 1995-06-01 at the Campus Test Site. Figure (a) shows the drawdowns over the full period of the test, while (b) shows an enlargement of the drawdowns centred on the time that the pump was switched off (t = 160 min).

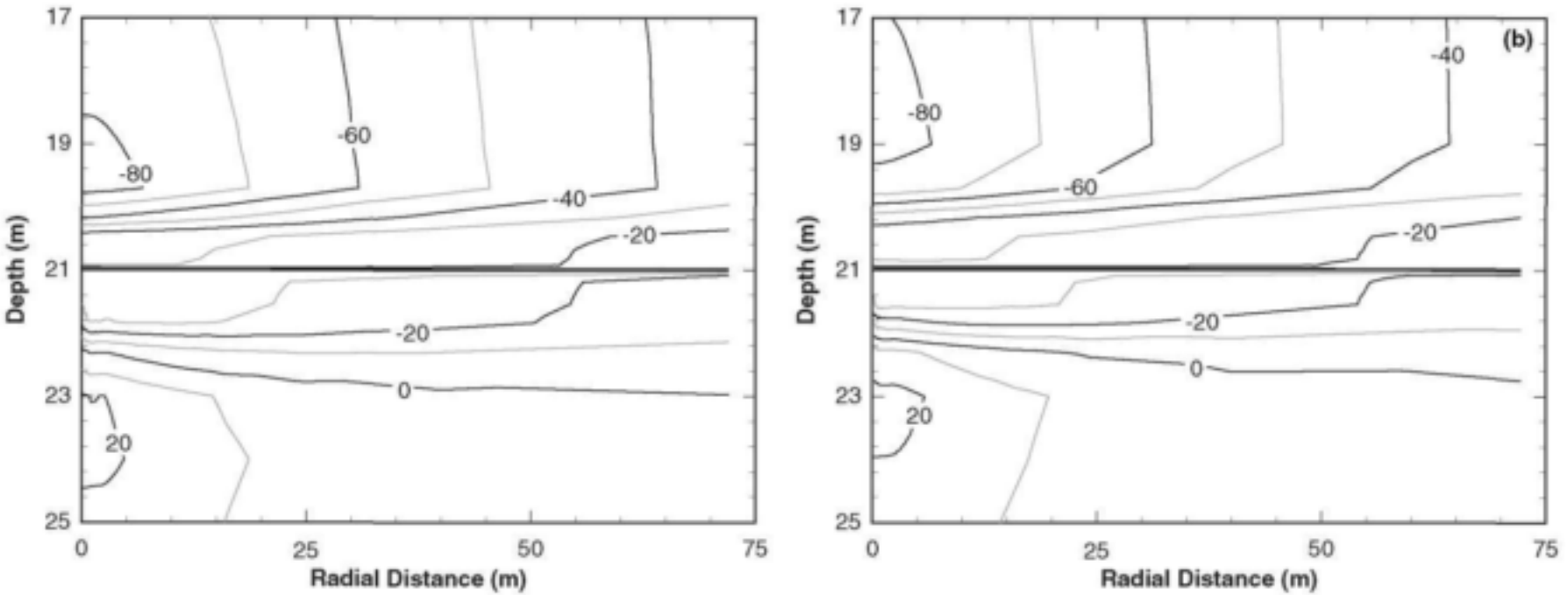

Figure 6–15 Contours of the vertical displacements (μm) in the Campus Test Site model after pumping the borehole for 2 h at a constant rate of 1,4 $m^3 h^{-1}$, using (a) the linear law of Hooke and (b) the non-linear law.

The dynamical forces created by the acceleration of the water and rock matrix during the pumping of a borehole will normally be the most likely cause for the deformation of an aquifer. It may therefore be interesting to see what effect different discharge rates have on the behaviour of the drawdowns and deformations in an aquifer. Two sets of numerical experiments were performed to study the behaviour of the drawdowns and deformations in the Campus Test Site model. In the first set, the borehole was pumped at a discharge rate Q = 1,4 m^3 h^{-1} for a period of approximately 500 minutes with the linear and the non-linear laws of Hooke in Equation (3.29). As shown by the graphs of the simulated vertical displacements in Figure 6–16, there is very little difference between the two sets of displacements. However, the situation changed drastically in the second set of simulations in which the borehole was pumped at a rate Q = 4,1 m^3 h^{-1}. As shown in Figure 6–17, the vertical displacements in the aquifer began to oscillate almost immediately after the pump was switched

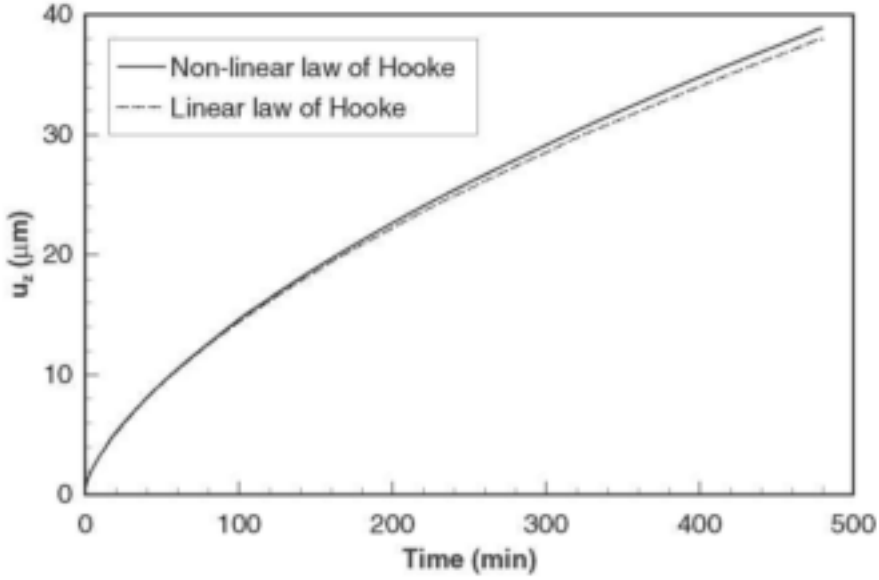

Figure 6–16 Magnitudes of the simulated vertical displacements in the Campus Test Site model at a position 25 mm above the fracture on the wall of the borehole for the linear and non-linear law of Hooke (Q = 1,4 m^3 h^{-1}).

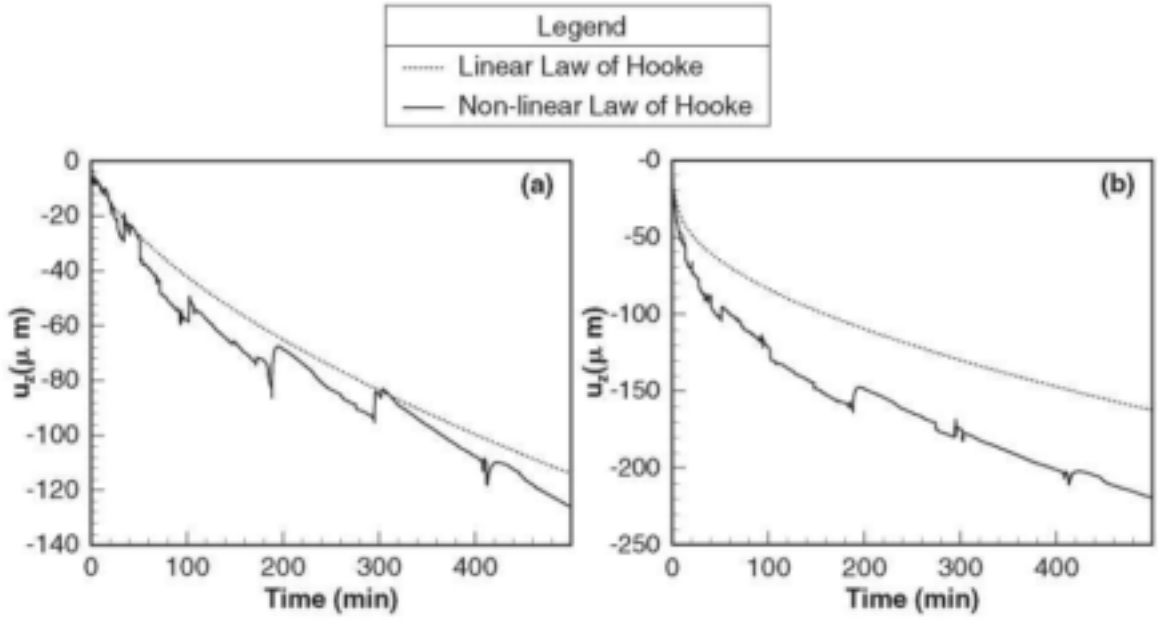

Figure 6–17 Simulated vertical displacements in the Campus Test Site model at positions (a) 25 mm and (b) 200 mm above the fracture on the wall of the borehole for the linear and non-linear law of Hooke (Q = 4,1 m^3 h^{-1}).

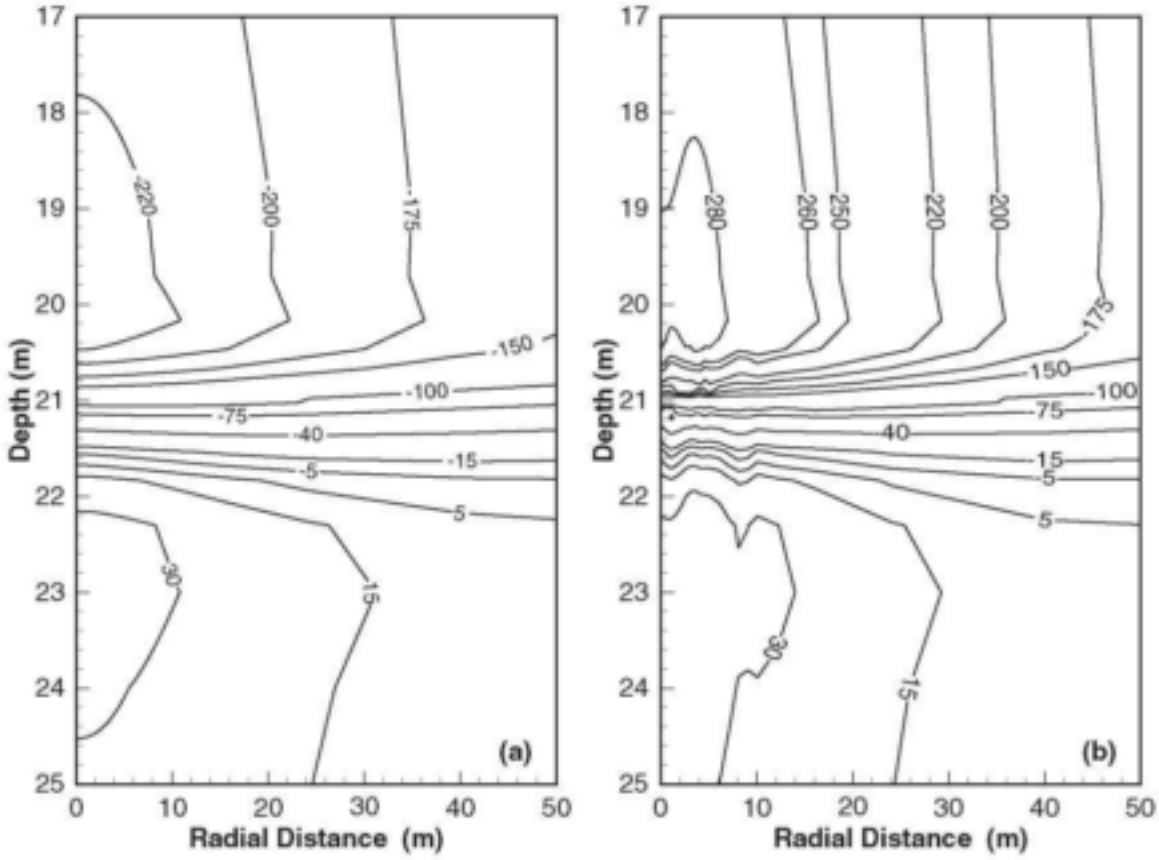

Figure 6–18 Contours of the vertical displacements (in μm) for the Campus Test Site model around the fracture after pumping the borehole for 8 h at a constant discharge rate of 4,1 m^3h^{-1} with (a) the linear law of Hooke and (b) the non-linear stress-strain relation.

on, with magnitudes that tends to increase with time.

An interesting feature of the non-linear oscillations is that they extend radially from the borehole into the aquifer, according to the contour maps of the simulated vertical displacements observed in the Campus Test Site Model after pumping the borehole for 8 h at a discharge rate of 4,1 m^3h^{-1} in Figure 6–18. It is also interesting to observe that the maximum magnitudes of the displacements do not occur at the fracture but at some distance above and below the fracture, with the absolute maxima in the upper aquifer. This could explain the difference in the behaviour of the drawdowns of the upper and lower aquifer in Figure 6–19, observed by Botha *et al.* (1998).

A rather surprising result that arose from the simulation is that the drawdowns for both the linear and non-linear law of Hooke in Figure 6–20 do not display any oscillations. A third simulation was therefore performed with a discharge rate of 8,3 m^3h^{-1} to see if this is behaviour may depend on the discharge rate. The contour maps of the simulated drawdowns in Figure 6–21 show that this is indeed the case. The drawdowns computed with the linear law of Hooke are still smooth, but the drawdowns computed with the non-linear relation are chaotic. The same behaviour is also displayed by the contour maps of the vertical displacements in Figure 6–22.

It is possible that the previously described behaviour of the non-linear deformation model for the Campus test site may be caused by deficiencies in the present model—the non-linear relation in Equation (3.29) may not be appropriate for this aquifer, for example. Nevertheless, it does show that non-linear deformations could have disastrous consequences for an aquifer if not taken care of, especially if it is kept in mind that non-linear deformations do not restore a body to its original form once the deforming force is removed, as illustrated in Figure 3.4, but create residual deformations that deform the body permanently. The contour maps of the simulated residual deformations for the model of the Campus Test Site in Figure 6–23 indicate

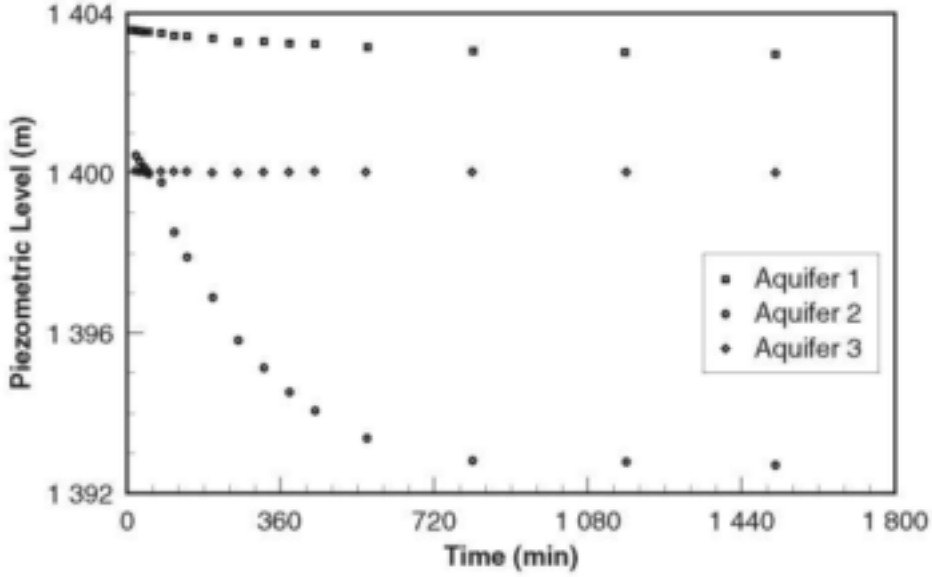

Figure 6–19 Graphs of the piezometric heads in the three aquifers on the Campus Test Site, as measured in piezometer UO18 (Botha *et al.*, 1998) during a constant rate test on Borehole UP16.

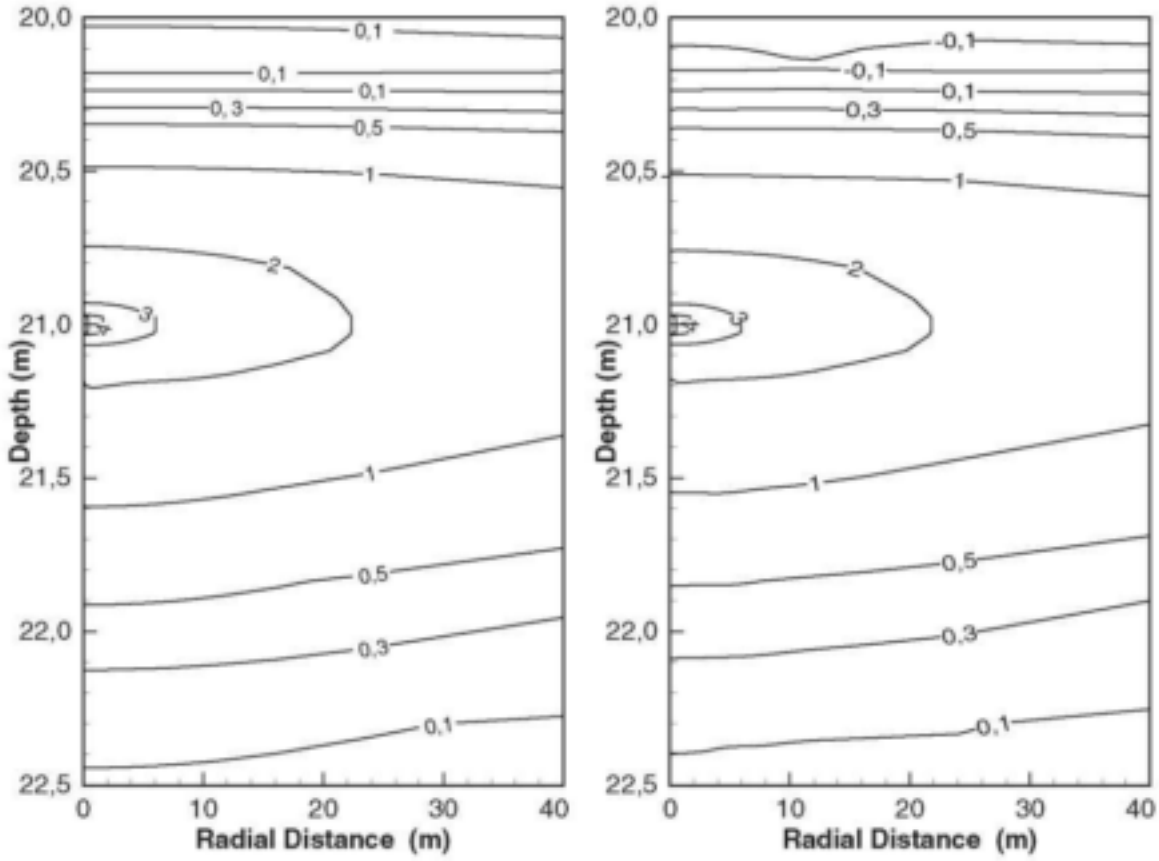

Figure 6–20 Contours of the simulated drawdowns (in μm) for the Campus Test Site model around the fracture after pumping the borehole for 8 h at a constant discharge rate of 4,1 $m^3 h^{-1}$ with (a) the linear law of Hooke and (b) a non-linear law of Hooke.

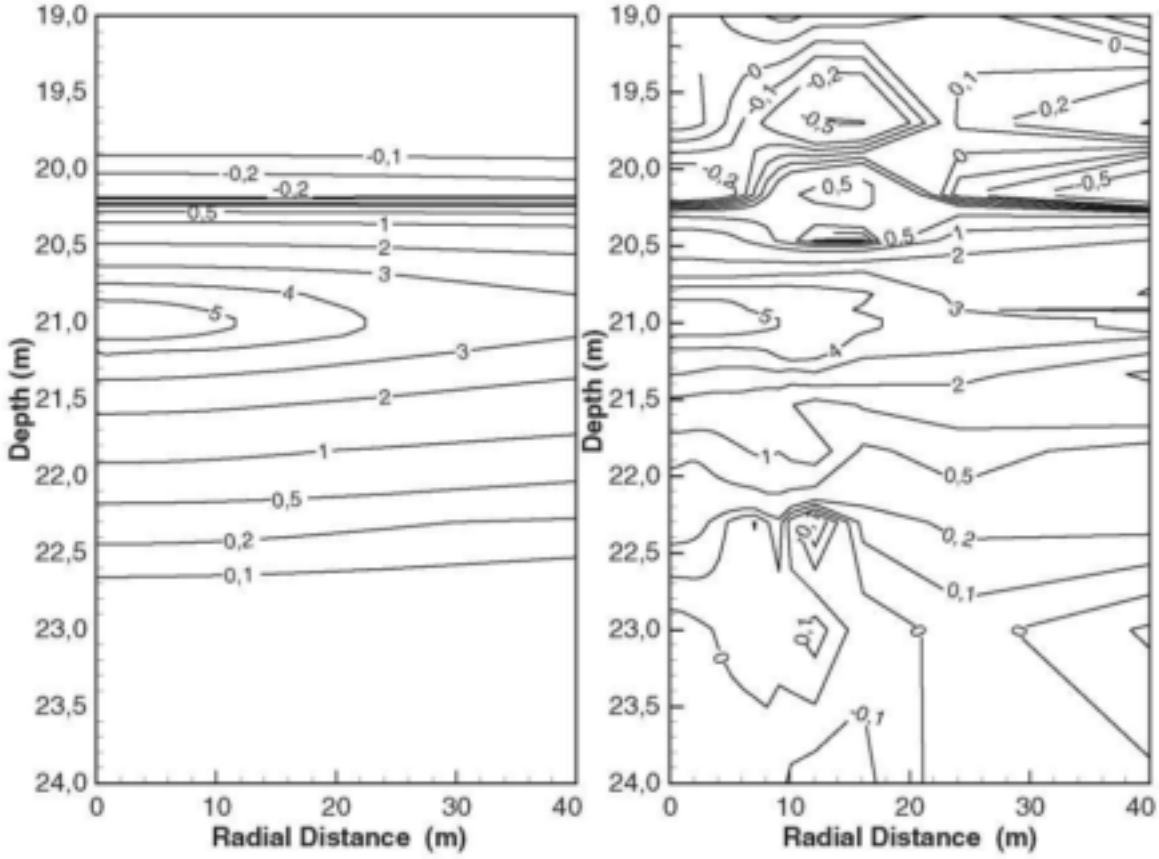

Figure 6–21 Contours of the simulated drawdowns (in m) for the Campus Test Site model around the fracture after pumping the borehole for 8 h at a constant discharge rate of 8,3 $m^3 h^{-1}$ with (a) the linear law of Hooke and (b) the non-linear stress-strain relation.

that residual deformations are most likely to develop close to the borehole and that the magnitudes of the deformations depend on the discharge rate. Notice also that the residual displacements are not uniform in the radial direction—an indication that the pumping of the borehole has changed the shape of the fracture from a flat horizontal plane into a non-linear wave-like surface over the first 20 m to 25 m from the borehole.

The formation of residual deformations is particularly important for Karoo aquifers, since they may ultimately constrict the aperture of a bedding-parallel fracture completely at one or more positions as suggested by the contours of the vertical deformations in Figure 6–22. This phenomenon is illustrated in Figure 6–24, which displays the constriction experienced by a 50 mm thick slice of the aquifer centred on the position of the fracture in the Campus Test Site model, after pumping the borehole for 8 h at the given discharge rates.

The magnitudes of the residual deformations in an actual aquifer will be determined by the elastic parameters of its rock matrix and the discharge rates of boreholes. However, the quadratic growth of the constrictions for the fracture in the model of the aquifer on the Campus Test Site with discharge rate in Figure 6–25, indicate that the discharge rates of boreholes will contribute the most to the constriction of a fracture.

Simulations performed with the Campus Test Site model also suggest that the deformations of the fracture behave very similar to drawdowns observed in natural aquifers. For, as shown in Figure 6–26, the constrictions develop very quickly at early times of pumping and then approach a pseudo steady state within approximately two hours of pumping.

Residual deformations of an aquifer obviously has important implications for the management and life expectancy of a given borehole, because it will cause irreversible structural damages to the porous matrix

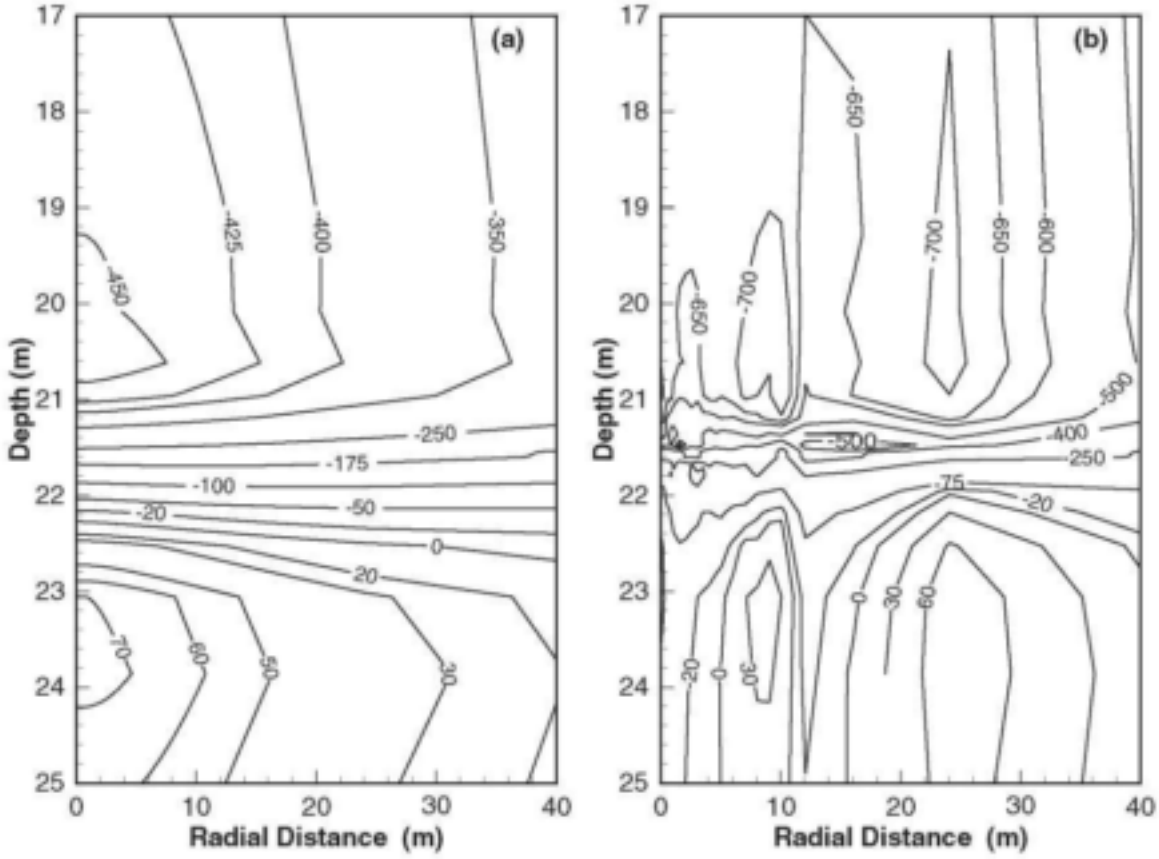

Figure 6–22 Contours of the vertical displacements (in μm) for the Campus Test Site model around the fracture after pumping the borehole for 8 h at a constant discharge rate of 8,3 $m^3 h^{-1}$ with (a) the linear law of Hooke and (b) a non-linear law of Hooke.

surrounding a borehole and even the borehole itself. As shown by the results above, residual deformations are usually very small and would not be important if the rock matrix obeyed the linear law of Hooke. However, this is no longer the case when the rock matrix obeys a non-linear law of Hooke, which allows the residual deformation to accumulate with time. Non-linear deformations may therefore slowly damage and ultimately destroy the ability of horizontal fractures to serve as conduits of water to boreholes over time.

The dependence of the deformations in an aquifer on the discharge rate of a borehole and the accumulation of residual deformations over time implies that the ability of a borehole to yield water must also depend on the discharge rate and how frequently the borehole is pumped. A series of simulations were therefore performed to try to find to what extent the pumping of the borehole in the model of the Campus Site will affect the yield of the borehole. Two basic assumptions were made in these simulations.

a) The borehole is pumped intermittedly for a continuous period of 8 h a day each day of the year, which is similar to the practice followed by many municipalities that depend on groundwater for their supply of water.

b) The borehole will dry up once the horizontal aquifer slice with an aperture of 50 mm (the fracture) has been closed due to the formation of residual constrictions.

The last assumption, which is based on the observation of Botha *et al.* (1998) that a borehole in a Karoo aquifer will only yield water if it intersects a horizontal fracture, allows one to derive an *expected mechanical life* for the borehole, defined as *the time it will take residual constrictions to reduce the aperture of the fracture to zero*. According to the results of the simulations, summarized in Table 6-2, a borehole on the Campus Site will fail in less than six years, if pumped at a rate of 8,3 $m^3 h^{-1}$ for 8 h a day, every day of the

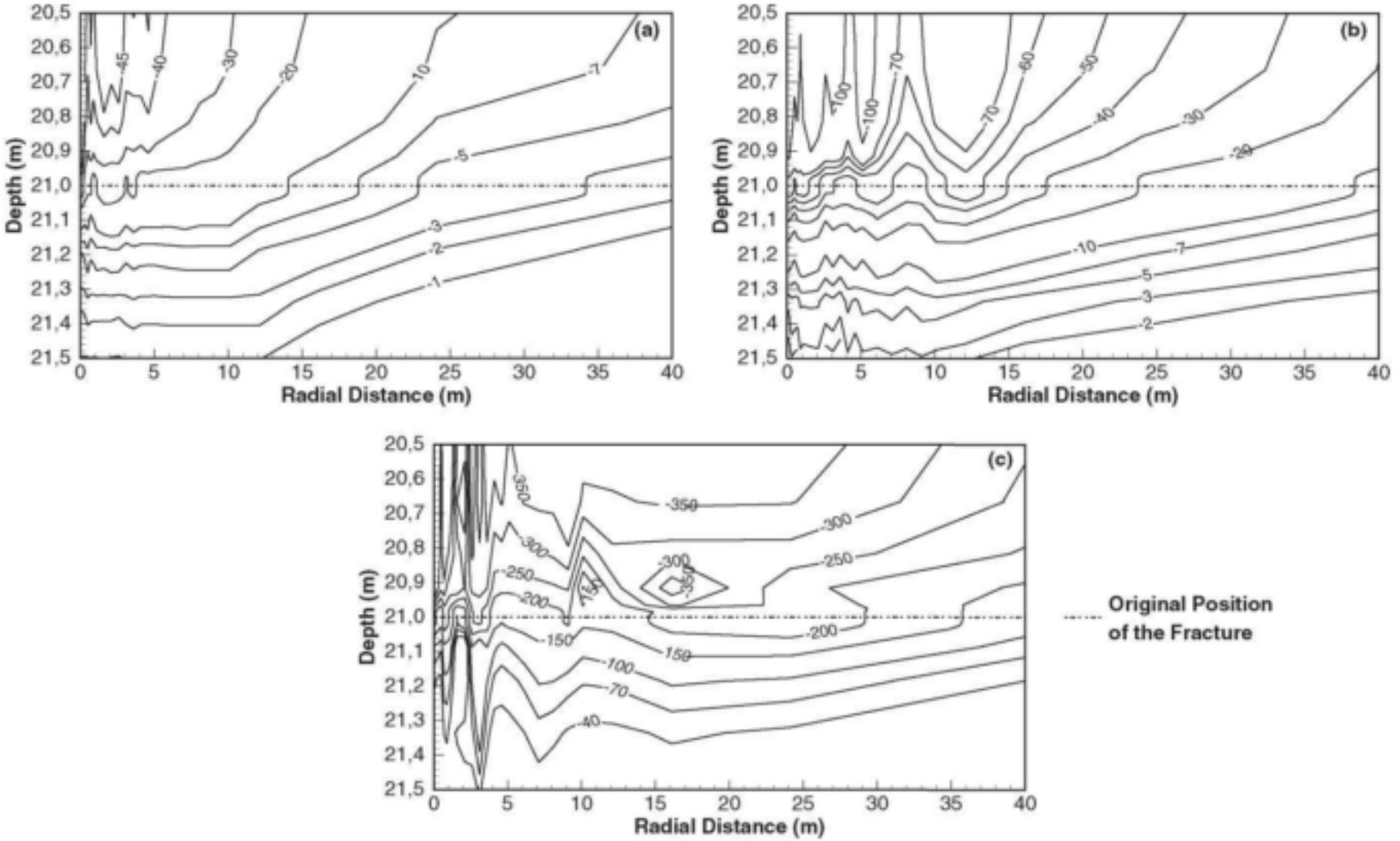

Figure 6–23 Contours of the simulated residual vertical displacements (μm) in the Campus Test Site model after pumping the borehole for 8 h at discharge rates of (a) 2,8 $m^3 h^{-1}$, (b) 4,1 $m^3 h^{-1}$ and (c) 8,3 $m^3 h^{-1}$.

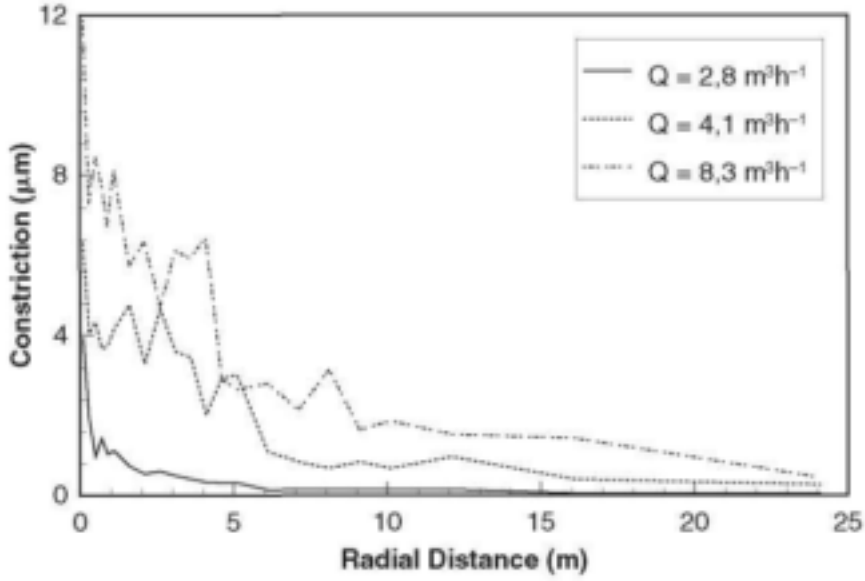

Figure 6–24 Residual constriction of the aperture of the fracture in the Campus Test Site model after pumping the borehole for 8 h at the given discharge rates.

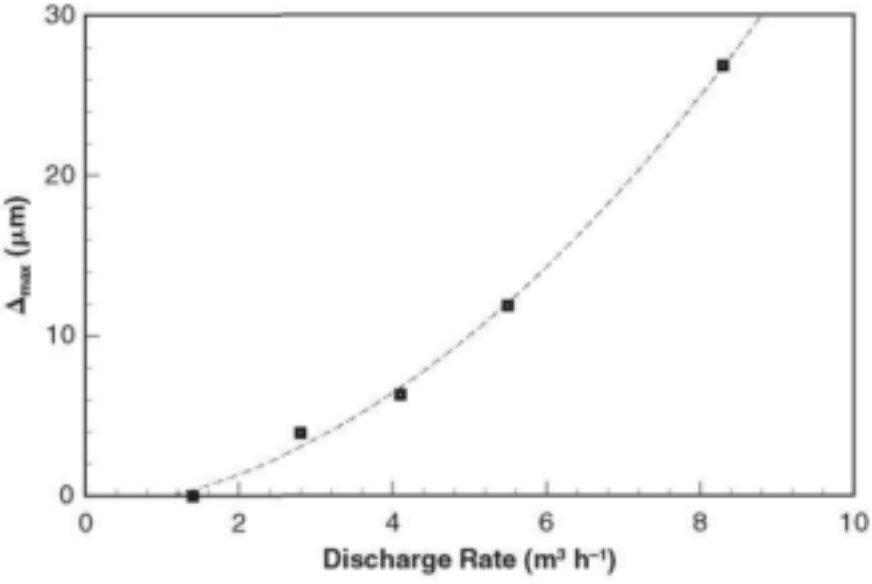

Figure 6–25 Relation between the simulated maximum constriction of the fracture in the Campus Test Site model and the discharge rate of the borehole after pumping the borehole for 8 h at the given discharge rates.

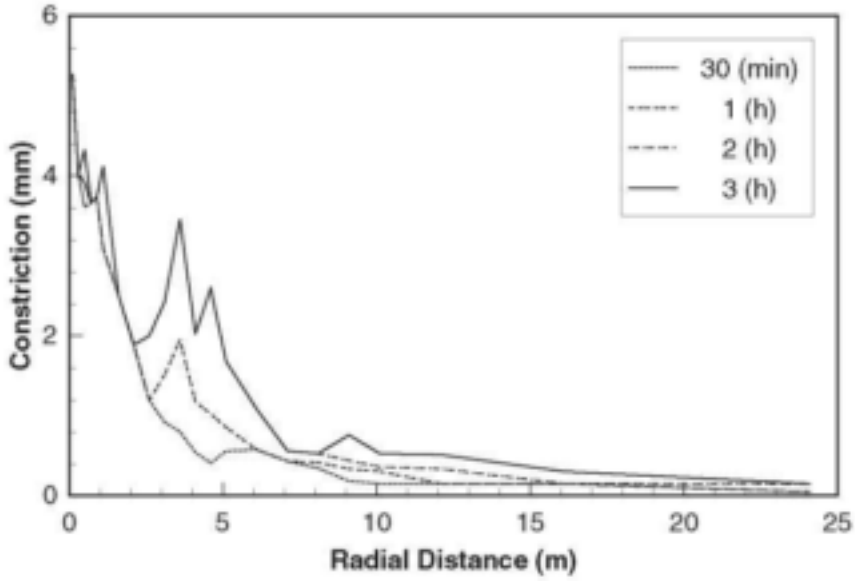

Figure 6–26 Variations of the simulated constrictions in the aperture of the fracture in the Campus Test Site model at various times during the period that the borehole was pumped at a rate $Q = 4{,}1\ \mathrm{m^3\,h^{-1}}$ as functions of the radial distance.

Table 6-2 Expected mechanical life (T_E) of the borehole in the model of the Campus Test Site pumped intermittedly for a period of 8 h a day, every day of the year, as a function of the discharge rate (Q).

Q ($\mathrm{m^3\,h^{-1}}$)	1,4	2,8	4,1	5,5	8,3
T_E (y)	Unlimited	34,85	21,68	11,54	5,10

year. However, the results also indicate that the fracture will suffer no significant mechanical damages, if the discharge rate is kept at or below $1{,}4\ \mathrm{m^3\,h^{-1}}$. These results indicate that the mechanical properties of a fractured aquifer are as important as the hydraulic properties of the aquifer in designing a discharge rate for a production borehole in such an aquifer. It is therefore important that more attention should be paid to the mechanical properties of the aquifer in the management and control of well fields, especially those based on fractured aquifers.

6.4 WATER RELEASED FROM STORAGE

There are in general three mechanisms that contribute to the volume of water pumped from an aquifer through a borehole: water that might flow across the aquifer boundaries, the expansion of the water caused by a reduction in pressure due to the pumping and matrix compression. The contribution of the last two mechanisms is described by the specific storativity, S_0, of an aquifer in the conventional theory of groundwater flow, which is based on the vertical compressibility of the aquifer and the compressibility of water. However, as shown by Equation (3.18), the release of water from matrix compression is actually determined by changes in the dilatational strain of the aquifer, which assumes in cylindrical coordinates the form

$$e = \nabla \cdot u = e_{rr} + e_{\theta\theta} + e_{zz} = \mathrm{D}_r u_r + u_r / r + \mathrm{D}_z u_z$$

It may therefore be interesting to compare the contributions of each member of the dilatational strain to the volume of water available for release in a deforming aquifer, given in cylindrical coordinates by the equation

$$V_w(t) = \iiint e\, r\, dr\, d\theta\, dz = 2\pi \iint e\, r\, dr\, dz = 2\pi V_e(t) \tag{6.1}$$

A basic assumption in the conventional theory of groundwater flow is that there are no horizontal strains in an aquifer during the pumping of a borehole and that the release of water from storage, represented by the

specific storativity, is caused by the strains in the vertical direction only. It may therefore be interesting to compare the contributions of each component of the dilatational strain to the volume of water released from storage. For this purpose use will be made of the *normalized radial yield*, S_r, the *normalized hoop yield*, S_θ and the *normalized vertical yield*, S_z, defined as

$$S_r(r,t)=\frac{1}{V_e(t)}\int_d e_r r dz,\quad S_\theta(r,t)=\frac{1}{V_e(t)}\int_d e_\theta r dz,\quad S_z(r,t)=\frac{1}{V_e(t)}\int_d e_z r dz$$

where d is the thickness of the aquifer and $V_e(t)$ is defined in Equation (6.1). The quantity S_α, with dimensions m^{-1}, can therefore also be viewed as the water that the α-th strain component release from storage per unit length in the radial direction of the aquifer at the position r. The graphs of the three normalized yields in Figure 6–27 clearly shows that the vertical strain contribute the most to the water released from storage in the model of the Campus Test Site, but that one cannot neglect the contributions of the radial strain and especially the hoop strain. This behaviour of the normalized vertical yield clearly support the view of Botha *et al.* (1998) that water predominantly flows vertically in Karoo aquifers. This conclusion is further supported by the graph of the normalized radial dilatational yield over the radius, R, of the borehole

$$S_e(z,t)=\frac{1}{V_e(t)}\int_R e r dr$$

in Figure 6–28. Since S_e can be interpreted as the water released from storage per unit thickness of the aquifer, Figure 6–28 indicates that the borehole withdraws its water essentially from two relatively small domains on both sides of the fracture that enlarges with the discharge rate of the borehole. Notice also that the fracture yields very little water.

An interesting feature of the graphs in Figure 6–27 is that the normalized yields at first increase and then decreases with radial distance from the borehole. The normalized radial yield, in particular, even assumes negative values after a distance of approximately 68 m from the borehole, which implies that the radial strains change at this distance from compressive to extensive. This means that instead of forcing an aquifer to only release water, as one would normally expect, the pumping of a borehole might also force water into storage. This behaviour of the normalized yields implies that the dilatational strain, e, must decrease continuously with distance from the borehole. However, as pointed out above, the dilatational strain is the real physical mechanism controlling the specific storativity, S_0, and storativity, $S = S_0 d$, in the conventional theory of groundwater flow. The specific storativity (or storativity) of an aquifer, determined from conventional hydraulic tests, should therefore be inversely related to the distance from the borehole, as suggested in

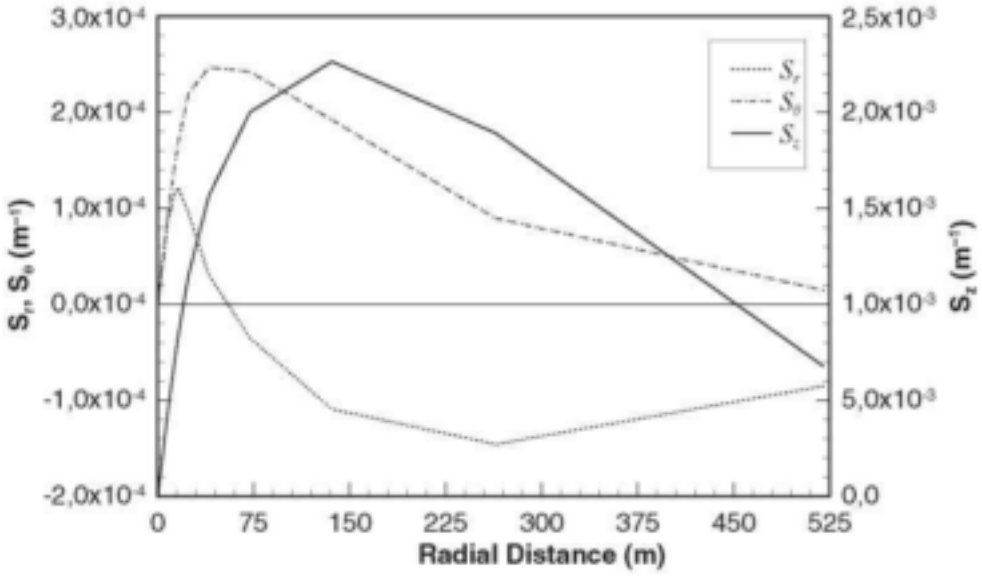

Figure 6–27 Graphs of S_r, S_θ and S_z, computed from the non-linear deformation model of the Campus Test Site after pumping the borehole at a rate of 4,1 $m^3 h^{-1}$ for a period of 8 h.

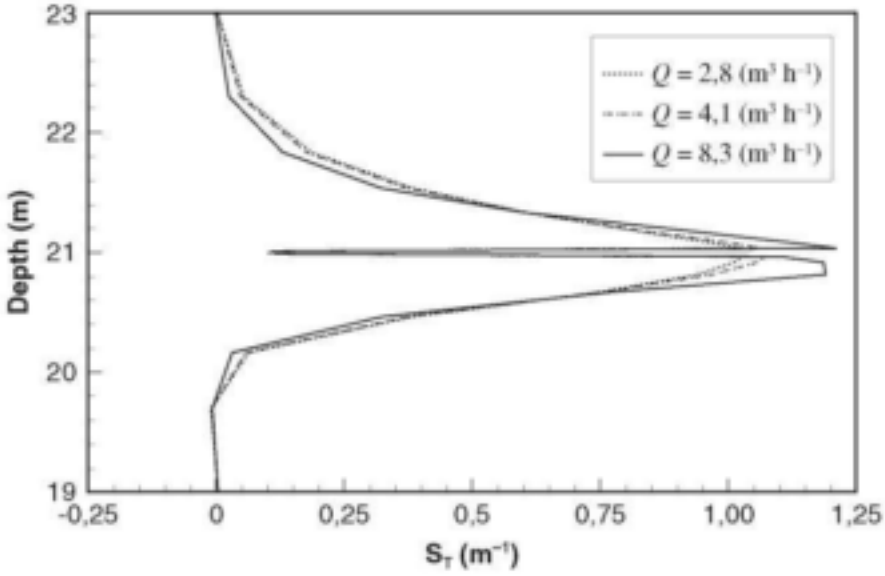

Figure 6–28 Graph of S_s computed from the non-linear deformation model of the Campus Test Site after pumping the borehole at rates of 2,8 $m^3 h^{-1}$, 4,1 $m^3 h^{-1}$ and 8,3 $m^3 h^{-1}$ for a period of 8 h.

Section 5.3.1. It should be noticed that this behaviour is not restricted to the three-dimensional poro-elastic theory under discussion, but should also be observed when only vertical deformations are taken into account. The addition of the hoop and radial strains will only exaggerate the effect. The decrease in the values of S with distance from the pumped borehole observed by Bredenkamp *et al.* (1995) and Botha *et al.* (1998) is therefore *not an artefact of the methods used in the analysis of the tests*, as suggested by Bredenkamp and his co-workers, but *a physical reality*! It is only when the pumping of a borehole stresses an aquifer slightly that this behaviour of the storativities may not be noticeable. This dependence of S on the distance from the pumped borehole is illustrated in Figure 6–29 for two constant rate tests. The values of S_1 were determined from a constant rate test in which borehole UO5 on the Campus Test Site was pumped at a discharge rate of 2,25 $m^3 h^{-1}$ and the S_2-values from a constant rate test in which borehole UP16 was pumped at the same discharge rate. (See Figure 6–2 for the positions of the boreholes.)

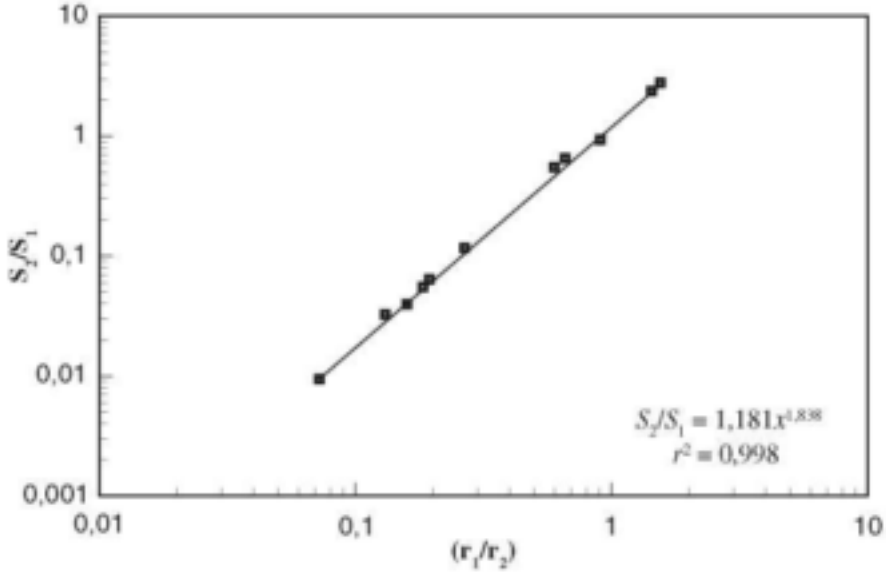

Figure 6–29 Dependence of the Theis-fitted S-value ratios on the inverse ratio of the distance between an observation borehole and the pumped borehole as determined from two constant rate tests performed on the Campus Test Site (Botha *et al.*, 1998). (Subscript 1 refers to a test performed with Borehole UO5 and subscript 2 to a test performed with Borehole UP16.)

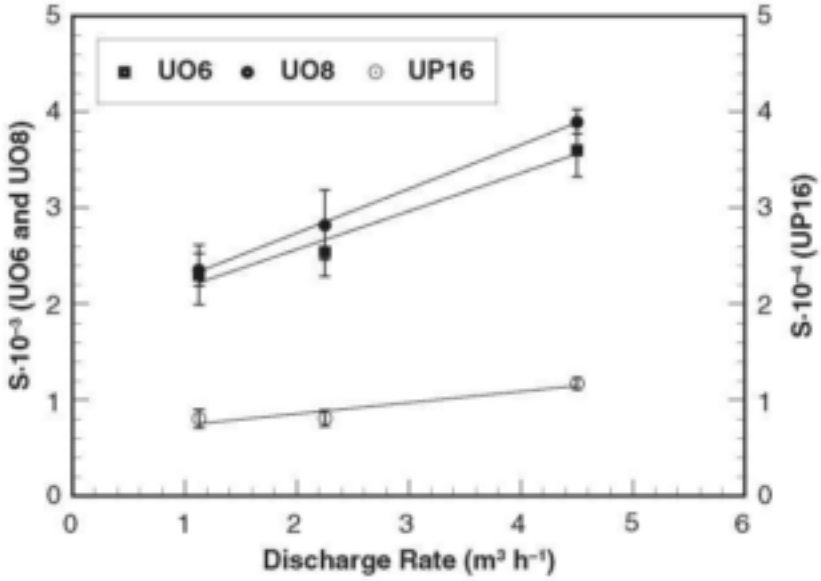

Figure 6–30 Storativity values for three boreholes on the Campus Test Site derived from a series of hydraulic tests in which Borehole UO5 was pumped at different discharge rates (Botha *et al.*, 1998). The variation between the maximum and minimum storativity values, expressed as a percentage of the minimum values are: UO6 56%, UO8 65% and UP16 46%.

It is interesting to note that the relation between S_2/S_1 and r_1/r_2 in Figure 6–29 indicates that one would obtain a different value of S for a borehole centred between UO5 and UP 16 ($r_1 = r_2$) from a constant rate test performed on UO5 than from one performed on U16. One explanation for this behaviour of S would be that the magnitudes of the deformations caused by the pumping of UO16 differ from the magnitudes of the deformations caused by the pumping of UO5 at this position. This implies that the flow of water towards a borehole in Karoo aquifers is not radial symmetric and that the flow paths may differ from one borehole to the next.

If it is kept in mind that the dilatational strains are functions of the displacements, **u**, which depend on the discharge rate of a borehole, see Figures 6–22 and 6–23, S_0 and hence S should also be functions of the discharge rate of a borehole. That this is indeed the case is shown by the graphs of S as a function of the discharge rate in Figure 6–30. (Notice again the inverse dependence of S on the distance from the producing borehole, given that UO6, UO8 and UP16 are situated respectively at distances of 5,08; 4,98 and 32,40 m from UO5.) *The specific storativity and storativity of an aquifer are therefore essentially determined by the discharge rate and are not independent parameters as assumed in the conventional theory of groundwater flow*. This behaviour of S raises the question whether a large fraction of the variations in values of S, derived from conventional hydraulic tests, should not be ascribed to differences in the discharge rates and distances of observation boreholes from the discharging borehole rather than heterogeneities in the aquifer, as is commonly assumed?

6.5 CONCLUSIONS

The most important result that emerged from the present study of a poro-elastic model for the Campus test Site, is that the pumping of a borehole always introduces stresses in an aquifer that could damage the aquifer and borehole permanently, particularly fractured aquifers, if not controlled properly. However, since the extent of the damage depends on the discharge rate of the borehole, it can be controlled by controlling the discharge rate of the borehole. Indeed, the model for the Campus Test Site indicated that every borehole has a critical discharge rate, and that the aquifer would suffer no irreversible, mechanical damage if the discharge rates of boreholes were kept below their critical rate. The discharge rates of boreholes, especially those used for water supply purposes, should therefore be kept as close as possible to (preferably below) this critical discharge rate.

The maximum mechanical damages caused by pumping a borehole in an aquifer that deforms non-linearly occur within a relatively short time after the pump has been switched on (2 h in the present model), and then

assume a pseudo steady state. However, it must be kept in mind that non-linear deformations are always accompanied by residual deformations that *accumulate with time* and that the magnitudes of the deformations increase with the discharge rate of a borehole. Too high discharge rates may therefore not only cause considerable difficulties for communities that depend on groundwater for their supply of water today, but may even deny future generations of water. Although it may take many years before the damage becomes noticeable, it can also occur literally overnight, for, it must be kept in mind that residual deformations are always accompanied by residual stresses, which will build-up steadily over the years. The possibility therefore exits that a water-yielding (or water-bearing) fracture can collapse suddenly and without warning.

A borehole or aquifer that has suffered mechanical damage can never be restored. It is therefore important that methods should be devised to eliminate, or at least limit the accumulation of residual stresses and strains. One approach to achieve this would be to include another parameter in the concept of the sustainable yield of a borehole—*the expected mechanical life of a borehole*. Unfortunately, the only method available today to determine this parameter, and the critical discharge rate, is to develop a poro-elastic model for the aquifer of concern. However, there is a practical (albeit unusual) approach to limit the effects of residual strains—pump the borehole continuously for as long as possible. For example, the model for the Campus Test Site shows that the expected mechanical life of a borehole could be tripled by pumping it continuously for 24 h over a period of 72 h, instead of pumping it intermittently for 3 sessions of 8 h each over the same period.

A very important result that emerged form this study is that the specific storativity and storativity of an aquifer, as defined in the conventional theory of groundwater flow, are not independent parameters, but depend inversely on the distance from the pumped borehole and linearly on its discharge rate. This behaviour of the storativity is caused by the fact that the water released from storage in an aquifer depends on the dilatational strain that decreases with distance from the borehole, while its magnitude increases with the discharge rate of a borehole.

The fact that storativity is not an independent parameter and therefore cannot account fully for the water released from storage in an aquifer, could have dire consequences for a number of practices commonly used in groundwater investigations. For example, the use of storativities, derived with conventional methods for the analysis of hydraulic tests and based on observation boreholes close to a pumped borehole (worse the pumped borehole itself), could lead to serious overestimates of quantities such as the sustainable yield of a borehole or the volume of water in an aquifer.

In conclusion, it can be said that the poro-elastic model for the Campus Test Site indicated that deformations play a much more important role in the physical behaviour of aquifers than commonly believed. Considerably more attention should therefore be paid to deformations in the management and control of groundwater resources than in current practices, to ensure that these resources will also be available to future generations.

CHAPTER 7

SENSITIVITY ANALYSIS

7.1 GENERAL

It follows from Equations (3.18) and (3.23) that the deformation of an aquifer does not depend only on the discharge rate, but is also a function of both the mechanical and hydraulic properties of the aquifer. This means that one must have a good knowledge of these parameters in order to protect an aquifer from mechanical damage. Unfortunately, it is not easy to determine the parameters in the field. It was thus thought worthwhile to perform a sensitivity analysis of the numerical results to see which of the major parameters that appear in Equations (3.18) and (3.23) might be particularly important in studies of aquifer deformations.

The results in Chapter 6 indicate that the drawdowns and displacements in the Campus Test Site model behaves very similar whether a linear on non-linear law of Hooke is used to describe the relation between the stresses and the strains. The investigation of the sensitivity of the model to the various parameters will consequently be restricted to the linear law of Hooke.

Since the discharge of a borehole is usually the main source for the development of unbalanced stresses in an aquifer, the discussion below begins with a study of the discharge rate in Section 7.2. This is followed by a study of the hydraulic conductivity in Section 7.3, the shear modulus in Section 7.4 and the porosity in Section 7.5. The major results and conclusions derived from the study is analyzed in Section 7.6.

7.2 THE DISCHARGE RATE

A series of simulations with various discharge rates were performed to investigate the sensitivity of the model to changes in Q. As shown in Figure 7–1, both the drawdown and the magnitude of the vertical displacements increase continuously and linearly with Q, at rates of 1,399 h m^{-2} and 7,509 10^{-6} h m^{-2} respectively. The contour maps of the drawdowns in Figure 7–2 and the vertical displacements in Figure 7–3 show that domain of the aquifer affected by the pumping also increases continuously with the discharge rate.

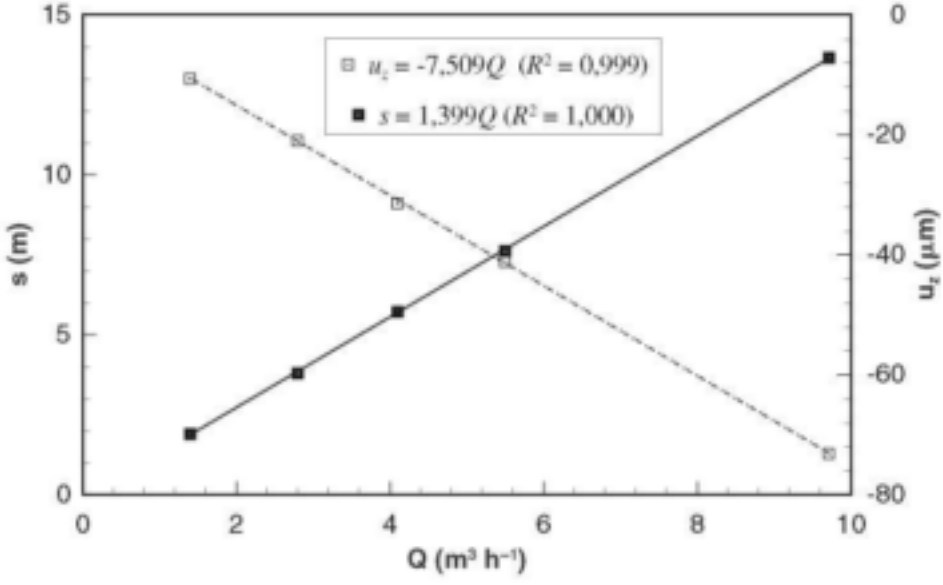

Figure 7–1 Simulated drawdowns (s) and vertical displacements (u_z) at a point 25 mm above the fracture on the wall of the borehole in the Campus Test Site Model after pumping the borehole for 1 h as a function of the discharge rate (Q).

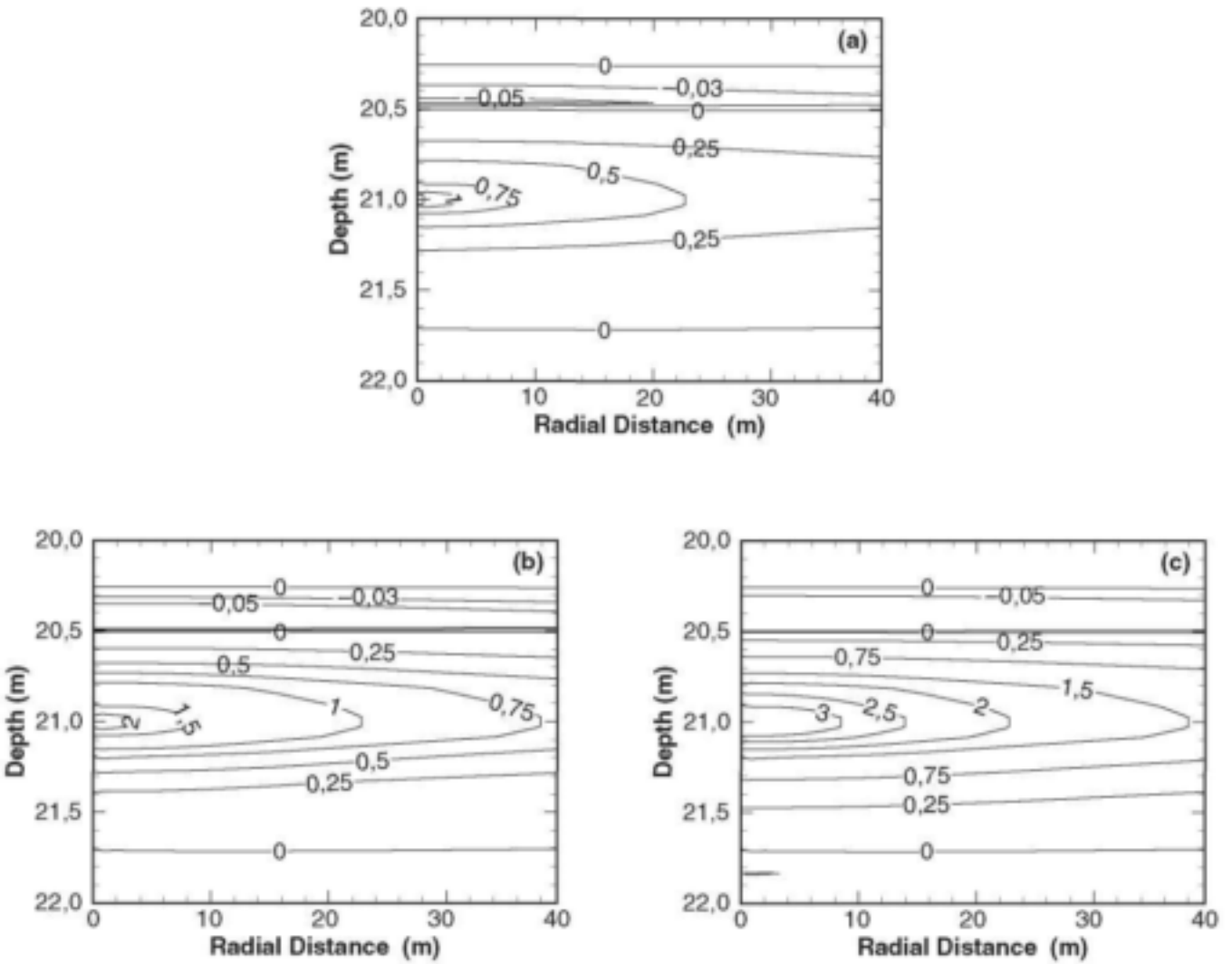

Figure 7–2 Influence of the discharge rate on the simulated drawdowns in the Campus Test Site Model after pumping the borehole for 1 h at discharge rates of (a) 1,4 $m^3 h^{-1}$, (b) 2,8 $m^3 h^{-1}$ and (c) 5,5 $m^3 h^{-1}$.

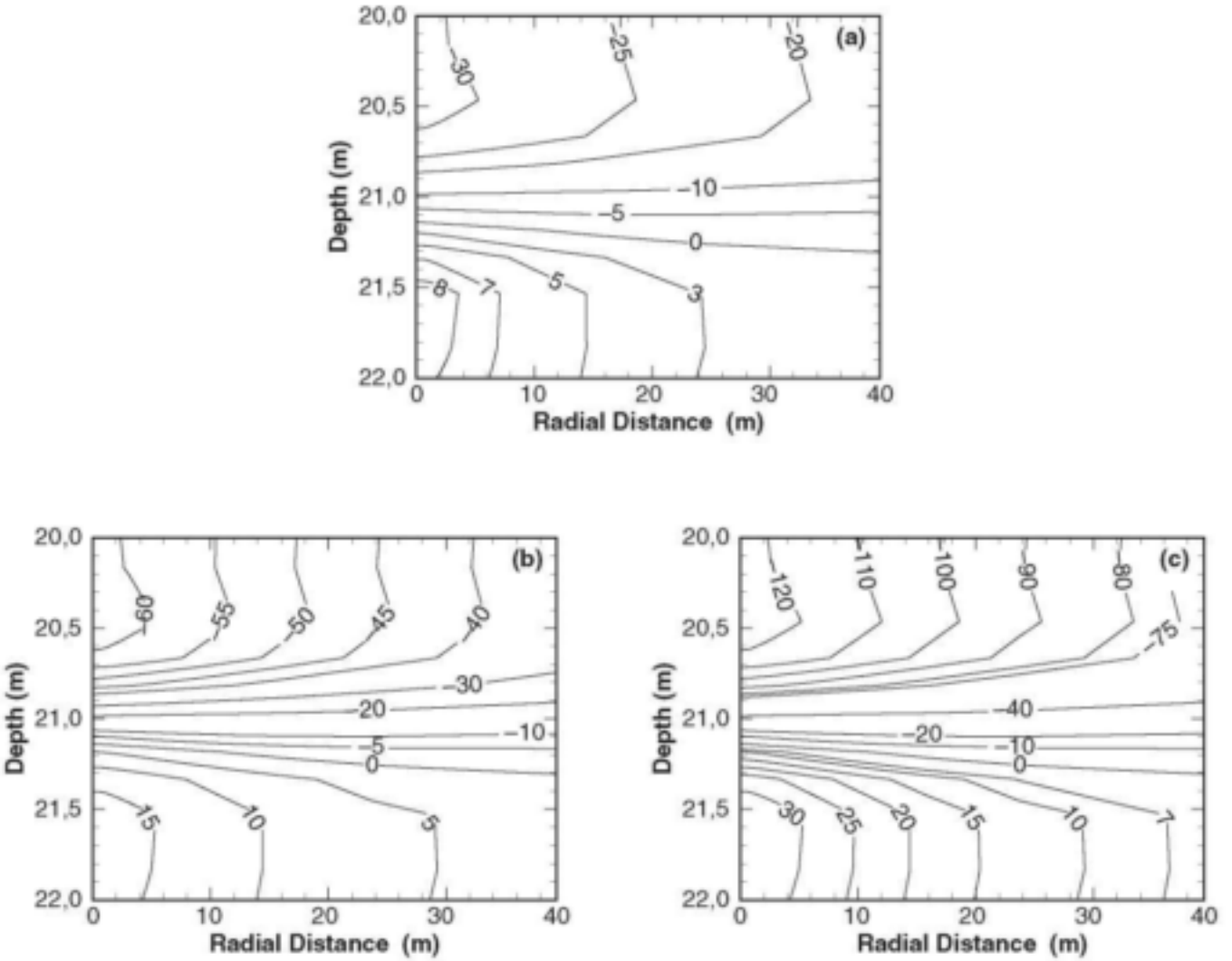

Figure 7–3 Influence of the discharge rate on the simulated vertical displacements in the Campus Test Site Model after pumping the borehole for 1 h at discharge rates of (a) 1,4 $m^3 h^{-1}$, (b) 2,8 $m^3 h^{-1}$ and (c) 5,5 $m^3 h^{-1}$.

An interesting feature of the contour maps in Figure 7–2 is that the borehole essentially obtains its water from the immediate neighbourhood of the fracture, between the depths 20,25 m and 21,7 m, in agreement with the full three-dimensional model of the aquifer developed by Botha *et al.* (1998). The domain affected, however, increases continuously in the radial direction with the discharge rate. This behaviour is not shared by the vertical displacements in Figure 7–3, which develop throughout the aquifer with magnitudes that increase with the discharge rate, but decrease with distance from the borehole. This implies that if a fracture fails the failure will most likely be confined to the immediate neighbourhood of the borehole. As conjectured by Botha *et al.* (1998), this behaviour of the vertical displacements may explain why it is often possible to drill another high-yielding borehole in the Karoo formations within a few metres from one that failed previously. It must be remembered though that if a fracture fails it will damage the aquifer in the neighbourhood of the failure permanently. One cannot therefore expect to replace mechanically damaged boreholes *ad infinitum* in a given aquifer.

7.3 THE HYDRAULIC CONDUCTIVITY

A similar analysis was carried out with the hydraulic conductivity. In this case numerical experiments were performed using a discharge rate of $Q = 2{,}8\ m^3 h^{-1}$ and multiples of the radial component of the hydraulic conductivity tensor, nK_{rr}, with K_{rr} computed as described in Section 6.1.1.

A very interesting result that followed from the simulations is that the drawdown and the magnitudes of vertical displacements are inversely related to the hydraulic conductivity, as illustrated in Figure 7–4. This implies that the drawdown and deformation of an aquifer decreases as the hydraulic conductivity increases. This behaviour is of course well-known in the case of the drawdown. However, the result for the deformations seems to be new, since no reference to such behaviour could be traced in the available literature.

The inverse dependence of the drawdowns and deformations on the hydraulic conductivity also applies to the domain of the aquifer affected by the pumping of a borehole, as can be seen from the contour maps of the simulated drawdown in Figure 7–5 and the simulated vertical displacements in Figure 7–6. The drawdowns are again restricted to the neighbourhood between 20,25 m and 21,7 m, while the displacements occur throughout the aquifer.

The inverse relation between the deformations and hydraulic conductivity, K_{rr}, raises the question: do the deformations depend inversely on K_{rr}, or is K_{rr} possibly a function of the deformations? It is difficult to answer this question in the absence of more detailed experimental information and certainly not in the context

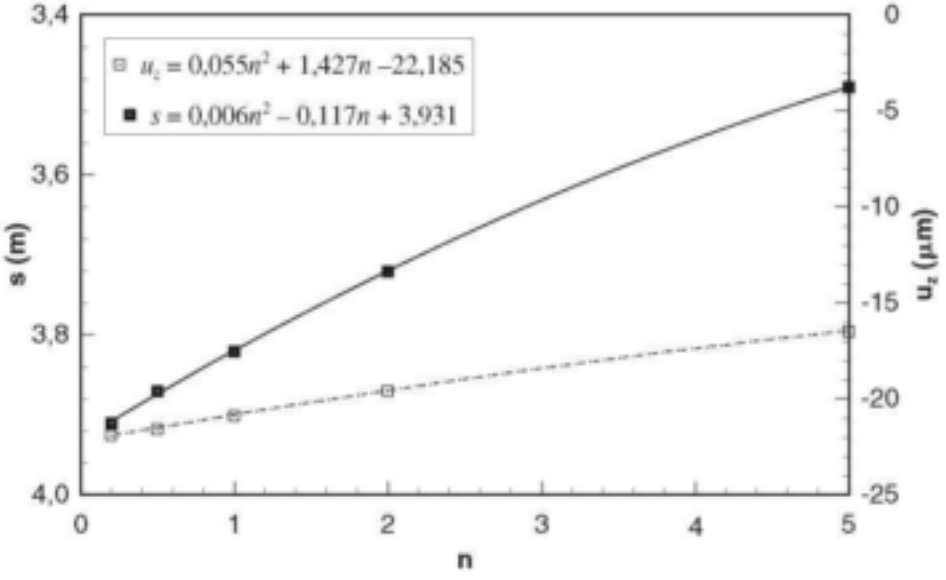

Figure 7–4 Simulated drawdowns (s) and vertical displacements (u_z) at a point 25 mm above the fracture on the wall of the borehole in the Campus Test Site Model after pumping the borehole for 1 h at a discharge rate of 2,8 $m^3 h^{-1}$ as a function of multiples, n, of the radial hydraulic conductivity (K_{rr}).

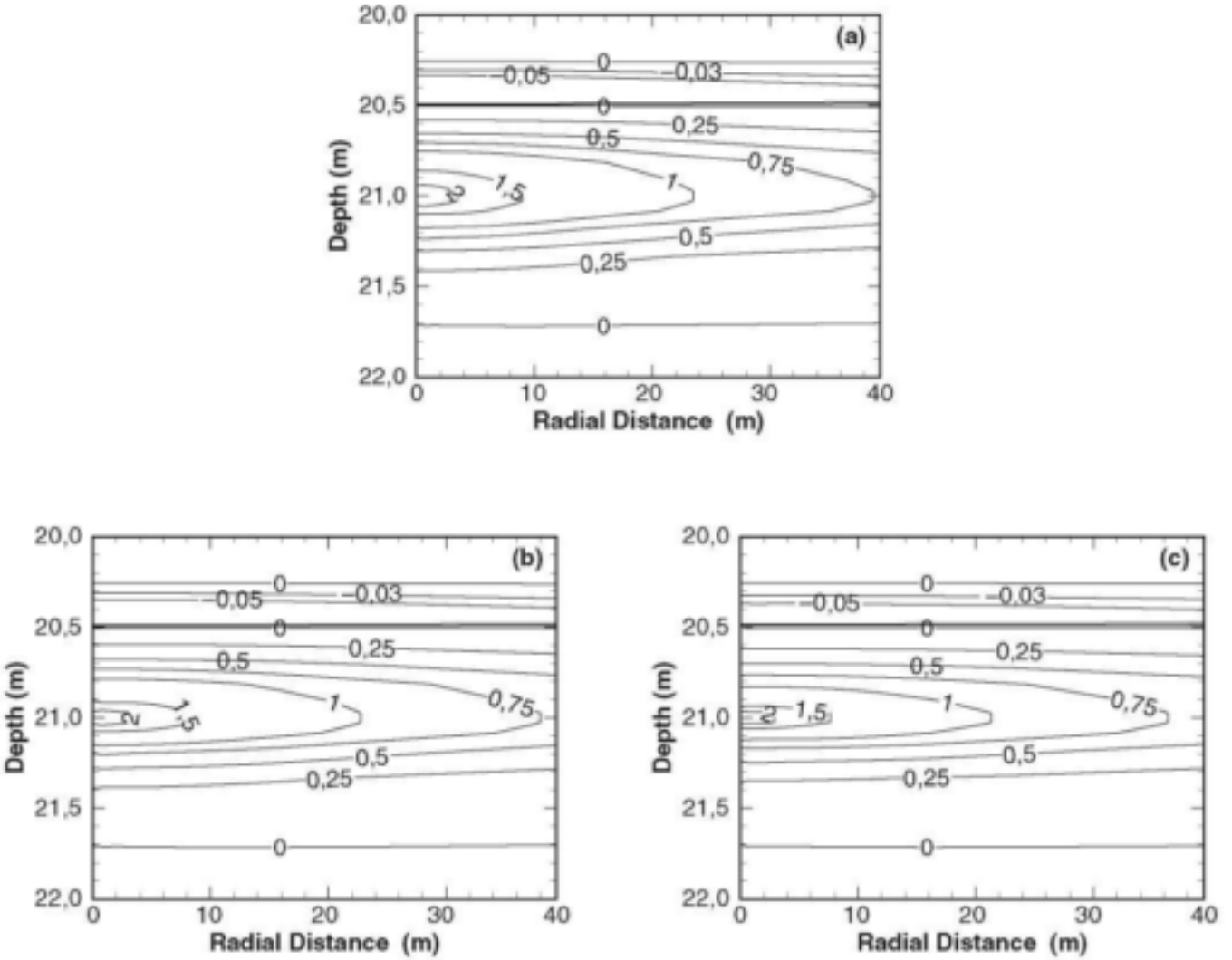

Figure 7–5 Influence of the hydraulic conductivity on the simulated drawdowns in the Campus Test Site Model after pumping the borehole for 1 h at discharge rate of 2,8 $m^3 h^{-1}$ with hydraulic conductivity values of (a) $K_x/2$, (b) K_x and (c) $2K_x$.

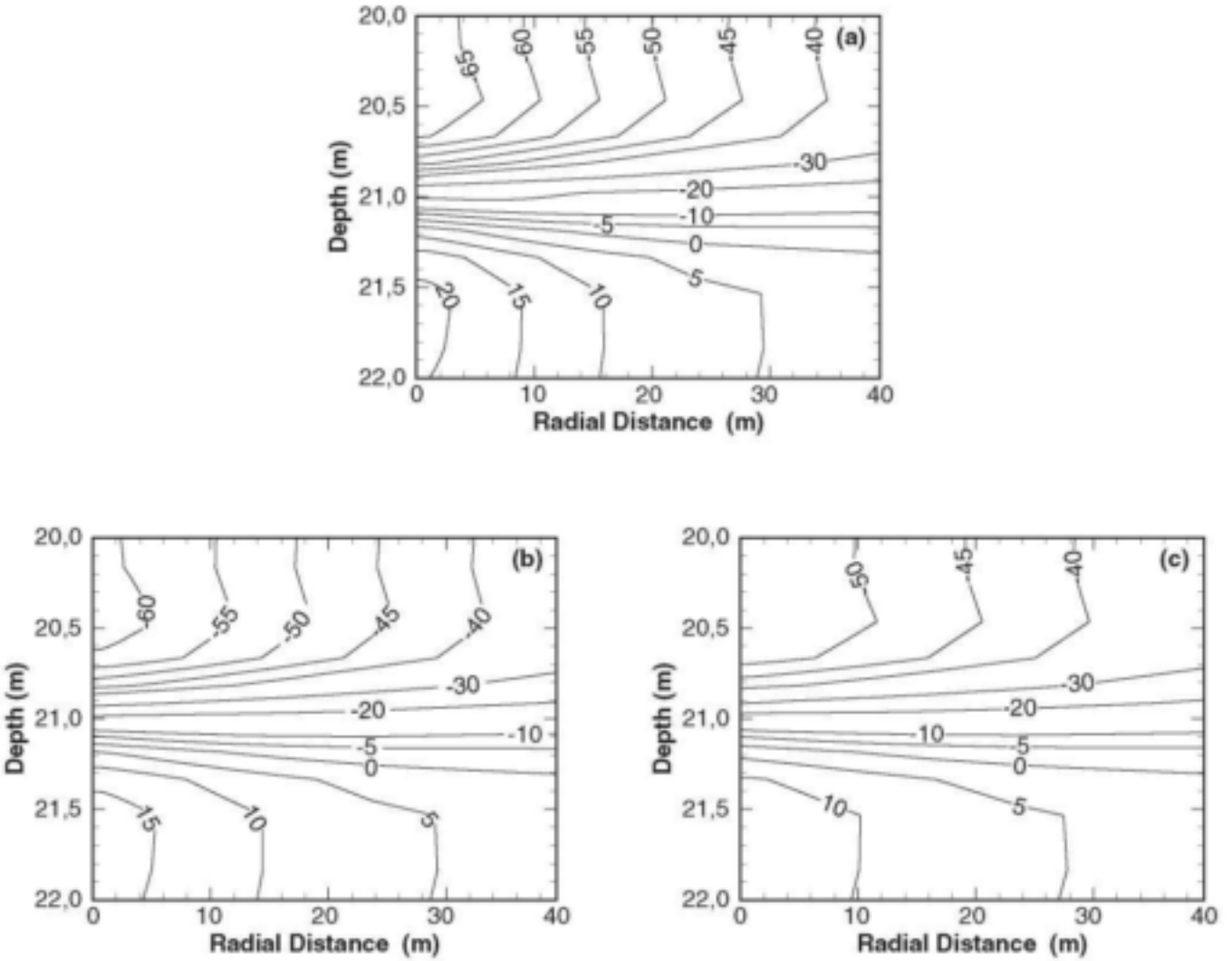

Figure 7–6 Influence of the hydraulic conductivity on the simulated vertical displacements in the Campus Test Site Model after pumping the borehole for 1 h at discharge of 2,8 m^3h^{-1} with hydraulic conductivity values of (a) $K_{rr}/2$, (b) K_{rr} and (c) $2K_{rr}$.

of the present model. However, it is worth to note that the hydraulic conductivity tensor (**K**) is introduced into the groundwater flow equation and Equation (3.18), the equation governing the flow of water in the present model, through Darcy's law, which is not related to deformations superficially. It is well-known though that **K**, which describes the ease with which water flows through the rock matrix, is related to the permeability tensor, **k**, of the rock matrix through the equation (Bear, 1972; Botha, 1996)

$$\mathbf{K} = \mathbf{k}\rho g/\mu$$

where, g is the acceleration of gravity, with ρ the density and μ the dynamic viscosity of the water. The permeability could therefore be interpreted as a parameter that describes the extent to which the rock matrix obstructs the flow of groundwater through its roughness and tortuosity, for example. Since deformations will obviously have an influence on the roughness and tortuosity of the rock matrix, it would make more sense, from the physical point of view, to invert the relation between the displacements and K_{zz} and interpret it as a relation between **K** and the deformations.

It is conceivable that small deformations might enhance **k** and thus **K**, but that large deformations might reduce it. The latter situation may especially develop at high discharge rates in an aquifer that deforms non-linearly and the deformations become chaotic, as illustrated in Figure 6-22. This presumed behaviour of **k** could explain the dependence of T (the scalar, two-dimensional equivalent of **K**) on the discharge rate of the boreholes in Figure 7–7.

Since the magnitudes of the deformations, which depend on the discharge rate, decrease with distance, one would expect that T, therefore **k**, should also decrease with distance from a pumped borehole. That this indeed the case with T, is illustrated by the transmissivities in Figure 7–8, determined from the same set of constant rate tests used in drawing Figures 6–29 and 7–7. It is important to remember though that **k** is a tensor that also depends on various properties of the rock matrix, particularly the orientation of the grains, and therefore cannot be described in terms of the deformations alone, as is the case with the specific storativity. This could explain the somewhat irregular behaviour of the transmissivities near the production borehole in Figure 7–8. For, although UO8 is situated closer to UO5 than UO6 (4,98 and 5,08 m respectively), Figure 6–2 shows that UO6 and UO5 are orientated in the main direction of the palæo-flows responsible for the deposition of the formations on the Campus Test Site, while UO8 is situated perpendicular to the main palæo-flow direction. The tensorial properties of the permeability and deformations may therefore play a much more important role in the behaviour of Karoo aquifers than currently assumed. It may therefore be worthwhile to

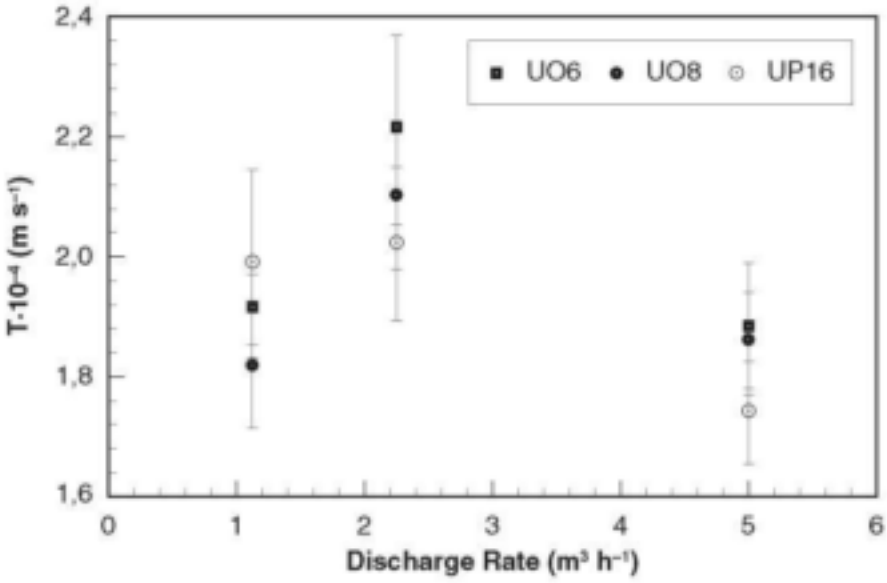

Figure 7–7 Dependence of the Theis-fitted T-values on the discharge rate of a borehole as determined from constant rate tests performed on Borehole UO5 at the Campus Test Site (Botha *et al.*, 1998). The variation between the maximum and minimum T-values, expressed as a percentage of the minimum T-value are: UO6 18%, UO8 13% and UP16 16%.

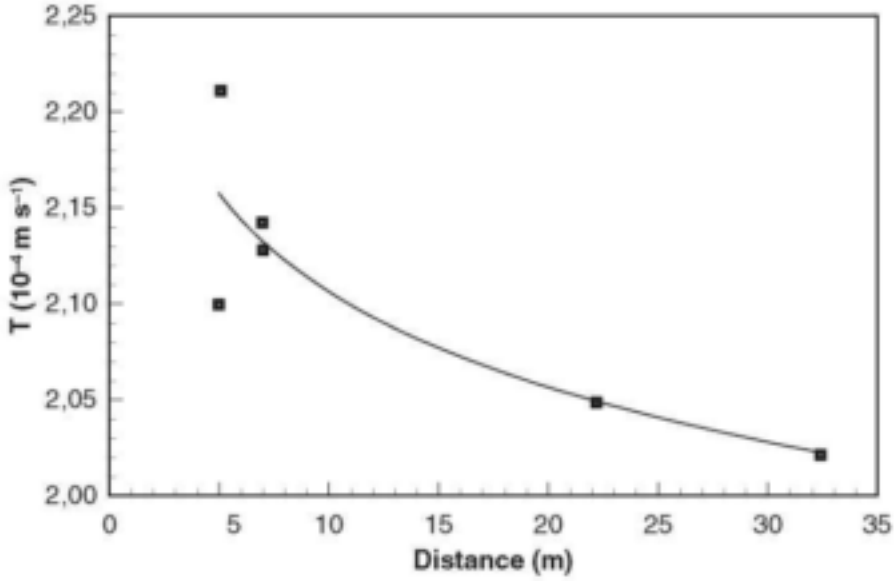

Figure 7–8 Dependence of the Theis-fitted T-values determined from the constant rate tests of (Botha *et al.*, 1998) on the distance from Borehole UO5.

study the behaviour of **k** in more detail experimentally, either through laboratory experiments or in the field, with the view to describe the relation between **k**, the rock properties and the deformations that may develop in the aquifer during the pumping of a borehole more exactly.

The previous results and the discussion of the volume of water released from storage in Section 6.4 clearly indicate that deformations not only control the volume of water that an aquifer is able to release from storage, but also how easily the water is transmitted by the aquifer. Aquifer deformations might therefore play a much larger role in the behaviour of aquifers, particularly Karoo aquifers, than assumed until now.

7.4 THE SHEAR MODULUS

The same approach used in studying the sensitivity of the Campus Test Site model to changes in the hydraulic conductivity was also used to study its sensitivity to multiple values of the shear modulus G, assumed to be a constant = 2,9 10^{+7} Pa. Since it is known that the drawdown in an aquifer depends inversely on its specific storativity, the expressions for the specific storativity and the isothermal compressibility of the rock matrix in Equations (5.1) and (5.2) indicate that the drawdown in the aquifer must be a direct function of the shear modulus. In other words, the more rigid the aquifer is the higher will the drawdown be for a given discharge rate, while the opposite must be true for the deformations. That this is indeed the case is illustrated by the behaviour of the drawdown and vertical displacements as functions of nG in Figure 7–9, which also show that the dependencies are non-linear.

The domain of the aquifer affected by the pumping of a borehole displays a similar behaviour. Although the major drawdowns in Figure 7–10 always occur in the neighbourhood of the fracture plane, the magnitudes of the drawdowns increase steadily across the aquifer as nG increases, while the opposite is true for the vertical displacements in Figure 7–11.

It is interesting to note that the vertical extent of the domain from which the borehole withdraws its water in Figure 7–2 and Figure 7–5 (as measured by the 0 m drawdown contour at depths of 20,25 m and 21,7 m) remained very much the same, notwithstanding the variation in both the discharge rate and hydraulic conductivities. However, this is not the case with the contour maps in Figure 7–10, where the 0 m contour at 20,25 m completely disappeared from the map and the one at 21,7 m shifted to a depth of approximately 21,9 m for n = 2. The more rigid an aquifer is the larger is the domain from which the borehole withdraws its water and the steeper the drawdown. Drawdowns observed in the field, might therefore be more sensitive to variations in the rigidity of an aquifer than the discharge rate. Nevertheless, it must be remembered that the discharge rate creates the strains, while G determines their magnitudes.

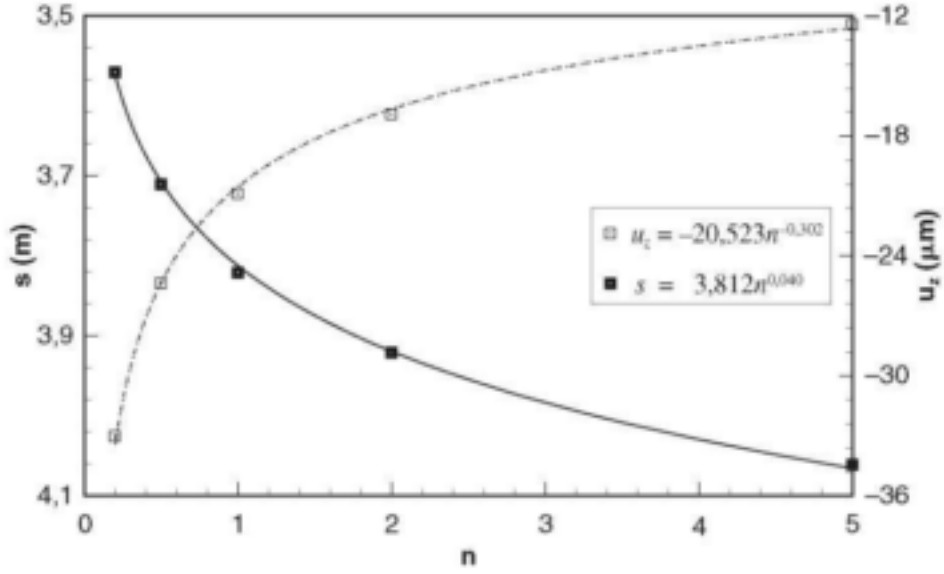

Figure 7–9 Simulated drawdowns (s) and vertical displacements (u_z) at a point 25 mm above the fracture on the wall of the borehole in the Campus Test Site Model after pumping the borehole for 1 h at a discharge rate of 2,8 m^3h^{-1} as a function of multiples, n, of the shear modulus G.

7.5 THE POROSITY

Since groundwater occurs only in the voids of geological formations, it is natural to expect that variations in the porosity may have a profound effect on both the drawdowns and the displacements. However, as can be seen in Table 7-1, this is not the case. The magnitudes of the vertical displacements show a slight decrease of

Table 7-1 Simulated drawdowns (s) and vertical displacements (u_z) at a point 25 mm above the fracture on the wall of the borehole in the Campus Test Site Model after pumping the borehole for 1 h at a discharge rate of 2,8 m^3h^{-1} as functions of the porosity ε of the aquifer.

ε	s (m)	u_z (µm)
0,15	3,82	–20,94
0,30	3,82	–20,85
0,60	3,82	–20,76

approximately 0,8% as ε increases fourfold, but the drawdowns remain constant. Although the porosity of the earth's subsurface may play an important part in unsaturated flow, it does not seem to be important in saturated flow, especially as far as the behaviour of the piezometric head is concerned.

7.6 CONCLUSIONS

The most important feature derived from the study of the dependence of the drawdown on the discharge rate in the model for the Campus Test site is that the borehole always withdraws its water from the immediate neighbourhood of the fracture, but that the domain increases continuously in the radial direction. This behaviour is, however not shared by the vertical displacements, which develop throughout the aquifer, but with magnitudes that decrease with distance from the borehole. The extreme displacements therefore always occur near the borehole. This implies that if a fracture fails the failure will most likely be confined to the immediate neighbourhood of the borehole.

Another interesting result that followed from the sensitivity analysis of the parameters in the model for the aquifer on the Campus Test Site is the inverse relations that exist between the drawdown and magnitudes of vertical displacements and the hydraulic conductivity. It is difficult to explain the inverse relation between

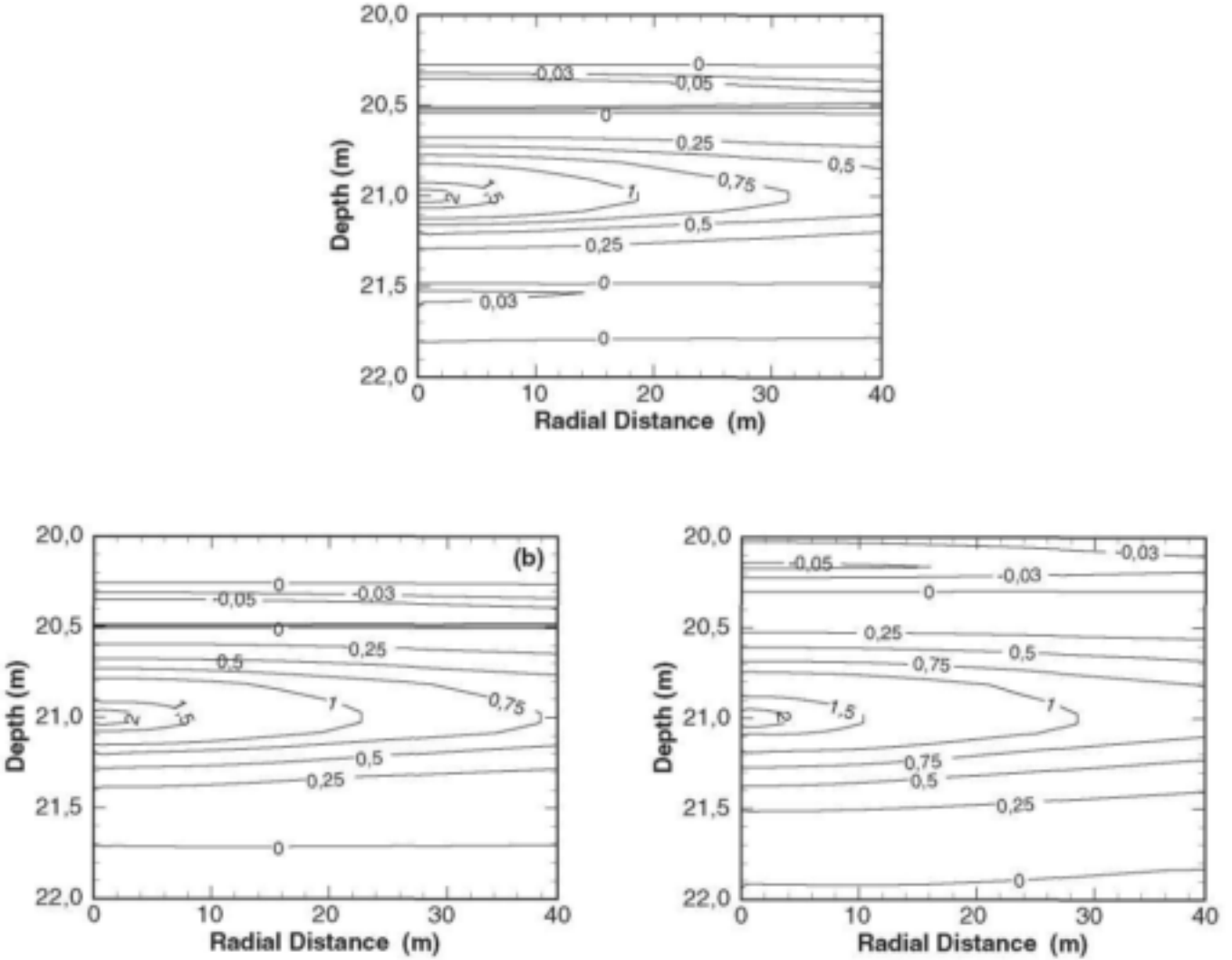

Figure 7–10 Influence of the shear modulus on the simulated drawdowns in the Campus Test Site Model after pumping the borehole for 1 h at discharge rate of 2,8 $m^3 h^{-1}$ with shear moduli of (a) $G/2$ (b) G and (c) $2G$.

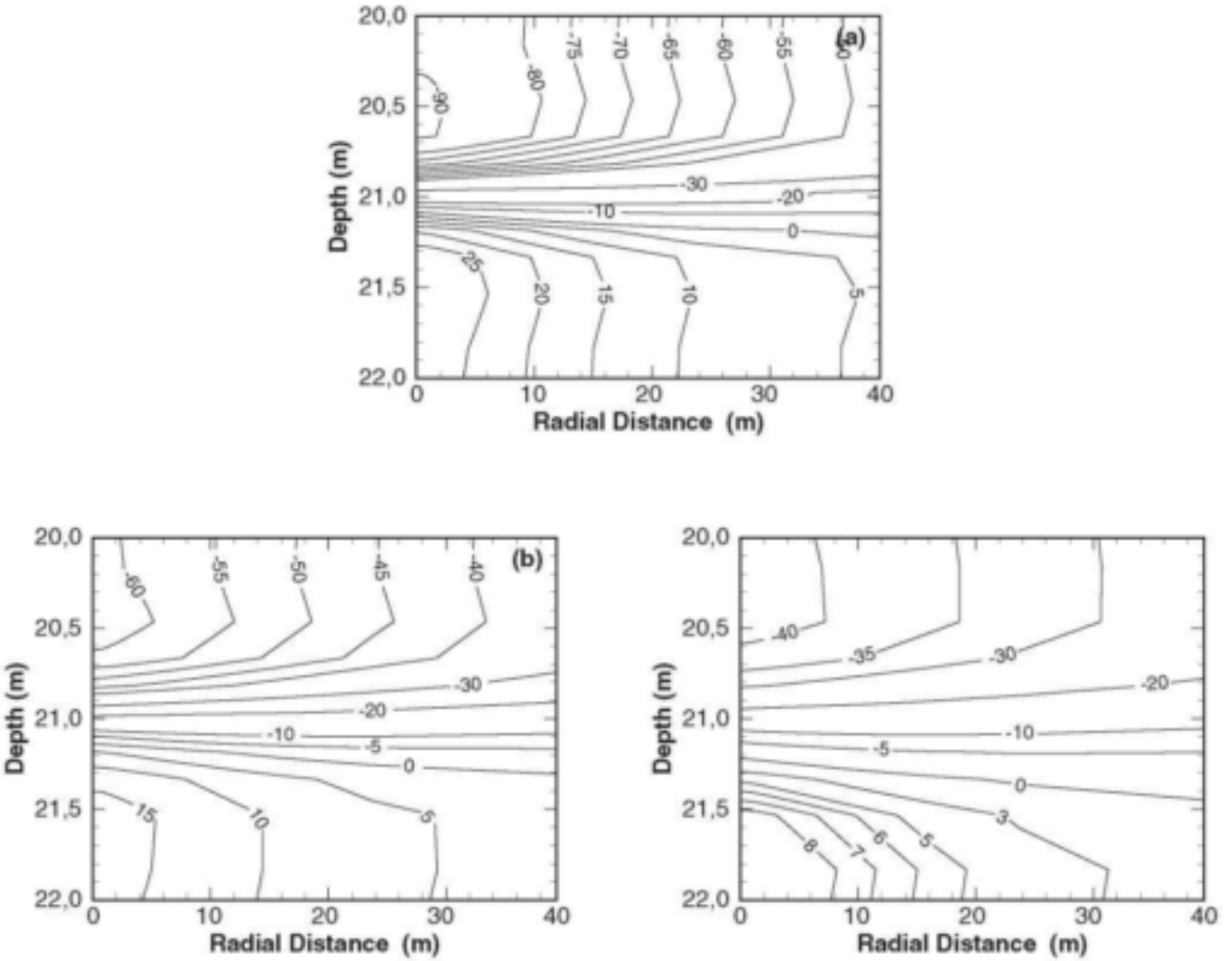

Figure 7–11 Influence of the shear modulus on the simulated vertical displacements in the Campus Test Site Model after pumping the borehole for 1 h at discharge of 2,8 m^3h^{-1} with shear moduli of (a) $G/2$ (b) G and (c) $2G$.

the vertical displacements and the hydraulic conductivity in the absence of more detailed experimental information. However, an analysis of the permeability tensor and the fact that values of the transmissivity determined from constant rate tests depend on the discharge rate of a borehole suggest that the relation may be reversed. It makes also more sense physically to assume that the permeability depends on the deformations, rather than the deformations on the permeability. One reason for this belief is that it is known that the permeability of rocks is determined by the ordering and orientation of their grains, which certainly would be effected by deformations. It is thus more natural to assume that the hydraulic conductivity of the aquifer also depends on the deformations rather than that the deformations depend on the hydraulic conductivity.

It is difficult to decide how deformations may affect the permeability. One possibility is that the permeability may be enhanced in areas where the rock matrix is stretched by the strains and reduced in areas that experience compressions. The permeability may therefore not only depend on the magnitude of the displacements, but also the signs of the displacement. However, it must be kept in mind that permeability is a tensor that also depends on variables intrinsic to the rock matrix, such as the orientation of grains and the surface area of the rocks exposed to the water. The best approach to demonstrate explicitly the dependence of the permeability on deformations will be to try to derive a more realistic expression relating the permeability of an aquifer to properties of the rock matrix and the deformations than is currently available. Since a better understanding of the behaviour of the permeability could aid in the management of deformable aquifers, it may be worthwhile to study such a relation in more detail.

It may seem strange at first that the rigidity of the aquifer has such a large effect on the simulated drawdowns. However, this behaviour should have been expected, if it is kept in mind that the drawdown is largely determined by the water released from storage, which is an inverse function of the rigidity of an aquifer.

The dependence of the drawdowns on the rigidity of the aquifer instead of the specific storativity and the possible dependence of the permeability on deformations may have profound consequences for numerical models of aquifers based on the conventional theory of groundwater flow. A common approach used in the development of such models, is to try derive a set of specific storativities and hydraulic conductivities by fitting water levels computed with the model from a limited set of 'observed' specific storativities and hydraulic conductivities for the aquifer (often only hydraulic conductivities) to a limited set of observed water levels. The partial differential equation conventionally used to describe the flow of groundwater in these models cannot account for the influence that deformations may have on the observed piezometric or water levels, although the influence will be reflected in the observed piezometric or water levels. The parameters derived from such models may therefore be biased and not representative of the aquifer.

The fact, well-known to anyone with some experience in this field, that these models are much more sensitive to variations in the specific storativity than the hydraulic conductivity of an aquifer, may be a sign of the influence that the rigidity of an aquifer has on the observed water levels.

The arguments above of course also apply to the methods conventionally used in the analysis of hydraulic tests. This may explain why it is so difficult to derive representative values of the storativities and transmissivities of fractured aquifers from conventional hydraulic tests, as well as the non-linearities that is often present in the drawdowns observed during these tests (Van Tonder *et al.*, 2001).

In conclusion, it can be said that there is little doubt that the pumping of a borehole will generate stresses in

Table 7-2 Qualitative effects that the discharge rate (Q), hydraulic conductivity (K), shear modulus (G) and porosity (ε) of an aquifer have on the observed drawdowns and displacements.

Parameter	Drawdown		Displacements	
	Magnitude	**Domain**	**Magnitude**	**Domain**
Q	Linear	Direct	Linear	Direct
K	Inversely	Inversely	Inversely	Inversely
G	Non-linear	Direct	Non-linear	Inversely
ε	Insensitive	Insensitive	Insensitive	Insensitive

an aquifer and that these stresses affect the two parameters— specific storativity and permeability. These two parameters, which are often regarded as fundamental independent parameters in the theory of groundwater flow, are therefore not really independent parameters in the sense that the word *independent* is used in the mathematical and physical sciences. Since groundwater practitioners tend to concentrate on these parameters in field investigations of groundwater resources, it was therefore thought worthwhile to summarize the effects that the various parameters may have on the drawdowns and displacements in an aquifer in Table 7-2. The reason for including the hydraulic conductivity, K, in this table is simply because the possible relation between the permeability of an aquifer and the deformations cased by the pumping is unknown and might remain unknown for a considerable period in the future.

CHAPTER 8

SUMMARY AND RECOMMENDATIONS

8.1 GENERAL

The present study was motivated mainly by the observations of Botha *et al.* (1998) that the behaviour of a stressed Karoo aquifer is determined by its complex geometry that results from the presence of bedding-parallel fractures and the multi-porosity of the rock matrix. Since the apertures of the bedding-parallel fractures are not very large, they cannot store large quantities of water, but serve as the main conduits of water for boreholes drilled into these aquifers. Indeed, there is little doubt that a borehole in these aquifers only has a significant yield if it intersects such a bedding-parallel fracture. Constrictions that developed in the aperture of such a water-yielding fracture, which is ~10 mm, could therefore have devastating consequences for a user who depends on a borehole that intersects such a fracture for his or her water supply.

Although the three-dimensional model developed by Botha *et al.* (1998) for the Campus Test Site explained many of the peculiarities associated with the behaviour of observed water levels in Karoo aquifers, there were a number of observations that the model could not account for. This applies in particular to the influence that the deformation of the fracture may have on the yield of a borehole and hence the ability of Karoo aquifers to supply water to local communities. This meant that the existing three-dimensional model had to be expanded to include deformations.

Previous studies of the deformation of aquifers (Biot, 1941; Burbey, 1999; Burbey, 2001; Hsieh, 1996) are all based on the linear law of Hooke. However, this law cannot account for residual deformations, which could play a significant role in Karoo aquifers, judging from the available information. A new non-linear form of the law was consequently introduced to study the relation between residual deformations and the discharge rates of boreholes with the emphasis on Karoo aquifers. Since there were no analytical solutions available for the coupled flow and momentum equations that describe the flow of groundwater through deformable aquifers, the finite element method (Botha and Pinder, 1983; Huyakorn and Pinder, 1983) was used to approximate the equations and to develop a computer program for the numerical computations. This computer program was first used to develop a model for a hypothetical aquifer system similar to the one discussed by Hsieh (1996), before it was applied to the study the behaviour of a Karoo aquifer. For this purpose, use was made of the Karoo aquifer underlying the Campus Test Site of the Department of Geohydrology on the campus of the University of the Free State in Bloemfontein, a complete description of which can be found in Botha *et al*., (1998).

8.2 SUMMARY OF THE RESULTS

The model for the hypothetical aquifer system was able to reproduce all the results of Hsieh (1996) and indicated that the vertical displacements, which developed in the aquifer during the pumping of a borehole, are restricted to the interfaces of the aquifer and confining layers where the elastic parameters are discontinuous. An interesting feature of this model, which is not discussed in any length by Hsieh, is that the deformation causes the aquifer to contract towards the screened segment of the borehole, both horizontally and vertically, while the confining layers contract horizontally and extend vertically. As it turns out later, this phenomenon, which is characteristic of all aquifers, plays the dominant role in the physical behaviour of all aquifers.

The first and most noticeable difference between the model for the aquifer on the Campus test Site and the aquifer of Hsieh is the way in which the drawdowns in the two aquifers behave. While the simulated drawdowns in Hsieh's aquifer steadily increase in time, the drawdowns in the Campus Test Site model, display a dependence on the position in the aquifer. In the fracture, its immediate neighbourhood and the region below it, the drawdowns increase steadily with time, as expected. However, there is a region, centred at approximately 800 mm above the fracture and extending over a distance of approximately 50 m from the borehole, where the simulated drawdowns decrease with time, after the pump was switched on. This behaviour may serve as

a numerical illustration of the somewhat paradoxal phenomenon, often observed during hydraulic tests of Karoo boreholes that the water level in an observation borehole begins to rise the moment the pump is switched on in the production borehole (Botha *et al.*, 1998).

The behaviour of the Campus Test Site model differs in another respect from that of Hsieh in that no sharp vertical deformations were generated along the discontinuous interfaces of the fracture, but at a vertical distance of approximately 0,25 m above and below the fracture. The deformations tend to compress the fracture and to bend it vertically in the form of a non-linear wave, while pushing the fracture plane downwards at the same time.

An interesting result that emerged from the model of the Campus Test Site is that there is almost no difference in the simulated drawdowns computed with the linear and non-linear law of Hooke, if the discharge rate of the borehole is not very high. However, both the vertical displacements and the drawdowns in the aquifer, computed with the non-linear law of Hooke, began to oscillate violently when the discharge rate exceeded a certain limit. The oscillations at first appear in the aquifer only near the fracture, where high strains developed, but then spread through the aquifer with increasing magnitudes. Such non-linear deformations could have disastrous consequences for an aquifer if not taken care of, especially if it is kept in mind that non-linear deformations do not restore a body to its original form once the deforming force is removed, but create residual deformations that deform the body permanently.

The model for the Campus Test Site indicated that residual deformations most likely would develop close to the borehole with magnitudes that depend on the discharge rate of a borehole, *if the discharge rate exceeds a certain limit*. The magnitudes of the residual deformations increase very quickly at early times of pumping, but then assume a pseudo steady state. The ability of a borehole to yield water therefore depends not only on the discharge rate, but also on how frequently the borehole is pumped. The model for the Campus Test Site indicated, for example, that a borehole on the site will fail in less than six years, if the borehole is pumped at a rate of 8,3 $m^3 h^{-1}$ for 8 h a day, every day of the year. The period before failure can be extended though by:

a) Decrease the discharge rate of the borehole,

b) Pump the borehole for longer periods,

c) Keep the discharge rate of the borehole below its critical limit.

This behaviour of a borehole, and consequently its ability to yield water, can be quantified by introducing a new parameter—*the expected mechanical life of a borehole*. Unfortunately, the only method available today to determine this parameter is to develop a poro-elastic model for the aquifer of concern.

A very important result that emerged from a study of the water released by the aquifer in the model of the Campus Test Site is that the two parameters: specific storativity (S_0) and its two-dimensional counterpart, storativity (S), depend on the dilatational strain, e. This variable not only decreases continuously with distance from a pumped borehole, but also increases in magnitude with the discharge rate of the borehole. The parameters S_0 and S are consequently inversely related to the distance from a pumped borehole and linearly related to the discharge rate of the borehole. *The decrease in the values of S with distance from the pumped borehole, observed by* Bredenkamp *et al.* (1995) and Botha *et al.* (1998) *is therefore not an artefact of the methods used in the analysis of the tests, as suggested by Bredenkamp and his co-workers, but a physical reality!* The parameters specific storativity and storativity are therefore not independent parameters, as implied in the conventional theory of groundwater flow, but *functions of the discharge rate*. The real independent parameters that determine how much water an aquifer is able to release is the rigidity of the aquifer, conventionally quantified by either Young's modulus, E, or the shear modulus, G and the discharge rate of the borehole. An aquifer in a rigid formation may therefore not be able to supply as easily in the demand of a borehole than an aquifer in a less rigid formation . Preference should therefore be given to aquifers in less rigid formations, if such a choice exists, in the siting of boreholes for production purposes.

A rather unusual property of aquifers that emerged from the sensitivity analysis of the parameters in the model for the Campus Test Site is that the magnitudes of the vertical displacements are inversely related to the hydraulic conductivity. However, this behaviour can be ascribed to the assumption that the hydraulic conductivity is independent of the deformations in the present model, which forces the deformations to depend on the hydraulic conductivity of the aquifer. A physical more meaningful interpretation is that the

deformations actually affect the permeability (**k**) of the aquifer, which is related to its hydraulic conductivity (**K**), through the equation

$$\mathbf{K} = \mathbf{k}\rho g/\mu$$

where, g is the acceleration of gravity, with ρ the density and μ the dynamic viscosity of the water. The advantage of this interpretation is that it can explain the dependence of the transmissivity (the scalar, two-dimensional equivalent of **K**) on the discharge rate of a borehole and the distance from the pumped borehole observed by Botha *et al.* (1998), see Figures 7–7 and 7–8. This implies that the hydraulic conductivity is not an independent parameter, as is the case with the specific storativity. It is important to remember though that **k** is a tensor that also depends on various properties of the rock matrix, particularly the orientation of the grains, and therefore should not depend on the deformations alone.

The conventional theory of groundwater flow accounts only for the rigidity of an aquifer, through the specific storativity, but not for the dependence of the hydraulic conductivity on the deformations, nor the dependence of both parameters on the discharge rate of a borehole. The values of specific storativities and hydraulic conductivities derived from this theory might therefore be biased and not representative of the aquifer for which they were derived. This may explain why it is so difficult to derive representative values of the transmissivity and storativity for a fractured aquifer from conventional constant rate tests and the non-linearities often observed in the drawdowns during such tests (Van Tonder *et al.*, 2001).

An attentive reader may at this stage ask: Why is so much emphasis placed on the discharge rate of the borehole and not the storativity or hydraulic conductivity—the two parameters conventionally used to characterize the flow of groundwater? To answer this question, one only needs to look at Equation (3.18) that governs the flow of water in the present model. This equation, which does not contain the specific storativity at all, contains just one parameter that can be controlled externally—the forcing function associated with the water, F_w, which is determined directly by the discharge rate of a borehole.

8.3 RECOMMENDATIONS

There are a number of results that followed from the present study that are of the utmost importance for the practical use, management and control of groundwater resources.

a) The pumping of a borehole causes deformations in an aquifer.

b) The magnitudes of the deformations depend linearly on the discharge rate and decrease with distance from the pumped borehole.

c) Groundwater levels observed in the field are implicit functions of the deformations.

d) The specific storativity of an aquifer is determined by the dilatational strains associated with the deformations and therefore depends on both the discharge rate of the borehole and the distance from the borehole.

e) The hydraulic conductivity of an aquifer is determined by properties of the rock matrix and the deformations and therefore depends on both the discharge rate of the borehole and the distance from the borehole.

There does not exist an explicit expression that relates the hydraulic conductivity or rather the permeability of an aquifer to the deformations. Since such a relation could improve the management of deformable aquifers considerably, it may be worthwhile to try to establish such an explicit relation. This could be achieved through more detailed laboratory studies, such as the experiments described by Mukarat (2001). Another approach would be to derive theoretical expressions for the permeability that include realistic and measurable parameters, such as the porosity, area of solids exposed to the flow and the volume of solids (Botha, 1996).

It follows from Equation (3.18) that the major contribution to the ability of an aquifer to yield water comes from the compressibility of the rock matrix, given by the dilatational strain, defined in Equation (2.38. There are thus two properties of aquifer deformations that will have a significant impact on the management and control of groundwater resources. The first is the magnitudes of the deformations and the second the nature of the deformations, i.e. are the deformations linear or non-linear.

Since the deformations are small, it is tempting to assume that the dilatational strain will also be small and can be neglected from the practical point of view. Unfortunately, this cannot be done, since such an assumption implies that one must also neglect the release of water by matrix compression in the conventional theory of groundwater flow. The real difficulty is how to detect the deformations and how to apply them in the management of an aquifer. Since there are no methods available today that can be used to detect the deformations directly and unobtrusively, the only viable option is to observe the behaviour of the aquifer continuously. This strategy of course requires a complete revision of many practices currently applied in the management and control of groundwater resources.

The reason why it is important to know whether the deformations are linear or non-linear is briefly the following. Linear deformations will only act during the time a borehole is pumped and then disappear, without causing any damage to the borehole or aquifer. Non-linear deformations, on the other hand, will generate residual deformations that accumulate with time; thereby damaging the aquifer permanently and eventually may lead to the complete destruction of the aquifer. The present study and the work of Botha *et al.* (1998) suggest that the deformations in Karoo aquifers are non-linear and therefore build-up steadily over the years, but this should be confirmed by further field investigations.

The discovery that the specific storativity and hydraulic conductivity of an aquifer are not independent parameters has far reaching consequences for the management of groundwater resources, especially since it does not depend on whether the deformations are linear or non-linear. To show this, consider the case where the management of an aquifer is based on a mathematical model derived from the conventional two-dimensional groundwater flow equation, as is often the practice today. A common approach used to develop such a model is to determine a few values for the storativity, S, and the transmissivity, T, of the aquifer from a few hydraulic tests performed on the aquifer. These parameters and water levels observed previously in a few boreholes are then used to derive a new set of storativities and transmissivities from the mathematical model that are supposed to be unique to the aquifer. This set of parameters is then combined with prescribed discharge rates for production boreholes to simulate the future behaviour of water levels in the aquifer with the mathematical model. This approach can be criticized for several reasons of which the following two are perhaps the most important.

a) The discharge rates used for the hydraulic tests will in most cases differ from the discharge rates of production boreholes for which the model is intended, which means that the S and T values derived from the hydraulic tests are not really valid for the model. There is thus no reason why the derived set of storativities and transmissivities or water levels simulated with the model should be representative of the aquifer.

b) The mathematical methods commonly used in the fitting of groundwater models are restricted to the degrees of freedom allowed for in the given model. The only way that these methods can handle the situation, where the given parameters depend on an additional parameter (not originally specified in the model), is to spread the dependence on the additional parameter over the given parameters. The parameters derived in this way will not only depend on one another, but may also loose their original physical interpretation.

A model for an observable derived by fitting a subset of the parameters, on which the observable actually depends, to a given set of realizations of the observable, will of course always describe the realizations of the observable with the accuracy specified in the fitting procedure. However, this does not mean that such a *phenomenological model* (as these models are sometimes called) will be able to describe all future realizations of the observable and that it can be used to obtain values of the observable in domains outside the one for which the model was derived originally. Extrapolation is an ill-conditioned mathematical exercise, i.e. small variations in one or more of the parameters can lead to large variations in the extrapolated values of the observable. There is thus no assurance that the extrapolated values will be true realizations of the observable, unless the whole fitting procedure is repeated, and it can be illustrated unambiguously that the model is not sensitive to extrapolations, which may be the case if the distance or time over which the model is extrapolated is small. It is therefore possible that a phenomenological groundwater model will predict the future behaviour of water levels in an aquifer within the accuracy normally associated with field observations in the immediate future, but not over extended periods. The question thus arises whether the inability of conventional, phenomenological, groundwater models to account for deformations, may not account for the heterogeneities often associated with hydraulic parameters derived from such models.

One approach to circumvent the ill conditioning of a groundwater model associated with the dependence of the storativity and transmissivity on deformations of an aquifer is to apply the model inversely. This means that one use the model repeatedly to derive values of the storativity and transmissivity from the discharge rates of the production boreholes and the water levels observed in the aquifer at different times and use these values to derive empirical relations for the storativity and transmissivity as functions of time. These functions are then used instead of the storativities and transmissivities in the direct application of the model. There are admittedly two difficulties associated with this approach. The first is that it may not be easy to fit the computed storativities and transmissivities to simple functions of time, indeed, any function of time. The second is that the inverse problem is also an ill-conditioned mathematical exercise. Considerable care must therefore be exercised in applying this approach to ensure that the derived storativity and transmissivity values are indeed representative of the aquifer. One approach to achieve this is to recompute the parameters from a new set of water levels obtained by introducing slight variations in the water levels originally used to compute the parameters and compare the variations in the simulated water levels.

The preceding discussion is broadly based on procedures used in the development of numerical models for aquifers. However, the same arguments can also be applied to conventional hydraulic tests, although the results of this study question the value of such tests.

The most unexpected result of the present study is that the motion of groundwater in an aquifer stressed by the pumping of boreholes is essentially controlled by the discharge rates of the boreholes and not the specific storativity or hydraulic conductivity as in the conventional theory of groundwater flow. The reason for this is that both these parameters are functions of the deformations created by the pumping of the boreholes and that the magnitudes of the deformations depend linearly on the discharge rate of the boreholes. It is therefore natural to ask: *Why are deformations of aquifers commonly neglected in investigations of groundwater resources, notwithstanding the fact that* Biot, (1941) *published the first significant paper on aquifer deformation more than 60 years ago*?

One answer to this question is that the effects deformations have on the parameters and variables observed in the field develop slowly with time and thus difficult to detect with the insensitive equipment used today in investigations of groundwater resources. It may therefore take a long time to notice the effects of the deformations, unless brought to the front by disastrous phenomena, such as the 'dried-up' borehole in Karoo aquifers. The result is that the effects are often not noticed or simply discarded in field investigations. However, such an approach could have dire consequences, not only for communities that depend today on groundwater for their supply of water, but perhaps more importantly for future generations. It is therefore paramount that more attention should be given to develop methods to observe the effects of deformations in the field, especially for Karoo aquifers on which properties the model discussed in this report is mainly based.

Two approaches can be used to observe deformations, or their effects, in the field: a qualitative approach and a quantitative approach. Qualitative methods could include, for example, the repetition of conventional hydraulic tests with different discharge rates. Quantitative methods, on the other hand, would consist of detailed theoretical and laboratory studies of the relation between observed drawdowns, deformations and the permeability of an aquifer and the verification of the results through actual field observations. Since it is not clear now how to relate the permeability to the deformations, it is recommended that preference should be given to laboratory and theoretical studies of the dependence of the permeability on deformations. There are many laboratory techniques that could be used to investigate the dependence of the permeability on deformations. However, there is only one method the project team is aware of that may be suitable for field investigations—the electrokinetic technique.

The advantage of the electrokinetic technique is that it is based on the same equations that govern the poro-elastic model developed in this study, with the addition of Maxwell's equations that govern the behaviour of electromagnetic fields. The method could therefore be used in principle to observe the effects that deformations have on the aquifer directly and to delineate regions of different mechanical properties in the aquifer. Although some positive results have already been obtained with the method during the present study, the progress has been slow because of the lack of financial resources.

The present report deals exclusively with results derived from a mathematical model for deformation in aquifers. Although some observational data from the aquifer on the test site of the Institute for Groundwater

Studies at the Campus of the University of the Free State have been used in the development of the model and some of the predictions of the model could be verified qualitatively with field data, the model must be regarded as generic. It is the hope of the authors that it will someday be possible to confirm the conclusions derived from the model in this report, or another appropriate model, with actual field data.

REFERENCES

Batchelor, G. K. (1967) *An Introduction to Fluid Dynamics*. Cambridge University Press, Cambridge.

Bear, J. (1972) *Dynamics of Fluids in Porous Media*. American Elsevier Environmental Science Series. American Elsevier Publishing Company, Inc., New York.

Bear, J. (1979) *Hydraulics of Groundwater*. Water Resources and Environmental Engineering. McGraw-Hill, Book Co., New York.

Biot, M. A. (1941) General theory of three-dimensional consolidation. *Journal of Applied Physics*. **12**, 155–164.

Biot, M. A. (1956) Theory of propagation of elastic waves in a fluid-saturated porous solid. I. Low frequency range. *Journal of the Acoustical Society of America*. **28** (2), 168–178.

Botha, J. F. (1994) *Models and The Theory of Groundwater Motion*. Unpublished Report. Institute for Groundwater Studies, University of the Orange Free State, P.O. Box 339, Bloemfontein.

Botha, J. F. (1996) *Principles of Groundwater Motion*. Unpublished Lecture Notes. Institute for Groundwater Studies, University of the Orange Free State, P.O. Box 339, Bloemfontein 9300.

Botha, J. F. and Pinder, G. F. (1983) *Fundamental Concepts in the Numerical Solution of Differential Equations*. John Wiley & Sons, New York, N.Y.

Botha, J. F., Verwey, J. P., Van der Voort, I., Vivier, J. J. P., Buys, J., Colliston, W. P. and Loock, J. C. (1998) *Karoo Aquifers. Their Geology, Geometry and Physical Behaviour*. WRC Report No 487/1/98. Water Research Commission, P.O. Box 824, Pretoria 0001.

Botha, J. F., Vivier, J. J. P. and Verwey, J. P. (1996) *Grondwaterondersoeke te Philippolis*. Verslag opgestel vir die Firma Cahi De Vries. Instituut vir Grondwaterstudies, Universiteit van die Oranje-Vrystaat, Posbus 339, Bloemfontein 9300.

Bredenkamp, D. B., Botha, L. J., Van Tonder, G. J. and Janse van Rensburg, H. J. (1995) *Manual on Quantitative Estimation of Groundwater Recharge and Aquifer Storativity*. WRC Report No TT 73/95. Water Research Commission, P.O. Box 824, Pretoria 0001.

Bredthauer, R. O. (1957) Strength characteristics of rock samples under hydrostatic pressure. *Transactions of the A.S.M.E.* **79**, 695.

Burbey, T. J. (1999) Effects of horizontal strain in estimating specific storage and compaction in confined and leaky aquifer systems. *Hydrogeology Journal*. **7**, 512–532.

Burbey, T. J. (2001) Storage coefficient revisited: Is purely vertical strain a good assumption? *Ground Water*. **39** (3), 458–464.

De Marsily, G. (1986) *Quantitative Hydrogeology*. Academic Press, Inc., New York.

El-Kadi, A. I. (1985) On estimating the hydraulic properties of soil. Part 1. Comparison between forms to estimate the soil water characteristic function. *Advances in Water Resources*. **8**, 136–147.

Filonenko-Borodich, M. (1965) *Theory of Elasticity*. Dover Publications, New York. N.Y.

Finlayson, B. A. (1972) The Method of Weighted Residuals and Variational Principles. Academic Press, New York, N.Y.

Fourie, F. D., Botha, J. F., Grobbelaar, R. and van Tonder, G. J. (2000) Application of the electrokinetic sounding technique for geohydrological investigations in a fractured rock aquifer system. In: Proceedings of the *XXXth IAH Congress on Groundwater: Past achievements and Future Challenges*. O. Sililo (eds.) Cape Town, South Africa. A.A. Balkema, Rotterdam.

Gringarten, A. C. and Ramey, H. J. (1974) Unsteady-state pressure distributions created by a well with a

single horizontal fracture, partial penetration, or restricted entry. *Society of Petroleum Engineers Journal.* **14** (5), 413–426.

Handin, J. and Hager, R. V. (1957) Experimental deformation of sedimentary rocks under confining pressure: Tests at room temperature on dry samples. *Bulletin of the American Association of Petroleum Geologists.* **41** (1), 1–49.

Hsieh, P. A. (1996) Deformation-induced changes in hydraulic head during ground-water withdrawal. *Ground Water.* **34** (6), 1082–1089.

Huyakorn, P. S. and Pinder, G. F. (1983) *Computational Methods in Subsurface Flow.* Academic Press, Inc., New York, N.Y.

Jaeger, J. C. (1969) *Elasticity, Fracture and Flow: With Engineering and Geological Applications.* Methuen & Co Ltd, London.

Love, A. E. H. (1927) *A Treatise on the Mathematical Theory of Elasticity.* (4th ed.) Cambridge University Press.

Meinzer, O. E. (1928) Compressibility and elasticity of artesian aquifers. *Geology.* **23**, 263–291.

Mukarat, A. (2001) Normal and shear stress dependent single phase fracture and fracture cross flow in different lithologies. In: Proceedings of the *Conference Fractured Rock 2001.* Toronto.

Pinder, G. F. and Gray, W. G. (1977) *Finite Element Simulation in Surface and Subsurface Hydrology.* Academic Press, Inc., New York, N.Y.

Strang, G. (1976) *Linear Algebra and Its Applications.* Academic Press, New York, N.Y.

Theis, C. V. (1935) The relation between the lowering of the piezometric surface and the rate and duration of discharge of a well using groundwater storage. *Transactions of the American Geophysical Union.* **16**, 519–524.

Tyldesley, J. R. (1975) *An Introduction to Tensor Analysis.* Longmans, London.

Van Genuchten, M. T. (1980) A Closed-form equation for predicting the hydraulic conductivity of unsaturated Soils. *Journal of the American Society of Soil Science.* **44**, 892–898.

Van Tonder, G. J., Botha, J. F. and Van Bosch, J. (2001) A generalized solution for step drawdown tests including flow dimension and elasticity. *Water SA.* **27** (3), 345–654.

Verwey, J. P. and Botha, J. F. (1992) *A Comparative Study of Two- and Three-dimensional Groundwater Models.* WRC Report No 271/1/92. Water Research Commission, P.O. Box 824, Pretoria 0001.

Zijl, W., Hendriks, M. A. N. and 't Hart, C. M. P. (2002) Numerical homogenization of the rigidity tensor in Hooke's law using the node-based finite element method. *Mathematical Geology.* **34** (3), 291–322.